KJELL WIIK

KINETICS OF REACTIONS BETWEEN SILICA AND CARBON

This thesis has been submitted

to

Institutt for uorganisk kjemi

Norges Tekniske Høgskole

Universitet i Trondheim

In partial fulfilment of the requirements for

the Norwegian academic degree

DOKTOR INGENIØR

March 1990

To believe what one expects

often leads to disappointment

Karl Remigius Fresenius

PREFACE

This work was carried out at the Institute of inorganic chemistry, Norwegian institute of technology, University of Trondheim.

First I want to thank my adviser Professor Ketil Motzfeldt, who initiated this investigation, and thereby introduced me into the exiting and demanding field of high temperature chemistry in the system Si-O-C. He has contributed with helpful advice and arguments and also helped with the English language, this is gratefully acknowledged.

I also want to thank siv. ing. Anders Schei at Elkem a/s (Vågsbygd, Kristiansand) for kind permission to use parts of his report: "Metallurgy of the Ferrosilicon Process", (1977). The report gives a valuable introduction into the chemistry of the industrial silicon and ferrosilicon process.

Thanks are due to dr. ing. Bjørn Myhre for valuable discussions and to ass. professor dr. techn. Stein Julsrud for encouragement and help. Furthermore, I want to thank the whole staff at the Institute of inorganic chemistry for help and interest during the years of my work.

The kind help given by siv. ing. Arne E. Arntsberg in carrying out the fluid dynamic calculations by means of the computer program FLUENT, must not be forgotten in this context.

Scholarships from the University of Trondheim for three years and NAVF for six months are gratefully acknowledged.

Financial support has been received from Norges Tekniske Høgskoles Fond and from Elkem a/s, Vågsbygd, Kristiansand and this is gratefully appreciated.

Last, but not least, I want to thank my family; Britt, Magnus and Kristina, for being patient and understanding during the turbulent completion of this work.

Trondheim, March 1990

Kjell Wiik

SYNOPSIS

The aim of this investigation has been to elucidate the mechanism by which solid silica reacts with solid carbon at elevated temperatures. The importance of the problem stems from the fact that reaction of silica with carbon is the basis for several large-tonnage process industries, and at the same time the kinetics of the reactions in these processes are poorly understood.

Investigations of kinetics must be based on a sound knowledge of the equilibria of the relevant reactions. Thus in Chapter 1, a review is given of the known compounds and the thermodynamics of the system Si-C-O, which is now quite well known. Chapter 2 deals with the phase transformations in silica which, as it turns out, have a profound influence on the experimental results.

In Chapter 3 a review is given of the previous investigations concerning the various reactions within the Si-C-O system. This review is made fairly comprehensive, with the intent that it may be useful also for future investigators in this area.

There are two main conclusions from this literature survey. One conclusion is that the reaction between silica and carbon in the presence of carbon monoxide most probably goes via the gas phase, viz.:

$$SiO_2(s) + CO(g) = SiO(g) + CO_2(g) \qquad (I)$$

and then
$$CO_2(g) + C(s) = 2CO(g) \qquad (II)$$

so that the sum gives

$$SiO_2(s) + C(s) = SiO(g) + CO(g) \qquad (III)$$

Depending upon the circumstances, the SiO(g) may react with carbon to give silicon carbide:

$$SiO(g) + 2C = SiC(s) + CO(g) \qquad (IV)$$
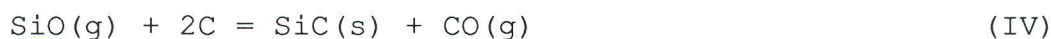
The second conclusion from the literature survey is that few, if any, of the published investigations give any reliable

information as to whether reactions (I) + (II) (or any other reactions) really represent the mechanism in question.

The experimental investigations were for the most part done by means of thermogravimetry, using a graphite-tube furnace and an associated electronic weighing cell, enclosed in a water-cooled vacuum system. It was thought expedient to conduct measurements at pressures of carbon monoxide varying from a good vacuum to somewhat above atmospheric pressure. On the other hand it was decided to limit the task by doing most of the measurements at the same temperature, about 1560 to 1570°C.

A considerable amount of work was spent investigating the rate of weight loss of a piece of silica glass tubing freely suspended inside the graphite-tube heating element, that is, investigating the reaction of silica enclosed in, but not in contact with carbon. The results from runs in a good vacuum are compared to the rate of weight loss expected from thermal dissociation of silica. Runs in carbon monoxide showed a marked influence of the gas. In the pressure range of about 10^{-2} to 10^{-1} bar the rate of weight loss was found proportional to the square root of the CO pressure. This is the expected dependence if the rate is controlled by the chemical reaction (I) on the silica surface, as shown in Chapter 5. At higher CO pressures the weight loss rate was found nearly independent of the gas pressure.

The main part of the investigations were done with charges of coarse-grained silica and graphite contained in graphite crucibles. The design of the crucible was shown to have a marked influence on the observations, and a relatively "open" design with a perforated body and large holes in the lid was chosen for the final series of experiments.

It was furthermore found advantageous to be able to vary the carbon monoxide pressure and the total gas pressure independently, in particular because gas diffusivities are inversely proportional to the total pressure. For this purpose, equipment was developed for the controlled mixing of carbon monoxide and argon.

Some of the observations may be summarized as follows:

- The crystal modification of silica at start may have a profound influence on the observed rates. Starting with silica that has in advance been converted to cristobalite gives reproducible results. The rates observed are higher than when starting with quartz, because the preceding

transformation has introduced micro-cracks and thus an enlarged reactive area on the cristobalite grains.

- At constant total pressure, the rates decrease with decreasing partial pressure of carbon monoxide. At constant partial pressure of carbon monoxide, the rates increase with decreasing total pressure

- In Chapter 7 a model is developed, based on the assumptions of local equilibrium of the reactions (I) and (II) on the silica and carbon surfaces, respectively, in combination with gas diffusion of CO_2 between the surfaces and of SiO out of the reacting system. Weight loss rates computed from the model show satisfactory agreement with the observed ones over substantial ranges of total pressures and carbon monoxide partial pressures. The observations and the model offer strong support that equations (I) and (II) above do indeed represent the mechanism of the initial reaction between silica and carbon.

It is further shown that throughout most of the experiments silicon carbide has not been formed, even under conditions where it should form according to the thermodynamics of reaction (IV). Thus it appears that the nucleation and growth of silicon carbide is a hindered process, as one might expect. Once silicon carbide has started to form on the graphite, however, a marked increase in the weight loss rate is observed. A qualitative explanation for this increased rate of reaction is offered, but a full elucidation of the part played by nucleation and growth of silicon carbide demands further investigations.

CONTENTS

BACKGROUND OF THE WORK

Reactions between silica and carbon occur in a number of important industrial processes. Silicon metal and ferrosilicon are produced by reacting silica (quartzite) with carbon (coke) in large submerged-arc electric furnaces. Silicon carbide is produced from essentially the same raw materials, but in this case the process takes place in the charge placed on a flat, rectangular bed and resistance heated by current running through the graphite core of the charge. Each of these commodities are produced in Norway in large tonnages annually, thus the reactions between silica and carbon are of considerable economic importance.

In the above examples it is desired that silica does react with the carbon to form the desired product. On the other hand, silica is also a major constituent of commonly used refractory materials, and when these materials are used under reducing conditions or in contact with carbon, reactions with silica are not wanted. This negative aspect of the reactions is also important technically and economically.

This short survey is given as background to the present work, that is, to show why it may be worthwhile to spend time on the study of reactions between silica and carbon. It is not, however, the intention of the present investigation to study these reactions in relation to any specific technological situation; the aim is to elucidate the reactions as such, with only brief comment to any tecnological implication that might occur.

It is furthermore noted that the thermodynamics, and hence the reaction equilibria, in the system Si-O-C are now quite well known, as will be related in Chapter 1. Reaction mechanisms and kinetics, on the other hand, are less studied and poorly understood. Hence the primary aim of the present investigation is to elucidate the mechanism or mechanisms by which solid silica may react with solid carbon at elevated temperatures.

1.   PHASES AND EQUILIBRIA IN THE SYSTEM Si-C-O

From the three elements silicon oxygen and carbon a large number of chemical compounds may be formed. This chapter treats the system Si-O-C from an equilibrium point of view; presenting the stability regions and composition of the various phases and species occuring in the Si-O-C system.

1.1.   Si

Silicon has the cubic diamond structure. The melting point is 1410°C with a volume contraction of 9.5%. The vapour pressure is low; e.g., at 2000 K it is about 4×10^{-5} bar (JANAF 1985). Elemental silicon, however, does not occur in the experimental studies of the present work.

1.2.   C

The stable modification of carbon at room temperature is graphite. Graphite may exist in two slightly different crystal structures: Hexagonal and rhombohedral. Normally the graphite is composed of about 90% hexagonal and 10% rhombohedral crystallites (Seltveit, 1980).

Graphite does not melt under normal pressure. The triple point has been estimated at about 4130 K and 120 bar (Bundy, 1980). The vapour in equilibrium with graphite consist predominantly of the species C_1, C_2 and C_3, with C_3 dominating at all temperatures above 1900 K. The vapour pressures are very low, however; e.g. at 2000 K the pressure of C_3 is about 4×10^{-11} bar (JANAF 1985). Hence the vapour species of carbon need not be taken into account in the present work.

1.3.   The system Si-O

Silica, or silicon dioxide with the composition SiO_2, appears to be the only thermodynamically stable compound in this system. This compound, however, occurs in a number of crystalline modifications as well as vitreous. With exception of the high-pressure modification stishovite (cf. Table 1.1), the SiO_4 tetrahedron is the building brick in all silica structures. This is a tetrahedron with Si at the centre and O at the four corners. In all of the structures except silica W, the tetrahedra are linked through the corners. The Si-O bonds have predominantly covalent character, and as a consequence, the Si-O-Si bonds are bent, with bonding angles in the range ~144° to ~150° for different structures (α-quartz: ~144°; α-cristobalite and β-cristobalite: ~147° and α-tridymite: ~150°; from Wells, 1984). This bending of the oxygen bridges is the main reason for the occurrence of the many silica structures. As regards the phase transitions, one distinguishes between displacive and reconstructive transformations. The displacive transformations, such as the α–β transition in quartz and in cristobalite, involve only the flipping of Si-O-Si bonds with resultant reorientation of the SiO_4 tetrahedra. As a consequence, displacive transformations take place readily during heating or cooling when the transformation temperature is passed. Reconstructive transformations, such as the transformation quartz→cristobalite or the crystallization of silica glass, involve the breaking of Si-O bonds and the establishment of new bonds; as a result these transformations occur much more sluggishly. We will return to the kinetics of these transformations in Chap. 2.

In analogy with carbon, silicon also appears with oxidation number +II in some compounds. The monoxide SiO, however, is thermodynamically stable only in the form of a gas at elevated temperatures. Upon rapid cooling this gas condenses to a brownish solid which is X-ray amorphous, but on heating, X-ray reflections from Si appear due to the disproportionation reaction

$$2SiO(g) = Si(s) + SiO_2(s)$$
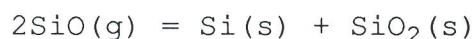
The possible stability of silicon monoxide in the condensed phase, however, has been a matter of controversy for many years. For instance Massalski (1986) in his collection of binary phase diagrams, reproduced an old tentative phase diagram in which SiO is shown as a stable solid compound, forming an eutectic on both sides with the neighbouring phases Si and SiO_2. The diagram is grossly erroneous, as can be verified by anyone who has melted silicon in a crucible of vitreous silica. The mutual solubility appears to be very small for both solid and liquid phases. Johnson and Muan (1968) have presented a phase diagram which is qualitatively correct.

Nagamori et al. (1986) claimed the existence of liquid SiO at elevated temperatures, in order to explain certain features of the carbothermal production of silicon. Neither these authors nor any others, however, presented any valid experimental evidence to show that condensed SiO exist as a stable phase, as was also pointed out by Rosenqvist and Tuset (1987).

The occurrence of sub-stoichiometric silicon oxides as metastable solid phases at moderate temperatures is a different matter. It was mentioned above that rapid condensation of SiO(g) yields a solid, usually brownish, product that appears amorphous on X-ray investigation. By various techniques of vapour deposition, sputtering, etc., colourless films may be obtained with composition SiO_x where $0<x<2$. The structure of these solids have been a matter of some controversy. Temkin (1975) claimed that they consist of phase-separated mixtures of silicon and silicon dioxide on a microscopic scale ("the microscopic mixture model"),which was supported by experimental investigation of Johannessen et al. (1976). On the other hand, Philipp (1972) on the basis of reflectance spectroscopy assumed that the structure of these sub-stoichiometric phases corresponds to the basic tetrahedral arrangement in SiO_2 with some oxygen replaced by silicon atoms, or more accurately: Tetrahedra of the type $Si-(Si_yO_{4-y})$ in which the distributions of atoms for all $y=0$ to 4 are statistical for any given atom ratio between silicon and oxygen ("the random bonding model"). This question of structure, however, is of little relevance to the subject of the present study, since none of the sub-stoichiometric phases are stable on heating.

The relevant phases to be considered here are quartz and cristobalite. The stability of the crystalline phases with respect to temperature is shown in Fig. 1.1, expressed as the Gibbs energy per mol of the phase relative to β-cristobalite.

Disregarding the tridymite phase, which most probably is not stable in the pure Si-O system (Flörke, 1956), it appears that β-

cristobalite is the stable phase above 1000°C. The kinetics of the β-quartz → β-cristobalite transformation is strongly influenced by temperature, ambient gas atmosphere and impurities and is given a more careful treatment in Chapter 2.1. Taking tridymite into account, β-cristobalite is still the only thermodynamically stable phase above 1470°C until it eventually melts at 1723°C (Fig. 1.1).

In addition we will have to consider vitreous silica, which is unstable relative to the crystalline phases at all temperatures below the melting point, but still appears as an important material in the laboratory (cf. Chap. 2 and 5).

Table 1.1.   Some crystalline phases of silica. The different phases of quartz, tridymite and cristobalite are referred to as modifications resulting from displacive transformations. The transformations between the listed phases are reconstructive. In addition to the crystalline phases there are also several amorphous phases of silica (e.g. Sosman 1955 and 1964).

Phase	Specific gravity [g/cm^3]	Hardness [Moh's scale]	Additional information
STISHOVITE	4.35	–	Synthesized by Stishov et. al (1961) at 1200-1400°C and pressures >160 kbar. Subsequently discovered in the Arizona meteor crater. Rutile structure (TiO_2); silicon is octahedrally coordinated by six oxygen.
COESITE	3.01	8	First prepared by Coes (1953) at 500°C and pressures >35 kbar. Found in the Arizona meteor crater along with stishovite.
QUARTZ (α)	2.65	7	Has a low temperature (α) and a high temperature (β) modification, with a transition point at 573°C.
KEATITE	2.50	–	Synthesized by Keat (1954) at 380-585°C and water pressures 350-1250 bar. The acidity, pH, is probably an essential parameter in the formation of keatite. It has the helical structure of quartz, but in the tetragonal instead of the trigonal system.
CRISTOBALITE	2.32	6.5	Has a low (α) and a high (β) temperature modification with transition point at 272°C.

Table 1.1. Continued.

Phase	Specific gravity [g/cm^3]	Hardness [Moh´s scale]	Additional information
TRIDYMITE (α)	2.26	7	This phase is probably not a pure SiO_2 phase, but is stabilized by small amounts of impurities (Flörke, 1956). It may occure in a number of modifications, Sosman (1964) states 9 possible modifications with stability fields in different temperature regions (even overlapping regions).
SILICA W	1.98	–	This is the lightest silica phase. Synthesized by Weiss and Weiss (1954) by condensation of SiO(g). The SiO_4-tetrahedra are joined at edges instead of corners. It´s lifetime is short in the presence of humidity (H_2O) which catalyses the rearrangement to SiO_4-tetrahedra joined at corners.
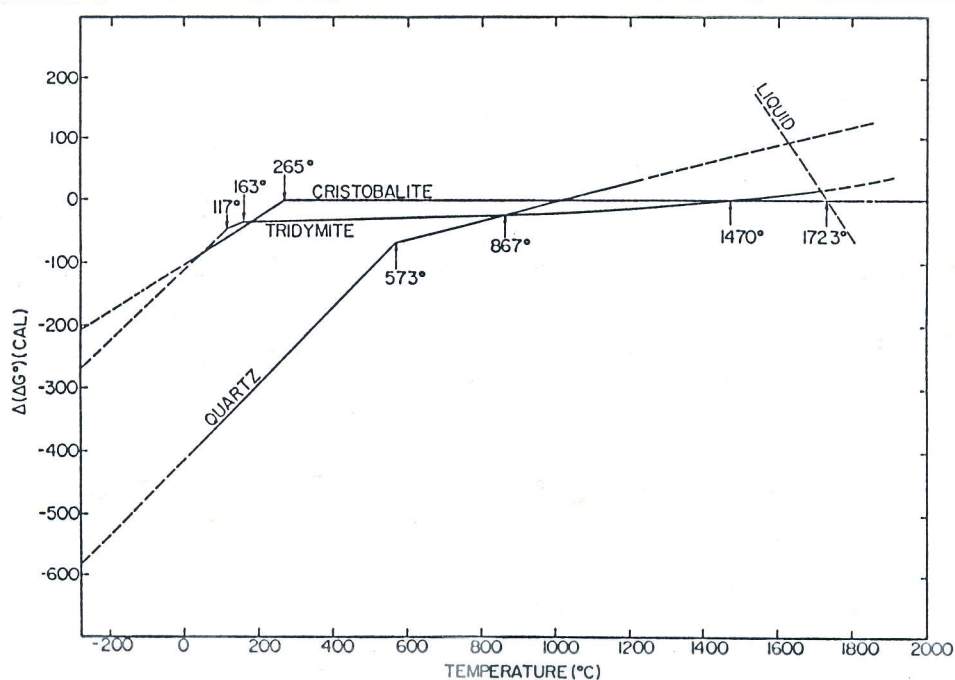
Fig. 1.1. Differences in standard free energy of formation, $\Delta(\Delta G^0)$, among various forms of SiO_2, using high cristobalite as reference state, as a function of temperature (after Muan and Osborn, 1965).

The thermal dilatation of the common silica phases is visualized in Fig. 1.2. and shows that the volume expansion associated with the displacive $\alpha \to \beta$ transformation of quartz and especially that of cristobalite is severe.
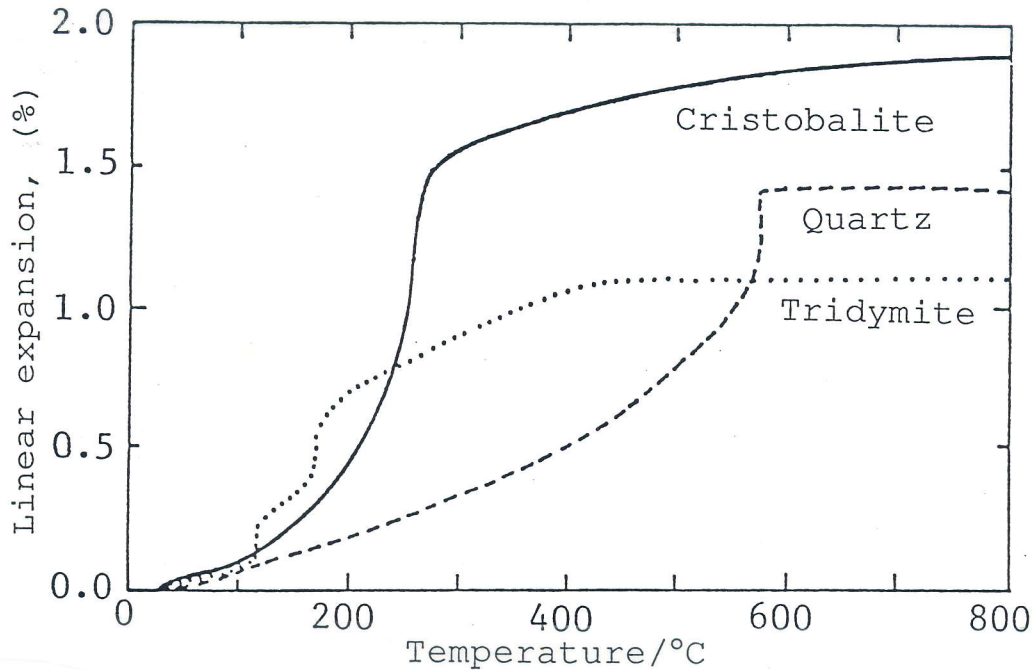
Fig.1.2.   Characteristic linear, thermal expansion of quartz, cristobalite and tridymite (after Seltveit 1980)

Silica vaporizes at elevated temperatures mainly by decomposition into silicon monoxide and oxygen:

$$SiO_2(s) = SiO(g) + 1/2\ O_2(g) \qquad (1.1)$$
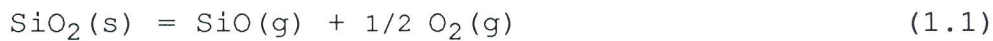
The thermal dissociation of oxygen

$$1/2\ O_2(g) = O(g) \qquad (1.2)$$

becomes noticeable at the high temperatures and low pressures in question. Some evaporation to molecular SiO_2 also takes place:

$$SiO_2(s) = SiO_2(g) \qquad (1.3)$$

The equilibrium partial pressures of the gaseous species in dependence of $1/T$ are given in Fig. 1.3 (JANAF, 1985). The principal species are seen to be $SiO(g)$ and $O_2(g)$.

Lamoreaux et al (1987) have compiled relevant thermodynamic data and have calculated equilibrium vapour phase composition above a number of oxides, including silica, under oxidizing, neutral and reducing conditions. They have computed the vapour pressure for a number of species (O, O_2, Si, SiO, SiO_2, Si_2, Si_2O_2 and Si_3) and shown SiO(g) to be the principal silicon containing vaporization product under neutral and reducing conditions, while SiO_2(g) is favoured under oxidizing conditions below about 2227°C.
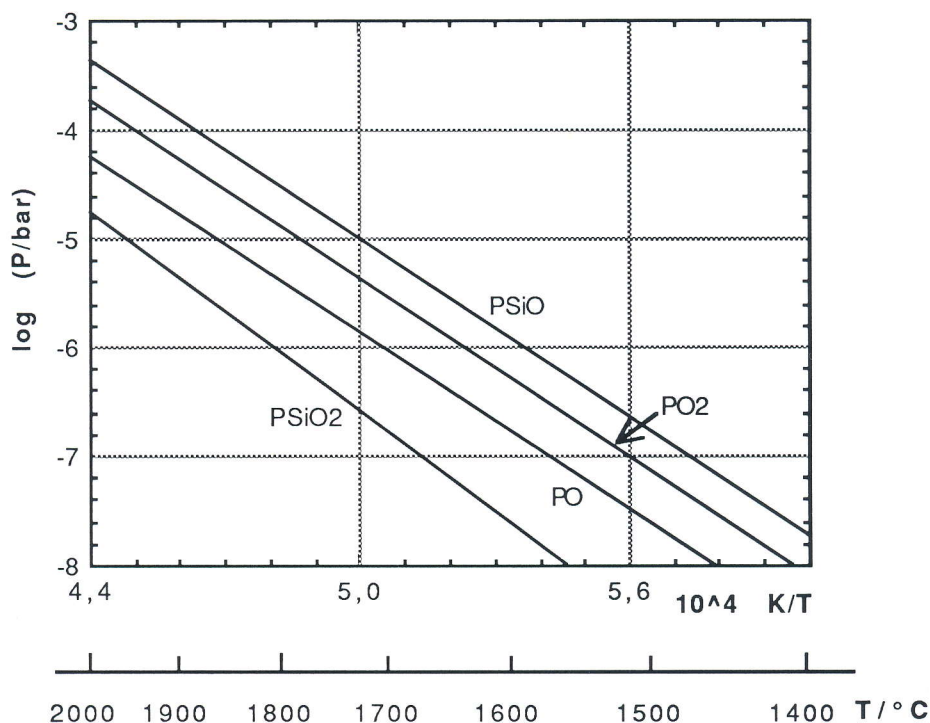
Fig. 1.3. Equilibrium pressures of the gaseous species resulting from congruent evaporation of silica as calculated according to reaction (1.1-3) (data from JANAF, 1985).

1.4.   The system Si-C

Silicon carbide is renowned for crystallizing in a number of different "polytypes". One of these is cubic, also denoted β-SiC. All of the others are hexagonal or rhombohedral with the common designation α-SiC. Shaffer (1969), in his review on the structure of SiC, tabulates 73 polytypes of α-SiC and one β-SiC. The basic crystal unit in SiC is always the tetrahedron consisting of a carbon atom tetrahedrally surrounded by four silicon atoms (CSi_4),

in the same way a silicon atom is tetrahedrally surrounded by four carbon atoms (SiC_4) and the crystal may be considered as layers of such tetrahedra. Accordingly the different structures result from different stacking sequences.

According to JANAF (1985) the β form is the thermodynamically stable phase in the whole temperature region (up to sublimation temperature). The commercial SiC process (Acheson) gives, however, mainly α-SiC with some β-SiC (e.g. Wecht, 1977).

According to Scace and Slack (1959) SiC decomposes peritectically at 2830°C into graphite and a silicon melt containing 19 atom% carbon. Olesinski and Abbaschian in their assessment of the system Si-C have preferred the results of Dolloff (1960), which give the peritectic decomposition at about 300°C lower (2545±40°C) with a corresponding solubility of carbon in liquid silicon of 27 atom%. This phase diagram appears in the collection edited by Massalski (1986). It is, however, reason to believe that the predicted solubility of carbon is too high and therefore the data given by Scace and Slack (1959) are believed to be more correct.

The total pressure of the gaseous species resulting from evaporation of SiC at high temperatures attains, according to Ruff (1935), 1 atmosphere at 2670°C. Drowart et al. (1958) performed a mass-spectrometric investigation of the gaseous species in equilibrium with the system SiC-C, and partial pressures are tabulated for 9 species (Si, SiC, SiC_2, Si_2, Si_2C, Si_2C_2, Si_2C_3, Si_3 and Si_3C) in the temperature interval 1876-2043°C. The predominant species found were Si, SiC_2 and Si_2C. Motzfeldt and Steinmo (1989) studied vaporization of SiC by mass-loss effusion and found the vapour pressures to be roughly a factor of 2 lower than the experimental results of Drowart et al.

However, an extrapolation of the measurements of Drowart et al. gives a total pressure of about 2×10^{-6} bar of the gaseous species in equilibrium with SiC-C at 2000 K. Thus the kinetics of interaction between silica and carbon at conditions where SiC is formed are assumed not to be affected by the presence of the gaseous species resulting from evaporation of SiC at the temperatures in question (~1830 K) in the present work.

1.5.   The system C-O

The reaction between carbon dioxide and carbon

$$CO_2 + C = 2CO \tag{1.4}$$

frequently referred to as the Boudouard reaction, plays an important role in the carbothermal reduction of a number of oxides. In the same way it will be assumed that reaction (1.4) is an important part of the reaction mechanism describing the interaction between silica and carbon.

In the presence of C at a given temperature and CO pressure the CO_2 pressure is uniquely given (invariant equilibrium) and Fig. 1.4. gives the CO_2 pressure against 1/T at 1 bar CO. The kinetics of the Boudouard reaction are treated in Paragr. 3.3.9.
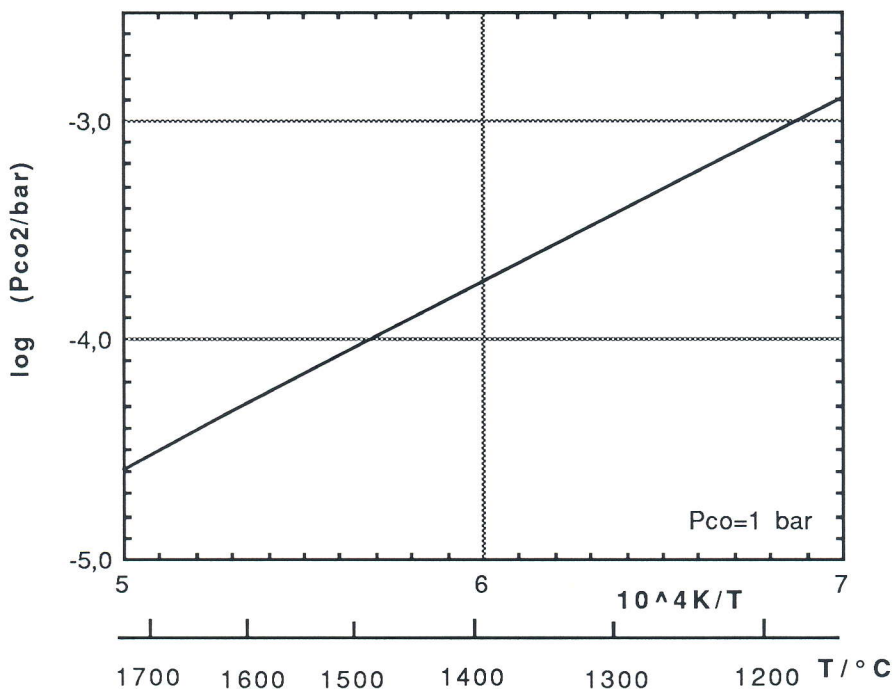
Fig. 1.4. Equilibrium pressure of CO_2 at 1 bar CO for reaction (1.4) (data from JANAF, 1985).

1.6.   The system Si-C-O

Gibb's phase rule in its simplest form may be written:

$$P + F = C + 2 \qquad\qquad (1.5)$$

P = number of phases
F = variance, or degrees of freedom
C = number of components

The simplest approach is to let the number of components equal the number of elements in the system, namely 3 (Si, O and C), which gives:

$$P + F = 3 + 2 = 5 \qquad\qquad (1.6)$$

The system is said to be invariant when the number of degrees of freedom equals zero (F=0); corresponding to 5 phases in mutual equilibrium, e.g., 4 condensed and a gas phase.

There are 4 known condensed phases in the system Si-C-O: Si, SiO_2, SiC and C.   Under reducing conditions at elevated temperatures there will always be a gas phase present where the most abundant species are SiO and CO.   Hence the invariant equilibrium is formally represented by the system:

(IA)   Si – SiO_2 – SiC – C – GAS
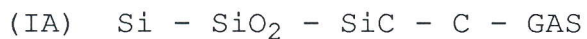
The coexistence of four phases, that is three condensed and one gas phase, leaves the system with one degree of freedom. Thus, the system is monovariant and one intensive variable (temperature, total pressure or gas composition) must be chosen before the system is in a determinate state.   The possible occurrence of four condensed phases may give rise to four different combinations of three phases each, indicating four possible monovariant equilibria.   However, two of these combinations require the simultaneous presence of Si and C[*] and these do not represent equilibrium conditions since the two

_____

[*] Only possible at the invariant point

elements will react and form SiC. The system is thus left with two possible monovariant equilibria viz.:

(IB) SiO_2 – C – SiC – GAS

(IIB) SiO_2 – SiC – Si – GAS
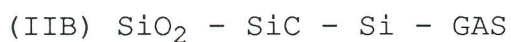
The coexistence of three phases, i.e. two condensed and one gas phase, leaves the system with two degrees of freedom and the system is divariant. Accordingly, two intensive variables must be chosen in order to get the system in a determinate state. With basis in the four condensed phases there are six possible combinations of divariant equilibria, but by reasons mentioned above the combination of Si and C is ruled out leaving the system with five possible divariant equilibria, viz.:

(IC)   Si – SiO_2 – GAS

(IIC)   Si – SiC – GAS

(IIIC) SiO_2 – SiC – GAS

(IVC) SiO_2 – C – GAS

(VC)   SiC – C – GAS
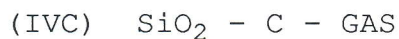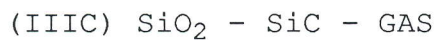
The relevant phases and combinations are shown in the schematic ternary diagram in Fig. 1.5. Solid solution among the phases is negligible.
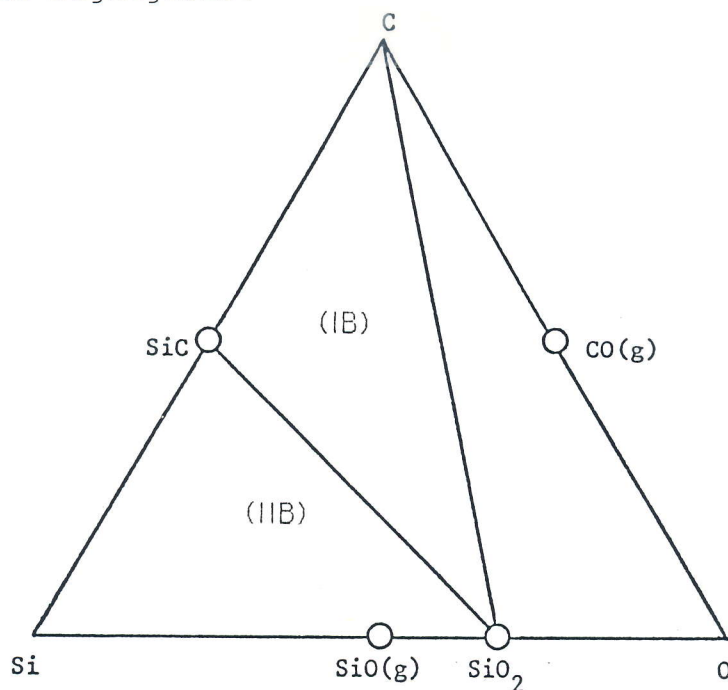
Fig. 1.5. Schematic diagram of the system Si-O-C.

1.7. Reaction equilibria

The virtual absence of solid solution among the phases simplifies the presentation of equilibria in the system.

There are a number of ways to present equilibria in the system Si-C-O. The challenge is to give as much adequate information as possible in a two-dimensional coordinate system.

Since the gas phase indeed is important in the system and the most prominent gaseous species are SiO and CO, it is convenient to represent the equilibria in a diagram with $\log P_{CO}$ and $\log P_{SiO}$ on the axes, cf. Fig. 1.6. Equivalent diagrams have previously been presented by Motzfeldt (1961) and by Poch and Dietzel (1962) (both based on the older and incorrect data for SiO_2), and by Gjerstad (1968) who also confirmed his data experimentally.

The equilibrium diagram is designed from the following five divariant equilibria:

$$SiO_2 + C = SiO + CO \qquad\qquad (1.7)$$

$$SiO + 2C = SiC + CO \qquad\qquad (1.8)$$

$$2SiO_2 + SiC = 3SiO + CO \qquad\qquad (1.9)$$

$$SiO + SiC = 2Si + CO \qquad\qquad (1.10)$$

$$SiO_2 + Si = 2SiO \qquad\qquad (1.11)$$

The above reactions may be adequately represented as planes in a three-dimensional coordinate system; the coordinates being $\log P_{CO}$, $\log P_{SiO}$ and $1/T$. However, choosing the $\log P_{CO}$-$\log P_{SiO}$ plane for the presentation of equilibria, each line in Fig. 1.6. is the projection of the line of interception by two planes: One plane described by the reaction in question and the other being the isothermal plane at right angle to the $1/T$-axis.

The main fields marked Si, SiC and C represent the fields where each of these phases may be present in equilibrium with SiO_2. Any gas composition above the lines (at a given temperature) will be unstable and condense into a mixture of SiO_2 and one of the species Si, SiC or C due to the reverse of reaction (1.7), (1.9) or (1.11).

The monovariant equilibria is represented by the dotted lines IB and IIB (Fig. 1.6) and refers to the following 4-phase equilibria:

$$SiO_2 + 3C = SiC + 2CO \qquad (1.12)$$

$$SiO_2 + 2SiC = 3Si + 2CO \qquad (1.13)$$

Considering only the monovariant equilibria (1.12) and (1.13), the phase diagram turns out as given in Fig. 1.7. The monovariant equilibria appear as almost straight lines which intercept at the invariant point IA, corresponding to the 5-phase equilibrium mentioned in Section 1.6. With data from JANAF (1985) the invariant point is calculated to 3048°C and at a total pressure (sum of SiO and CO) of about 6.6 kbar. This calculated result, however, cannot be quite correct. It is noted that the invariant point represents the conditions for simultaneous presence of Si, SiC and C, and this was found experimentally by Scace and Slack to occur at 2830°C.

An alternative way of presenting the equilibria appears in Fig. 1.8. (originally presented by Motzfeldt, 1961) where the restriction $P_{SiO} + P_{CO} = 1$ bar is put on the system. Accordingly, the invariant equilibria is reduced to four coexisting phases corresponding to the points of interception at 1514°C (SiO_2, SiC, C, gas) and 1811°C (Si, SiO_2, SiC, gas). This diagram has been frequently applied in discussing the chemistry of the Si-metal production.
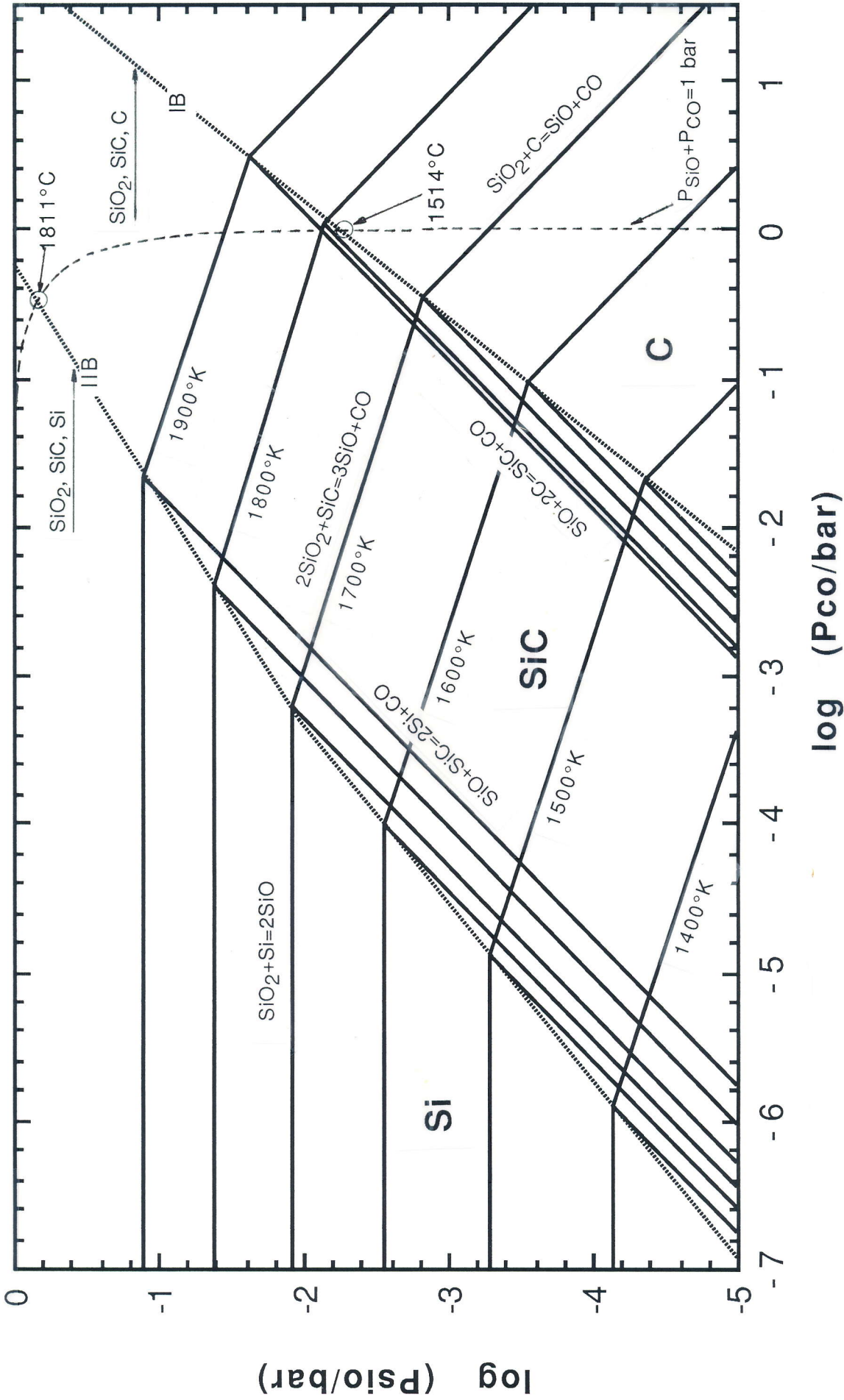
Fig. 1.6. Equilibrium gas composition for the five divariant equilibria in the system Si-O-C (solid lines). The dotted lines, IB and IIB, are the monovariant equilibria. The isobar at 1 bar total pressure is included (calculated with data from JANAF, 1985).
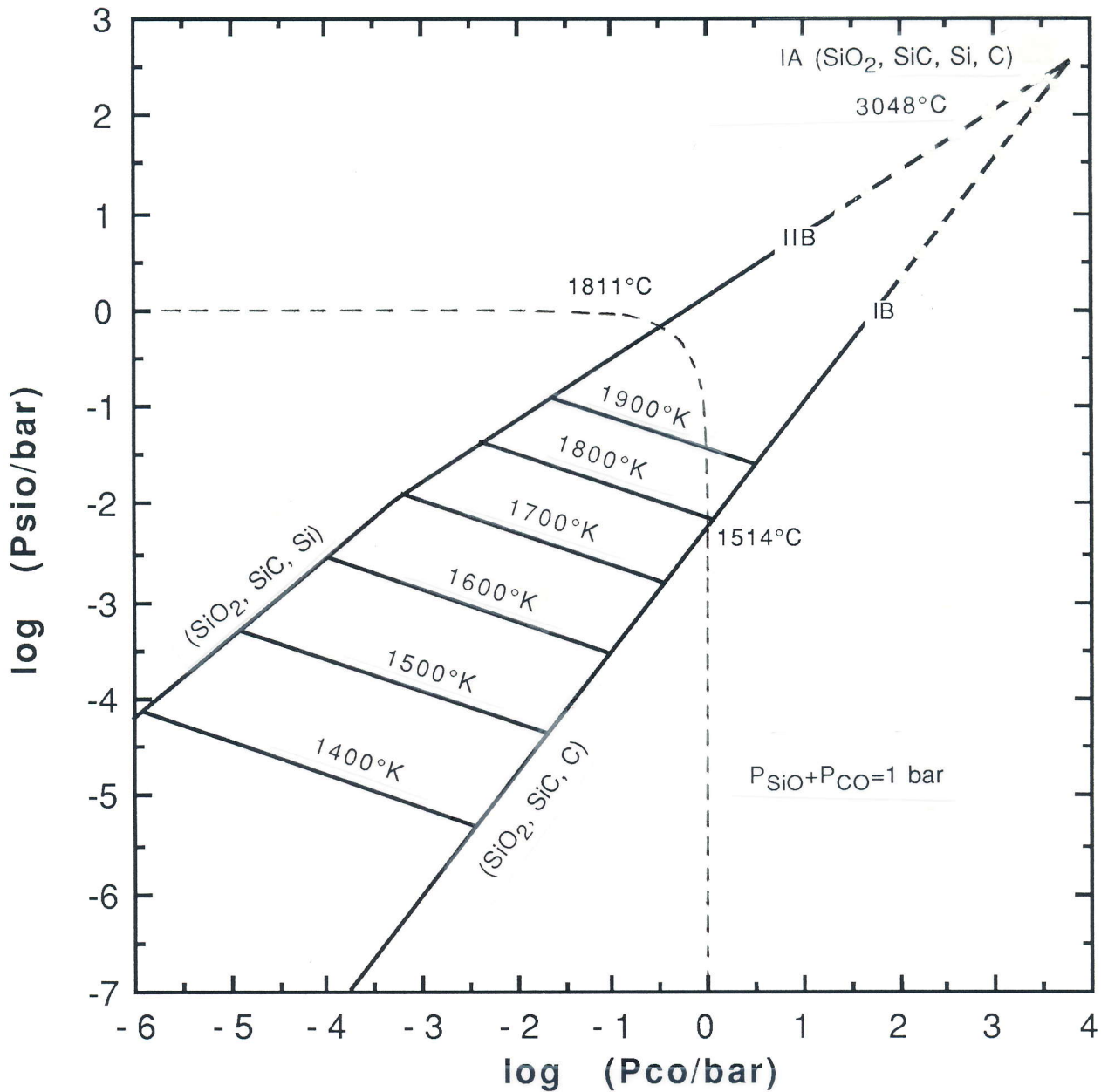
Fig. 1.7. Equilibrium gas composition for the monovariant equilibria in the system Si-O-C   The point of interception between the lines represents the invariant equilibrium at 3048°C assuming unit activity of the condensed phases.   However, since the solubility of carbon in silicon becomes significant at high temperatures (~19 atomic % at 2830°C according to Scace and Slack) the corresponding activity of silicon is less than unity and hence the "true" invariant point lies at a somewhat lower temperature (data from JANAF, 1985).
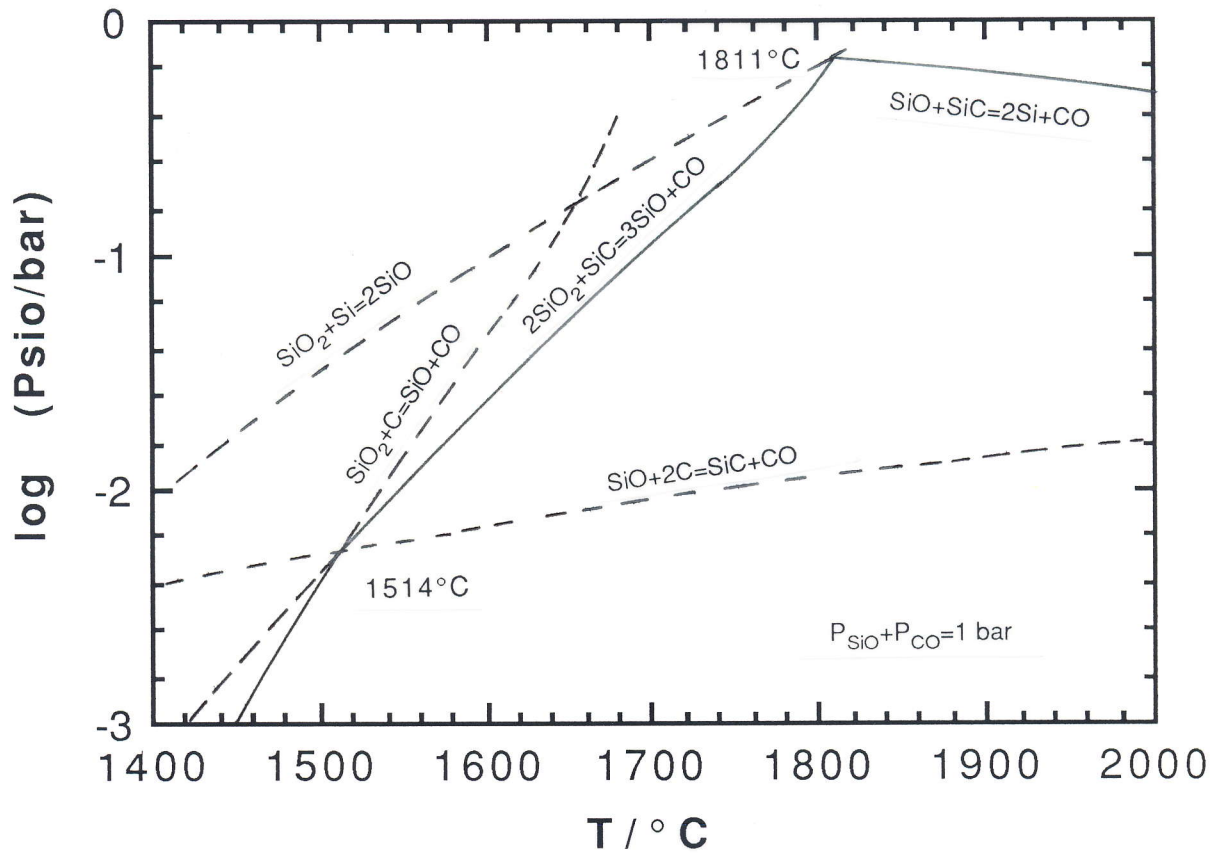
Fig. 1.8. Partial pressure of SiO at a total pressure of 1 bar for the divariant equilibria in the system Si-O-C (data from JANAF, 1985).

2.   KINETICS OF PHASE TRANSFORMATIONS IN SILICA

It has been found in the present experimental studies (Chap. 5 and 6) that phase transformations in the silica used as reactant has important effects on the rates of reaction. Hence it appears necessary to include a discussion of these transformations, in particular that from quartz to cristobalite, and the crystallization of vitreous silica.

2.1.   Quartz → Cristobalite

Chaklader and Roberts (1961) and Chaklader (1963) showed from DTA and XRD-determinations that the quartz → cristobalite transformation was indirect and involved an intermediate non-crystalline (amorphous) transition phase, viz.:

$$Quartz \xrightarrow{k_1} Transition\ phase \xrightarrow{k_2} Cristobalite \qquad (2.1)$$
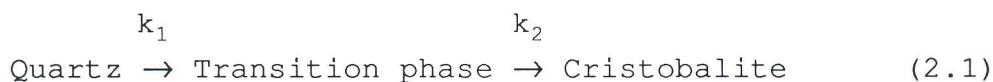
Chaklader and Roberts (1961) found that a Madagascar quartz quality, fired at 1500°C, was initially very slow to decompose into the transition phase and assumed this to be due to a nucleation period. The more rapid conversion that followed, represented the propagation of the nucleated zones. A similar result from Chaklader (1963) is given in Fig. 2.1.
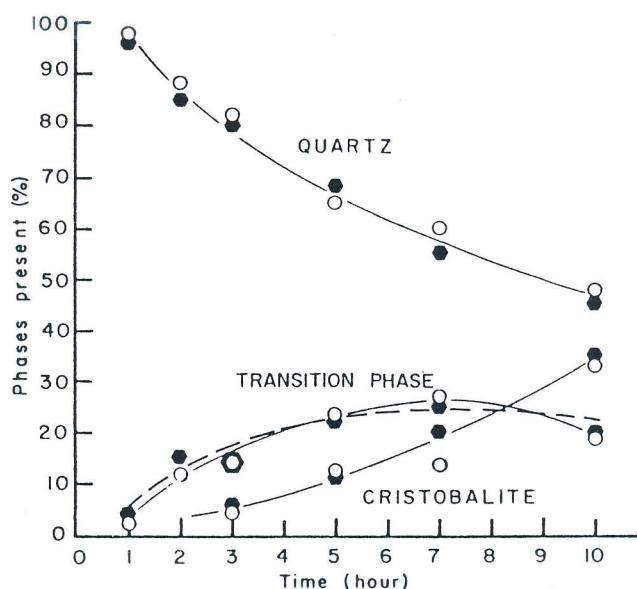
Fig. 2.1.   Transformation of Brazilian quartz (average diameter 137 μ) at 1560°C (after Chaklader, 1963).

It is seen that the reconstructive transformation into cristobalite is rather sluggish: After 10 h at 1560°C only approximately 35 % of the quartz was transformed into cristobalite.

Mitra (1977) studied the phase transformations of two varieties of high-purity quartz at 1400°C and developed a model aiming at describing the rate of formation of the intermediate and cristobalite phase respectively. The results of the model are shown by dashed lines in Fig. 2.2. The composition
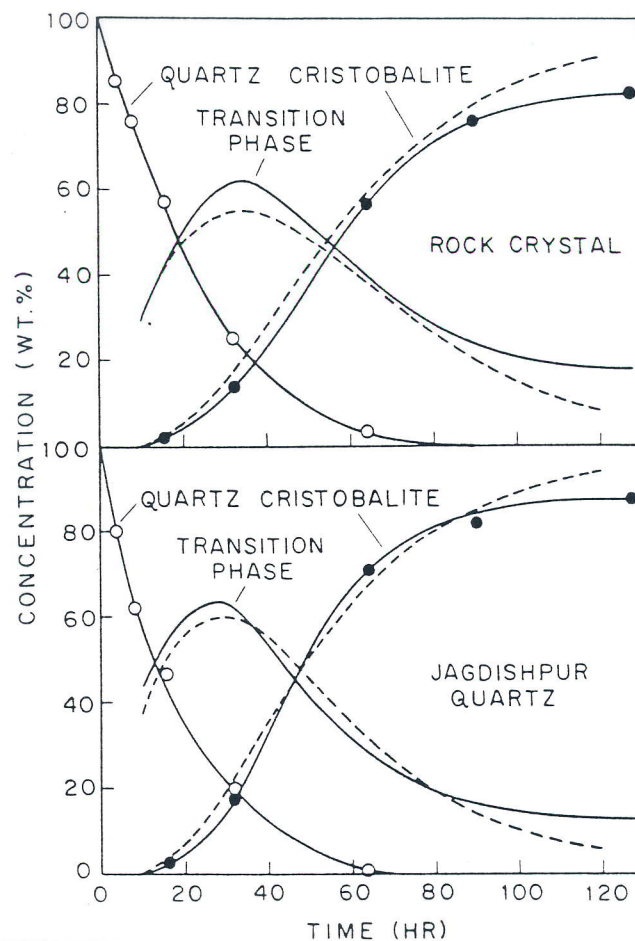
Fig. 2.2. Concentration of quartz, transition phase, and cristobalite on firing rock crystal and Jagdisphur quartz at 1400°C Particle size of the quartz samples were 20-40 μ (after Mitra, 1977).

of the silica was found by subjecting the fired samples to DTA for determination of quartz and cristobalite contents from their high-low inversion peaks. The amount of the transition phase was obtained by deducting the sum of quartz and cristobalite percentages from 100.

The first step of the conversion, quartz → transition phase, was shown to be a phase boundary process following the rate equation:

$$A_f = \left(1 - \frac{ut}{r_0}\right)^3 \qquad\qquad (2.2)$$

where A_f is fraction of quartz remaining unconverted after time t, u is radial velocity of decomposition, i.e., linear rate of propagation of quartz/transition phase boundary, and r_0 is the initial average radius of the particles present.

Furthermore, Mitra (1977) assumed that the rate of formation of cristobalite was proportional to the relative amount of the transition phase (or more accurately: the concentration of critical-size nuclei of cristobalite in the transition phase). This would explain the sigmoidal cristobalite curves in Fig. 2.2. The reason why cristobalite is nucleated throughout the body of the transition phase is explained as follows: Because of its much lower density[*] compared with quartz, the transition phase layer would occupy a greater volume than the parent phase, and the resulting tension would produce cracks in the former. Furthermore, the reconstructive transformation involving the breaking of silicon-oxygen bonds would result in an extensive fragmentation of the transition phase. They did find that partially converted quartz particles, containing large portions of transition phase but no cristobalite, looked opaque white and were easily crumbled to a powder on application of pressure by the fingers. This indicated that the transition phase was a highly fragmented material and it is probable, therefore, that a large number of homogeneously distributed internal nucleation centres would be available, so that nucleation and growth of cristobalite would occur throughout the whole volume of the transition phase instead of being localized at its outer surface.

The rate of the respective steps is likely to be influenced by the nature of contaminating species, the impurity level, and ambient atmosphere. Chaklader (1963) found that UO_2 catalyzed the transformation reaction, but that the catalytic effect was much more pronounced in the last stage, i.e., transition phase to cristobalite. Moreover, Chaklader and Roberts (1961) found that a

---

[*] The density of the transition phase was measured by Chaklader and Roberts (1961) and found to be 2.30 g/cm^3. The density of quartz is 2.65 g/cm^3

Madagascar quartz quality transformed substantially faster into cristobalite than did a Brazilian quartz quality, despite the fact that no significant difference in the chemical composition of the two materials could be found. The discrepancy was left unexplained and indicates some of the difficulties associated with quantitative studies of phase transitions or solid state kinetics in general.

2.2. Devitrification of silica glass

Ainslie et al. (1962) reported that devitrification of silica occurs at perceptible rates at temperatures from about 1000 up to 1710°C. They applied a fused silica having the commercial designation 204A (General Electric Company) with an exceptionally low water content throughout their investigation. The nucleation of cristobalite was found to take place mainly on the external surface and only rarely in the interior of the glass. The nucleation showed a heterogeneous nature, strongly catalyzed by superficial condensed phase impurities. E.g. a flame polished silica specimen fired for one hour at 1400 °C showed essentially no devitrification whereas a specimen subjected to the same treatment, with the exception of a drop of tap water placed on the silica surface, showed cristobalite nucleation in profusion. This was consistent with the mineral residue, which was left behind while the water evaporated, catalyzing the nucleation, as an experiment with triply distilled water showed virtually no devitrification. They concluded that most fused silica objects had enough "dirt" on their surfaces to catalyze nucleation uniformly and that the rate of devitrification as it is ordinarily seen is controlled , not by the nucleation rate, but by the rate at which the cristobalite grows into the glass.

For the silica glass quality in question the authors reported that the thickness of the cristobalite layer increased parabolically with time for the experiments conducted in O_2 and/or H_2O-atmosphere. Furthermore the crystal growth was found to be severely inhibited when fired in carefully dried inert gases (Ar and N_2). Devitrification was found to be effectively retarded,

but linear with time when the silica surface was coated with a thin layer of pyrolytic graphite.

From the parabolic behaviour in O_2 and H_2O the authors suggested that the rate of crystal growth was controlled by O_2 and/or H_2O diffusion through the increasing cristobalite layer to the crystal/glass interface. This was supported by the retarding effect of the pyrolytic graphite coating which is a effective reducing agent for O_2 and H_2O.

The rate of devitrification in air (parabolic behaviour) was found to increase from 1350°C all the way up to 1655°C. Above this temperature the rate decreased and became zero as the melting point was attained.

Wagstaff et al. (1964) investigated crystallization rates in the temperature range 1300-1580°C for four types of carefully classified vitreous silica. The work deals with the rate of crystal growth from the surface into the body of the glass, and is not concerned about the rate of nucleation. Some difficulties with the formation of a homogeneous layer of cristobalite on the glass surface was, however, reported for the high-purity glasses, but cleaning with hydrofluoric acid and subsequent treatment with a very dilute sodium silicate solution or tap water ensured a satisfactory nucleation.

Wagstaff found that the nature of the crystal growth in various gaseous media indeed was sensitive to the stoichiometry of the glass: The thickness of the cristobalite layer was found to increase parabolically with time for unstoichiometric glasses[*] (initially with a short linear dependence) both in O_2 and H_2O atmosphere, consistent with the observations of Ainslie et al. (1962). The rate was also found to increase with increasing concentration of both O_2 and H_2O in the ambient atmosphere. Furthermore, they were able to separate the effects of O_2 and H_2O and found a substantial increase in rate by the presence of H_2O compared to O_2.

However, for stoichiometric glasses, SiO_2, the growth of cristobalite was linear with time and enhanced rate was not observed in the presence of O_2. The rate was found to increase with increasing concentration of H_2O in the atmosphere, but still

---

[*] The quality of the applied unstoichiometric glasses had the commercial designation GE 201 and GE 204A (General Electric Company). The -X in SiO_{2-X} was estimated by T.Bell et al (1962) to be between 3×10^{-5} and 10^{-4}.

exhibit linear growth with time. Moreover, stoichiometric glasses was found to devitrify more rapidly than the unstoichiometric.

The experimental results led to the following conclusions: The diffusion controlled rate dependence for the unstoichiometric glasses is due to O_2 and/or H_2O diffusion through the increasing layer of cristobalite to the glass/crystal interface. It is assumed that the tendency to crystallize would be greater if the proper stoichiometry (that is SiO_2) was satisfied. This was supported by the linear growth behaviour, independent of O_2-concentration in the gas atmosphere, for the stoichiometric glass. However, since the presence of H_2O was found to increase the growth rate both for unstoichiometric and stoichiometric glasses, the role of H_2O was believed to be twofold: First, it may act as a source of oxygen and thereby diminish the unstoichiometry. Secondly, hydroxyls in the glass have the effect of weakening the structure (breaking oxygen bonds) and thereby lower the viscosity and softening point. As a result the ease with which the glass can re-arrange into a crystalline lattice is increased. The work of Wagstaff et al. thus explains the observations of Ainslie et al. (1962).

Bihuniak (1983) investigated the effect of trace impurities on the rate of crystal growth in a series of unstoichiometric vitreous silica glasses doped with trace levels of alkali metal oxides and aluminium oxide. The work does not deal with the rate of nucleation of cristobalite on the silica surface, but the author points out that because devitrification is a high-temperature occurrence, and a typical furnace environment is not chemically inert, experimental details can strongly influence nucleation. Uniform nucleation was ensured by soaking the silica specimens in a solution of $Na_2O \cdot SiO_2$. The rate of growth was found to exhibit the expected parabolic behaviour, and was furthermore found to increase as the molar ratio of alumina (Al_2O_3) to alkali metal (Na_2O, Li_2O and K_2O), designated $R_{Al/M}$, in the silica glass decreased, the dopants all being at the molar ppm level. As the viscosity of glass increased with increasing $R_{Al/M}$, Bihuniak concluded that impurities in vitreous silica at the trace level affect the devitrification rate only insofar as they affect viscosity. That is, increasing viscosity correspond to decreasing growth rate.

Leko and Komarova (1975) investigated nucleation and growth rates of anhydrous glasses and glasses containing OH-groups, in

different gaseous media at temperatures in the region 1400-1500°C. They found that cristobalite nucleated in a continuous surface layer in glasses containing more than o.1 wt.% OH-groups independent of gas composition (air, oxygen, argon or vacuum). Nucleation of anhydrous glasses in dry media exhibited a rather inhomogeneous nucleation: Nuclei were formed at individual local zones and were distributed at random throughout the glass surface. Surface sectors with no sign of nucleation were observed for a long time. The formation of a uniform, homogeneous crystalline layer was observed when any silica glass was crystallized in an atmosphere containing a large amount of water vapour. The anhydrous glass however, exhibited both types of nucleation when fired in moist air, that is, simultaneous formation of a homogeneous layer and crystallization in individual local zones.

It may be concluded that pure unstoichiometric silica glasses in dry reducing or inert atmosphere should stay vitreous at high temperatures for quite some time, while stoichiometric glasses will devitrify rather rapidly independent of atmosphere if the nucleation of cristobalite on the surface of the glass takes place without significant hindrance. The rate of devitrification may be increased by the presence of H_2O in the ambient atmosphere and the presence of alkali impurities in the glass.

3. KINETICS OF REACTIONS BETWEEN SOLIDS

3.1. Direct reaction between solids

The aim of this work is to investigate the interaction between silica and carbon at elevated temperatures. A number of experiments with silica-carbon grain mixtures, have been performed under experimental conditions where the formation of SiC does not take place. This type of interaction may be characterized as gasification of the reactants. It is generally agreed upon that the net stoichiometry of this interaction is adequately described by the equation:

$$SiO_2 + C = SiO + CO \qquad (1.7)$$

Some of the experiments have been performed under conditions where the formation of SiC does take place, for which the net stoichiometry may be written:

$$SiO_2 + 3C = SiC + 2CO \qquad (1.12)$$

The temperatures in question are well below the melting point of any of the condensed phases (SiO_2, SiC and C). Thus equations (1.7) and (1.12), respectively, suggest that the reactions actually take place between solid phases, that is between $SiO_2(s)$ and $C(s)$.

Assuming a solid-solid type of reaction mechanism, the interaction in question would be entirely confined to the points of contact between the reactants. For reaction (1.12) the reactants will even be spatially separated as SiC is formed, leaving further reaction to the solid-state diffusion of either C or SiO_2 through SiC or counterdiffusion of both. The calculations carried out in Paragraph. 3.3.6. shows that diffusion of C in SiC is an extremely slow process.

The number of contact points between the reactants is low for the loosely packed, coarse grain mixtures of SiO_2 and C which are applied in this work, and thus the corresponding rates of a

solid/solid reaction would be imperceptibly low at the temperatures in question. However, as substantial rates are observed for the gasification reaction (1.7) as well as for reaction (1.12), the solid-solid mechanism is ruled out.

3.2. Reactions via the gas phase

In the absence of a liquid phase, a solid may react with a gas in three different ways as given below:

$$A(g) + bB(s) = \text{Gaseous products} \qquad (3.1)$$

$$= \text{Solid products} \qquad (3.2)$$

$$= \text{Gaseous and solid products} \qquad (3.3)$$

Reaction (3.1) may be characterized as a gasification reaction, and a representative example is the Boudouard reaction (1.4). This reaction has been the subject of intense research activity during the years (Paragraph 3.3.9). An adequate example of (3.2) type of reaction is the oxidation of metals which has been extensively studied. Comprehensive reviews are given by Rao and Gopalakrishnan (1986) and Fromhold and Fromhold (1984). Reaction (3.3) is frequently encountered in extractive metallurgy; representative examples are the roasting (oxidation) of sulfide ores to yield metal oxides, and the carbon reduction of iron ore to produce sponge iron.

In the presence of two solid reactants another important reaction sequence becomes possible, that is, reactions between solids proceeding through gaseous intermediates:

$$A(g) + bB(s) = cC(g) + eE(s) \qquad (3.4)$$

$$C(g) + dD(s) = aA(g) + fF(s) \qquad (3.5)$$
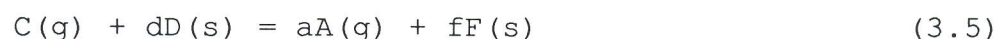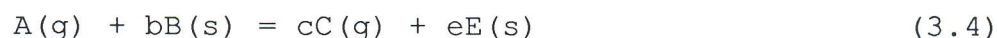
The requirement for a self-sustaining reaction is that there must be a net gas production, i.e. $ac > 1$. It is generally accepted

that the reduction of iron oxide takes place according to this reaction scheme:

$$FeO + CO = Fe + CO_2 \qquad\qquad (3.6)$$

$$CO_2 + C = 2CO \qquad\qquad (1.4)$$

Reaction (3.6) and (1.4) yields the total reaction

$$FeO + C = Fe + CO \qquad\qquad (3.7)$$

Rao (1971) has done extensive experiments on the "direct" reduction of hematite (Fe_2O_3) with carbon in the temperature range 850 - 1087°C at atmospheric pressure of Ar. The samples in question were hematite fines and carbon powders mixed together and contained in a cylindrical alumina crucible. The overall rate of reaction was found to be limited by the reaction between CO_2 and C, that is reaction (1.4) (Rao, 1974).

The literature on the kinetics of gaseous reduction of solids is voluminous (e.g. Szekely et al., 1971, 1976; Levenspiel, 1972; Koga and Harrison, 1984; Sohn and Wadsworth, 1979; Robertson and Sohn, 1986), but the examples given are all concerned with the more easily reducible oxides such as FeO, MnO, NiO, etc. The reduction of silica and other stable oxides is not mentioned in any of these texts. Motzfeldt (1988) considered reaction mechanisms for the carbothermal reduction of some refractory oxides (Al_2O_3, SiO_2, $3Al_2O_3 \cdot 2SiO_2$, MgO, BeO and ZrO). We will return to his views regarding silica in Chapt. 7.

3.3. Kinetics of reactions in the Si-C-O system. A survey of previous work.

As indicated in the introduction, the reaction between silica and carbon is poorly understood, and no valid model for the kinetics of this reaction has been established. Nevertheless, a substantial number of investigations have been carried out on various aspects of reactions in the system Si-O-C.

Rather than to review these investigations arranged according to chronology or authors, we have chosen to consider separately the various possible reaction systems or combination of reactants. The first one, SiO_2 + C, represents the system which is the central topic of the present work. The following eight systems are included in part because results from these may shed light upon the kinetics of the first one, in part also to provide the background for further studies in this area.

3.3.1. Reaction between SiO_2 and C

Poch and Dietzel (1962) investigated the behaviour of a mixture of silica (quartz sand, 10-20 μm) and carbon ("zuckerkohle", < 60 μm) at elevated temperatures in a stream of Ar and CO respectively (1 atm total pressure). They continuously recorded the weight change at constant temperatures in the range 1350 to 2200°C for charges with a total weight of 4 g pressed into a graphite crucible. The molar ratio between silica and carbon was 1/3.15. After each run the charge was quantitatively analyzed for SiO_2, Si and SiC.

The experiments conducted in CO showed no SiC formation at temperatures lower than 1530°C, and furthermore there was a large jump in the reaction rate (i.e. weight change per unit time) between 1450°C and 1530°C which was not observed in Ar. These observations are consistent with the equilibrium diagram in Fig.1.6 : The charge, being surrounded by ~1 bar CO, is most likely to follow the $P_{SiO}+P_{CO}=1bar$ line (one restriction) when heated. It is seen that the formation of SiC is not expected until 1514°C is obtained: The observed reaction rate is also expected to "make a jump" as the temperature is increased beyond 1514°C. This because the equilibrium pressure ($P_{SiO}+P_{CO}$) exceeds 1 bar at temperatures above 1514°C, and the transport of gaseous species (SiO, CO) out of the crucible is expected to take place at a faster rate.

Incipient formation of SiC in Ar was observed at 1350°C, that is, at lower temperature than in CO. The reaction rates in Ar were also considerably faster at temperatures below 1550°C compared to reaction rates in CO. Above 1550°C there was no

significant distinction between reaction rates in Ar and CO respectively.

The above observations may be interpreted in terms of the equilibrium diagram in Fig.1.6 : Assuming that a SiO_2/C-charge heated in inert atmosphere at first will proceed according to:

$$SiO_2 + C = SiO + CO \qquad\qquad (1.7)$$

with equimolar formation of SiO and CO ($P_{SiO}=P_{CO}$) The gas phase composition at first will move along the $P_{SiO}=P_{CO}$-line, but this is in the predominant stability field of SiC, and as soon as it is kinetically possible SiC will be formed. When SiC is present, the gas phase composition will move to the monovariant line and move along this line until interception with the $P_{SiO}+P_{CO}=1bar$ line at 1514°C.

Independent of atmosphere they observed another large jump in reaction rate between 1600 and 1700°C, this is, according to the authors, probably due to the reaction

$$2SiO_2 + SiC = 3SiO + CO \qquad\qquad (1.9)$$

becoming increasingly more dominant above 1600°C.

Klinger, Strauss and Komarek.(1966) investigated powder mixtures of silica (α-quartz, 105-149 μm) and carbon (graphite, <44μm) in the temperature range 1378 - 1765°C under vacuum conditions (< 0.1 torr). The weight ratio of silica to graphite was 0.555 ($n_C/n_{SiO_2}=9$) i.e. an approximate 50 to 1 particle ratio of graphite to silica. The charge was put into a graphite crucible and the rate of interaction between silica and graphite was determined by measuring the amount of CO evolved.

They found that the amount of CO evolved was a linear function of time in the temperature interval 1445 to 1610°C, but when the experiment proceeded beyond a certain time a substantial increase in rate took place and the rate continued to accelerate steadily. The duration before the abrupt increase in reaction rate; decreased with increasing temperature: 120 min at 1545°C and 7 min at 1610°C. At temperatures above 1610°C the accelerating reaction began almost immediately and no linear dependence was observed.

They found the reaction rate to be proportional to $t^{3/2}$ in the accelerating region. The apparent activation energy was calculated to be 117 kcal in the linear region and 122 kcal in the $t^{3/2}$-region. Solid residues of the runs carried out to completion, were subjected to XRD-examination, and SiC along with carbon was found.

Through effusion calculations the authors assume that the reaction proceeds by the thermal decomposition of silica; making this the rate determining step. They assumed the silica decompose viz. (cf. Fig. 1.3):

$$SiO_2 \rightarrow SiO(g) + O_2(g) + SiO_2(g) + O(g) \qquad (3.8)$$
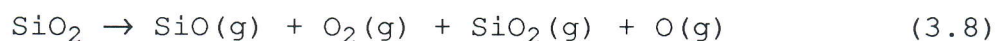
It is known that the transformation of quartz into cristobalite proceeds via a transitional noncrystalline phase (e.g. Chaclader and Roberts, 1961) and the authors postulate that the sudden increase in reaction rate is due to this transformation. That is, the transitional phase is the reactive one, speeding up the reaction as soon as it is formed.

Khalafalla and Haas (1972) made an isothermal thermogravimetric examination of an equimolar mixture of quartz and highly porous graphite particles (-70 +100 mesh) in the temperature region 1375 to 1515°C. The charge was placed in a Mo-crucible and the weight change was continuously recorded under vacuum conditions (10^{-6} torr) and at modest CO pressures (10^{-3} to 0.25 torr).

Significant reaction rates were observed at 1400°C in a vacuum, but presence of CO seriously retarded the reaction rate: A presence of 0.25 torr CO was found to inhibit the reaction. This was claimed to be due to the reaction proceeding via a gaseous intermediate of such a low pressure that the presence of even 10^{-3} torr of CO may suppress it.

The remainder of their results, experiments carried out in a vacuum, resemble the results of Klinger et al (1966). That is; a linear rate initially at low conversions is followed by an accelerating rate beyond a certain time. The duration of the linear part decreases with increasing temperature. Like Klinger et al. the authors assume that the transitional phase may be the active form of silica, and that probably the rate of carbothermal reduction of quartz is controlled by its rate of transformation

into the transitional phase. This is justified by the following observations: Arrhenius plots give an apparent activation energy of 77 kcal/mol which they claim is similar to the the apparent activation energy (72 kcal/mol) calculated by Roberts (1959) for the transformation of Madagascar quartz into the transitional phase. Furthermore, only small quantities of cristobalite were found in the discharge when graphite was present; indicating that the transitional phase, mainly, is consumed at a faster rate than it is transformed to cristobalite.

An important difference between the two investigations is that Khalafalla and Haas did not find any, or at most very little, SiC in the charge after a run. Hence they assume that the main reaction is adequately described by

$$SiO_2 + C = SiO + CO \qquad\qquad (1.7)$$

Klinger, on the other hand, found a mixture of SiC and graphite in the solid residues of the runs carried out to completion at 1590, 1640, 1670 and 1765°C.

Lee, Miller and Cutler (1977) proposed the following mechanism for the carbothermal reduction of silica:

$$SiO_2 + CO = SiO + CO_2 \qquad\qquad (3.9)$$

$$CO_2 + C = 2CO \qquad\qquad (1.4)$$

$$SiO + 2C = SiC + CO \qquad\qquad (1.8)$$
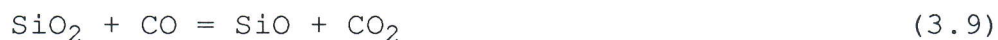
Reaction (3.9) and (1.4) resembles the classical reaction cyclus for carbothermal reduction of iron oxide. The total stoichiometry of the process is then (reaction (3.9) + (1.4) + (1.8)):

$$SiO_2 + 3C = SiC + 2CO \qquad\qquad (1.12)$$

The authors performed thermogravimetric experiments with silica/carbon-charges at 1500°C and investigated how the surface area of the reactants affected the rate and the degree of formation of SiC. They found increased rates by increasing the surface area of both reactants and conclude that the controlling steps are reaction (3.9) and (1.4). The presence of iron was

found to increase the overall reaction rate and it is concluded that this is due to the catalytic effect of iron on reaction (1.4). The effect of iron indicates, therefore, that reaction (1.4) is the rate determining reaction. When excess silica was present, SiO loss was observed . This was suggested to be due to the reaction:

$$2SiO_2 + SiC = 3SiO + CO \qquad\qquad (1.9)$$

Miller, Lee and Cutler (1979) conducted thermogravimetric experiments on intimately mixed silica/carbon-charges in the temperature region 1375 - 1530°C. The samples were prepared from cristobalite and carbon black and put into a graphite or Mo crucible. The crucible was continually exposed to a constant flow of Ar during a run.

While recording the weight change of a equimolar charge at 1450°C it was observed that at a certain fraction reacted, the reaction slowed down significantly. The fraction reacted at this "break point" coincided with all the carbon consumed according to:

$$SiO_2 + 3C = SiC + 2CO \qquad\qquad (1.12)$$

XRD-analysis of partly reacted samples confirmed that the SiC content increased to a maximum at "the break point". Beyond the break point there was a successive decrease in SiC.

It was concluded that when excess silica is present the reaction proceeds in two steps:

Initial: $SiO_2 + 3C = SiC + 2CO$ $\qquad\qquad$ (1.12)

Final $\qquad 2SiO_2 + SiC = 3SiO + CO$ $\qquad\qquad$ (1.9)
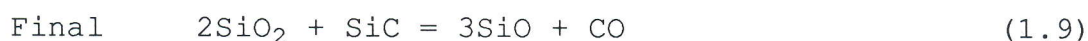
An apparent activation energy for the initial step was found to be 76 - 82 kcal/mol, whether iron was present or not. The activation energy of the final step was found to be 131 kcal/mol without addition of iron and 86 kcal/mol in the presence of iron.

Vodop´yanov et al. (1978) investigated the "non contact" interaction between silica and carbon in the following manner: Silica specimens (sintered silica, presumably cristobalite?) were placed between carbon tablets (graphite or charcoal). The

distance between the reactants (0.35-3.0 mm) was kept constant by spacers of tungsten (W). The experiments were carried out in an inert atmosphere in the temperature region 1250 - 1680°C. The degree of interaction was determined by the weight loss of the silica briquette in 30 min. Furthermore, silica and carbon were examined by XRD after each run.

The following reactions were assumed to take place during the "non-contact" interaction:

$$SiO_2 = SiO + \frac{1}{2} O_2 \qquad\qquad (1.1)$$

$$SiO + 2C = SiC + CO \qquad\qquad (1.8)$$

$$\frac{1}{2} O_2 + C = CO \qquad\qquad (3.10)$$

Hence, by determining the weight loss of silica the authors claimed to determine the rate of dissociation; reaction (1.1).

The results showed increasing dissociation rate with increasing temperature; except for a slight decrease in the temperature range 1530 - 1560°C. This slight decrease coincided with a decrease in the intensity of the 4.04 A diffraction line of α-cristobalite for the silica specimen. Thus the lowering of the rate of dissociation was explained by the formation of liquid non-stoichiometric silica which filled the pores in the specimen and thereby reduced its surface area. The rate of reaction was also shown to increase with decreasing distance between the reactants.

The authors concluded that the reduction of solid silica by carbon occurs by means of a non-contact reaction via the dissociation of silica. The possibility of a mechanism similar to that outlined by Lee et al (1977) was not considered, and may not even be likely in an inert atmosphere.

Finally, it was assumed that the dissociation pressure of SiO was 2-5 orders of magnitude higher than would be expected according to reaction (1.1). This was, quoting the authors, due to the formation of an oxygen deficiency in the initial oxide. That is, the silica may be considered as a solid solution of SiO(s) in SiO_2(s). This part of the explanation appears very dubious.

Bentsen, Jørgensen, Wiik and Motzfeldt (1985) conducted a thermogravimetric investigation on the behaviour of silica and

silica/carbon charges at 1570°C in the presence of CO. In line with Lee et al. (1977), the following reaction sequence was assumed:

$$SiO_2 + CO = SiO + CO_2 \qquad\qquad (3.9)$$

$$CO_2 + C = 2CO \qquad\qquad (1.4)$$

The curve for weight loss as function of time at constant CO pressure (1.5 atm) was taken to indicate that mass transfer due to gas phase diffusion was rate controlling. Furthermore, the rate of weight loss of silica and silica/carbon charges was found to decrease with increasing CO pressure in the pressure range 0.4 - 2 atm. At pressures below 0.5 atm the reaction rate was fairly constant, independent of CO pressure. The same sort of results were also obtained by Sigurjonsson (1986). These results will be further discussed in Chapt. 6.

Biernacki and Wotzak (1989) used finely divided silica and carbon, of particle size about 40 μm and 1 μm, respectively, intimately mixed in a 1:1 molar ratio. Charges were put in an alumina crucible of 0.25 cm^3 nominal volume, and heated at a specified rate in a commercial thermoanalyzer (that is, a thermobalance) connected to a mass spectrometer. The runs were performed at a pressure of about 0.01 bar of flowing argon, and the CO content in the off-gas was continuously monitored by means of the mass spectrometer. Combining this information with the initial weights and the weight loss, the authors were able to verify the stoichiometry of the various steps in the reaction:

$$SiO_2 + C = SiO + CO \qquad\qquad (1.7)$$

followed by $\qquad SiO + 2C = SiC + CO \qquad\qquad (1.8)$

and finally also $\quad 2SiO_2 + SiC = 3SiO + CO \qquad\qquad (1.19)$
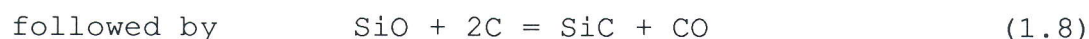
It appears, however, that Biernacki and Wotzak have used advanced equipment and elaborate calculations, only to establish what other people in this area have taken for granted during the last decades.

Blaha and Komarek (1989) made an isothermal thermogravimetric investigation of powder mixtures of silica (α-quartz and quartz glass fibres, < 56 μm) and carbon (graphite, 44 μm) in vacuum between 1395 and 1761°C. The molar ratios of silica to carbon was varied in the range 1:5 to 1:50. The silica/graphite charges were put into graphite crucibles closed with a triple lid consisting of three graphite disks with a 1 mm hole rotated 180° so that escaping gas would hit a solid C-surface before leaving the crucible system. With this arrangement the experimental weight losses agreed with the stoichiometry of reaction (1.12):

$$SiO_2 + 3C = SiC + 2CO \qquad\qquad (1.12)$$

The relative weight loss, Δw, for all of the experiments was found to obey the following relation:

$$-\ln(1-\Delta w) = kt$$

where k is a reaction rate constant and t is reaction time. The mean apparent activation energy was found to be 379 kJ. It was concluded that the interaction between silica and carbon followed a first-order rate law based on gaseous diffusion in porous pellets.

However, the order of reaction is usually expressed in terms of concentration of reactants, and the term should not be used for reactions between solids where there are no concentrations, only amounts of the reactants. The relation found by Blaha and Komarek may be easily deduced from the assumption that the rate of the reaction is proportional to the amount of reactant. (that is, silica) remaining in the charge. Let w designate the amount of silica relative to the amount at start. The above assumption may then be formulated

$$-\frac{dw}{dt} = k \ (1 - \Delta w)$$

On integration, the above relationship found experimentally is obtained.

However, the reason why the rate should be proportional to the remaining amount of silica remains unknown. The rate may equally well be expected to vary in proportion to the surface area

of the remaining silica, which would introduce $(1-\Delta w)^{2/3}$ rather than the first power. The question remains unsettled.

3.3.2. The behaviour of SiO_2 in the presence of reactive and inert gases.

Schwerdtfeger (1966) examined the behaviour of silica (silica balls manufactured from fused quartz glass, that is vitreous silica) at 1500°C in a stream of H_2, H_2/H_2O and CO/CO_2 mixtures respectively. He also investigated the effect of diluting H_2 with Ar and He. The total pressure was kept constant equal to 0.96 atm in all experiments. The reactions in question were:

$$SiO_2(s) + H_2(g) = SiO(g) + H_2O(g) \qquad (3.11)$$

$$SiO_2(s) + CO(g) = SiO(g) + CO_2(g) \qquad (3.9)$$
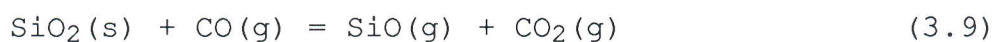
For H_2 containing gases he observed that the reaction rate increased with increasing mass transfer coefficient, indicating that mass transfer is rate controlling.

For CO/CO_2-mixtures the rate of silica consumption approached a constant value as the mass transfer coefficient increased, suggesting that the rate becomes controlled by a surface reaction. Furthermore, the rate was shown to be proportional to the CO/CO_2-ratio in the region of surface reaction control. Schwerdtfeger observed no devitrification of silica in H_2 containing gases whereas in CO/CO_2 mixtures the silica balls were always crystallized to cristobalite. Hence the silica source in reaction (3.11) is permanently vitreous and for reaction (3.9) the silica is continuously transforming to cristobalite. This may affect the kinetics.

Ozturk and Fruehan (1985) conducted experiments similar to those of Schwerdtfeger at a somewhat higher temperature; 1650°C. The rate of silica reduction in H_2 was found to be controlled by gas phase mass transport in accordance with Schwerdtfeger. Based on Schwerdtfeger's and their own results an activation energy of 75 kcal is calculated for reaction (3.11). Furthermore, experiments carried out in a stream of purified CO confirmed that the rate of reaction (3.9) was almost independent of the velocity

of the gas stream, hence the authors suggested that the rate of reaction (3.9) was controlled by chemical kinetics on the silica surface; which is consistent with the observations of Schwerdtfeger.

The silica was, however, poorly characterized; quoting the authors: "The silica spheres were made from commercially available fused quartz." That is, the silica was vitreous at the start of the run; but the silica specimens apparently were not subjected to XRD-analysis after a run. Hence, no information is given about the possible crystallization to cristobalite.

3.3.3. Reaction between C and SiO(g).

Poch and Dietzel (1962) exposed C ("zuckerkohle") to a stream of SiO-Ar at 1100, 1200, 1300,......., 1900°C. The SiO was generated by a mixture of SiO_2+Si, and Ar was used as a carrier gas, transporting the SiO through the carbon layer. The C was exposed to the same amount of SiO in every run.

The formation of a thin layer of cubic (ß) SiC was recognized at 1200°C, whereas at 1100°C no SiC was found. The fraction of C reacted increased with temperature, but even at 1600°C the product layer on each carbon particle was only a thin shell. Above 1700°C SiC could be found in pores inside the C particles. The main product was SiC, although some SiO_2 was found at temperatures up to 1600°C, and small amounts of Si at even higher temperatures.

The SiC formation was assumed to be due to the reaction:

$$SiO(g) + 2C = SiC + CO \qquad\qquad (1.8)$$
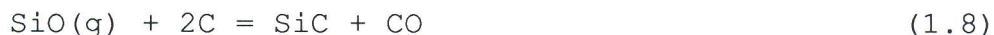
SiC was exposed to a CO-Ar atmosphere at 2000 and 2200°C and subsequent weight loss and formation of C was recognized; accordingly reaction (1.8) may be reversed.

Raaness and Tuset (1972) developed a method to determine the reactivity of carbon materials. The criterion of reactivity was based on the ability of the carbon to react with SiO and form SiC, according to reaction (1.8). The reactivity test was carried out by admitting a stream of Ar saturated with SiO-CO through a fixed bed of granulated carbon materials (coke, petrol coke, charcoal

etc...). The temperature of the carbon bed was 1650°C and the gas mixture was generated from a mixture of SiO_2 and SiC.

They did find a rather good correlation between SiO-reactivity and specific surface, volume weight, and CO_2-reactivity (CORMA) respectively. That is, a carbon material which is characterized by a large specific surface, a low volume weight and a large CO_2-reactivity, will generally show up with a large SiO-reactivity.

In the beginning of a run all SiO was found to be consumed, indicating that reaction (1.8) is fast. After some fraction reacted (depending on carbon quality) the reaction rate slowed down and calculations showed that the rate probably became controlled by interdiffusion of SiO and CO through the porous product layer and pores in the carbon material.

Kozhevnikov et al. (1972, 1973) conducted a thermogravimetric investigation of reaction (1.8) and found the reaction rate to be slow below 1680°C, but rapidly increasing above this temperature. Fraction carbon reacted was found to increase when metal oxides (SiO_2, Al_2O_3) were present in the carbon material.

Vodop´yanov et al (1983a/1983b) investigated reaction (1.8) in the temperature range 1850 – 2200°C. SiO and CO were generated by a mixture of SiO_2 and C which was placed inside a graphite crucible. Inside the upper part of the crucible were plates of carbon reducing agent tightly clamped to an annular protrusion with a graphite cover. Plates from carbon fibre, charcoal and oil coke were used as specimens for the investigation.

For carbon fibres it was shown that the thickness of the SiC layer increased proportional to $t^{0.5}$ after a certain time of reaction, obeying the parabolic law. According to the authors this is due to the diffusion of carbon through the product layer to the SiC/gas-phase-boundary being rate controlling. On the basis of experimental data the diffusivity of C through the product layer is calculated:

$$D[cm^2/s] = 2.099 \times 10^8 \exp\left(\frac{(-778.2 \pm 26.0 \text{ kJ})}{RT}\right) \quad (3.12)$$

valid in the temperature range 1900 – 2100°C.

A comparison of the diffusivity from this expression at, e.g., 2300K with that from Hong and Davis (1980) (cf. p. 59) shows that the value from Vodop´yanov et al. is just about a power of ten higher. This indicates that the diffusivity they observed must in part be due to surface and/or pore diffusion..

3.3.4. Reaction between SiO_2 and SiC

Poch and Dietzel (1962) investigated the reaction between SiO_2 and SiC in Ar atmosphere. The molar ratio between SiO_2 and SiC was 1:2.5 and the weight change of the charge was recorded continuously at constant temperatures in the range 1480 – 2000°C.

The reaction rate (rate of weight loss) was found to be rather slow at temperatures below 1550°C but increased rapidly with temperature above 1550°C. Below 1790°C the final weight loss agreed with the stoichiometry of the reaction:

$$2SiO_2 + SiC = 3SiO + CO \qquad\qquad (1.9)$$

Above 1790°C there was an additional weight loss of about 5%. This was probably due to the loss of Si-vapour formed according to the reaction:

$$SiO + SiC = 2Si + CO \qquad\qquad (1.10)$$

No reaction mechanism was, however, suggested. Reaction (1.9) is undoubtly not a reaction between to condensed phases; it is most likely to proceed via gaseous intermediates.

Pultz and Hertl (1966) studied the reaction between finely divided SiO_2 (74 μ) and SiC (0.1 μ) in the temperature range 1270 – 1610°C. The molar ratio between SiO_2 and SiC was 2 and the experiments were carried out in a vacuum. The effect of adding inert and reactive gases was also investigated. The amount of SiO_2 and SiC consumed after each run was determined by chemical analysis, and the reaction rate was determined in terms of the weight loss of silica.

Experiments conducted in CO atmosphere with a mixture of SiO_2 and tagged (C^{14}) SiC demonstrated that SiC was re-formed during a run: The specific activity of the remaining SiC was found to be

SiC was formed from the added CO. On the other hand, no "new" SiC was found to be formed during runs with SiC only in CO atmosphere at elevated temperatures. In this case SiC was found to lose weight, and deposits of carbon were found on the residual SiC particles, probably due to the reverse of reaction (1.8):

$$SiC + CO = SiO + 2C$$
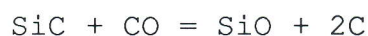
In conclusion the re-formation of SiC must proceed through some reaction with SiO_2.

Moreover, a vast number of experiments conducted under a variety of conditions showed one general trend: The molar ratio between reacted SiO_2 and SiC varied from <1 up to about 2; it increases with the degree of reaction. The ratio between SiO_2 and SiC reacted is expected to equal 2 if the overall stoichiometry of the interaction is adequately described by reaction (1.9).

The reaction scheme proposed by the authors looks as follows:

$$2SiC + SiO_2 = 3Si_{(ad)} + 2CO_{(ad)} \qquad (3.13)$$

$$2Si_{(ad)} + CO = SiO_{(ad)} + SiC \qquad (3.14)$$

$$Si_{(ad)} + SiO_2 = 2SiO_{(ad)} \qquad (3.15)$$

$$Si_{(ad)} = Si(g) \qquad (3.16)$$

$$SiO_{(ad)} = SiO(g) \qquad (3.17)$$

$$CO_{(ad)} = CO(g) \qquad (3.18)$$
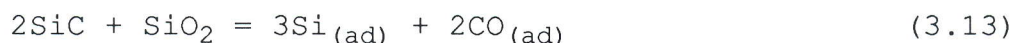
Subscript "(ad)" denotes adsorbed species. It is not clearly stated on which surfaces the adsorbtion takes place, presumably it is on the SiC surfaces. It was assumed that the initial few % of reaction takes place with a ratio SiO_2/SiC of 0.5, that is, reaction (3.13) followed only by reaction (3.16) (which is very unlikely at the temperatures in question). The remainder of the reaction was assumed to take place with a stoichiometry of 2, that is, reaction (3.13) followed by (3.14) and (3.15). Reaction (3.14) explains the re-formation of SiC.

The reaction rate was found to increase with decreasing particle size of SiC, but not as much as expected from the increased number of contacts between the reactants. Hence reaction (3.13) was ruled out as the rate determining step.

On the other hand, the fact that added CO depressed the reaction rate and, further, that the reaction rate was about twice as fast in a constantly evacuated system as in a closed system, led the authors to the conclusion that desorption of CO from the SiC surface was the rate determining step. An adsorption isotherm of the form

$$(1-\theta) = \left(1 - \frac{P_{CO}}{k + P_{CO}}\right) \qquad (3.19)$$

($(1 - \theta)$ = fraction of uncovered surface sites) is reasonably well fitted to experimental data at 1435°C.

The apparent activation energy of CO desorption from the active sites was found to vary from 131 - 97 kcal/mole in the temperature range 1270 - 1430°C.

It is somewhat puzzling that Pultz and Hertl propose an initial reaction between solid SiC and solid SiO₂, without.ever mentioning that this reaction between two solids is very unlikely. While the experimental observations may be worth considering, their reaction scheme, as reproduced above, probably has very little basis in reality.

Borisov (1967) investigated the behaviour of briquettes of SiO₂/SiC in a stream of Ar at elevated temperatures. The amount of SiC was varied in the interval 2 to 95 weight% . The reaction was run to completion during 40 min at 1800°C and during 5 min at 2000°C. Above 1800°C some Si was formed, and the amount increased with temperature. The silicon yield decreased with decreasing amount of SiC in the briquettes; probably due to the reaction:

$$Si(l) + SiO_2(s,l) = 2SiO(g) \qquad (1.11)$$
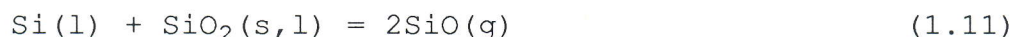
Below 1800°C the stoichiometry was

$$2SiO_2 + SiC = 3SiO + CO \qquad (1.9)$$

which, with increasing temperature above 1800°C, was gradually supplied with

$$SiO_2 + 2SiC = 3Si + 2CO \qquad (1.13)$$

On the basis of thermodynamic calculations Yudin et al (1968) expected the reaction in a vacuum to proceed according to equation (1.9) as above. Experiments carried out at 10^{-6} to 10^{-7} atm (1500 to 1650°C) with pressed mixtures of SiO_2 and SiC (molar ratio 2:1) showed that the initial ratio between SiO_2 and SiC did not change during a run; indicating that (1.9) is correct. The interaction is described as a diffusion of SiO_2 into SiC, and the apparent activation energy was reported to be 77 kcal/mol (1500 - 1650°C). Once again the proposed mechanism appears unlikely

A thermogravimetric investigation carried out by Tuset (1972) characterized the interaction between SiO_2 and SiC, below the melting point of silica, in the following manner:

1. Rate of weight loss is faster in the presence of Ar than in CO.

2. Rate of weight loss is rather insensitive towards the quartz quality.

3. Rate of weight loss increased by a factor of 10 when recrystallized SiC was exchanged with an equivalent volume of SiC formed from charcoal.

4. The molar ratio between consumed SiC and SiO_2 was found to be below 2 after a run. Depending on experimental conditions the ratio was found to be somewhere between 1 and 2, which is consistent with the findings of Pultz and Hertl (1966).

The following reaction mechanism was put forward:

$$SiC(s) + SiO(g) = 2Si(g) + CO \qquad (1.10)$$

$$2Si(g) + 2SiO_2(s,l) = 4SiO \qquad (1.11)$$

$$\overline{}$$

$$2SiO_2(s,l) + SiC(s) = 3SiO(g) + CO \qquad (1.9)$$
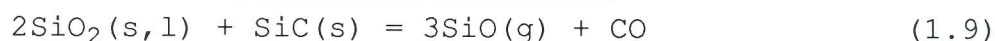
The vaporization of Si(g) was taken as the reason why the observed ratio between SiO_2 and SiC reacted is below 2. Above the melting

point of quartz a significant increase in reaction rate with time
was observed.

3.3.5. Reaction between $SiO_2(s,l)$ and $Si(l)$.

Ryabchikov et al. (1966 a, b) heated SiO_2, Si, and SiO_2 +Si,
respectively, in inert environments at 1 atm and observed the rate
of weight loss. Below 1850°C only vaporization of SiO_2 and Si was
observed, whereas above 1850°C there was a significant reaction
between SiO_2 and Si forming SiO(g) (According to JANAF (1985) the
equilibrium pressure of SiO(g) above SiO_2 + Si will exceed 1 atm
above 1860°C) The apparent activation energies was reported to
be 105 kcal/mole for the reaction between SiO_2 and Si, 75 and 200
kcal/mole for the vaporization of SiO_2 and Si respectively. The
authors find that Si is a less effective reducing agent for SiO_2
than C is and proposed the following reaction mechanism:

$$SiO_2(l) = SiO(g) + O(g) \qquad\qquad (1.1)+(1.2)$$

$$Si(l) + O(g) = SiO(g) \qquad\qquad (3.20)$$

They claimed that carbon would be more effective in binding O(g).

Hirata and Hoshikava (1980) observed the dissolution rate
(i.e. weight loss) of various silica glass qualities immerged into
a silicon melt in the temperature region 1450-1510°C. The
experiments were conducted in a Czochralski crystal growth
furnace; facilitating relative motion between silica samples and
silicon melt. The relative velocity between silica and melt was
varied in the region 0-9.4 cm/sec. The rate of dissolution was
found to increase significantly as the relative velocity between
the melt and silica specimen increased. On the other hand by
rising the temperature, only a slight increase in dissolution rate
was observed.

They conclude that the transportation of dissolved oxygen
atoms from the reaction interface (i.e. $SiO_2(s)/Si(l)$-interface)
to the melt is the rate determining step. The dissolution rate
was found to be rather insensitive to the silica quality.

3.3.6. Reaction between Si(s,l,g) and C

Poch and Dietzel (1962) investigated the reaction :

$$Si(s,l) + C(s) = SiC(s) \qquad\qquad (3.21)$$

at temperatures above and below the melting point of silicon. The formation of SiC was reported at temperatures down to 570°C with molten silicon alloys, while formation of SiC with pure silicon was reported at temperatures above 1150°C. Experiments carried out with carefully polished silicon- and carbon plates, which were tightly pressed together at 1380°C, indicated that C diffused through the SiC layer. The thickness of the SiC layer was found to increase proportionally to the square root of time ($t^{1/2}$), that is, obeying the parabolic law.

Above the melting point of silicon the rate of formation of SiC was significantly increased. This was, according to the authors, due to the presence of Si(l) which caused the SiC to exfoliate, thereby exposing unreacted carbon to the silicon.

Konijnenburg (1977) conducted similar experiments to those of Poch and Dietzel: A diffusion couple consisting of silicon and carbon (ash-free carbon refractory brick) was fired at 1300°C in pure Ar and in Ar with the addition of 200 ppm O_2, respectively. Microprobe analysis of the specimens after a run indicated that the SiC was formed by Si-vapour diffusing into the carbon specimen.

The addition of 200 ppm O_2 to the inert atmosphere speeded up the rate of SiC-formation significantly, probably due to the SiC-formation taking place via gaseous intermediates. The following reaction mechanism was suggested:

$$C + \frac{1}{2} O_2 = CO \qquad\qquad (3.10)$$

$$2Si + CO = SiC + SiO \qquad\qquad (3.22)$$

$$SiO + 2C = SiC + CO \qquad\qquad (1.8)$$
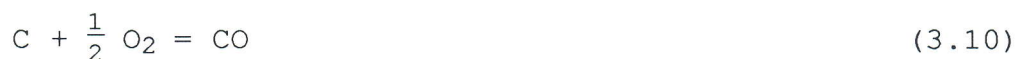
That is, once CO is formed (reaction (3.10)) it is consumed at the silicon (reaction (3.22)) but regenerated at the carbon (reaction (1.8)).

Minnear (1979) investigated the kinetics of the interaction between carbon and Si(l) by considering the morphologies of the resulting SiC reaction layer. The SiC formation was indeed affected by the carbon quality exposed to the silicon melt: Highly oriented pyrolytic graphite showed rapid conversion to SiC due to Si penetration parallel to the C planes and resulting in exfoliation of SiC. In this case it is suggested that the rate of reaction is controlled by surface wetting and capillary effects; i.e., the transport of Si(l) to unexposed regions of graphite.

On the other hand, reaction with glassy carbon (poorly graphitized and poorly aligned) formed rapidly a continuous polycrystalline SiC layer on the surface of the carbon (if the density of the carbon was greater than 0.96 g/cc). The SiC layer was essentially only one crystallite thick and further conversion took place at a slow rate. The rate of conversion was, however, found to increase significantly by imposing conditions which lead to convection currents in the melt. This is explained in the following manner: Agitation of the melt will lead to coarsening of the SiC crystallites and a given volume of large crystals will cover less surface area than small crystals, thus speeding up the rate. A mathematical model was established describing the conversion of C to SiC.

In a later work (Minnear, 1982) the reaction mechanism for the SiC formation on glassy carbon is further discussed. The conversion to SiC is claimed to take place by carbon diffusion at the SiC grain boundaries followed by reaction with Si(l) near the SiC/Si interface. Coarsening of the SiC crystallites in Si(l) causes the SiC grain boundaries to sweep across the carbon surface, thus uniformly reacting the carbon.

We may consider in more detail the possible formation of SiC by solid-state diffusion

Poch and Dietzel (1962) claimed that C is diffusing through the SiC layer and obeying the parabolic law. At 1380°C they found:

$$X = 8.9 \ t^{0.5} \qquad\qquad\qquad (3.23)$$

where X is the thickness of the SiC layer [μm] and t is the time of reaction [h].

Having a diffusion couple of Si(s) and C(s) (plane sheets, "infinite" in two dimensions) the thickness of the SiC layer formed, X, by carbon diffusing through the SiC, is given by Eq. (3.24) (the parabolic law).

$$X = \left(2 \ V_{SiC} \ D_{C-SiC} \left(\rho_2 - \rho_1 \right) \ t \right)^{0.5} \qquad (3.24)$$

where V_{SiC}=0.3155 cm^3/g is the specific volume of SiC, ρ_2 = 2.25 g/cm^3 is the density of carbon at the C/SiC interface (taken as the density of graphite), the density of carbon at the SiC/Si interface, ρ_1, is taken equal to zero and t is the time of reaction.

The diffusivity of C in SiC single crystal has been measured by Hong and Davis (1980):

$$D_C [cm^2/s] = (8.62 \pm 2.01) \times 10^5 \ exp\left(\frac{(-715 \pm 5 \ kJ)}{RT} \right) \qquad (3.25)$$

The measurements were conducted at 1850 to 2180°C, but assuming that Eq.3.25 is valid at lower temperatures, the diffusivity at 1380°C is calculated to be: D_{C-SiC} = 2.226x10^{-17} cm^2/s. Inserted into Eq.3.24 gives:

$$X = 3.4 \times 10^{-3} \ t^{0.5} \qquad\qquad\qquad (3.26)$$

where X is given in [μm] and t in [h]. Assuming 1380°C and a reaction time of t = 120 h, the expected thickness of the SiC layer according to Poch and Dietzel (Eq. 3.23) is 97.5 μm while Eq.3.26 gives 0.04 μm. That is, only an infinitesimal fraction of the SiC formed may be due to solid state diffusion of C through SiC. Thus the reaction rate for the formation of SiC observed by Poch and Dietzel is far too fast to be controlled by diffusion of C through SiC.

By taking the opposite view, that is, Si(s) diffusing through SiC, the reaction rate will be even slower than is the case with C diffusion, due to the diffusivity of C in SiC exceeding the diffusivity of Si in SiC by a factor of approximately 100 (Hong,

Davis and Newbury, 1981). Hence Si diffusion is definitely ruled out as the major contributor to the formation of SiC.

A more probable mechanism is Si(g) (evaporating from the Si(s) specimen) diffusing into the carbon, preferably through the grain boundaries of the SiC crystallites (cf. Konijnenburg, 1977).

3.3.7. Reaction between SiC and SiO(g).

Poch and Dietzel (1962) conducted experiments where SiC was exposed to a flowing mixture of SiO(g) and Ar(g). The investigation was carried out in the temperature range 1400 – 2050°C and in every run the SiC was exposed to the same amount of gas. The formation of Si was observed from 1500°C onwards due to the reaction :

$$SiO(g) + SiC = 2Si(l) + CO \qquad (1.10)$$

The amount of Si formed was found to increase with temperature: 0.01 % at 1500°C and 6 % at 2050°C. The reversion of reaction (1.10) was also demonstrated. Below 1550°C the reaction was found to proceed according to:

$$3Si(s,l) + 2CO = 2SiC + SiO_2 \qquad (3.27)$$

and above 1500°C:

$$2Si(l) + CO = SiC + SiO(g) \qquad (3.22)$$
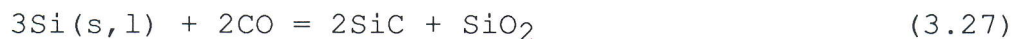
3.3.8. Reaction between SiO(g) and CO(g).

Poch and Dietzel (1962) brought together gas streams of CO(g) and Ar(g) +SiO(g) in a reaction chamber containing pieces of corundum at temperatures between 1300 and 1500°C. Thermodynamically the employed gas compositions should give the reaction

$$SiO(g) + CO(g) = SiO_2(s) + C(s) \qquad (3.28)$$

or else $\quad 3SiO(g) + CO(g) = 2SiO_2(s) + SiC(s)$ $\qquad$ (3.29)
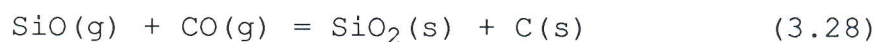
However, only SiO_2 and Si were found on the corundum pieces. formed by the simple dispropornation reaction

$$2SiO(g) = SiO_2(s) + Si(s) \qquad (3.30)$$

However, in the cold parts of the furnace a condensate composed by SiO_2, Si and SiC was found, which could be due to reaction (3.28) and (3.29), or else the reaction

$$3Si(s) + 2CO(g) = 2SiC(s) + SiO_2(s) \qquad (3.27)$$

Schei and Sandberg (1966) conducted experiments with a SiO_2/C-charge in a 40kW single-phase submerged-arc electric furnace. Large quantities of a brown condensate, situated above the electrode crater, were found in-between the pieces of original charge components. Examination of the condensate showed only the occurrence of SiO_2 and Si, hence the authors concluded that the dominating back reaction is reaction (3.28). Similar condensates containing Si are also found in the upper part of the charge when digging out industrial furnaces.

3.3.9. Kinetics of the Boudouard reaction

The thermodynamics and kinetics of the Boudouard reaction

$$CO_2(g) + C(s) = 2 CO(g) \qquad (1.4)$$

have been investigated by a large number of scientists during this century. Comprehensive reviews on the subject are given by Walker et al. (1959), Fredersdorff and Elliot (1963), Ergun and Mentser (1965) and Essenhigh (1981). Moreover, Rao and Jalan (1972) discuss several mechanistic schemes representing the most prominent opinions during the years. Since the early work of Gadsby et al. (1946) and Long and Sykes (1948) the rate of the Boudouard reaction has often been expressed by a Langmuir-type equation:

$$\frac{dn_C}{dt} = \frac{k_I P_{CO_2}}{1 + k_{II} P_{CO} + k_{III} P_{CO_2}} \qquad (3.31)$$

Here, dn_C/dt is the rate of carbon gasification and the k's are related to specific rate constants.

Eq. 3.31 may be deduced from the following two-stage mechanistic scheme, first proposed by Reif (1952) and later reformulated by Ergun (1956). It involves initially the detachment of an oxygen atom from a gaseous CO_2-molecule, viz.:

$$CO_2 + C_f \underset{k'_1}{\overset{k_1}{\rightleftharpoons}} CO + C_O \qquad (3.32)$$

followed by transfer of carbon to the gas phase, that is, formation of carbon monoxide:

$$C_O \overset{k_2}{\rightarrow} CO + nC_f \qquad (3.33)$$

C_O and C_f refer to active centres or reaction sites that are occupied by oxygen or free of oxygen respectively. (3.32) is often referred to as "the oxygen exchange reaction" while (3.33) is termed "the gasification reaction". The value of the integer n in reaction (3.33) is taken as unity if there is no increase or decrease in the number of reaction sites accompanying gasification (Ergun and Mentser, 1965). The rate constants k_1, k'_1 and k_2 are functions of temperature only and are common to all carbons having trigonal (coplanar) bonds, regardless of origin, particle size, porosity and crystallinity (Ergun, 1956). The above mechanism is supported by many scientists.

The oxygen exchange reaction (3.32) is reversible with rate constants k_1 and k'_1 of the same order of magnitude and the activation energy of the forward reaction was found to be 53 kcal/mol while the reverse was 36 kcal/mol (Ergun, 1967). The larger activation energy for the forward reaction indicates that the process of attachment of oxygen from CO_2 to a surface carbon atom is energetically more difficult than its removal by CO.

Equilibrium data of reaction (3.32) are reported by Ergun (1956) in the temperature interval 700 - 1400°C.

The gasification reaction (3.33) is assumed to be the slowest step, hence the rate of carbon gasification is determined by the rate of reaction (3.33). Ergun (1967), on the basis of C^{14} - tracer experiments, claimed that there was no carbon transfer from gas to solid at "gasification temperatures", thus reaction (3.33) was regarded as unidirectional[*]. The activation energy of reaction (3.33) was measured by Ergun (1956) for three different carbons and was found to be 59 kcal/mol. Because the oxygen exchange reaction is much faster than the gasification reaction in the temperature region 750 - 850°C and the difference in activation energy between the forward reaction (3.32) and the gasification reaction (3.33) is small, Ergun (1967) points out that it is unlikely that the oxygen exchange reaction would become the rate controlling process for the CO_2 - C reaction at high temperatures.

The detachment of oxygen, according to reaction (3.32), is supposed to take place at active sites at the carbon surface. Furthermore, the fraction of the total surface containing active centres is assumed to be constant at a given temperature. That is, expressed in concentration units, with active sites denoted C_t:

$$C_{C_t} = C_{C_o} + C_{C_f} = \text{constant} \tag{3.34}$$

C_{C_t} is expected to decrease with increasing temperature due to surface migration of carbon atoms to more stable positions in the lattice (annealing). However, the temperature question has to be relatively high in order to produce thermal annealing effects, that is, at a moderate temperatures the C_{C_t} is essentially constant.

As reaction (3.33) is the slowest reaction, the rate of gasification of carbon is accordingly given by:

$$-\frac{dn_C}{dt} = k_2 \, C_{C_o} \tag{3.35}$$

---

[*] The unidirectionality of reaction (3.33) was claimed already by Ergun in 1956 with reference to a C^{14} -tracer study conducted by Bonner and Turkevich (1951). However, from my point of view, the data of Bonner and Turkevich seem to have been incorrectly interpreted, as they did find some active carbon on the carbon surface; indicating that some carbon transfer from gas phase to solid had taken place.

64

Under steady state conditions the net rate of formation of occupied sites must be zero:

$$\frac{dC_{C_O}}{dt} = k_1 \, P_{CO_2} \, C_{C_f} - k_1{}' P_{CO} \, C_{C_O} - k_2 \, C_{C_O} = 0 \qquad (3.36)$$

Combination of Eq.3.34, Eq.3.35 and Eq.3.36 yields:

$$-\frac{dn_C}{dt} = \frac{k_1 \, k_2 \, C_{C_t} \, P_{CO_2}}{k_1 \, P_{CO_2} + k_1{}' P_{CO} + k_2} \qquad (3.37)$$

The similarities between Eq.3.37 and the empirical rate Eq.3.31 is obvious. When reaction (3.33) is rate determining it is reasonable to assume that $k_1 \, P_{CO_2} > k_2$ and $k_1{}' P_{CO} > k_2$, furthermore, by introducing the equilibrium constant for reaction (3.32), $K_1 = k_1/k_1{}'$, Eq.3.37 is transformed into the simplified equation:

$$-\frac{dn_C}{dt} = \frac{K_1 \, k_2 \, C_{C_t}}{K_1 + P_{CO}/P_{CO_2}} \qquad (3.38)$$

K_1 and k_2 are independent of the type of carbon and functions of temperature only, whereas C_{C_t} depends strongly on the type of carbon.

Ergun (1956) reports numerical values for $k_2 \, C_{C_t}$ for three different carbon qualities as well as values for K_1 which give the opportunity to calculate the expected rate of gasification at a given P_{CO}/P_{CO_2} ratio if the applied carbon quality is one of those reported in the work of Ergun (1956).

Turkdogan and Vinters (1970) have been concerned about the effect of CO on the rate of the Boudouard reaction, hence they conducted a vast number of experiments with P_{CO}/P_{CO_2} ratios ranging from 0 to 10 for three different carbon qualities in the temperature range 700 - 1400°C. The retarding effect of CO on the Boudouard reaction is well known, and Ergun (1967) explains this in terms of reaction (3.32). That is, increasing CO-pressure decreases the equilibrium ratio of occupied sites to free sites, C_{C_O}/C_{C_f}, which in turn decreases the rate of gasification according to Eq.3.35.

Turkdogan and Vinters (1970) were not able to interpret their results in terms of a Langmuir-type relation and as a consequence they proposed a reaction scheme in which the oxygen exchange reaction is radically different from reaction (3.32). The first

step (oxygen exchange) is supposed to take place by CO_2 dissociating on the carbon surface:

$$CO_2(g) = CO_2(ad) = (CO_2)^{\#} \rightarrow C(gr) + 2 O(ad) \qquad (3.39)$$

followed by carbon gasification by formation of CO:

$$C + O(ad) = (CO)^{\#} \rightarrow CO(ad) = CO(g) \qquad (3.40)$$
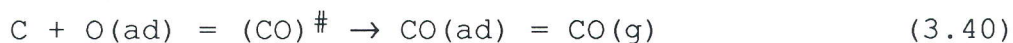
The superscript $^{\#}$ denotes activated complex. Reaction (3.39) predicts carbon transfer from gas phase to the solid phase, which, as previously pointed out, was claimed not to take place according to Mentser and Ergun (1967). However, Bonner and Turkevich (1951) did find some exchange.

Turkdogan and Vinters found that the rate of carbon gasification was proportional to P_{CO_2} at high CO contents (>10 %) and concluded that reaction (3.39) was rate determining when "sufficient" CO was present. At low CO contents the rate was found proportional to $(P_{CO_2})^{0.5}$ and they concluded that reaction (3.40) was rate determining when the CO content of the gas was "sufficiently low".

By the introduction of a rate parameter, Φ_1, and an activity coefficient ϕ_{CO}, the following rate equation was developed for the case with high CO content in the gas phase:

$$R_t = -\frac{1}{w}\left(\frac{dw}{dt}\right) = \frac{\Phi_1 \ (P_{CO_2} - P_{CO_2,e})}{1 + \dfrac{P_{CO}}{\phi_{CO}}} \qquad (3.41)$$

where R_t is the rate of oxidation per unit mass of carbon and $P_{CO_2,e}$ is the equilibrium pressure according to reaction (1.4) for a given temperature and P_{CO}/P_{CO_2} ratio, w is the weight of C at time t. The temperature dependence of the Φ_1 and ϕ_{CO} parameters was reported for three different carbon qualities and is given here for National grade AUC-graphite:

$$\log \Phi_1 = -\frac{13200}{T} + 7.68 \qquad (1000-1200°C) \qquad (3.42)$$

$$\log \phi_{CO} = -\frac{5940}{T} + 3.46 \qquad (800-1200°C) \qquad (3.43)$$

where Φ_1 is given in [min^{-1} atm^{-1}], ϕ_{CO} in [atm] and T in [K].

The mechanism represented by reaction (3.39) and (3.40) was considered by Rao (1972) to be of doubtful value , especially the $(P_{CO_2})^{0.5}$ rate proportionality at low CO contents was suggested to result from incomplete pore diffusion rather than chemical control by reaction (3.40).

3.4. Conclusive remarks on the survey of previous works.

Although a large number of investigations have been carried out, it still appears that there is a lack of fundamental understanding on the kinetics of reactions in the system Si-O-C. The present work is restricted to studies of the primary reaction or reactions between silica and carbon. Somewhat unfortunately, it appears that none of the previous experimental studies of the interaction between these two reactants were conducted in such a way as to clarify the mechanism of the interaction

Lee et al. (1977) suggested that the reaction between silica and carbon takes place in two steps:

$$SiO_2 + CO = SiO + CO_2 \qquad\qquad (3.9)$$

$$CO_2 + C = 2CO \qquad\qquad (1.4)$$

These authors, however, offered only very meagre evidence in support of the suggested mechanism.

Both Schwerdtfeger (1966) and Ozturk and Fruehan (1985) studied the first of these, reaction (3.9), as a reaction between samples of silica and a flowing gas phase. They concluded that reaction (3.9) in a flowing gas was controlled by reaction at the silica surface (chemical reaction control), but none of them extended their studies to the simultaneous presence of carbon.

The Boudouard reaction, Eq. (1.4), has been described with two quite different mechanisms by Ergun (1956, 1965 and 1967) and by Turkdogan and Vinters (1970), respectively. The temperatures considered, however, are in the range of about 700 to 1400°C; and it is doubtful whether the kinetic data obtained in this range may

be applied at the temperatures of around 1560°C encountered in the present work. For this reason no attempt is made in the course of the present work to treat the Boudouard reaction quantitatively.

In the above, the formation of silicon carbide has not been taken into account. When the SiO pressure is high enough, silicon carbide is formed by reaction on the carbon surface:

$$SiO + 2C = SiC + CO \qquad (1.8)$$

Although the study of this reaction has not been a central topic, some of the experiments in the present work have been performed under conditions where silicon carbide was formed. The quality of the carbon material is probably an important parameter with respect to the rate of silicon carbide formation. Raaness and Tuset (1972) examined reaction (1.8) for a number of commercially available carbons, and their results indicated that reaction (1.8) generally is fast. Vodop´yanov et al., on the other hand, found reaction (1.8) to be rather slow when the carbon quality in question was carbon fibres. More quantitative kinetic studies considering nucleation and growth seem to be missing.

Two different reaction mechanisms for the reaction between silica and silicon carbide

$$2SiO_2 + SiC = 3SiO + CO \qquad (1.9)$$

are being put forward by Pultz and Hertl (1966) and Tuset (1972), respectively. However, a third possibility is suggested in Sect. 3.6.

3.5. Proposed mechanism for the reaction between SiO$_2$ and C

At elevated temperatures silica is known to undergo decomposition according to reaction (1.1):

$$SiO_2 = SiO + \frac{1}{2} O_2 \qquad (1.1)$$

In the presence of CO, the most likely reaction to take place is reaction (3.9)(Schwerdtfeger, 1966; Lee et al., 1977 and Ozturk & Fruehan, 1985):

68
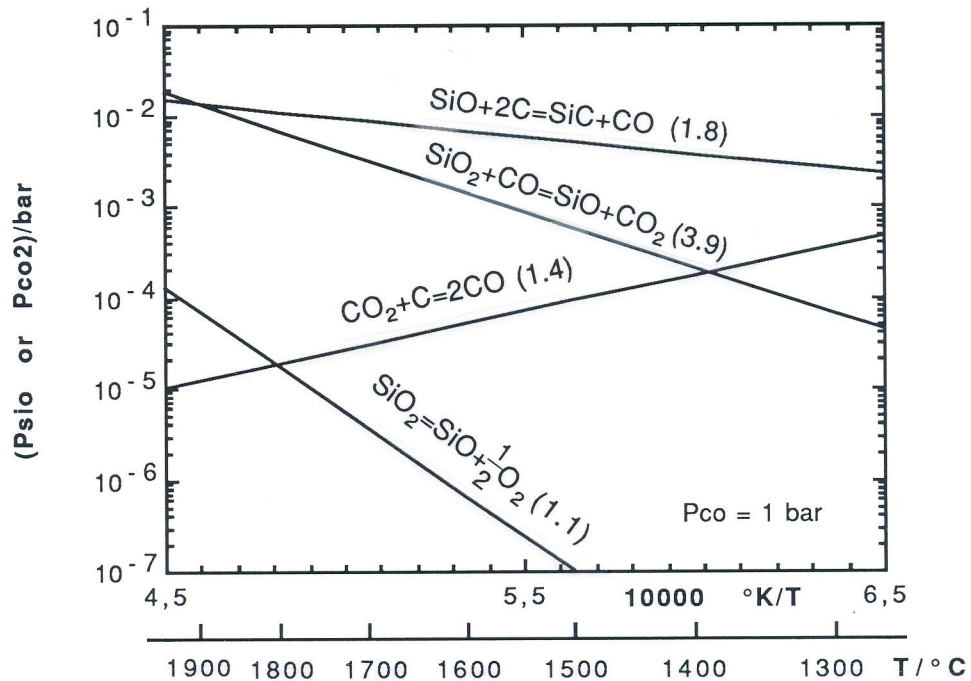
Fig. 3.1. Equilibrium pressures of SiO and/or CO_2 for some relevant reactions in the system Si-O-C. Reactions (1.4), (1.8) and (3.9) are calculated at 1 bar CO, reaction (3.9) with the additional restriction $P_{SiO}=P_{CO_2}$. For reaction (1.1) $P_{SiO}=2P_{O_2}$ (data from JANAF, 1985).

$$SiO_2 + CO = SiO + CO_2 \qquad\qquad (3.9)$$

From Fig. 3.1 it is seen that the SiO pressure resulting from decomposition (1.1) is substantially lower than the pressure resulting from reaction (3.9) (at 1 bar CO) over the entire temperature range given.

As is reported in Sect. 5.2 (Fig. 5.5), a pronounced increase in the rate of weight loss of the silica specimen is observed when the furnace conditions are altered from a vacuum to the presence of CO, indicating that the reaction in question is changed from decomposition (1.1) to reaction (3.9). Thus it is believed that, in the presence of CO, the prevailing reaction is adequately described by (3.9).

Some of the relevant reactions are given in Fig. 3.2 in dependence of CO pressure at 1558°C. The temperature is chosen in accordance with the "final experiments" presented in Chapt. 6. In the presence of both SiO_2 and C it is seen that the CO_2 pressure

resulting from reaction (3.9) is lowered by immediate contact with C, according to the Boudouard reaction (1.4).

Fig. 3.2. Equilibrium pressures of SiO and/or CO_2 for some relevant reactions in the system Si-O-C at 1558°C. For reaction (3.9) $P_{SiO}=P_{CO_2}$ and for reaction (1.1) $P_{SiO}=P_{O_2}$ (data from JANAF, 1985).

Hence, it is believed that the reaction between silica and carbon in the presence of CO is adequately described by the following reaction sequence:

$$SiO_2 + CO = SiO + CO_2 \tag{3.9}$$

$$CO_2 + C = 2CO \tag{1.4}$$

A mixture of silica and carbon heated in an inert atmosphere may react according to the following scheme:

$$SiO_2 = SiO + \tfrac{1}{2}O_2 \tag{1.1}$$

$$\tfrac{1}{2}O_2 + C = CO \tag{3.10}$$

$$CO + SiO_2 = SiO + CO_2 \tag{3.9}$$

$$CO_2 + C = 2CO \qquad\qquad (1.4)$$

That is, the decomposition of silica (1.1) releases oxygen which reacts with C (3.10) and forms CO. The CO will next react with silica (3.9) and the resulting CO_2 will in turn react with carbon (1.4) and produce CO. It is seen that reaction (3.9) plus reaction (1.4) have an avalanche potential in terms of generating CO: One CO_2 molecule formed (3.9) produce two molecules of CO (1.4). Two CO molecules generates two molecules of CO_2 (3.9). The two molecules of CO_2 will then generate four molecules of CO and so on....., thus building up the partial pressure of CO. Successively increasing rates in terms of time have been observed for silica/carbon-mixtures in Ar atmosphere (run 18C), thus indicating that the CO generating sequence takes place. Hence, the prevailing reactions taking place in silica/carbon-mixtures are assumed to be (3.9) and (1.4) both in CO and in inert atmosphere (apart from the eventual formation of SiC, cf. below).

If there is equilibrium between the two condensed phases (silica and carbon) at a given temperature and CO pressure, the total reaction is adequately described by Eq.s. (3.9) + (1.4), viz.:

$$SiO_2 + C = SiO + CO \qquad\qquad (1.7)$$

That is, at a given temperature and CO pressure (i.e. two restrictions) the system is invariant, and the composition (and total pressure) of the gas phase are uniquely given (Fig. 3.2). The above reaction sequence is in agreement with the reaction mechanism proposed by Lee et al (1977) and by Motzfeldt (1985, 1988).

However, if there exist equilibrium between silica and carbon, reaction (1.11) (Fig. 3.2) predicts formation of SiC at CO pressures below ≈ 1.5 bar, corresponding to reaction (1.8) taking place:

$$SiO + 2C = SiC + CO \qquad\qquad (1.8)$$

Carbon is thus consumed corresponding to reaction (1.4) and (1.8) taking place simultaneously. From an equilibrium point of view the coexistence of three condensed phases (SiO_2, SiC and C) is a univariant equilibrium, and fixing the temperature yields a

nonvariant equilibrium, that is, the gas phase composition is uniquely given by the point of interception between the lines representing reaction (1.7) and (1.8), respectively (Fig. 3.2). The total reaction may be expressed as:

$$SiO_2 + 3C = SiC + 2CO \qquad (1.12)$$

If the carbon source , for some reason, is unable to lower the CO_2 pressure in accordance with the Boudouard reaction (1.4), the resulting SiO pressure will be lower than predicted by reaction (1.8). Hence, the formation of SiC will be expected to take place only at a somewhat lower CO pressure than predicted in Fig. 3.2. This will be further considered in Chap. 7.

3.6. Proposed mechanism for the reaction between SiO_2 and SiC

The present work does not include experiments where the only condensed phases present are silica and silicon carbide, nevertheless a possible reaction cyclus, based on equilibrium considerations, is included:

Assuming that the total reaction in question is (1.12) when SiO_2, SiC and C are present; how do the system respond when all of the C is consumed? It is generally believed (Chap. 3.3.4) that the total reaction in this case is

$$2SiO_2 + SiC = 3SiO + CO \qquad (1.9)$$

However, as previously indicated, solid/solid interaction is not likely to occur at perceptible rates. Thus the existence of a gas phase mechanism is indicated. By analogy with the previously proposed mechanism for the interaction between SiO_2 and C; the following reaction sequence may describe the reaction between SiO_2 and SiC in the presence of CO:

$$SiO_2 + CO = SiO + CO_2 \qquad (3.9)$$

$$2CO_2 + SiC = SiO + 3CO \qquad (3.44)$$

72

The sum of reaction (3.9) and (3.44) yields reaction (1.9). The reactions in question are given in terms of CO pressure at 1527°C in Fig. 3.3.
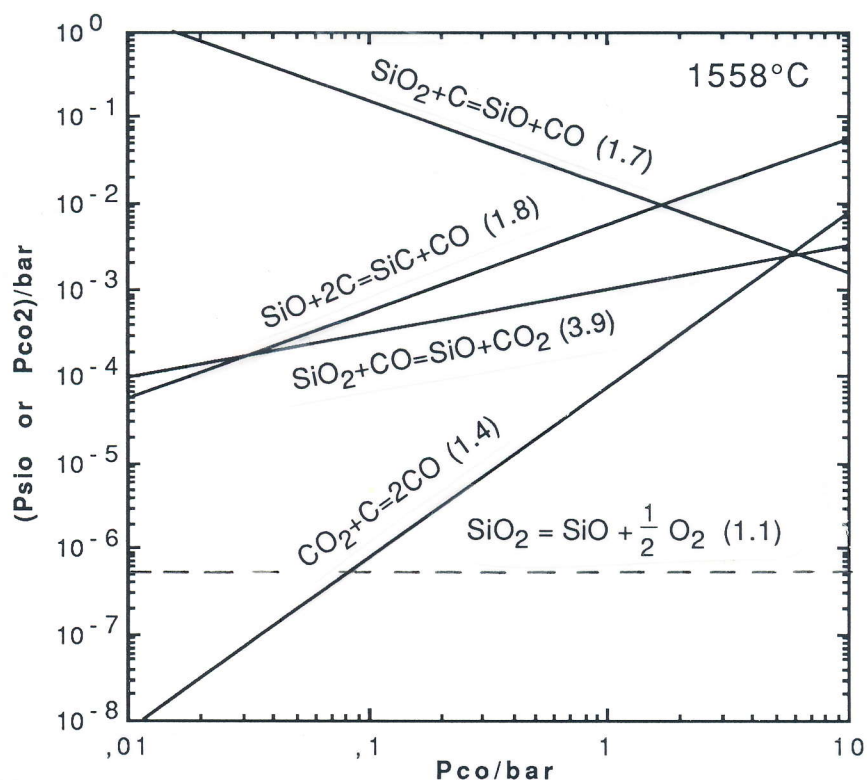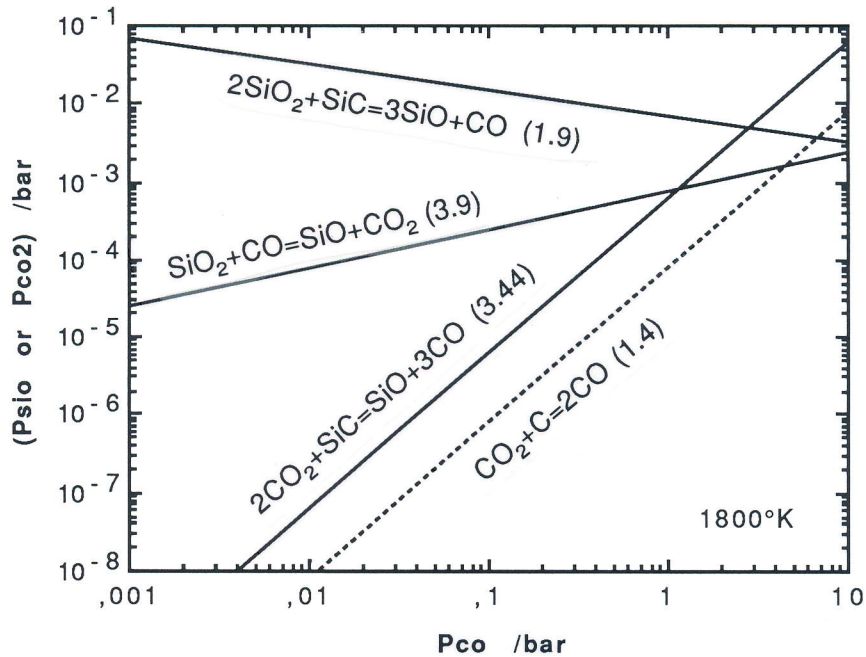

Fig. 3.3. Equilibrium pressures of SiO and/or CO_2 for some relevant reactions in the system Si–O–C at 1527°C. For reaction (3.9) $P_{SiO}=P_{CO_2}$ and for reaction (3.44) $P_{CO}=3P_{SiO}$ (data from JANAF, 1985).

With the restrictions given for reaction (3.9) and (3.44) it is seen that SiC defines a lower CO_2 pressure than reaction (3.9) at CO pressures below ~1.2 bar. Thus, in the absence of C, SiC may take over the role of C and react with CO_2 to form SiO and CO (3.44). At equilibrium between SiO_2, SiC and a gas phase, the gas composition is given by reaction (1.9) (Fig. 3.3). The Boudouard reaction (1.4) is included in Fig. 3.3 (dotted line) and is seen to define a CO_2 pressure roughly a factor of ten lower than reaction (3.44) throughout the CO pressure range. This, indicates that SiC is not consumed by CO_2 in the presence of C.

4. EXPERIMENTAL METHOD AND EQUIPMENT

4.1. Choice of method

The type of reactions encountered in the present investigation may roughly be divided into three categories:

$$B(s) = \text{Gaseous products} \qquad (4.1)$$

$$A(g) + bB(s) = \text{Gaseous products} \qquad (3.1)$$

$$A(g) + bB(s) = \text{Gaseous and solid products} \qquad (3.3)$$

All the reactions in question produce gaseous species and, except from the vaporization reaction (4.1), the consumption of gaseous species also takes place. Accordingly, a kinetic study may be performed either by means of a flow system with analysis of the exit gas or by means of a thermobalance continuously monitoring the weight change of the system. Thermogravimetry has been preferred in this work due to its simplicity. However, since the only information obtained by this method is the weight change of a given sample, the method invites to a substantial portion of "educated guesses".

A study of the kinetics of interaction of silica and silica/carbon mixtures, respectively, in the presence of CO, has to take into account a considerable number of variables. Some of the variables are readily controlled by the experimentalist, while others are not:

Variables affecting the kinetics are:

The reactants $SiO_2(s)$, $C(s)$ and $CO(g)$

    * Impurity composition and impurity level

    * Crystal structure of the solid reactants SiO_2 and C.

* Porosity of SiO_2 and of C.

* Grain size of SiO_2 and of C.

* Ratio of SiO_2 to C in the charge

* Absolute pressure and molar fraction (when diluted with inert gas) of CO in the bulk gas.

Sample container (crucible).

* Choice of material.

* Size and place of openings for gas exit.

The vacuum thermobalance "Versatilie", which was used throughout the experimental part of the present investigation, is shown in Figs. 4.1-2. It was designed by Motzfeldt about 25 years ago, and it has been used and described by a number of dr. ing.-students including Blegen (1976) and Sandberg (1981). In its present form it consists essentially of a graphite-tube furnace, a vacuum system including gas pressure gauges, an optical pyrometer for temperature measurement and control, an electronic weighing system, and equipment for gas mixing and gas inlet. In the following, each of these parts will be described in some detail.

4.2. The graphite-tube furnace

The furnace is a "cold wall" type, i.e. the heating element is placed inside a water cooled furnace chamber. On top of the furnace chamber is a rotatable flange carrying three silica windows, which, in combination with a total reflecting prism, permits application of optical pyrometry for temperature reading and control.

The heating element is a graphite tube, and Figs. 4.3-4 show design, dimensions and temperature distribution of two different elements applied during the experimental period.
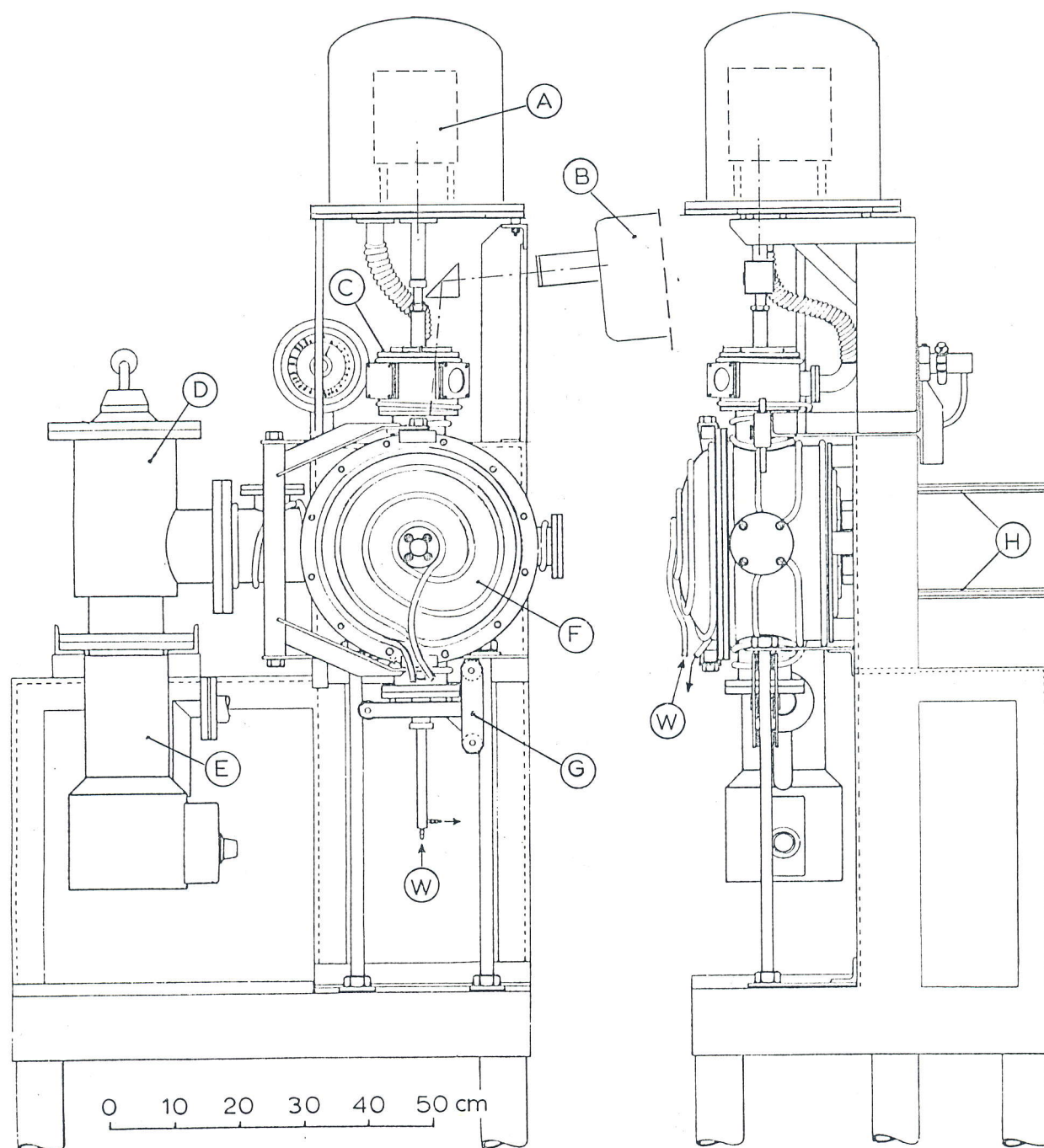
Fig. 4.1. The vacuum thermobalance "Versatilie". A: Weighing cell in bell jar. B: Automatic optical pyrometer. C: Revolving flange with three silica glass windows. D: High-vacuum valve. E: Oil diffusion pump. F: Front door of furnace enclosure. G: Carriage for bottom flange. H: Copper rails for heater current. W: Cooling water.

76
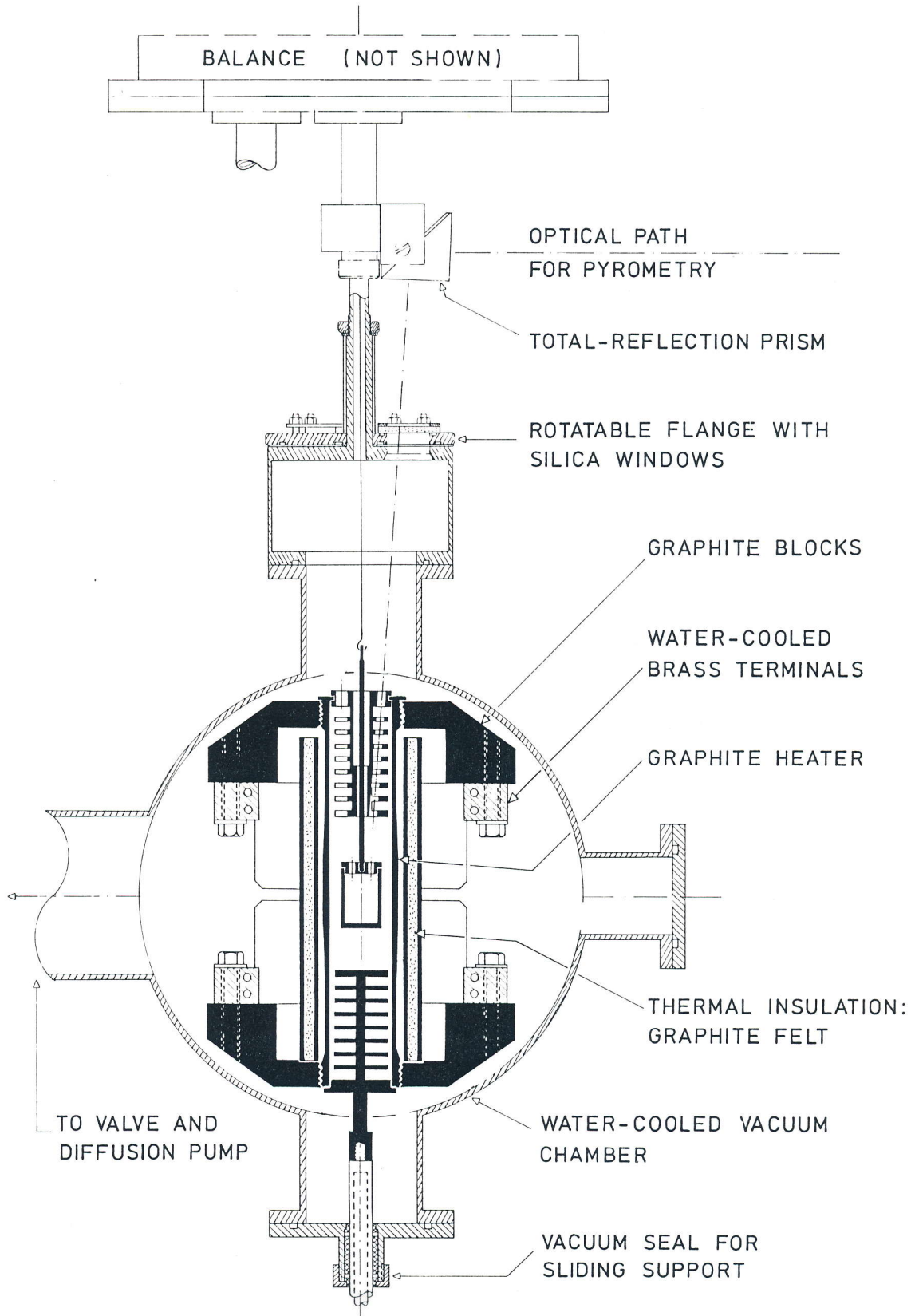
Fig. 4.2. Front view of furnace part of vacuum thermobalance "Versatilie" (access to furnace through hinged front door, not shown).
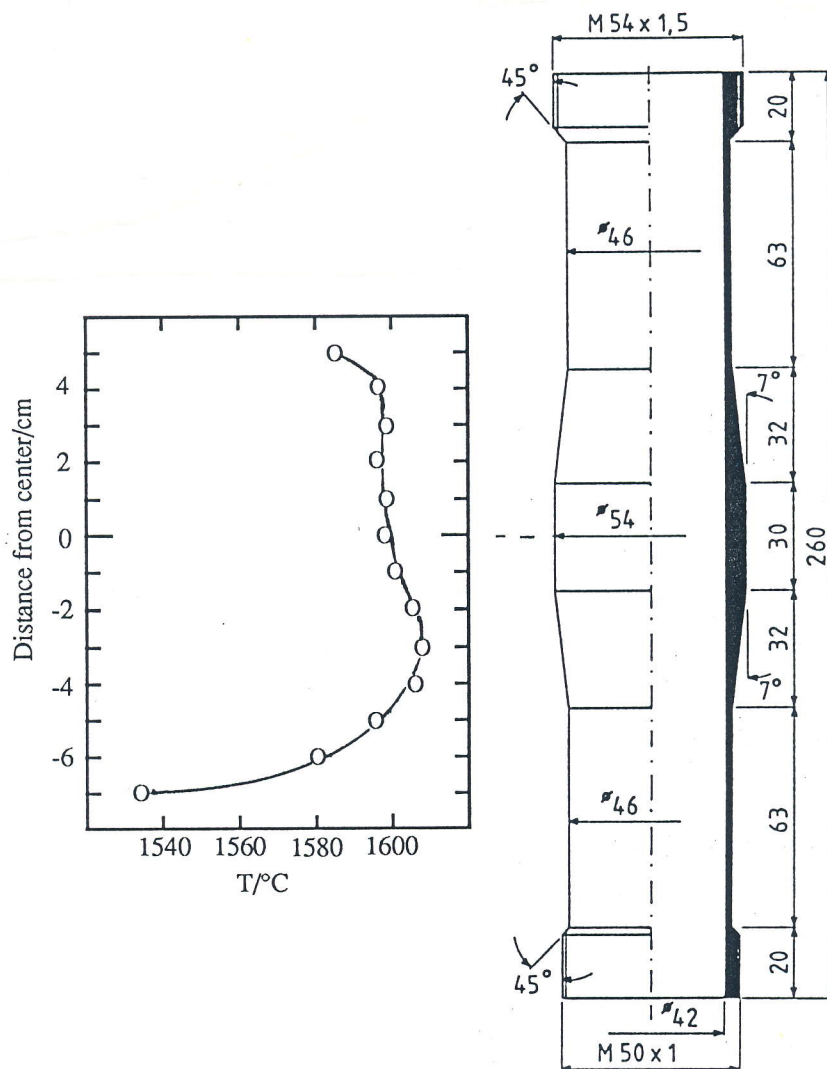
Fig. 4.3. Graphite-tube heating element including the observed temperature distribution measured at vacuum conditions without horizontal radiation shields. Graphite-felt isolation as indicated in Fig. 4.4. (The element was applied in run no. 1-20).

Fig. 4.4. Graphite-tube heating element including the observed temperature distribution measured at vacuum conditions without horizontal radiation shields (the element was applied in run no. 21-46).

The lower and upper end of the heating element may be supplied with horizontal radiation shields (made of graphite) as indicated in Fig. 4.2. The lower end of the lower radiation shield is fitted across the bottom opening of the furnace element to prevent the "chimney effect", i.e. vertical gas drafts through the furnace. Some experiments were performed without radiation shields, with only a graphite lid fitted across the bottom opening of the furnace element. It was possible to lower the graphite lid in order to create a substantial increase in the vertical gas draft through the furnace due to the "chimney effect".

The heating element is supplied with electric power from a low voltage transformer (max. 1800 A at 9 V).

4.3. Vacuum system and pressure gauges

The furnace chamber is evacuated by a standard vacuum line consisting of an oil diffusion pump, an angle valve, and a rotary forepump.

Pressures in the range 1000 - 0.5 torr is measured by an electronic pressure transmitter (cf. Fig. 4.7, manometer I). The pressure transmitter has an analog output permitting continuous monitoring of furnace pressure on a chart recorder. Pressures in the range $1 - 10^{-3}$ torr is measured by a Pirani gauge model M 6A[1] and in the range $10^{-2} - 10^{-5}$ torr by a Penning gauge type 5 MF[1]. The ultimate vacuum attainable is in the range 10^{-5} to 10^{-6} torr.

4.4. Temperature measurement and control

Temperature measurement in Versatilie was done by radiation pyrometry by means of a Leeds & Northrup 8642 Mark II High Precision Automatic Optical Pyrometer[2]. The instrument automatically adjusts the current in the built-in pyrometer reference lamp to match the brightness temperature of the target.

---

[1]Edwards High Vacuum Ltd., Crawley, Sussex, England.
[2]Leeds and Northrup Co., Philadelphia, USA.

The pyrometer measures at a effective wavelength of about 655 nm
and a passband having a bandwith of about 16.3 nm. The resolution
given is 0.15°C at 1064.4°C and the stability is claimed to be
within 0.5°C for a 300 h period. The pyrometer may measure
temperatures from 775°C up to 5800°C divided into four ranges
(Low, Medium, High and Extra High). Readout from the pyrometer
was accomplished by a digital meter and followed continuously on
the chart recorder. The millivolt signal from the pyrometer is
also used to control the furnace temperature via an Eurotherm
controller[1] connected to a thyristor unit.

Light from the hot target in the furnace is reflected to the
pyrometer through a silica window and a total-reflection silica
prism (cf. Fig. 4.2). A window or a prism will always absorb some
light. That is, the temperature T_2 as seen from the pyrometer is
somewhat lower than the true temperature T_1 in the furnace. The
absorption in the prism was determined "once and for all" by
sighting the pyrometer on a glowing filament lamp, first through
the prism (T_2), and then without prism (T_1), at the same distance.
The absorption, A, may then be calculated from Wien's law:

$$A = \frac{1}{T_2} - \frac{1}{T_1} \qquad\qquad (4.1)$$

and is a characteristic constant for any particular prism or
window. Absorption in the windows was determined by a similar
procedure. Results are given in Table 4.1.

Table 4.1. Results from determination of absorption in prism based
on 8 measurements. A typical absorption factor for a
silica window is included (based on 3 measurements).

	Absorption factor $A \times 10^5$	Resulting uncertainties in temperature at 1560°C [°C]
Prism	0.541 (±0.0019)	±0.1
Window	0.341 (±0.005)	±0.2

The absorption factors are additive and the total absorption
between sample and pyrometer is accordingly the sum of absorption
in prism and window.

---

[1]Model no. 090-008-97-154-02-61, Eurotherm Ltd., Worthing, West Sussex, England.

Calibration of the pyrometer was accomplished by means of a ribbon filament lamp[1] calibrated at NBS. The calibration report from NBS (Appendix A5) reports the following uncertainties:

$$800°C (\pm2.5); \quad 1100°C (\pm1.5); \quad 2300°C (\pm3)$$

The uncertainties are seen to be much larger than the uncertainties which are introduced by determination of absorption factors in prism and windows respectively. Thus the maximum error in the temperature read by the pyrometer is believed to be somewhere between $\pm1.5°C$ and $\pm3°C$.

A major problem attached to the application of radiation pyrometry was, however, obstruction of the optical path between sample and pyrometer due to condensation of SiO(g) in the holes through the upper radiation shields and/or on the silica window. In order to prevent condensation in the optical path of the upper radiation shields, it was designed as shown in Fig. 4.5. This design proved successful when running experiments with gas in the furnace; most of the SiO deposit was found at the opposite side from the optical path. At high vacuum conditions, where vapour molecules travel in straight lines, deposition of a film of the evaporating substance on the silica window, is a potential source of error. No precautions where made to avoid this, but it was possible to check whether the repeated use of one window had resulted in an observable increase in its absorption by turning to another window. This was frequently done when running experiments in vacuum.

4.5. The electronic weighing system

Previously "Versatilie" was equipped with an old-fashioned beam balance using a combination of manual weight-changing and electronic weighing.

---

[1] Gas-filled tungsten ribbon filament lamp. General Electric Co., USA.
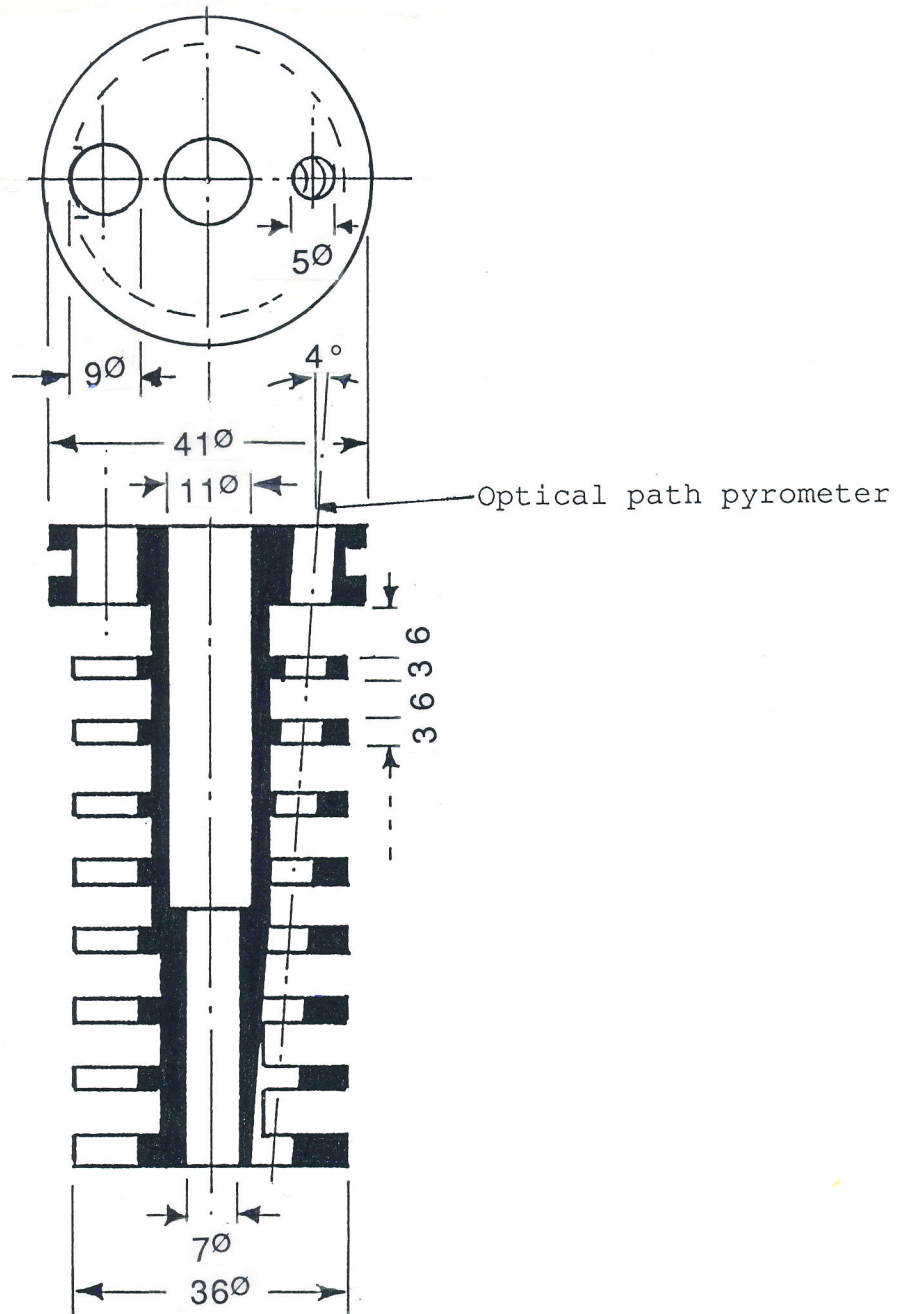
Fig. 4.5. Upper horizontal graphite radiation shield, as it was
designed to prevent obstruction of optical path due to
condensation of SiO(g) (dimensions in mm).

In the course of the present work this was replaced by an all-electronic weighing cell with 160 g loading capacity and a sensitivity better than 0.5 mg[1] . An obvious advantage of the latter is that it lends itself to the automatic recording of data in conjunction with a small on-line computer.

The weighing system is visualized in Fig. 4.6. The results are monitored on the chart recorder (6)[2] where sample weight, sample temperature and furnace pressure are continuously recorded. Weight data (absolute weight, %weight change and rate of weight change) are continuously displayed on the monitor of the microcomputer (4)[3] and may also be dumped on the printer (5)[4].

The microcomputer communicates with a Solartron 7151 Computing Multimeter (3)[5] thus the sensitivity of the analog output ("the weight signal") from the multimeter may be freely chosen. Hence, full range (weight) on the chart recorder may be chosen whatever is convenient for the experiment in question. The software part along with the procedure for running the weighing system is given in Appendix A1.
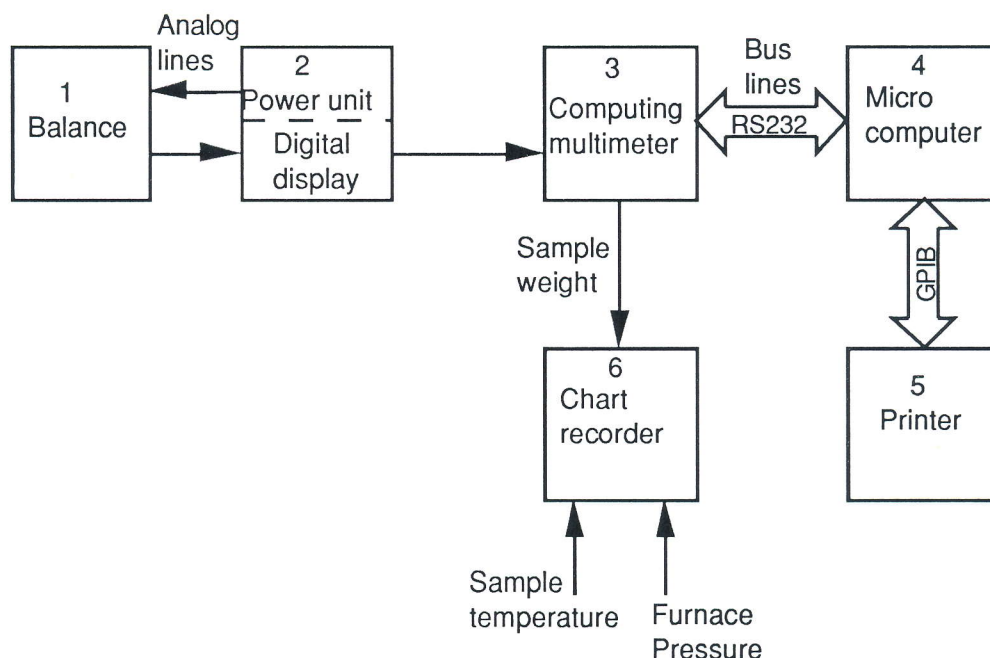
Fig. 4.6. The electronic weighing system.

[1] Sartorius Electronic Weighing Cell Model 5405 with power supply and readout unit A7048; Sartorius-Werke AG, 3400 Göttingen, BRD.
[2] Servogor, Type SE 330, Goerz Electro Ges. m.b.H., A-1101 Wien, Austria.
[3] BBC-Microcomputer, Type ANB 03, Acorn Computers Ltd., Cambridge, England.
[4] Brother, Model M-1009, Japan.
[5] Solartron Instruments, Farnborough, Hampshire England.

84

However, the weighing system suffered from an unpleasant temperature drift for a period of time. That is, small changes in room temperature caused a response in the weighing signal from the balance, corresponding to about 18 mg/°C. It took quite some time to locate the temperature sensitive component: Using a thermistor the temperature on different locations of the weighing system and the weighing signal from the balance were recorded simultaneously. Following this procedure the temperature sensitive component was found to be an operational amplifier located at "the position reader" part of the balance itself. The operational amplifier (designated LH0042CH[1]) was replaced with an operational amplifier with a better temperature characteristic (designated LH0022CH) and the typical temperature drift of the weighing system was reduced to about 1.6 mg/°C.

4.6. Gas mixing and inlet

The peripheral gas support system is given in Fig. 4.7. Gas mixtures are synthesized in a 40.6 l gas cylinder. The lightest gas specie (CO) is allowed first into the cylinder followed by the heavier gas specie (Ar). The composition of the gas mixture is controlled by manometer II (Fig. 4.7).

The total pressure of the final gas mixture in the mixing cylinder is chosen to be 2.9 bar (2200 torr), which is sufficient to run experiments at total pressures up to 1.3 bar (1000 torr) in the furnace (the volume of the furnace is 42.8 l).

A heating tape, keeping the bottom end of the cylinder at about 75°C, works as a "convective impeller" providing a homogeneous gas composition during a relatively short time.

The quality of mixing was investigated by means of gas chromatography for a 50% CO 50% Ar mixture. Mixing procedure: CO admitted into the mixing cylinder until the manometer read 1.133 bar (850 torr); subsequent admittance of Ar until the manometer read 2.266 bar (1700 torr). Gas analysis of the mixture was taken 15, 30 and 45 min after admittance of the last gas specie (Ar) and the results are given in Table 4.2.

---

[1] National Semiconductor Ltd., Greenock, Scotland, UK.

Table 4.2.   Composition   of   a   "50/50
              mixture"   of   Ar   and   CO   as
              function of time elapsed (time
              of mixing) after admittance of
              the last gas specie (Ar).

Time of mixing	Composition [%]		
[min]	Ar	CO	N_2
15	51.8	48.0	0.2
30	51.7	48.1	0.2
45	51.8	48.0	0.2

The composition is seen to be virtually constant after 15 min of
mixing, indicating that 15 min is sufficient to obtain a
homogeneous gas mixture. Analyses of the applied gases (CO and
Ar) , as given from the manufacturer, are given in the next
paragraph.
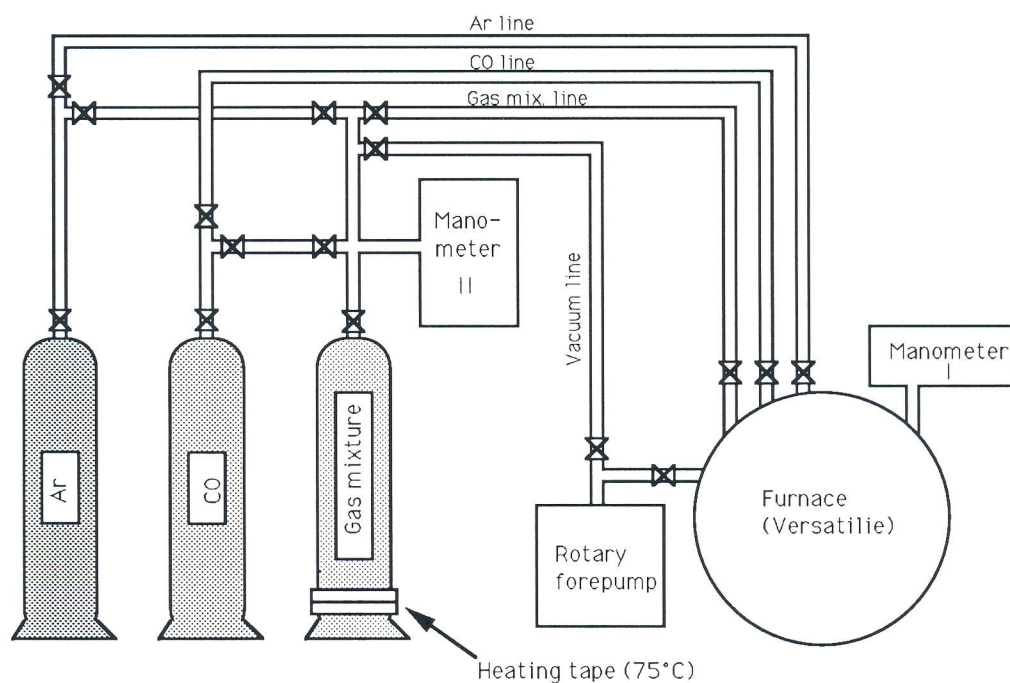
Fig. 4.7. Peripheral gas support system. Manometer I[1] monitors
          the furnace pressure (range 0-1000 torr, accuracy ±0.1
          torr) while manometer II[2] is applied when preparing
          mixtures from Ar and CO (Range 0-10000 torr, accuracy
          better than ±1 torr).

[1] Barocel pressure sencor, type 571D-1000T-3C2-H5 and Electronic manometer
type 1018.Datametrics, Wilmington, Mass., USA.
[2] Precision pressure gage, model 145. A differential Bourdon capsule type 801
is applied. Texas Instruments, Texas, USA.

4.7. Chemicals

The chemicals used are listed in Table 4.3, and the pore size distribution of the applied graphite is given in Fig. 4.8.

Table 4.3. Chemicals

Compound	Quality	Manufacturer
Vitreous silica[1] (silica tubings)	See footnote	–
SiO_2 (Quartz)	99,98% 60 ppm Al 50 " Ca 3 " Cr 50 " Fe 2 " Mn <0.1 " Mo 5 " Ti 0.03 " V 0.6 " Zr 1 " B 1 " P	Mount Rose,British Columbia. Received from Elkem R&D Center, Vågsbygd, Norway
C (CS49 graphite)	99.5%	Union Carbide
CO(g)	99.0% <2000 ppm N_2 <5000 " $Ar+O_2$ <2000 " H_2 <1000 " C_nH_m	Hydro Industri Gasser Herøya, Norway
Ar(g)	99.99% <5 ppm O_2 <5 " H_2O <5 " C_nH_m	"

---

[1] Unfortunately it was not possible to find out the origin of the silica glass tube. It is, however, reason to believe that it was of high purity, and that the impurity level of alkali was less than 1 ppm.
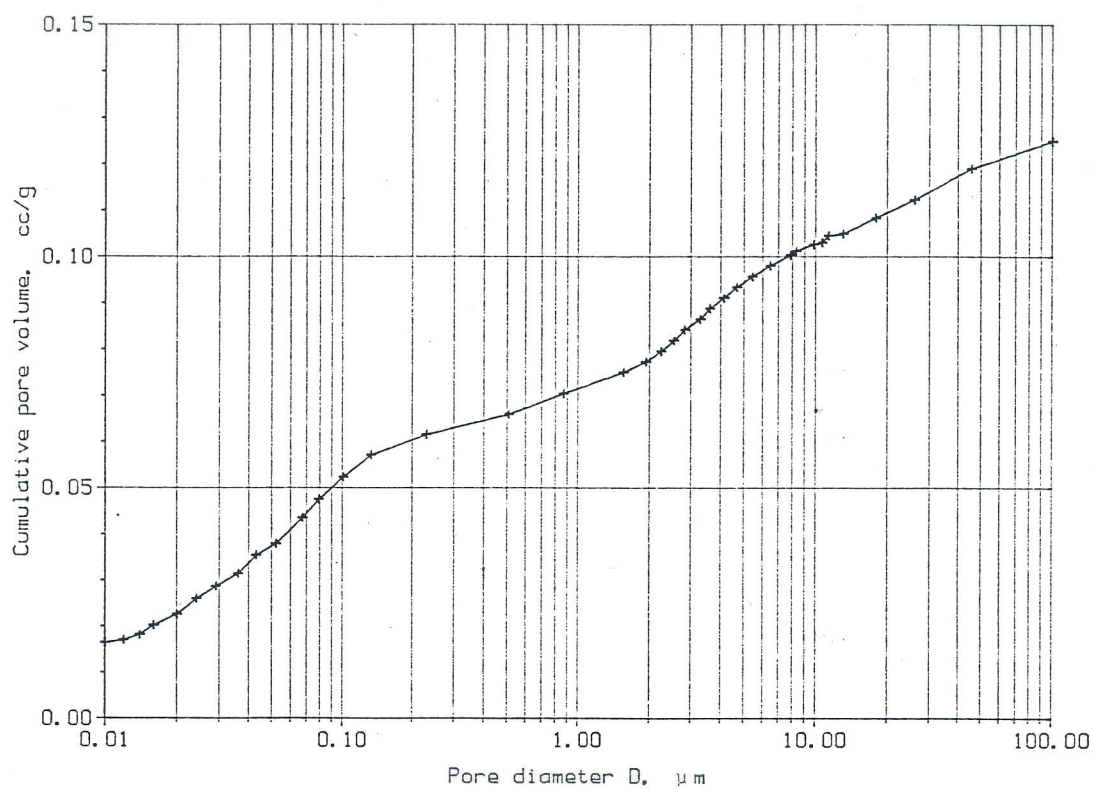
Fig. 4.8.   Pore size distribution of CS49 graphite as measured by
a mercury porosimeter.

4.8. Investigation of reaction products

A Philips X-ray diffractometer with CuK_α radiation was used
for phase identification. The equipment consists of an X-ray
generator (PW 1730/10) with vertical goniometer (PW 1050/25)
controlled by a PW 1710 diffractometer control.

5. REACTIONS WITH VITREOUS AND DEVITRIFIED SILICA

This chapter reports on the behaviour of silica in vacuum and in the presence of CO respectively:

$$SiO_2(s) = SiO(g) + \frac{1}{2} O_2(g) \qquad\qquad (1.1)$$

$$SiO_2(s) + CO(g) = SiO(g) + CO_2(g) \qquad\qquad (3.9)$$
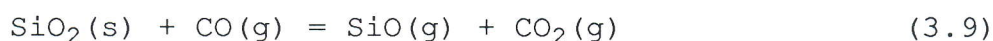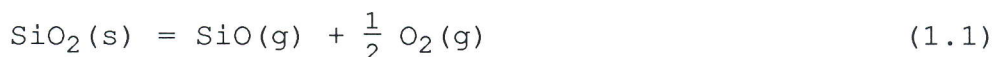
For this purpose it was found convenient to apply silica glass tubing because of its defined surface geometry. The evaporation reaction (1.1) was investigated for vitreous silica as well as for devitrified silica (cristobalite) whereas reaction (3.9) was studied with devitrified silica only.

All experiments performed in this section are referred to with a run number and relevant information concerning experimental parameters, weight data and rate data are tabulated in Appendix A2.

5.1. Thermal decomposition in vacuum

5.1.1. Experimental

A series of experiments were conducted with specimens of pure silica glass tubing freely suspended from the balance into the graphite heating element. The specimens were 39 mm long with inner diameter 15.1 mm and outer diameter 18.5 mm.

Every run followed the same procedure: The furnace was evacuated to about 5×10^{-5} mbar, heated to 1000°C and degassed at this temperature until the pressure was down to 5×10^{-5} mbar. The temperature was subsequently increased to the reaction temperature. A vacuum of 5×10^{-5} mbar was maintained during the reaction period.

The temperature of the specimen was measured by aiming the pyrometer on the edge of the silica tubing. Since the edge of the silica tubing is not expected to show black body behaviour, blank experiments were run afterwards with a black body placed inside the furnace in order to assign a correct temperature to each run. The weight loss of the silica tubings as functions of reaction time is shown in figure 5.1.
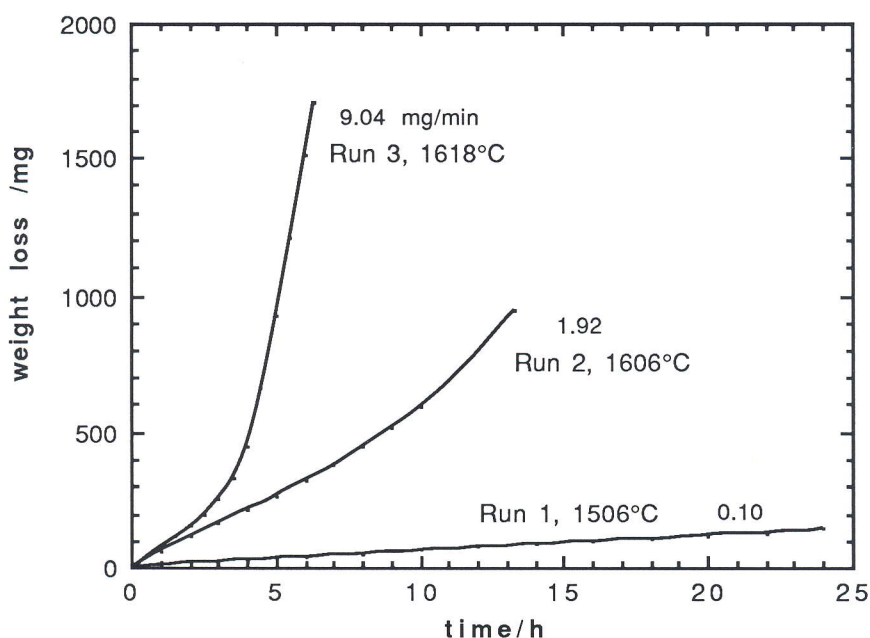
Fig. 5.1. Weight loss against reaction time for three different, but identical silica tubings at vacuum conditions. The numeric value of the final rate of weight loss (i.e. at the end of each run) is given.

Run 2 at 1606°C and run 3 at 1618°C show a non-linear behaviour with an accelerating rate beyond a certain time. The acceleration seems to cease and the rate becomes constant towards the end of the run. At 1506°C (run 1) the rate appears to be nearly constant throughout the run.

Inspection of the specimens after each run showed devitrification due to the formation of cristobalite on the surface: The specimens run at 1506°C and 1606°C showed devitrification at both the inner and outer surface of the tubings. Additionally, the specimen run at 1606°C showed a large number of bubbles in the body of the silica and some deformation due to incipient melting. The specimen run at 1618°C was mainly devitrified at the inner surface of the tubing, the outer surface remained essentially glassy clear, and the specimen was considerably deformed due to incipient melting.

Another series of experiments were conducted following essentially the same procedure as described above. One difference was a small Mo crucible, with a lid with a 5 mm hole, placed inside the silica tubing and, furthermore, the same piece of silica tubing was used throughout the series. The Mo crucible provided black-body conditions; sighting the pyrometer on the 5 mm hole in the crucible lid. The results are shown in Fig. 5.2. The first run was conducted at 1568°C (run 4A) and the silica specimen was cooled and visually inspected before continuing the experiment at 1582°C (run 4B-I), thereafter the temperature was raised to 1632°C (run 4B-II) and 1682°C (run 4B-III) respectively.
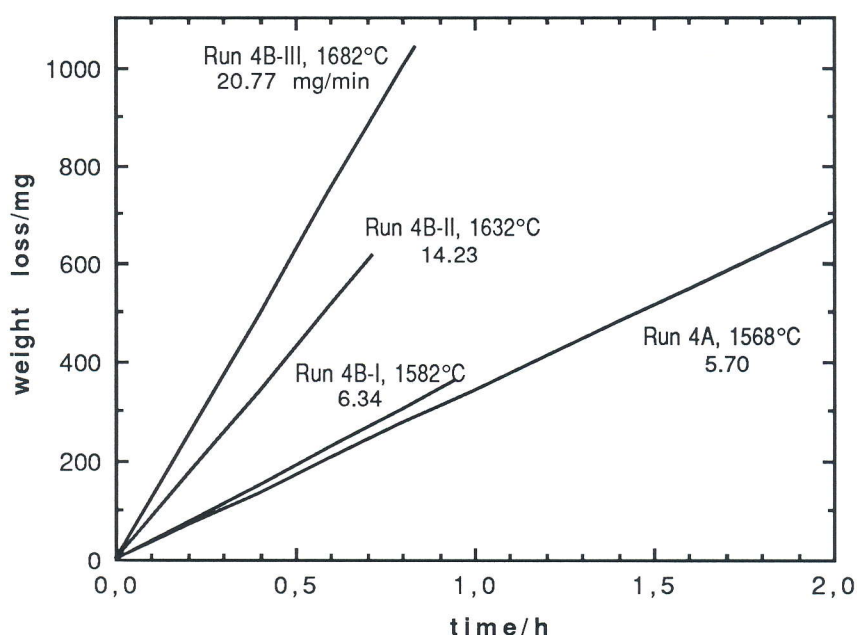
Fig. 5.2. Weight loss against reaction time for a silica tubing at four different temperatures and vacuum conditions. The rate of weight loss was constant throughout each run and the numeric values are given (note the time scale compared to Fig. 5.1).

The rate of weight loss was quite high already from the start of the run compared to those in Fig. 5.1 (5.7 mg/min at 1568°C) and furthermore the rate stayed constant during the reaction period. Inspection of the silica tubing after the experiment showed a very low degree of devitrification, that is, only a faint, milky white 15 mm broad band on the inside of the tubing was observed. Apart from this the silica specimen was glassy clear and considerably deformed.

In order to show how devitrified silica behaved at elevated temperatures in a vacuum, a silica tubing of the same size and quality as described above was fired for 24 hours in 1 bar Ar

atmosphere at 1550°C (run 5). A tiny Mo crucible, similar to that described above, was placed inside the tubing providing black body conditions. During the firing period the silica specimen lost 70 mg corresponding to a average weight loss rate of 0.049 mg/min. The specimen appeared milky white after the run, and examination of a cross section of the specimen showed the formation of a 0.1 mm thick crystalline layer at the outer and inner surfaces. XRD-analysis confirmed the formation of cristobalite. A uniform layer of 0.1 mm thickness corresponds to 12 % of the silica transformed to cristobalite.

The specimen was subsequently held at 1563°C (run 6) in a vacuum. The weight loss in dependence of reaction time is shown in Fig. 5.3.
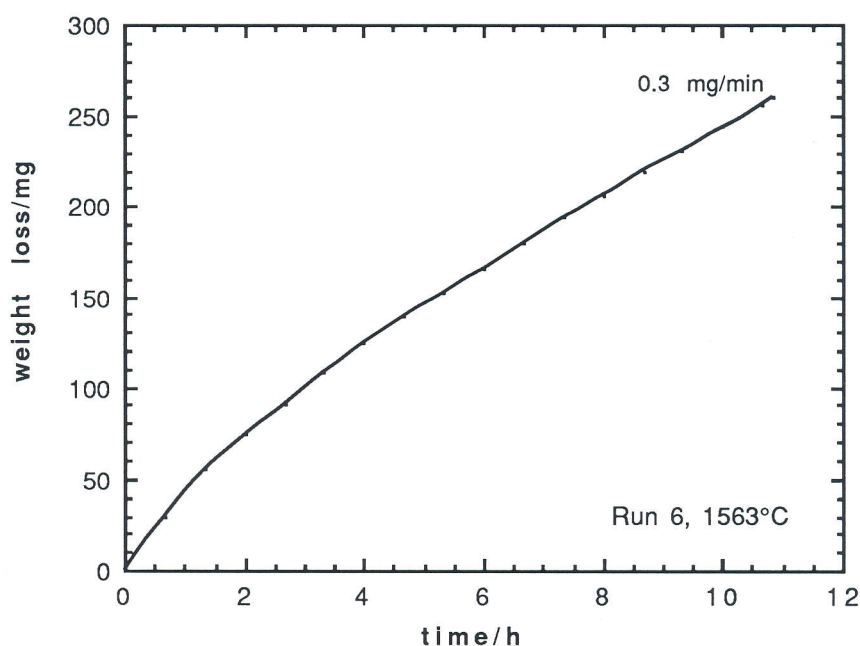
Fig. 5.3. Weight loss against reaction time at vacuum conditions for a silica tubing pretreated for 24 h at 1550°C in Ar atmosphere. The numeric value of the rate at the end of the run is given.

It is seen that the rate of weight loss decreases during the first few hours and approaches a nearly constant rate of about 0.3 mg/min. Furthermore this rate is far lower than observed with vitreous silica, and while vitreous silica, according to Fig. 5.1, shows an increase in rate with time, devitrified silica shows a considerable decrease in rate.

5.1.2.   Discussion

Silica will evaporate in a vacuum at elevated temperatures mainly according to the reaction

$$SiO_2(s) = SiO(g) + \frac{1}{2} O_2(g) \tag{1.1}$$
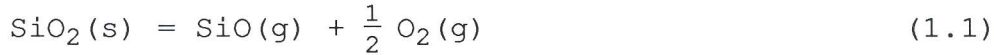
Assuming equilibrium pressures of the gaseous species SiO and O_2 at the silica surface, the rate of mass loss per unit area, dq/(Adt), may be calculated from the Langmuir equation (e.g. Paule and Margrave, 1967):

$$\frac{1}{A} \frac{dq_i}{dt} = P_i \left(\frac{M_i}{2 \pi R T} \right)^{0.5} \tag{5.1a}$$

Here, P_i and M_i is the partial pressure and molar mass, respectively, of the vapour, T is absolute temperature and R is the gas constant. With all quantities on the right-hand side expressed in SI units, Eq. 5.1a gives the rate of evaporation in kg/m^2 s. The evaporation coefficient, α, is assumed unity; meaning that we will calculate the theoretical maximum evaporation rate. It has been found convenient to express dq_i/dt in mg/min, A in cm^2, M_i in g/mol and P_i in bar. This gives

$$\frac{1}{A} \frac{dq_i}{dt} = 2.625 \times 10^6 \, P_i \left(\frac{M_i}{T} \right)^{0.5} \tag{5.1b}$$

When reaction (1.1) takes place at steady state, the ratio between the number of moles per unit time of SiO and O_2, respectively, leaving the silica surface will be $(dn_{SiO}/dt)/(dn_{O_2}/dt) = 2$. Hence, the ratio between the partial pressures of SiO and O_2, respectively, at the silica surface must be different from 2. In order to calculate the maximum rate of evaporation from a silica specimen, assuming that reaction (1.1) takes place at the silica surface without significant kinetic hindrance, the ratio between the partial pressures of SiO and O_2 must be known: The total rate of mass loss is given viz.:

$$\frac{dq_v}{dt} = \frac{dq_{SiO}}{dt} + \frac{dq_{O_2}}{dt} = \frac{dn_{SiO}}{dt} M_{SiO} + \frac{dn_{O_2}}{dt} M_{O_2} \tag{5.2a}$$

The relationship between the number of moles of SiO and O_2 leaving the silica surface per unit time:

$$\frac{dn_{SiO}}{dt} = 2\frac{dn_{O_2}}{dt} \tag{5.2b}$$

Now, dq_{SiO}/dt and dq_{O_2}/dt (hence $(dn_{SiO}/dt)M_{SiO}$ and $(dn_{O_2}/dt)M_{O_2}$) are given from Eq. 5.1 and combination with Eq. 5.2b gives:

$$P_{SiO} = 2\left(\frac{M_{SiO}}{M_{O_2}}\right)^{0.5} P_{O_2} \tag{5.2c}$$

$$= 2.348\, P_{O_2}$$

The equilibrium pressure of O_2 and SiO, respectively, may be expressed in terms of the equilibrium constant for reaction (1.1), viz.:

$$P_{SiO}\left(P_{O_2}\right)^{0.5} = K_3 \tag{5.3}$$

K_3 is calculated from JANAF (1985), assuming evaporation from β-cristobalite. Combination of Eq. 5.2c and 5.3. yields on a logarithmic form:

$$\log P_{SiO} = \log P_{O_2} + \log 2.348 = -27298\frac{1}{T} + 8.6551 \tag{5.4}$$

The expected rate of weight loss from the silica tubing is given from Eq. 5.1:

$$\frac{dq_v}{dt} = 2.625\text{x}10^6\ A\left(P_{SiO}\left(\frac{M_{SiO}}{T}\right)^{0.5} + P_{O_2}\left(\frac{M_{O_2}}{T}\right)^{0.5}\right) \tag{5.5}$$

The area, A, of the silica tubing contributing to the evaporation is assumed equal to the outer cylindrical surface area plus the circular cross-section area (πr^2) at both ends, that is A=28 cm^2. Combination of Eqs. 5.4-5 gives, on a logarithmic form, the final expression for the expected rate of weight loss:

$$\log \left(\frac{dq_v}{dt}\right) = -27298 \frac{1}{T} - 0.5 \log T + 17.478 \qquad (5.6)$$

where dq_v/dt is given in mg/min and T is absolute temperature.

The $1/T$ term is much more temperature sensitive than the $\log T$ term and a plot of $\log(dq_v/dt)$ v.s. $1/T$ will essentially give a straight line with a slope close to 27298. That is, the slope is mainly given by the enthalpy and stoichiometry of reaction (1.1) (cf.. Eq. 5.4). The rate of weight loss, on a logarithmic scale, v.s. $1/T$ is given in Fig. 5.4 for all of the experiments with the silica tubings. The solid line represents the theoretical rate of weight loss according to Eq. 5.6 and the corresponding slope is ~26900, that is 1.5% lower than would be expected if the slope was determined by the enthalpy and stoichiometry of reaction (1.1) alone.
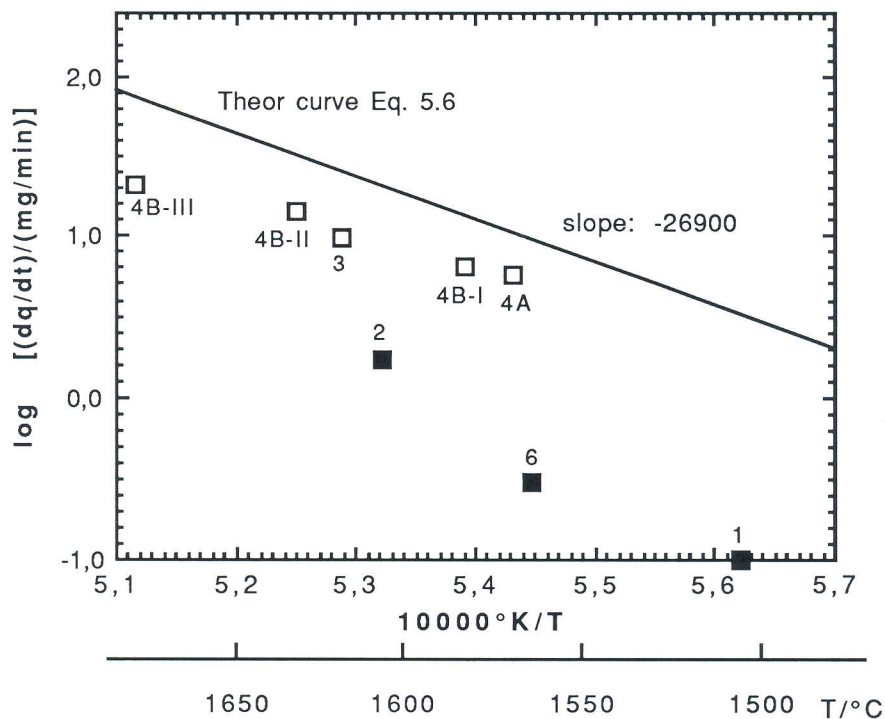
Fig. 5.4. The logarithm of the rate of weight loss against $1/T$ for the silica tubings presented in Figs. 5.1-3. Numbers refer to run no. and the rates given are the observed rates at the end of each run. Open squares indicate that low conversion into crystalline silica was observed after the run while filled squares indicate high conversion. Solid line represents the theoretical maximum rate of evaporation from β-cristobalite as calculated from Eq. 5.6.

The open squares (cf.. Figs. 5.2-3) is seen to agree with the theoretical curve within a factor of approximately two, except from the measurement at the highest temperature, 1682°C, which is a factor of 3.6 lower than the theoretical value. Furthermore, the silica tubings, represented by the open squares in Fig. 5.4, have one common feature: After the experiments, the tubings showed some devitrification only at the inner surface of the tubings, the outer surface was still glassy (transparent) and showed no formation of crystals.

On the other hand, the measurements represented by the filled squares in Fig. 5.4 is seen to be substantially lower than predicted from Eq. 5.6. An examination of the tubings after the experiments showed that both the inner and outer surfaces of the silica tubings were covered with crystals; apparently no vitreous silica was freely exposed to the vacuum.

Accordingly the following tentative postulates may be extracted from the results:

1. Vitreous silica evaporates in a vacuum at a rate fairly close to that expected from the Langmuir Eq. 5.1. Induction periods may, however, occur; that is, a period of accelerating rate until it becomes constant. The nature of this induction period is unknown, but it indicates that the vitreous silica is transformed into a more reactive modification of amorphous silica.

2. Devitrified silica (cristobalite), evaporates at a rate far lower than expected according to the Langmuir Eq. 5.1. Hence, devitrified silica exhibits a considerable kinetic hindrance to evaporation.

From a thermodynamic point of view the evaporation from an amorphous silica specimen (glass) is expected to take place at a faster rate than from a crystalline (β-cristobalite) silica specimen due to the exothermic reaction.

$$SiO_2 \text{(amorphous)} \rightarrow SiO_2 (\beta\text{-cristobalite}) \qquad (5.7)$$
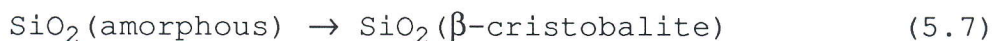
Richet et al. (1982) reported the enthalpy of transformation to -7 kj/mol at 1700 K. However, the free energy change for reaction (1.1) at 1700K, when the silica in question is amorphous, is 366.5 kJ/mol (combining data from Richet et al. and JANAF, 1985), while the corresponding free energy change, when the silica is high

cristobalite, is 367.5 kJ/mol (JANAF, 1985). Thus the calculated rate of evaporation from amorphous silica gives rates which are only infinitesimally higher than the rates calculated for evaporation from crystalline silica (Eq. 5.6), due to the small free energy differences between crystalline and amorphous silica. At e.g. 1506°C (run 1) the rate of evaporation from amorphous silica is expected to be a factor of 1.036 higher compared to crystalline (β-cristobalite) silica while at 1682°C (run 4B-III) the factor is only 1.003. This modest increase is hardly measurable, thus the observed differences in rates of evaporation between vitreous and crystalline silica cannot be explained from the differences in thermodynamic stability of the condensed phases.

5.2. Behaviour in the presence of carbon monoxide.

Fig. 5.3. shows the weight loss of a sample of devitrified silica in vacuum. The very same devitrified sample was employed in the subsequent investigation concerning the behaviour in carbon monoxide.

5.2.1. Experimental

The temperature was again measured by aiming the pyrometer at a Mo-crucible placed inside the silica tubing; as previously described. The first run (run 9) recorded the rate of weight loss of the silica specimen at 1575°C in a vacuum and in CO with pressures ranging from $2x10^{-3}$ to 1 bar. The whole series was recorded at constant temperature and successively increasing pressure, and every CO-pressure was kept constant for approximately 0.5 h while recording the rate of weight loss of the silica specimen. The results are given graphically in Fig. 5.5.

The rate of weight loss in vacuum was 0.25 mg/min and is seen to be significantly increased by the presence of CO. A maximum of about 1.25 mg/min is attained at approximately 0.27 bar. The rate descends as the pressure is increased beyond 0.27 bar and becomes practically independent of pressure above 0.53 bar.

Fig. 5.5. Rate of weight loss of a devitrified silica tubing in dependence of CO pressure at 1575°C (run 9). Upper and lower graph in linear and logarithmic scales respectively (data from Table A2.13).

Another series, varying the CO pressure in a random way (run 10), conducted with the very same silica tubing at a slightly lower temperature, 1570°C, confirmed the results from the first run. The results are given in Fig. 5.6. The results from the first run (run 9) is included in the same figure.

A third (run 12) and a fourth run (run 13) were performed with the very same devitrified silica tubing, recording the rate of weight loss in the temperature range 1412-1573°C at 0.100 and 0.267 bar CO respectively. The results are given as Arrhenius

98

plots in Fig.5.7 and 5.8. The Arrhenius plot at 0.267 bar (Fig 5.8) is strictly linear and an apparent activation energy of 302 kj/mol is calculated from the slope of the curve. The Arrhenius plot at 0.100 bar seems, however, somewhat curved. By fitting the low temperature and high temperature region of the Arrhenius plot separately into straight lines, apparent activation energies of 483 and 325 kj/mol, respectively, are calculated. Apparently, the AE is reduced from 483 to 325 kj/mol (33 %) as the temperature is raised from 1430 to 1574°C.
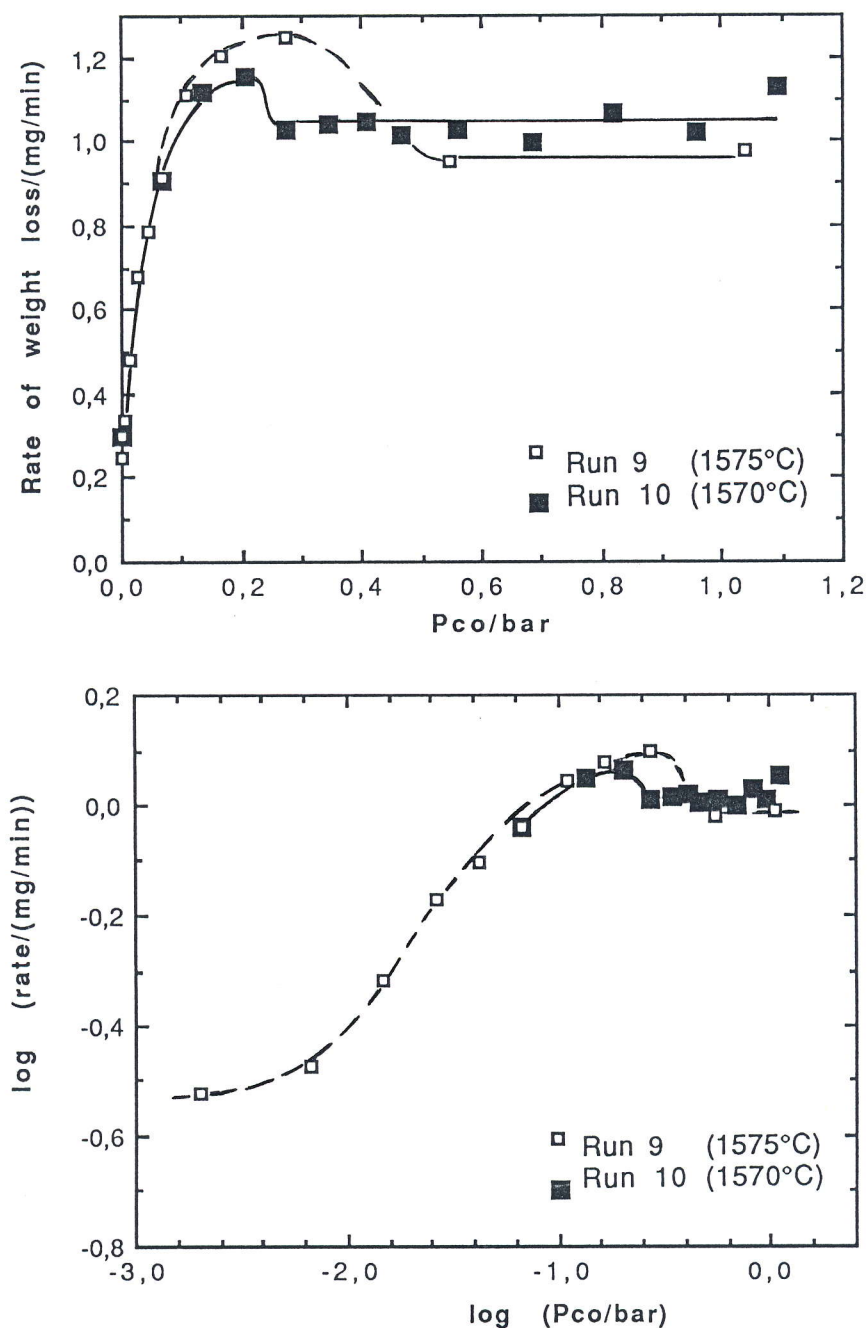
Fig. 5.6. Rate of weight loss of a devitrified silica tubing at 1570°C and 1575°C respectively in dependence of CO pressure. Upper and lower graph are in linear and logarithmic scales respectively (data from Table A2.13-14).

A last run (run 14) was conducted with the devitrified silica tubing; to see how the bulk gas (CO) flow rate affected the rate of weight loss. The gas flow rate was controlled to a certain extent by means of a graphite lid in the lower end of the graphite heating element; as illustrated in Fig.5.9.
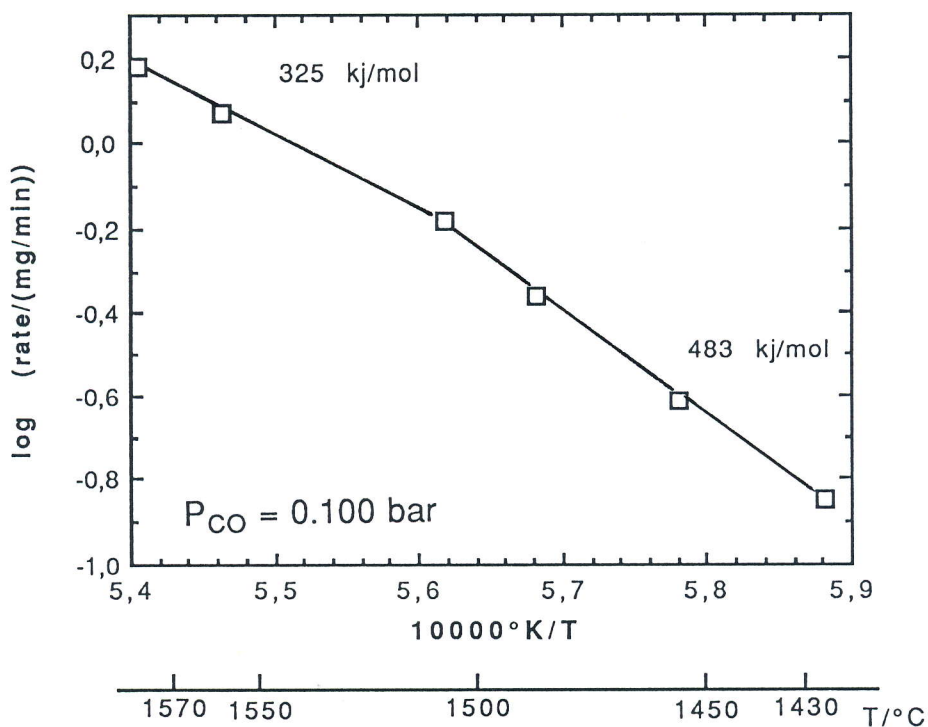
Fig. 5.7. The logarithm of the rate of weight loss against 1/T for a devitrified silica tubing (run 12) (data from Table A2.15).
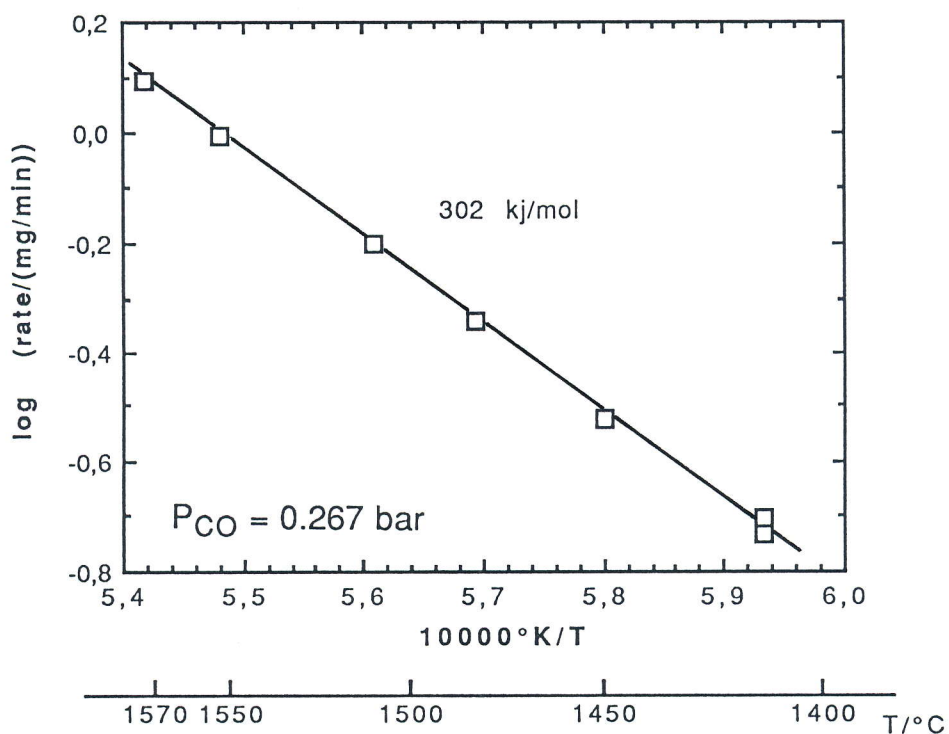
Fig. 5.8. The logarithm of the rate of weight loss against 1/T for a devitrified silica tubing (run 13) (data from Table A2.16).

Case A (closed)   Case B (open)
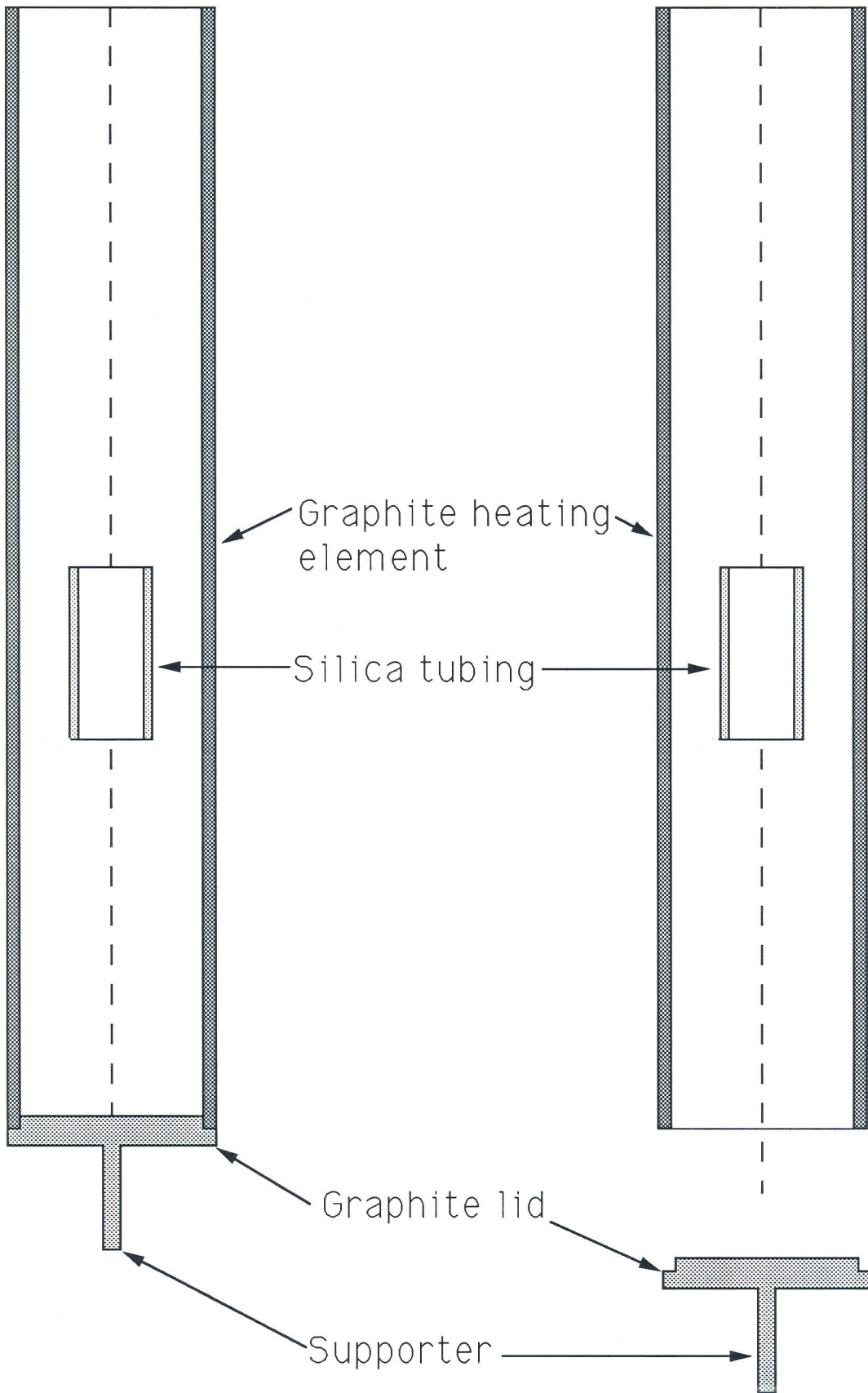
Fig. 5.9. Schematic drawing of graphite heating element, illustrating a closed and an open element, respectively.

Only a moderate gas flow around the tubing due to convection is
expected in case A, whereas a fast rate is expected in case B
where the lid is removed and gas is allowed to flow ("chimney
effect"). The rates of weight loss of the silica tubing at 1575°C
and 0.100 bar CO with a closed and a open heating element,
respectively, are given in Fig.5.10.
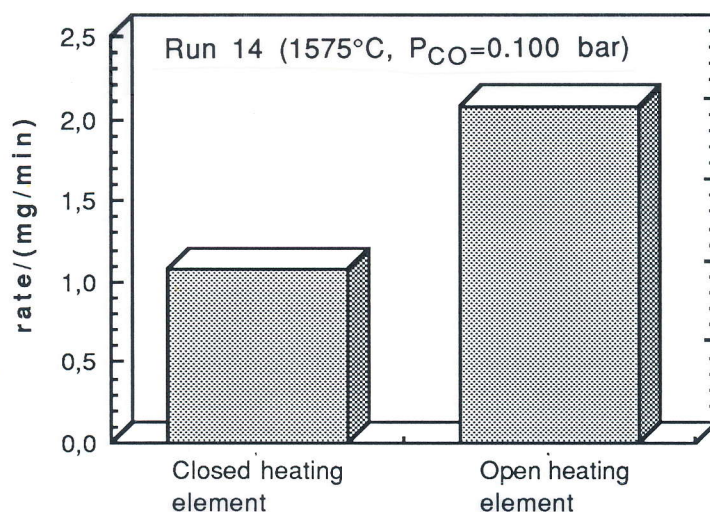
Fig. 5.10. The rate of weight loss of a devitrified silica tubing
at 1575°C and 0.100 bar CO when the graphite heating
element is closed and open, respectively (run 14).

It is seen that the rate is increased by a factor of about 2 when
the lower end of the graphite heating element is opened.

-oOo-

The results given in Fig.5.5 are reproduced on a log-log
scale in Fig.5.11. The rate as function of the CO pressure is
divided into 5 different regions. In the low pressure region (I)
the rate is not very sensitive to the CO pressure whereas region
II show a pronounced dependence. In region IV the rate decreases
with CO pressure while in region V it is independent of pressure.
Region III is a transition region between II and IV.

It is assumed that in the presence of CO the primary reaction
may be written:

$$SiO_2 + CO = SiO + CO_2 \qquad\qquad\qquad (3.9)$$
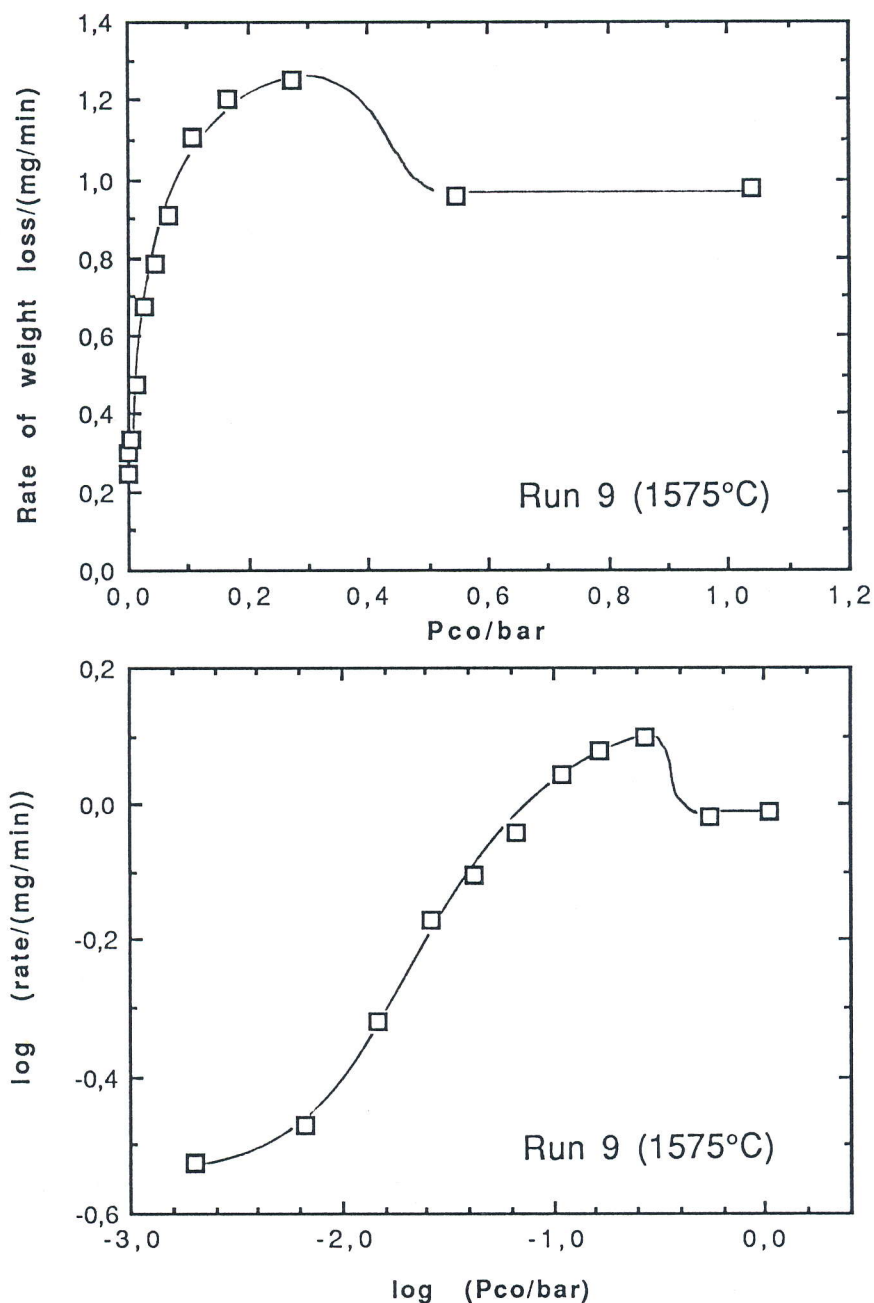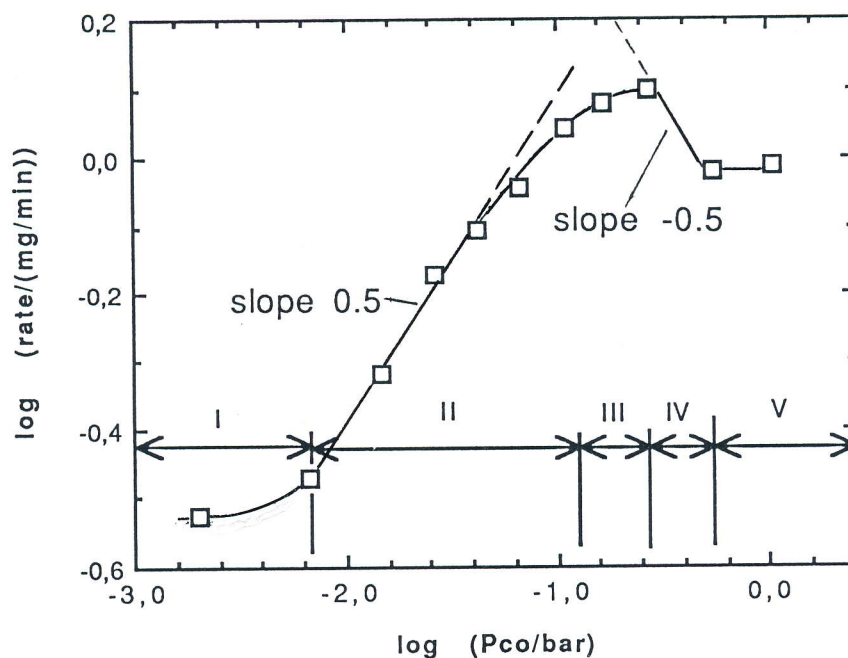
Fig. 5.11. Rate of weight loss of a devitrified silica tubing in dependence of CO pressure at 1575°C (run 9). Log-log scale (data from Table A2.13)

Accordingly there are three possible rate controlling processes to be considered:

    i) Transport of product gases (CO_2 and SiO) away from the silica surface by bulk gas flow.

    ii) Transport of product gases (CO_2 and SiO) away from the silica surface by gas diffusion.

    iii) Chemical reaction on the silica surface.

It is noted that transport of reactant gas (CO) to the surface is not included as a possible rate-controlling process. This is because the equilibrium partial pressures of CO_2 and SiO are so low that the gas surrounding the silica will remain nearly pure CO in spite of reaction (3.9) (cf. Fig. 3.1).

5.2.2. Calculation of gas flow by FLUENT

From the results depicted in Fig. 5.10 it is clear that the rate of gas flow past the silica surface does have an influence on the reaction rate. For a more quantitative evaluation of this effect, information was needed about the rates of gas flow around

the silica tube in a closed and an open heating element, respectively. This information was obtained by means of calculations in fluid dynamics, taking into account the geometry of the silica tube and the heating element, the temperature distribution in the heating element, and the density, heat capacity, thermal conductivity and viscosity of the gas (carbon monoxide) as functions of temperature. The calculations were done by means of the computer program FLUENT, which was put at the author´s disposal by siv. ing. Stein Tore Johansen and his research group at the Department of Metallurgy, NTH. The calculations are documented in Appendix A3, and only the main results will be presented here.

The results for the conditions of closed heating element, 0.10 bar of CO and a furnace temperature of 1570°C are shown graphically in Fig. 5.12. Note that in this drawing, the diameters have been enlarged with a factor of 4 relative to the heights in order to obtain a legible graph. The pattern of motion of the gas is more clearly shown on Fig. 5.13 which shows the countours of the streamlines, across which there is no mass flow.

The main result for our purposes is that the gas velocity in the vicinity of the silica tubing is essentially nil. This is even more clearly shown in Fig. 5.14, which shows the calculated velocities in the central part of the heating element, this time with a correct ratio diameter/height. The blank fields around the silica tube correspond to velocities below 5×10^{-6} m/s, which means 0.3 mm per minute. Thus we may conclude from the calculations that the gas convection inside this sort of closed heating element results in essentially no gas flow at all along the silica surfaces.

The calculated velocity distribution for 0.1 bar and an open heating element, on the other hand, is shown graphically in Fig. 5.15. Only the centre part of the heating element is shown here, for comparison with Fig. 5.14. Note the difference in the scales for velocity, shown to the right of the two figures. Numerical values for the mean velocity of the gas in the interspace between
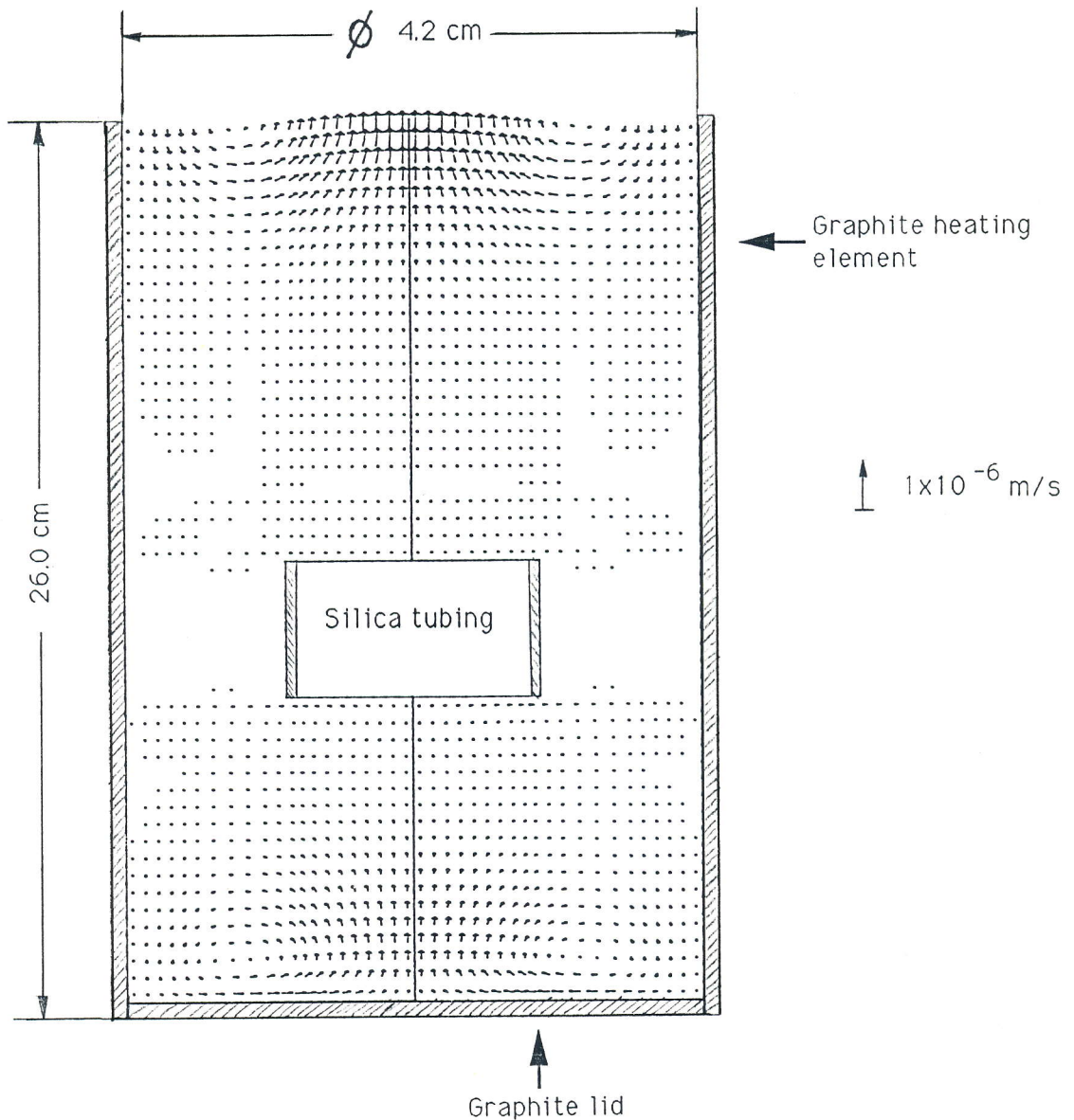
Fig. 5.12 Calculated velocity distribution in the gas in the closed heating element at o.1 bar CO and furnace temperature 1570°C. Blank fields in the central part indicate velocities below 5×10^{-6} m/s. Note that, for purpose of clarity in plotting the velocities, the ratio of width to height of the drawing is 4 times the real diameter-to-height ratio of the heating element.

silica and graphite tubes are shown in Table 5.1 for the two cases. It is seen that, compared to the closed heating element, the velocity in the open heating element is about 10^5 larger at 0.1 bar, and about 10^4 larger at 1.0 bar of CO.
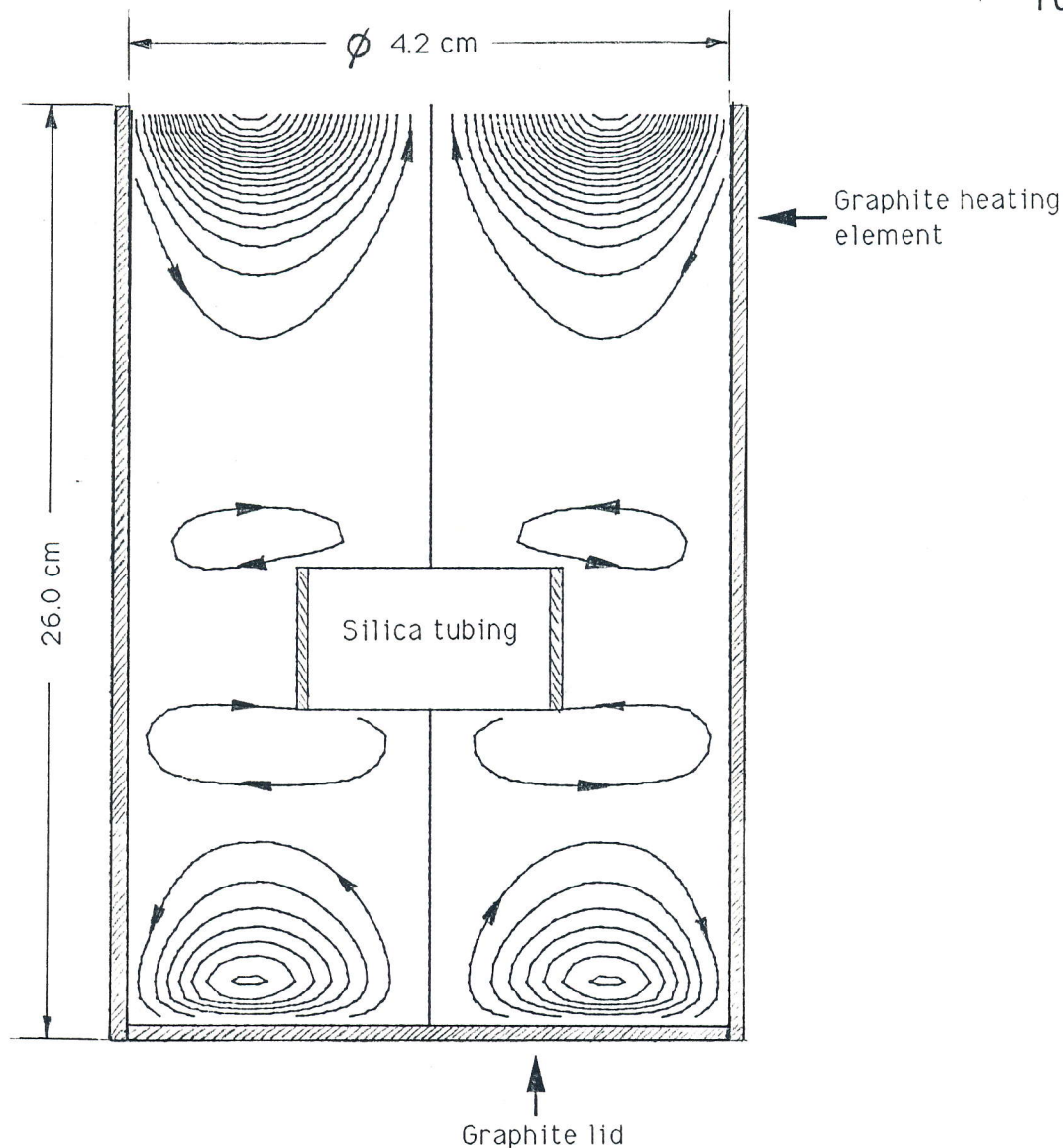
Fig. 5.13. The same results as in Fig. 5.12, re-plotted to show
        contours of the streamlines. There is no mass flow
        taking place across the streamlines. It is seen that
        the gas will have a sort of rotating motion towards
        both ends of the heating element, while a very slow
        rotation in the opposite direction is noted around the
        ends of the silica tube. Ratio of diameter to height
        enlarged 4 times as in Fig. 5.12.

Table 5.1. Mean bulk gas flow rates [m/s] in the open space
        between the silica tubing and the graphite heating
        element. The silica tubing is at 1570°C. Calculated
        by means of the data program FLUENT, Appendix A3.

CO pressure in the furnace chamber [bar]	Gas velocity [m/s]		Factor increase by changing from closed to open heat. elem.
	Closed graphite heating element	Open graphite heating element	
0.100	$\sim 10^{-6}$	0.320	$\sim 10^5$
1.013	$\sim 5 \times 10^{-5}$	1.1	$\sim 10^4$
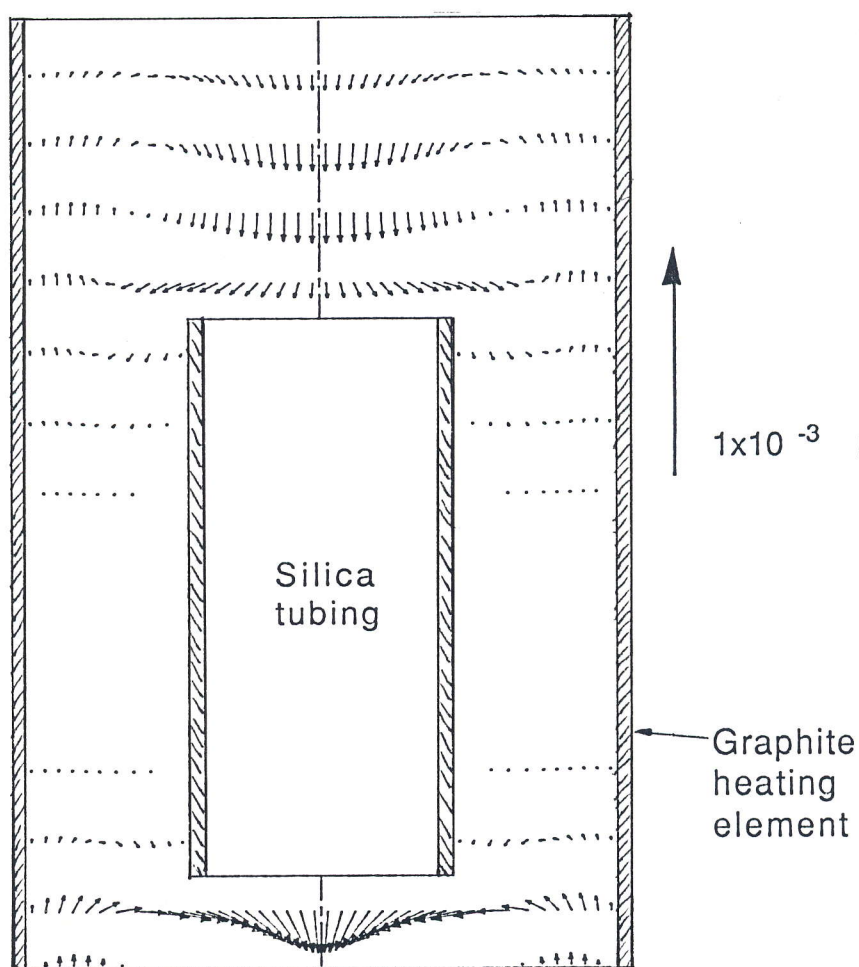
Fig 5.14. The results of Fig. 5.12, re-plotted to show detailed velocity distribution in the vicinity of the silica tubing, here shown with the correct ratio of diameter to height. Note also the difference in the scales for the velocity, shown to the right in both figures. Blank fields indicate gas velocities below about 5×10^{-6} m/s.

Returning now to the chemical reaction, it was shown in Fig. 5.10 that opening the heating element gave an increase in the rate of weight loss by a factor of 2. This is a modest increase, however, when compared to the increase in gas velocity by a factor of 10^4 to 10^5. Thus it is concluded that while mass transfer by gas flow contributes somewhat to the reaction rate when the heating element is open, the main control of the reaction rate occurs by some other mechanism.
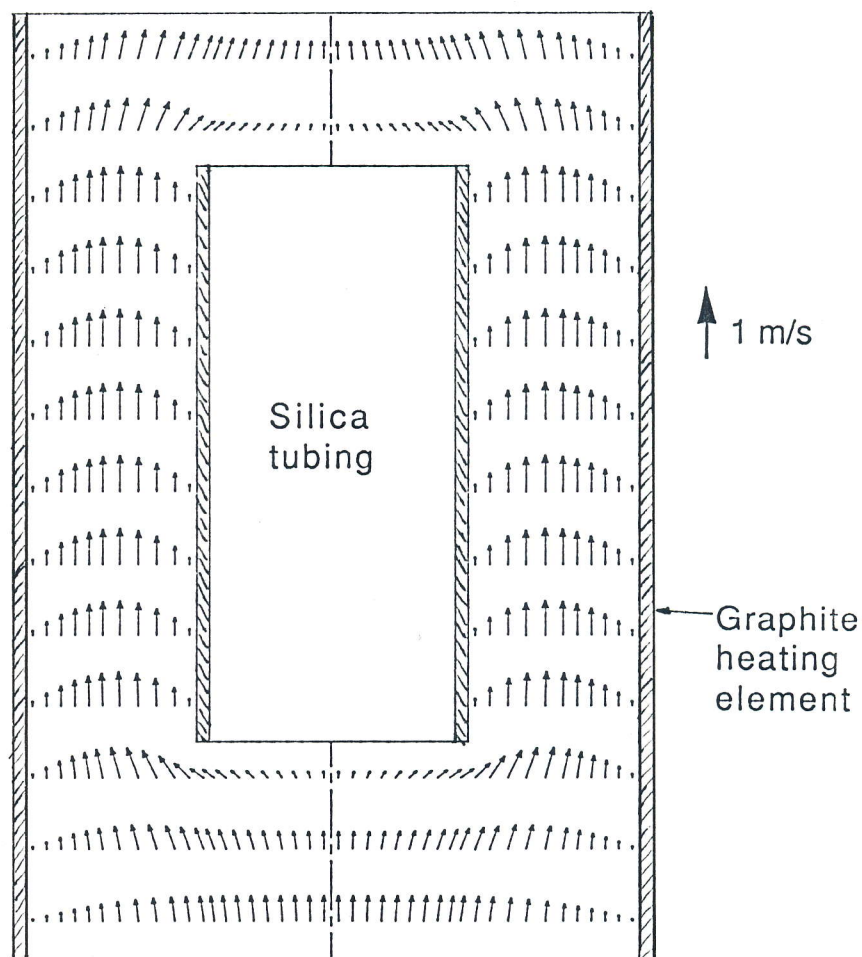
Fig. 5.15. Calculated gas velocity distribution in the open heating element at 0.1 bar CO and 1570°C furnace temperature. Only the central part of the heating element with the silica tube is shown in the figure, which may be compared to Fig. 5.14. Note the difference in the scales for velocity on the two figures.

5.2.3. Calculation of diffusive transport

It was concluded in the preceding section that mass transfer by gas flow (or convection) cannot be rate determining for the reaction taking place in the closed heating element. Thus mass transfer due to diffusion of product gases (SiO and CO_2) has to be considered

Fick´s 1st law of diffusion on the general form is

$$J_i = \frac{dn_i}{A\ dt} = -D_i\ \frac{dc_i}{ds} \qquad (5.8)$$

where J_i is molar flux of specie i [moles time^{-1} length^{-2}], n_i is number of moles of specie i, A is area [length^2], t is time, D_i is diffusivity of specie i [length^2 time^{-1}], c_i is concentration of specie i [moles length^{-3}] and s is length.

Data are needed for the diffusivity of SiO in CO and for CO_2 in CO respectively. Reliable data on the diffusivity of SiO in CO have not been found, hence it is taken to be equal to the diffusivity of CO_2 in CO. Marrero and Mason (1972) have constructed semi-empirical functions to fit experimentally determined diffusivities over a large temperature range for a number of gas pairs. Thus, D_{CO_2-CO} is calculated according to Eq. 5.9a, as recommended by Marrero and Mason:

$$D_{SiO-CO}[cm^2/s] \approx D_{CO_2-CO} = \frac{3.15 \times 10^{-5}\ T^{1.570}}{P\ \exp\left(\frac{113.6}{T}\right)} \qquad (5.9a)$$

where T is absolute temperature in the range 288 – 1800K and P is the total pressure in atmospheres. The diffusivities are inversely proportional to the total pressure P.

The theoretical expression for the diffusivity of gas 1 in gas 2 is given by the following expression (e.g. Present 1958, p. 55):

$$D_{12} = \frac{3}{8} \left(\frac{\pi k}{2m^*}\right)^{0.5} \frac{k}{\pi (d_{12})^2} \frac{1}{P} T^{1.5} \qquad (5.9b)$$

where $m^* = m_1 m_2/(m_1+m_2)$ is the reduced mass of a pair of molecules and m_1 and m_2 are the molecular masses, k is the Boltzmann constant, $d_{12} = (d_1+d_2)/2$ and d_1 and d_2 are the diameters of the molecules treated as rigid elastic spheres, P is the total pressure of the gas mixture and T is absolute temperature. Eq. 5.9b reveals two important features associated with the diffusivity, that is, proportional to $T^{1.5}$ and inversely proportional to the total pressure. Eq. 5.9b does not account for the small composition dependence of the diffusivity, cf. Appendix A4.

The formation of SiO and CO_2 is supposed to take place according to the reaction

$$SiO_2 + CO = SiO + CO_2 \qquad (3.9)$$

The rate expression for the flux of SiO away from the SiO_2-surface due to diffusion is:

$$J_{SiO} = D_{SiO-CO} \frac{dC_{SiO}}{ds}$$

$$= D_{SiO-CO} \frac{\Delta P_{SiO}}{R \, T \, \Delta s} \qquad (5.10)$$

Assuming equimolar formation of SiO and CO_2, the SiO pressure may be expressed in terms of the CO pressure and the equilibrium constant, K_4, of reaction (3.9), viz.:

$$P_{SiO} = P_{CO_2} = \left(K_4 \, P_{CO}\right)^{0.5} \qquad (5.11)$$

If reaction (3.9) is controlled by diffusive transport of SiO and CO_2, then equilibrium according to reaction (3.9) is established on the silica surface. Assuming that P_{SiO} is virtually zero at some distance, Δs, away from the silica surface, due to the dilution of the product gas, the driving force for diffusion may be approximated to the equilibrium pressure of SiO, that is, ΔP_{SiO} is given by Eq. 5.11. This gives:

$$J_{SiO} = D_{SiO-CO} \frac{\left(K_4 \, P_{CO}\right)^{0.5}}{R \, T \, \Delta s} \qquad (5.12)$$

Furthermore, the diffusivity of SiO in CO, D_{SiO-CO}, is inversely proportional to the total pressure, which in this case is the CO pressure:

$$J_{SiO} = \frac{D'_{SiO-CO}}{P_{CO}} \frac{\left(K_4 \, P_{CO}\right)^{0.5}}{R \, T \, \Delta s} \qquad (5.13)$$

D'_{SiO-CO} and Δs are assumed to be independent of pressure, thus at constant temperature, the following rate expression is obtained.

$$J_{SiO} = const. \; P_{CO}^{-0.5} \qquad (5.14a)$$

That is, the rate should be inversely proportional to the square root of the CO pressure. On a log-log scale the rate as function of the CO pressure would describe a straight line with slope -0.5. It is seen in Fig. 5.11 that region IV fulfils the -0.5 slope requirement. Hence, in this rather limited region IV, the

reaction rate could be controlled by the diffusion of product gases away from the silica surface.

The rate of weight loss from the silica tubing in dependence of temperature was recorded in the low pressure end of region IV, $P_{CO} = 0.267$ bar, and an apparent AE of 302 kj/mol was calculated (cf. Fig. 5.8). Now, if the rate was solely controlled by gaseous diffusion of product gases one would expect an apparent AE of about 253 kj/mol, that is one half the enthalpy of reaction (3.9), since the contribution from the activation energy of gaseous diffusion is small. The observed response in rate, is thus of similar magnitude as expected if gaseous diffusion was rate controlling.

What would the expected rate of weight loss be, if the rate was controlled by gaseous diffusion of product gases from the silica surface into the bulk gas? Consider the geometry of the system as given in Fig. A3.1. It is assumed that equilibrium concentrations of SiO and CO_2, are established on the silica surface according to reaction (3.9). Furthermore, the diffusive path is taken to be the distance from the silica surface to the inner surface of the graphite heating element. The concentration of product gases at the graphite surface are assumed to be 0, thus the concentration gradient equals the equilibrium concentration of product gases at the silica surface. The rate of molar transport of the gaseous species may be calculated from the following general expression:

$$\frac{dn_i}{dt} = \frac{2\ \pi\ l\ D_i\ \Delta P_i}{\ln\left(\frac{r_2}{r_1}\right)\ R\ T} \qquad (5.14b)$$

In this case $dn_i/dt = dn_{SiO}/dt = dn_{CO_2}/dt$ and D_i is the diffusivity of SiO and CO_2, respectively, in CO, given by Eq. 5.9a. $\Delta P_i = P_{SiO} = P_{CO_2}$, that is, the equilibrium pressure of product gases at the silica surface. r_1 and r_2 are the radius of the silica tube and graphite heating element, respectively, while l is the length of the silica tube (cf. Fig. A3.1). Given a temperature of 1575°C and a CO pressure of 0.4 bar (which is well within region IV, Fig. 5.11), the corresponding equilibrium pressures of SiO and CO_2, respectively, are 7.3×10^{-4} bar. These assumptions yield an expected rate of weight loss, as calculated from Eq. 5.14b, of 7.5 mg/min. That is, about a factor of 7 larger than the observed

rate, which indicates that the rate controlling step in this case is not likely to be the diffusion of product gases.

5.2.4. A model for chemical reaction control

Region II in Fig. 5.11 shows a marked slope of +0.5, which is opposite to the expectations based on the assumptions of gas diffusion. Ruling out also the rate control due to gas flow, chemical reaction control is moved into focus.

Assuming that the total reaction is adequately described by reaction (3.9) the following tentative reaction mechanism is put forward.

Adsorption of CO on the SiO_2 surface:

$$CO(g) = CO(ad) \qquad\qquad (5.15)$$

"Rearrangement" (breaking Si-O bonds) on the silica surface producing adsorbed CO_2 and SiO respectively:

$$SiO_2(s) + CO(ad) = CO_2(ad) + SiO(ad) \qquad\qquad (5.16)$$
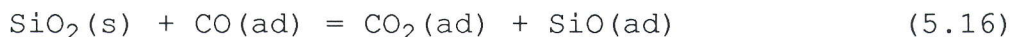
Desorption of CO_2 and SiO, that is, the gasification step:

$$SiO(ad) \xrightarrow{k_3} SiO(g) \qquad\qquad (5.17)$$

$$CO_2(ad) \xrightarrow{k_4} CO_2(g) \qquad\qquad (5.18)$$

It is assumed that reactions (5.15) and (5.16) are fast, hence at equilibrium. Expressed in terms of concentration of adsorbed species, C, the following expressions are obtained:

$$C_{CO(ad)} = K_5 \, P_{CO} \qquad\qquad (5.19)$$

$$C_{CO_2(ad)} \, C_{SiO(ad)} = K_6 \, C_{CO(ad)} \qquad\qquad (5.20)$$

K_5 and K_6 are the equilibrium constants of reaction (5.15) and (5.16) respectively.

The gasification steps, reaction (5.17) and (5.18) are assumed to be slow and hence rate determining. That is, the rate of formation of SiO and CO_2, respectively, may be expressed:

$$\frac{dn_{SiO}}{dt} = k_3\, C_{SiO(ad)} \qquad\qquad (5.21)$$

$$\frac{dn_{CO_2}}{dt} = k_4\, C_{CO_2(ad)} \qquad\qquad (5.22)$$

Assuming that k_3 and k_4 are of similar magnitude and much larger than their reverse, and furthermore that SiO and CO_2 are adsorbed in equal amounts, the following expression is obtained for the rate of consumption of SiO_2:

$$-\frac{dn_{SiO_2}}{dt} = \frac{dn_{SiO}}{dt} = \frac{dn_{CO_2}}{dt} = k_3\, C_{SiO(ad)} = k_4\, C_{CO_2(ad)} \qquad (5.23)$$

Let $k_3 = k_4 = k$ and $C_{SiO(ad)} = C_{CO_2(ad)}$, this gives:

$$-\frac{dn_{SiO_2}}{dt} = k\, C_{SiO(ad)} = k\, C_{CO_2(ad)} \qquad\qquad (5.24)$$

Combining with Eqs.5.19 and 5.20, the following expression for the concentrations of SiO and CO_2 adsorbed is obtained:

$$C_{SiO(ad)} = C_{CO_2(ad)} = \left(K_5\, K_6\, P_{CO} \right)^{0.5} \qquad\qquad (5.25)$$

Combining with Eq. 5.24 gives the expected rate of silica consumption in terms of the CO pressure:

$$-\frac{dn_{SiO_2}}{dt} = k\, \left(K_5\, K_6\, P_{CO} \right)^{0.5} \qquad\qquad (5.26)$$

That is, if desorption of SiO and CO_2 is the rate determining step, the rate of gasification of silica would be proportional to the square root of the CO pressure. Thus, region II of Fig.5.11 may be chemically controlled by the desorption of SiO and CO_2 respectively.

It is seen from Fig. 5.11, however, that below 0.007 bar CO, region I, the rate of weight loss does not decrease as pronounced as predicted by the $(P_{CO})^{0.5}$ dependence. The observed rate of

weight loss from the silica tube at vacuum conditions (5×10^{-5} mbar) was 0.25 mg/min (cf. Table A2.13), thus it is likely that region I is controlled by the thermal decomposition of silica:

$$SiO_2(s) = SiO(g) + \frac{1}{2} O_2 \qquad (1.1)$$

The processes of decomposition (1.1) and reaction with CO (3.9) are assumed to take place in parallel.

At CO pressures above 0.5 bar (region V, Fig. 5.11) the rate is seen to be virtually independent of the CO pressure. If the interaction between silica and CO is correctly described in terms of an adsorption/desorption mechanism, one would expect that the silica surface became saturated with respect to adsorbed CO at some CO pressure. The rate of desorption would, accordingly, become independent of CO pressure at pressures beyond saturation. This is consistent with the observed behaviour in region V. Thus, one may say that the rate changes from proportional with $(P_{CO})^{0.5}$ (rate controlled by desorption) to independent of CO pressure (consistent with saturation of silica surface with respect to adsorbed CO).

Claiming chemical reaction control in region V, would be in accordance with the observations of Schwerdtfeger (1966) and Ozturk and Fruehan (1985), respectively. They suggested that the rate of reaction (3.9) was controlled by "chemical kinetics on the silica surface" (cf. Paragraph. 3.3.2).

There are, however, several objections to the above interpretation: First, the existence of region IV, where the rate is seen to decrease with increasing CO pressure until it becomes independent in region V. Second, the rate was found to increase in the high pressure part of region II, when a gas flow was generated in the surroundings of the silica tube (cf. Fig 5.10), which indicates that the rate is not entirely chemically controlled. And, finally, the apparent AE measured at 0.100 bar CO was found to be 483 kj/mol in the low temperature range and 325 kj/mol in the high range (cf. Fig. 5.7), which indicates that the nature of the rate controlling step changes with temperature. E.g., a decrease in AE with increasing temperature is expected when the rate determining process is changed from a chemically controlled process to a process where gas diffusion becomes rate controlling.

However, an adsorption/desorption mechanism seems to be the most reasonable explanation, and the above objections must be left unexplained for the time being.

5.2.5.   Conclusions

With reference to Fig. 5.11 the following rate determining processes are suggested to describe the interaction between SiO_2 and CO (reaction (3.9)) at ~1575°C. The interpretations are based on the results obtained from a silica tube suspended concentrically inside a graphite tube (heating element) with closed bottom.

Region I: P_{CO} < 7 mbar. The reaction with CO becomes less dominant, as the CO pressure is decreased below 7 mbar, indicating that the rate becomes dominated by the thermal decomposition of silica.

Region II: 0.007 < P_{CO} [bar] < 0.100. Controlled by chemical reaction on the silica surface. A tentative proposal for the rate controlling step is the simultaneous desorption of CO_2 and SiO.

Region III: 0.100 < P_{CO} [bar] < 0.267. The silica surface becomes saturated with respect to adsorbed CO.

Region IV +V: P_{CO} > 0.267 bar. The silica surface is saturated with respect to adsorbed CO, and rate is, accordingly, independent of CO pressure.

6. REACTIONS WITH CRYSTALLINE SILICA

The experiments described in the preceding chapter have shown beyond doubt that solid silicon dioxide, when heated in a graphite-tube furnace in a carbon monoxide atmosphere, will react to form gaseous silicon monoxide plus carbon dioxide. It has also been surmised that this reaction represents the first step in the reaction between silica and carbon, although this has not been directly demonstrated since the mass change of the carbon source (the graphite heating element) could not be measured.

A more direct way to study the reaction between silica and carbon is to heat a more or less finely divided mixture of the two solid reactants. Experiments of this sort have been carried out by a number of investigators, as discussed in Chap. 3. Most of these experiments, however, have been done on finely ground and intimately mixed samples. From a kinetic point of view this is unfortunate for a number of reasons: It makes it difficult to distinguish between solid/gas reaction and solid/solid reaction (if any); the surface areas of the reactants are largely unknown, and gas phase transport within the sample or exchange between the sample and its surroundings are difficult to assess because of the narrow interspaces between grains. Furthermore, in most of the previous investigations, one or at most a few specific experimental conditions have been used, with little attempt at systematic variation of reaction parameters such as grain size, reaction geometry, and gas pressure.

For these reasons, the present experiments were performed with mixtures of coarse grains of silica and graphite, of known grain sizes, loosely packed in graphite crucibles. Most of the runs were done at a fixed temperature, with systematic variation of the carbon monoxide pressure in the furnace atmosphere.

6.1. The influence of crucible design

The aim has been to elucidate the kinetics of the interaction by studying the rate of weight loss as a function of the carbon monoxide pressure. Ideally, every particle in the sample should be exposed to the same pressure and composition of the gas, including

product gases. With this in mind, it is clear that the design of the container (crucible) may also considerably influence the results.

Fig. 6.1 shows three different crucible designs which have been used in the present work. All of them were machined from graphite CS49, which is a pure, fine-grained, but porous graphite quality (cf. Section 4.7 and Fig. 4.8). The closed crucible (denoted type A) has no machined holes; accordingly, any exchange of reactant/product gases is forced to take place solely through the pores in the body of the graphite. The semi-open crucible (type B) has additional machined holes in the lid of the crucible, while the open crucible (type C) is perforated with 0.5 mm holes in the bottom and side wall of the crucible cup in addition to six holes in the crucible lid. The type C crucible is believed to provide easy access for reactant/product gases.

Type A (closed)   Type B (semi open)   Type C (open)

Suspension   Lid   Crucible cup   Cross-section lid   20 mm
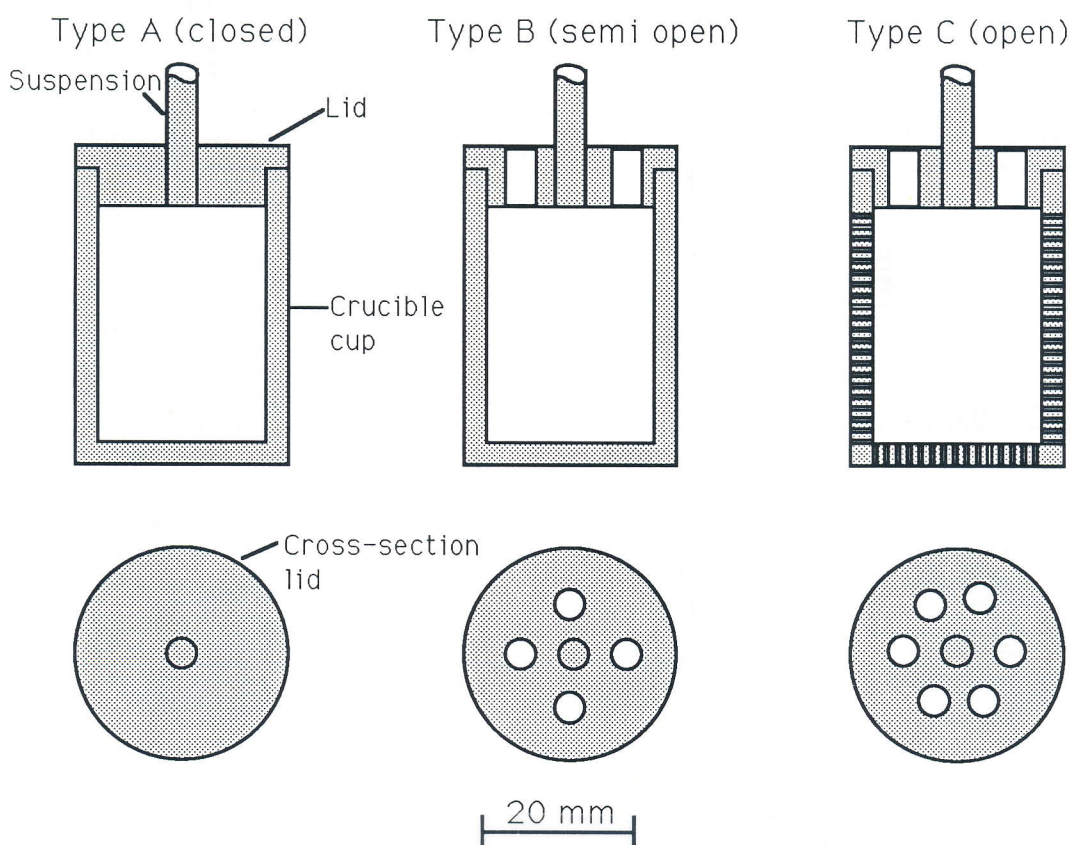
Fig. 6.1. Schematic drawing of the three different graphite crucibles (CS49-graphite) applied in this investigation. The crucible cup of type C is perforated with 0.5 mm holes.

The material of the crucibles is the same as the graphite used as reactant. Hence the crucible may also take part in the

reaction; this is particularly so in experiments with silica grains only (no graphite grains) in the charge.

An illustrative example of how crucible design affects the observed rates is given in Fig. 6.2. The figure shows the observed rates of weight loss in dependence of CO pressure for quartz/graphite mixtures contained in the three different graphite crucibles described in Fig. 6.1. The observed rates for the closed crucible (run 24) and open crucible (run 26), solid curves, are to be compared directly as they were performed at 1558°C with identical quartz/graphite mixtures. At pressures above 0.5 bar the sequence of the curves is as expected, with the rate of weight loss from the open system (run 26) larger than that from the closed system (run 24). At CO pressures below 0.4 bar, on the other hand, the rate of weight loss from the closed crucible greatly exceeds that from the open one. This rather unexpected feature of the curves must be left un-explained for the time being; the main point of Fig. 6.2 is to demonstrate that the geometry of the container has a profound effect both on the reaction rate and on its variation with the CO pressure.

Run 20 with the semi-open crucible was done with a slightly different charge mix and at a slightly higher temperature (1570°C), thus it should not be used for quantitative comparison, but the general trend fits in with that of the two other curves.
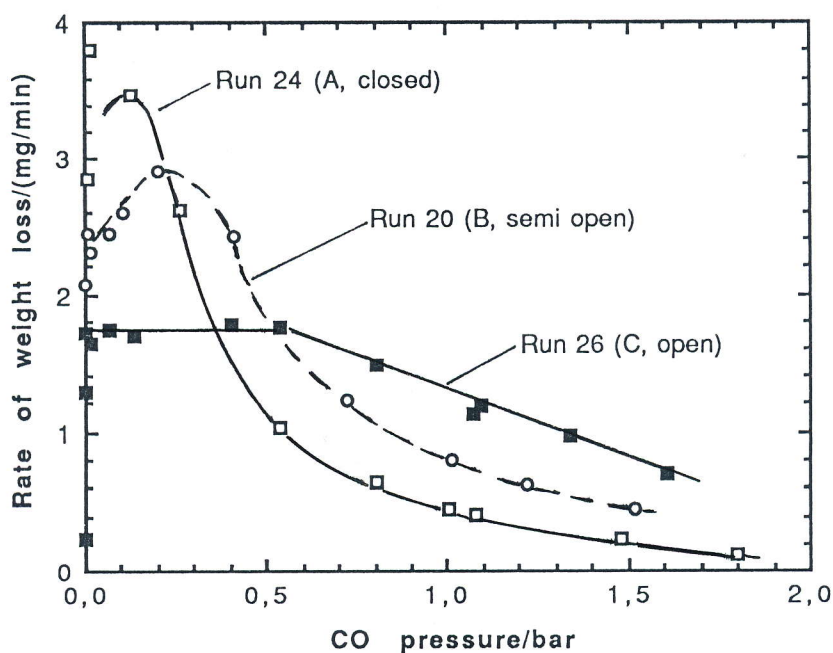
Fig. 6.2. Illustrative example on how crucible design affects the rate of weight loss of SiO_2/C-charges against ambient CO pressure. The letters A, B and C refer to the crucible types given in Fig. 6.1.

The closed type of crucibles (type A) was used by Sigurjonsson (1986) who performed a large number of experiments with observation of the rate of weight loss in dependence of the CO pressure Some further comments on his work are given below, Paragraph 6.2.2.

In the first part of the present chapter (Section 6.2), experiments with semi-open (type B) crucibles are reported. As the work progressed, however, it was increasingly felt that easy exchange of gas between the sample and the furnace atmosphere would be advantageous, and thus that the open (type C) crucible is the most favourable. This type, then, has been used in the final series of experiments, reported in Section 6.5.

6.2.   Quartz plus carbon in pure carbon monoxide

As indicated in the heading, the characteristic features of these experiments are that charges were made up with silica in the form of quartz, and that the furnace atmosphere contained carbon monoxide only. The temperature during the runs was kept at 1570°C. It is clear from the discussions in Section 1.3 and in Chapter 2 that at this temperature, a slow transformation of quartz to cristobalite will take place, but this transformation was not taken into account in the runs of the present section.

The grain size of the quartz was between 1.00 and 1.19 mm, while carbon was used in the form of graphite with grain size between 0.105 and 0.177 mm. The semi-ope "type B" graphite crucible was used. The crucible was freely suspended from the balance into the graphite tube furnace. The temperature was measured by the automatic pyrometer while the holes in the lid served as targets offering black body conditions. Standard procedure for each run was evacuating the furnace to approximately 5×10^{-5} mbar and subsequently heating to about 1000°C. The furnace and sample were degassed at 1000°C for at least one hour before admitting carbon monoxide and raising the temperature to the desired level.

Please note that all experiments referred to in this chapter are identified by a run number, and all relevant informations on

experimental parameters, including weight and rate data, are tabulated for each run in Appendix A2.

6.2.1.   Reaction to completeness

In the initial runs the aim was to follow the weight change of oxide plus carbon at constant temperature and gas pressure until complete reaction (that is, constant weight). Initially it was thought that the over-all reaction would correspond to the equation

$$SiO_2 + 3C = SiC + 2CO \qquad\qquad (1.12)$$

It was soon found, however, that the weight loss actually observed was considerably larger than corresponding to this equation, and in fact that little or no silicon carbide had been formed. Thus the reaction corresponded more closely to the equation

$$SiO_2 + C = SiO + CO \qquad\qquad (1.7)$$
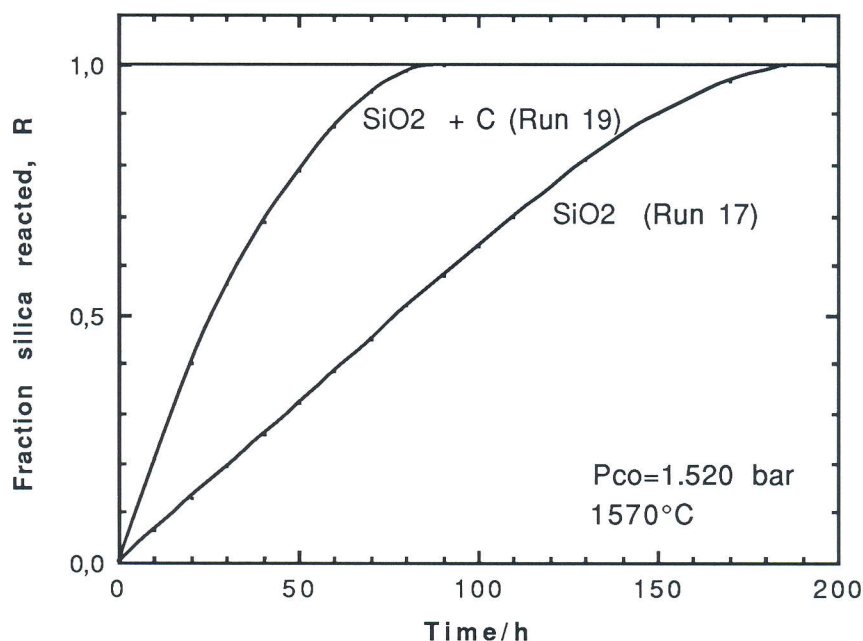
Fig. 6.3. Fraction silica reacted, R, as a function of time for two runs at 1570°C and 1.52 bar CO. Run 17: 1.022 g quartz grains only. Run 19: 0.721 g quartz grains plus 1.255 g graphite powder. Both runs in a semi-open ("type B") graphite crucible.

In order to study explicitly the rate of this reaction, the reaction parameters were chosen so that silicon carbide would not be thermodynamically stable and thus could not be formed. From Fig. 1.6 is seen that this will be the case at a temperature of, e.g. 1514°C and $P_{CO} > 1.0$ bar. The slightly higher temperature of 1570°C and $P_{CO} = 1.5$ bar also fulfil the requirement and were chosen for the experiments.

The results of two such experiments are shown graphically in Fig. 6.3. In the first of these (run 17) the charge consisted of 1.022 quartz of the grain size specified above, and no graphite powder. In the other (run 19) the charge consisted of 0.721 g quartz grains mixed with 1.255 g graphite powder. In both cases the total weight loss observed corresponded quite closely to that expected for the above reaction (1.7). The curves of Fig. 6.3 were previously presented in the publication together with Bentsen et al. (1985); they are repeated here as a basis for the discussion in Paragraph 6.2.3.

6.2.2. Rate as function of CO pressure

Experiments of the type shown in Fig. 6.3, in which a reaction is followed to completeness at constant temperature and gas pressure (or in a vacuum), have been quite common in work on the kinetics of reactions with solids. It appears, however, that the kinetic information to be extracted from this sort of curves is rather limited. It was felt that more information could be derived by investigating the rate (that is, the derivative of the curve for weight versus time) as a function of the carbon monoxide pressure, similar to what has been described in Chapter 5 for the silica glass tube.

The reaction temperature again was chosen at 1570°C. At this temperature, lowering the carbon monoxide pressure substantially below 1.5 bar brings the system into the region where silicon carbide is thermodynamically stable and thus in principle could be formed, see Fig. 1.6. Experimentally, however, no silicon carbide was detected in the graphite residue even after prolonged runs at fairly low carbon monoxide pressures. This is a consequence of the kinetics of the initial reaction, as will be further discussed in the next paragraph.

Fig. 6.4 shows the results of two runs with variation of the CO pressure. Run 18 was done with a charge of 3.066 g quartz only, while run 20 was done with 3.066 g quartz plus 5.335 g graphite, both of the grain sizes specified above. The CO pressure was decreased or increased stepwise in a random sequence to avoid systematic error. Each chosen pressure was kept constant for about half an hour, and the rate of weight loss was determined from the slope of the recorder curves. Fig. 6.4 shows these rates as functions of the CO pressure on log log scales.
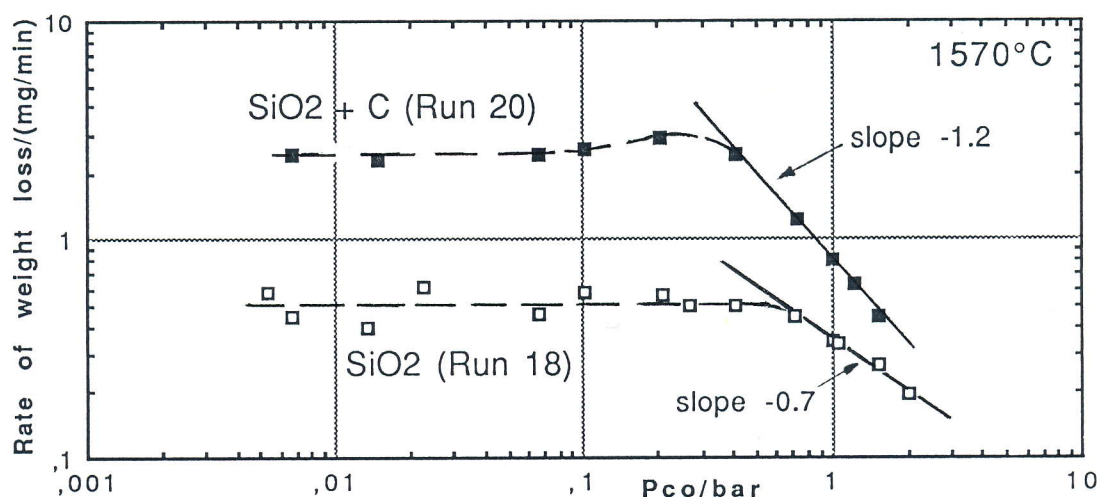
Fig. 6.4. Rate of weight loss for two runs at 1570°C, plotted as functions of CO pressure (log-log scales). Run 18: 3.066 g quartz grains. Run 20: 3.066 quartz grains plus 5.335 g graphite powder. Both runs in a semi open ("type B") graphite crucible.

6.2.3.   Discussion of Section 6.2

First some words about the formation or non-formation of silicon carbide. Initially we considered the reaction

$$SiO_2 + C = SiO + CO \qquad\qquad (1.7)$$

When the CO pressure is kept high, the SiO pressure of this reaction at equilibrium will be low. As the CO pressure is reduced, the SiO pressure will increase. With reference to Fig. 1.6 it is found that a temperature of 1570°C and a CO pressure of 1.0 bar would give an equilibrium pressure of SiO from reaction (1.7) of about 2×10^{-2} bar, amply, sufficient to produce silicon carbide by the reaction

$$SiO + 2C = SiC + CO \tag{1.8}$$

Based on this line of thought, the CO pressure in runs 17 and 19 (Fig. 6.3) was kept at about 1.5 bar to avoid the formation of SiC.

There is no reason to believe, however, that reaction (1.7) reaches equilibrium or anything near equilibrium under our experimental conditions, considering that formally it is a reaction between two solid reactants. It was pointed out repeatedly above that, most probably, the initial step is the reaction with the carbon monoxide gas:

$$SiO_2 + CO = SiO + CO_2 \tag{3.9}$$
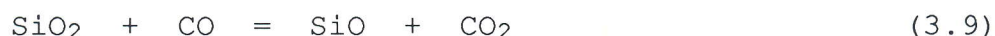
According to the equation, SiO and CO_2 are formed in equimolar amounts. Assuming that reaction (3.9) goes to equilibrium with $P_{SiO} = P_{CO_2}$, this gives at 1570°C and 1 bar CO, $P_{SiO} \cong 1 \times 10^{-3}$ bar (see Fig. 3.1). This is about a power of ten lower than required for the formation of silicon carbide.

When carbon is present at close distance from the silica surface, the carbon dioxide first formed may be rather quickly reduced again by the reaction

$$CO_2 + C = 2CO \tag{1.4}$$

As a consequence, the effective SiO pressure from reaction (3.9) may increase somewhat, but still it is a long way to go before it increases to the point where SiC can be formed. This reaction mechanism is the reason why silicon carbide was not formed in the runs 18 and 20 (Fig. 6.4), even though these were conducted down to rather low carbon monoxide pressures.

$$-o\ O\ o-$$

Next we turn to the question of the rate-determining step. We assume that the reaction (3.9) and the subsequent (1.4) are the reactions we have been studying. There are then a number of separate steps to be considered as possible contributors to the over-all reaction resistance:

—   Reaction (3.9) on the silica surface.

—   Reaction (1.4) between CO_2 and graphite.

—   Gas diffusion of CO_2 through CO, from its origin at the
     silica surface to the nearest carbon surface.

—   Gas diffusion of SiO out of the crucible.

Let us consider the assumption of a hindered reaction on the silica surface first. If this is rate determining, then the reduction of the particle radius should go linearly with time. Assuming an initial radius r_0 and that the time for complete reaction is τ, then a plot of r/r_0 versus t/τ should give a straight line as shown in Fig. 6.5, taken from Levenspiel (1972). Alternatively we may assume that the rate-limiting step is gas diffusion, which we may think of as diffusion through a spherical shell of gas with constant outer radius, surrounding each silica particle. It is then readily shown from the solution of Fick's first law for spherical symmetry that the rate, expressed in terms of dr/dt, at first will be fairly low, and then will increase as r decreases, approaching infinite as r goes to zero. The curve for r/r_0 will have the shape shown in Fig. 6.5 (even if Levenspiel's model for gas film diffusion is not directly analogous to the present case).
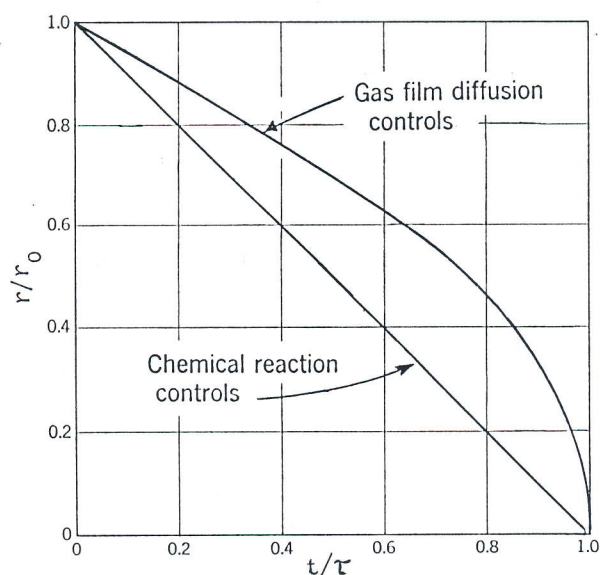
Fig. 6.5. Progress of reaction of a single spherical particle with surrounding fluid. r_0 is initial radius of particle, and τ is time to complete reaction. The straight line is characteristic for processes controlled by a chemical reaction on the particle surface. The upper solid curve is characteristic for gas film diffusion being rate controlling. Mainly after Levenspiel (1972).

From Fig. 6.3 it is seen that the time for complete reaction, τ, is 185 h for run 17 and 90 h for run 19, respectively. It is further noted that the fraction reacted, $R = 1 - (r/r_0)^3$, from which follows that $r/r_0 = (1 - R)^{1/3}$. The results of Fig. 6.3 thus recalculated are shown in Fig. 6.6. It is seen that these curves definitely do not correspond to chemical reaction control on the silica surface: they indicate instead that gas diffusion may be rate controlling. Deviations occur particularly for large degrees of reaction; it is seen that for r/r_0 approaching zero, the slope dr/dt of the theoretical curve in Fig. 6.5 goes towards minus infinity while the curve of run 19 in Fig. 6.6 goes to zero with finite slopes. This is readily explicable, however, since in the terminal stages of this reaction some other mechanism, such as the chemical reaction on the silica surface, would be expected to take over as rate-controlling.
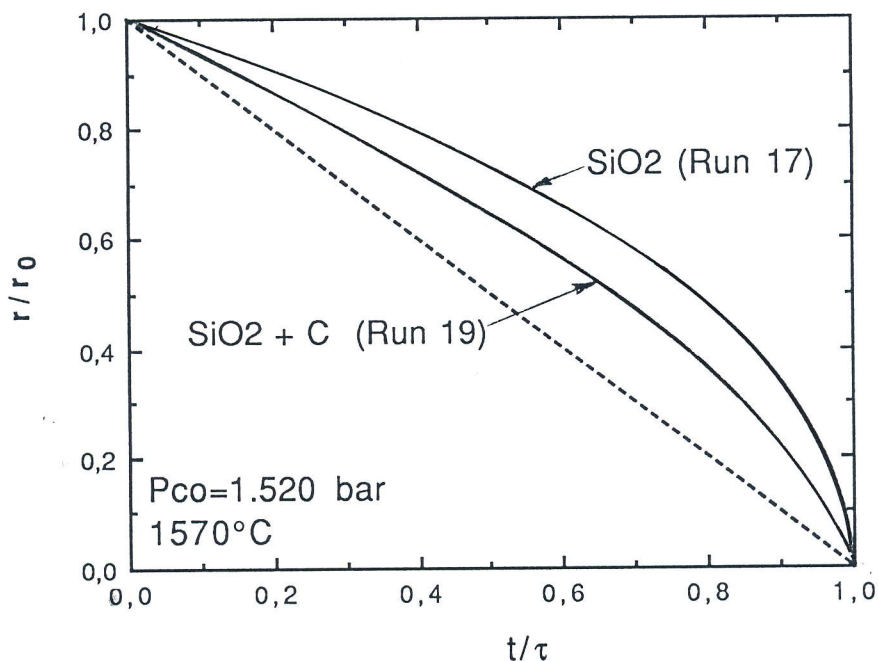
Fig. 6.6. The results of Fig. 6.3 given as r/r_0 against of relative time t/τ. The upper curve (run 17) is for silica only and the lower curve (run 19) is for silica embedded in graphite powder. The dotted line represents expected progress of reaction if chemical reaction were rate determining.

Moreover, with reference to the run without addition of graphite powder (run 17) in Fig. 6.3, it is seen that the rate of silica consumption is strictly constant until almost 70 % of the silica is consumed. Speaking in terms of the surface area of silica it means that the rate is constant until the surface area of the silica is less than one-half the original area. This

certainly rules out chemical reaction control on the silica surface to be the rate determining step.

The other chemical reaction listed above is that between carbon dioxide and carbon, reaction (1.4). If this were rate determining, both of the runs (17) and (19) should show constant rate throughout when plotted as in Fig. 6.3, since the available carbon (graphite) surface hardly changes during the runs. Particularly run 19 shows nothing near a constant rate. For this and other reasons, reaction (1.4) is discounted as being rate determining.

Thus it appears that the rate of reaction in runs 17 and 19 has been controlled primarily by gas diffusion. Two such alternatives were indicated above: Diffusion of CO_2 from its origin at the silica surface to the nearest carbon surface, and diffusion of SiO out of the crucible. Since the diffusion path in the latter case is much longer than in the former, while the diffusivities are taken as nearly equal (section 5.2.2), we will assume that the diffusion of SiO is rate determining. Furthermore, we will use the results of run 17 for a semi-quantitative check on this assumption.

In order to calculate the expected rate for run 17, the following assumptions are made:

- The SiO pressure inside the graphite crucible is uniform and at equilibrium with the ambient CO-atmosphere according to reaction (3.9). (In the absence of carbon this is the largest SiO pressure attainable.)

- The SiO-pressure outside the crucible, in the bulk gas, is assumed to be zero.

- SiO diffuses only through the holes in the graphite lid.

Assuming equimolar formation of SiO and CO_2 (reaction (3.9)) the equilibrium pressure of SiO at 1.52 bar CO and 1570°C is 1.3 mbar (JANAF, 1985). The diffusivity of SiO in CO is taken to be equal to the diffusivity of CO_2 in CO, and is calculated according to Eq. 5.9a as recommended by Marrero and Mason (1972):

$$D_{SiO-CO} \approx D_{CO_2-CO} = \frac{3.15 \times 10^{-5} \ T^{1.570}}{P \ \exp \left(\frac{113.6}{T} \right)} \qquad (5.9a)$$

126

where D is expressed in cm^2/s and P in atm. Eq. (5.9a) refers to an equimolar binary mixture and is valid in the temperature range 15 to 1527°C. It is, however, assumed that Eq. (5.9) is also valid in the dilute range of CO_2 as well as at temperatures slightly above 1527°C.

An approximate value for D_{SiO-CO} at 1.52 bar CO and 1570°C is then calculated to be: D_{SiO-CO} = 2.65 cm^2/s. If SiO is diffusing only through the 4 holes (each of 0.4 cm diameter) in the graphite lid the diffusing area will be: A = $4\pi(0.2)^2$ = 0.503 cm^2. The lid is 0.8 cm thick, which is taken to be equal to the path of diffusion, s. Fick's first law of diffusion in the general form is:

$$J_i = \frac{dn_i}{A\ dt} = -\ D_i\ \frac{dc_i}{ds} \qquad (5.8)$$

By expressing the concentration, c_i, in terms of the partial pressure of SiO, the rate of SiO diffusing out of the crucible is:

$$\frac{dn_{SiO}}{dt} = -\ \frac{A\ D_{SiO-CO}}{R\ T}\ \frac{dP_{SiO}}{ds} \qquad (6.2)$$

$$= \underline{1.477 \times 10^{-8}}\ mol\ SiO/s$$

Furthermore, for every mole SiO formed by reaction (3.9) one mole of CO_2 is also formed. It is assumed that CO_2 does not enter the bulk gas but is consumed by the graphite according to the Boudouard reaction (1.4). This is confirmed experimentally: With reference to run 17 in Fig. 6.1 all of the silica was consumed, that is 1.0220 g. The corresponding weight loss of the graphite crucible was found to be 0.2015 g. Hence, the molar ratio between SiO_2 and C consumed was n_{SiO_2}/n_C = 1.01, indicating that practically all CO_2 produced was consumed by the graphite crucible.

The expected rate of weight loss is then calculated to be:

$$\frac{dw}{dt} = (M_{SiO_2} + M_C)\ \frac{dn_{SiO}}{dt} \qquad (6.3)$$

$$= 1.065 \times 10^{-6}\ g/s = \underline{0.064\ mg/min}$$

The observed linear rate for run 17 without addition of graphite powder (Fig. 6.3) was 0.131 mg/min; that is, of the same order of magnitude as calculated. This suggest that the assumption of SiO diffusion as the rate determining step may indeed be correct for this case.

It should be emphasized that the above calculation is based on several rather rough and approximate assumptions. In particular the assumption that diffusion is confined only to the holes in the lid cannot be strictly true. The crucible was made from a porous graphite (quality CS49), and it is well known, e.g., from work of Kvande et al.(1979) that considerable gas transport by diffusion takes place through the pores of this graphite. Thus the observed rate of weight loss would be expected to be somewhat larger than that calculated, as is actually the case.

$$- o \ 0 \ o -$$

Next we will turn to the dependence of the rate of weight loss on the applied carbon monoxide pressure, with runs 18 and 20 in Fig. 6.4 as the experimental examples. If the primary reaction is adequately described by Eq. (3.9), and if this reaction is at equilibrium with $P_{SiO} = P_{CO_2}$, we will have

$$P_{SiO} = (K_4 \ P_{CO})^{0.5} \tag{5.11}$$

where K_4 is the equilibrium constant of reaction (3.9) at the temperature in question. At constant temperature, the diffusivity is proportional to the inverse of the total pressure, which is identical to the pressure of CO in the present investigation. The diffusivity may then be expressed in terms of the CO-pressure viz.:

$$D_{SiO-CO} = \text{constant}/P_{CO} \tag{6.4}$$

Substituting Eq. 5.11 and 6.4 into Eq. 6.2 the following expression is obtained for the diffusive transport of SiO:

$$\frac{dn_{SiO}}{dt} = \text{constant} \times P_{CO}^{-0.5} \tag{6.5}$$

That is, the observed rate should be inversely proportional to the square root of the CO-pressure if SiO diffusion is rate

determining, and a plot of log rate versus log P_{CO} should give a straight line with slope -0.5. It should be added that the assumption of carbon dioxide diffusion as rate determining would lead to the same $(P_{CO})^{-0.5}$ dependence, hence this feature cannot be used to distinguish between the two alternatives. For reasons outlined above, however, rate control by SiO diffusion is considered the more probable.

It is seen (Fig. 6.4) that the inverse square root dependence of the lower curve (run 18) is reasonably well fulfilled in the range 0.6 to 2.0 bar (experimental slope -0.7). Hence, this simple approach still points in the same direction, namely SiO diffusion being the rate determining step. On the other hand, silica with addition of graphite powder (run 20, Fig. 6.4) has a more pronounced CO-pressure dependence than can be explained by the simple gas diffusion model. At CO-pressures below 0.5 atm the rate becomes nearly independent of the pressure, this will be discussed in more detail in Chapt. 7.

A number of further runs similar to run 20 were performed (listed as runs 21 to 26 in Appendix A2). They substantiated the general shape of the curve of run 20 in Fig. 6.4, although the reproducibility was not very good. Furthermore these runs are difficult to interpret, for reasons that will be made more evident throughout the remainder of this chapter. Hence it was chosen not to report on these runs in the main text.

Observations from a large number of similar runs are also available from the work of Sigurjonsson (1986). Examples of Sigurjonsson´s experimental curves are given by Motzfeldt (1988). They too show rather steep increase in rate with diminishing CO pressure, quite often with slopes of about -1.4 on a log-log plot, and then a region of more or less pressure-independent rate at lower pressures. Sigurjonsson´s experiments were done with closed crucibles (type A of Fig. 6.1), this does not make the interpretation any easier.

6.3.   Reaction in carbon monoxide mixed with argon

A change in the applied carbon monoxide pressure will affect the reacting system of silica plus carbon in several ways: The

situation is changed for all the relevant equilibria, cf. Fig. 3.2; the rate expected from chemical reaction control on the silica surface would change, cf. Paragraph 5.2.4; and above all, the rates of diffusion change since gas diffusivities are inversely proportional to the total gas pressure. This latter change, however, will be avoided if the carbon monoxide pressure is varied at constant total pressure. Conversely, the diffusivities may be varied at constant CO pressure by using different total pressures. Thus the desire to separate the diffusivity from the other variables led to the idea of using mixtures of carbon monoxide and an inert gas.

6.3.1. Preliminary experiments with gas mixing

The first experiments with mixed gases were performed by admitting the gases directly into the furnace enclosure. Using the electronic manometer attached to the furnace enclosure, the mixing ratio was easily determined from the pressures.

There is a serious snag in this procedure, however. As seen from Fig. 4.1, the thermobalance has a furnace compartment and a balance compartment, each of about equal volumes and connected by a flexible hose. After evacuation, when the first gas is admitted, it flows equally into the two volumes. When the second gas is admitted to the furnace compartment, however, the first will to a considerable extent be compressed into the balance compartment. Thus the gases in the two compartments will have different compositions, and none of them will have the composition aimed at by the experimentalist. Also, the actual composition in the furnace compartment, where the reaction takes place, will depend upon which gas is admitted first.

This effect, once one thinks about it, is so obvious that the first series of experiments may rightly be considered a blunder. Nevertheless, experimental proof of the effect is shown in Fig. 6.7. The upper curve shows the recorded rates of weight loss when gas mixtures were prepared by admitting argon first into the furnace chamber, while the lower curve shows the results when carbon monoxide was admitted first.
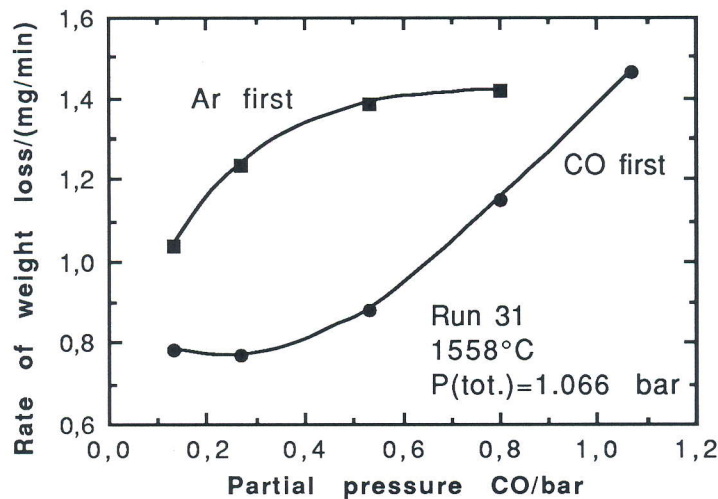
Fig. 6.7. Rate of weight loss of a quartz/graphite charge (run 31) in terms of partial pressure of CO at 1558°C and constant total pressure 1.066 bar (800 torr). Perforated graphite crucible is applied as charge container. The gas mixtures (Ar-CO) are prepared directly in the furnace chamber, and the upper curve illustrates the effect of admitting Ar first, while the lower curve shows the effect of admitting CO first.

6.3.2. Conclusion regarding gas mixing

The above experiments showed clearly the need for proper mixing of the gas. It was chosen to prepare the mixtures in advance, and the gas mixing equipment was developed which has already been described in Section 4.6. This was used throughout the remainder of the present work.

6.4. Effects of the phase transformation quartz — cristobalite

6.4.1. Problems of reproducibility

The first series of experiments with the gas-mixing equipment were conducted with charges of quartz plus graphite in the open "type C" crucibles. The intention was to investigate the effect of

varying CO partial pressure at 1558°C and a constant total pressure of 1.066 bar (800 torr). Each chosen gas composition was admitted to this total pressure, and the rate of weight loss was recorded for about one-half hour. Next the furnace was evacuated to about 1 mbar, and a new gas composition was admitted to the same total pressure.

The results of three similar but independent runs (32, 35 and 37) are shown in Fig. 6.8. It is immediately apparent that there is a severe lack of accordance between the results, and it appears that at least one experimental parameter is beyond control.
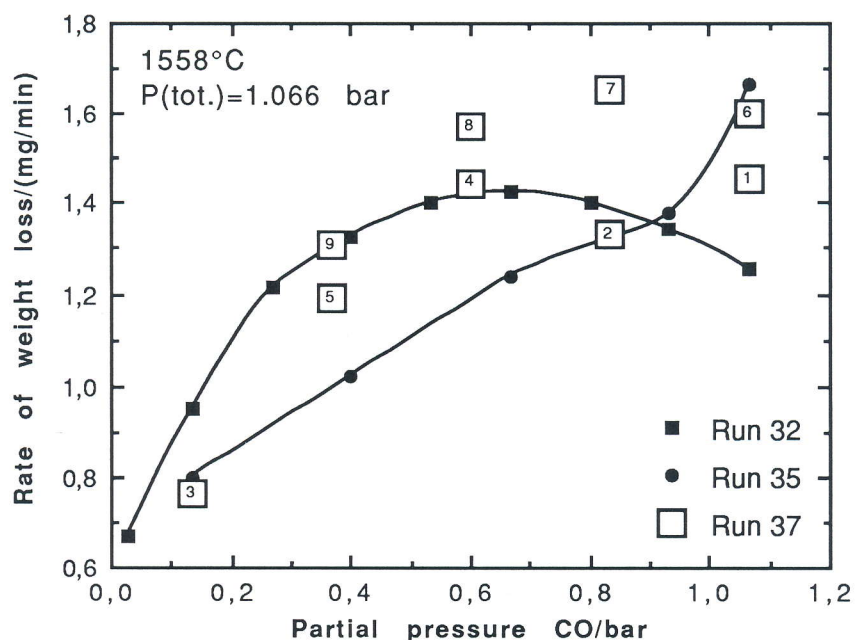
Fig. 6.8. Rates of weight loss for three independent runs (32, 35 and 37) with quartz/graphite charges in "open" crucibles at 1558°C, plotted as functions of the partial pressure of CO in CO-Ar mixtures with constant total pressure 1.066 bar (800 torr). Runs 32 and 35 were conducted with successively decreasing partial pressure of CO, while run 37 was conducted as numbered. Evacuation of furnace between each measurement of weight loss rate in all three runs.

We may consider first the fact that the reactants are continuously consumed during a run, this leads to decreasing surface area which in turn may lead to decreased rate of reaction. The mass loss during any one of these runs, however, is a fairly small fraction of the total amount of reactants. Furthermore, in run 37 of Fig. 6.8 the rate of weight loss has increased for consecutive runs at the same gas composition, see runs 1 and 6, 3 and 7, 4 and 8, etc. Thus the diminishing surface area cannot explain the scatter of the observations.

Next we turn attention to the fact that in these runs, silica was used in the form of quartz, and at 1558°C a transformation to cristobalite will certainly take place, most probably via the intermediate, amorphous phase. This continuous, reconstructive transformation may well affect the reactivity of silica and hence the rate of weight loss.

Finally we may also consider the fact that the furnace was every time evacuated to less than 1 mbar before admitting a new gas composition. Could this repeated evacuation affect the rate of reaction?

We will consider each of these effects in turn.

6.4.2. Phase transformation under constant pressure or vacuum

Both Klinger et al. (1966) and Khalafalla et al. (1972) postulated that the intermediate amorphous silica phase was the reactive phase in carbothermal reduction of quartz under vacuum conditions. As Khalafala only found small quantities of cristobalite in the discharge it was claimed that the rate of carbothermal reduction of quartz was controlled by its rate of transformation into the intermediate phase. That is, the rate of reaction was enhanced substantially as the intermediate phase was formed, and the rate of consumption of the intermediate phase was larger than its rate of transformation into cristobalite.

In order to test this assumption a quartz/graphite-charge was held at 1558°C in a vacuum (5×10^{-5} mbar) for 1.8 h (run 36). XRD-analysis confirmed the formation of cristobalite but the recorded rate of weight loss was strictly constant throughout the reaction period.

Another run conducted with quartz particles only in the open graphite crucible (run KR 4) was held at 1558°C for 5 h in a vacuum (5×10^{-5} mbar). Although XRD-analysis of the discharge demonstrated that most of the quartz was transformed into cristobalite, the recorded rate of weight loss stayed practically constant during the five hours.

A last run (run KR 3) was performed with only quartz particles, as above, keeping the sample for 7 h at 1558°C in 1.066 bar (800 torr) CO. XRD-examination of the discharge confirmed a

substantial transformation of quartz into cristobalite. In spite
of this, the recorded rate of weight loss was constant throughout
the reaction period.

That is, under constant vacuum conditions or at constant CO-
pressure, the rate of reaction does not seem to be influenced by
the continuous transformation of quartz into cristobalite via the
intermediate transition phase. Hence, the lack of reproducibility
is believed not to be caused by continuous phase transformations.

6.4.3.   Effect of intermittent evacuation

The first experiment, investigating the influence of repeated
evacuation and admittance of CO, was performed with a
quartz/graphite-charge (run 38). After subjecting the charge to
the standard degassing procedure, the temperature was raised to
1558°C and the CO pressure was adjusted to 1.066 bar (800 torr).
This pressure was kept constant for about 0.5 h while recording
the rate of weight loss of the charge. Thereupon the furnace was
evacuated below 1 mbar with subsequent admittance of CO up to
1.066 bar, and the rate of weight loss once again was recorded.
This procedure was repeated until the observed rate of weight loss
did not change significantly on further evacuation plus gas
admittance.
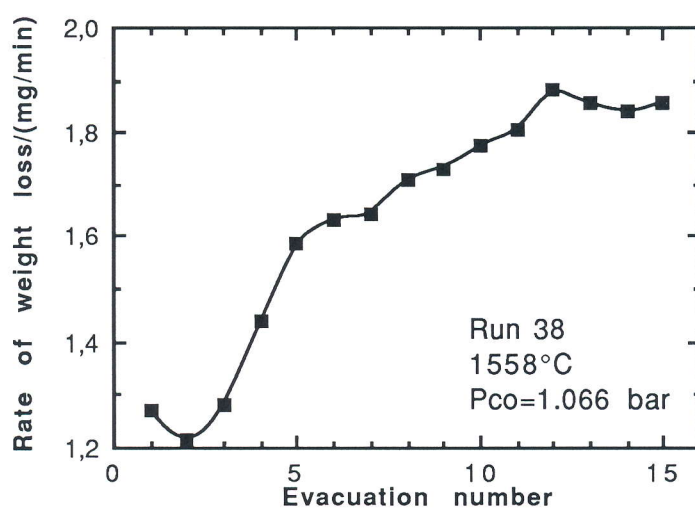
Fig. 6.9. Rate of weight loss of a quartz/graphite-charge, at
          1.066 bar (800 torr) CO and temperature 1558°C, in
          dependence of number of evacuations. Open ("type C")
          graphite crucible applied. "Between" every data point
          the furnace has been evacuated below 1.3 mbar (1 torr).

The results are given in Fig. 6.9. Every point in the graph represents the rate of weight loss of the charge at 1.066 bar CO and 1558°C, and "between" every point the furnace has been evacuated below 1 mbar. It is seen that evacuation has a rather pronounced effect on the rate; varying from 1.22 mg/min after the second evacuation to 1.88 mg/min after the twelfth evacuation. Furthermore, after the second evacuation the rate seems to increase rather steadily and levels out at about 1.86 mg/min.

This variation in rate is of the same order of magnitude as the scatter in experimental data in Fig. 6.8. Hence it is believed that the lack of reproducibility has its origin in the effect of evacuation on the rate of weight loss.

Fore comparison the same sort of experiment should be done with silica in the form of cristobalite. For this purpose, cristobalite was synthesized by firing quartz grains for 5 days at 1430°C in an alumina crucible in air at ambient pressure (runs KR 5 and KR 6). XRD confirmed that the quartz was essentially transformed into cristobalite (cf. Fig. 2.2).
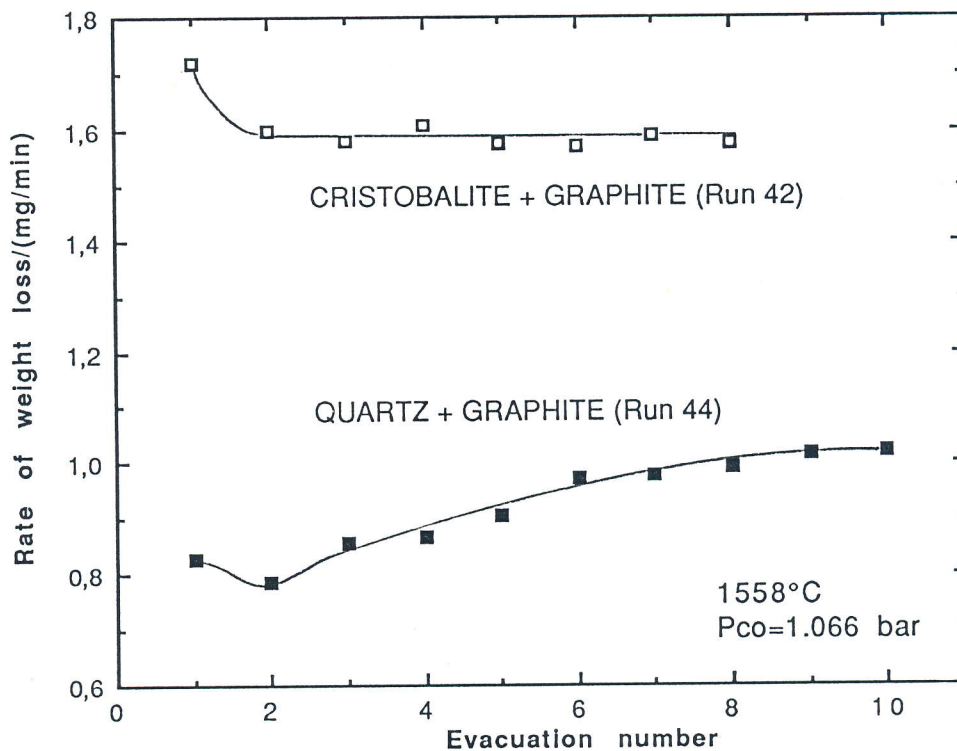
Fig. 6.10. Rate of weight loss of a quartz/graphite-charge (run 44) and a cristobalite/graphite-charge (run 42), at 1.066 bar (800 torr) CO and temperature 1558°C, in terms of number of evacuations. Perforated graphite crucible applied. "Between" every data point the furnace has been evacuated below 1.3 mbar (1 torr).

In previous runs with evacuation, serious problems with the control and measurement of temperature had occurred because of SiO condensing in the optical path for pyrometry. It was thought that this problem would be lessened by using less silica in the charge. For this reason, the first run with cristobalite (run 42) was done with an amount of silica only one-third of the amount of quartz used in the previous run. Apart from this, the experiment was conducted in exactly the same manner as described above. The results in terms of rate of weight loss are given in Fig. 6.10, upper curve. For the sake of comparison, an additional experiment (run 44) was conducted with quartz as the silica source, but reduced to one third of the former amount, thus being identical to the cristobalite charge in terms of mass. The results are given in Fig. 6.10, lower curve.

The rate of the upper curve, which resulted from the cristobalite/graphite-charge, are essentially independent of number of evacuations. That is, after the first evacuation the rate of weight loss is practically constant. The results from the quartz/graphite-charge, on the other hand, show the same characteristic behaviour as given in 6.9, although the magnitude of the rates is less because of the reduced amount of charge. The relative increase in the rate upon evacuation/re-filling is also somewhat less than in Fig. 6.9, but this merely suggests that the effect in itself may depend upon incidental circumstances such as the duration of each evacuation, etc.

The most striking difference between the two curves of Fig. 6.10 is that the observed rates with cristobalite are nearly a factor of 2 larger than the rates with quartz. This would seem to suggest that silica in the form of cristobalite is more reactive than the quartz. On the other hand, as reported above, it was found experimentally that the continuous transformation of quartz to cristobalite under constant conditions of pressure or vacuum does not have any effect on the rate of reaction. This seeming contradiction demands an explanation.

6.4.4. On the surface area

The enhanced rate with silica in the form of cristobalite is believed to be connected with the thermal history. When cristobalite is synthesized in a separate furnace it has to pass the displacive α-β-transformation at 272°C downwards when removed from that furnace, and upwards again during the heating in the actual run. The volume contraction, and the subsequent volume expansion as cristobalite goes from the α- to the β-modification, is rather pronounced, (cf. Fig. 1.2) and it is known to cause micro-cracks in the material. (It is interesting to note that Mitra (1977) found extensive fragmentation of the silica caused by the transformation from quartz to transition phase, cf. Section 2.1.) Thus the enhanced rate shown in Fig. 6.10 is believed to be caused by the formation of micro-cracks in the silica, which in turn increase the total surface area.
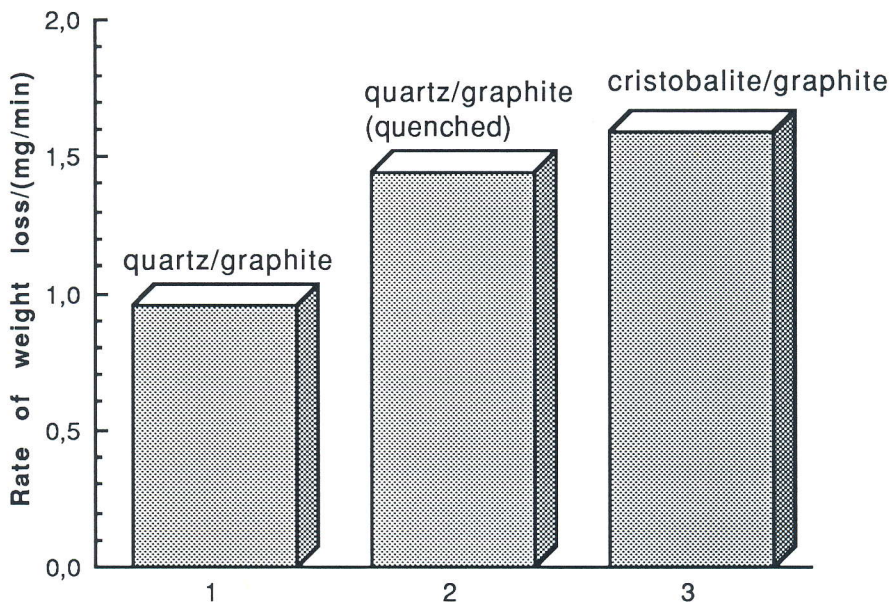
Fig. 6.11. Rate of weight loss of a quartz/graphite-charge (run 45) at 1.066 bar (800 torr) CO and 1558°C showing the rate before (column 1) and after (column 2) the charge has been allowed to cool down to roomtemperature. Column 3 is the rate of a corresponding charge but with cristobalite as the silica source (run 42). Open ("type C") graphite crucible applied.

This conclusion was corroborated by yet another experiment. A charge of quartz + graphite of the same composition and mass as in run 42 and 44 (Fig. 6.10) was held at 1558°C and 1.066. bar of CO

for 5.3 h (run 45) while recording the rate of weight change. The furnace was subsequently turned off, and the charge was allowed to cool to room temperature. Next it was again heated to 1558°C at a fairly high rate of heating. The results are illustrated in Fig. 6.11. It is seen that the cooling and subsequent re-heating caused the rate of weight loss to increase by nearly 50 %. The rate after re-heating is comparable to that obtained with cristobalite in the charge, cf. the column to the right in Fig., 6.11 which represents the upper curve in Fig. 6.10.

Further evidence was sought by measuring the specific surface areas of samples of the quartz and the cristobalite which were used to make up the charges prior to runs 44 and 42. The surface areas was measured by the BET method, and the results are given in Table 6.1. It is seen that the measured surface area of the cristobalite is a factor of 20 larger than that of quartz.

Table 6.1. The surface area per unit mass of the cristobalite (run 42) and the quartz (run 44) particles referred to in Fig.6.10. The particle size was the same for both silica sources: $0.513<d[mm]<0.710$. The area was measured by means of the BET-isotherm method using Kr as the adsorbing gas. (Measurements kindly performed by Mr. Olav Tronstad, at the Institute of Industrial Chemistry, NTH.)

Surface area [m^2/g]

QUARTZ	CRISTOBALITE
0.025 ± 0.008	0.50 ± 0.05

The increase in rate, on the other hand, amounted to not more than about a factor of 2. The discrepancy may be explained by assuming that a large part of the surface area measured by the BET method is present in the form of pores (or micro-cracks) and thus not available for the reaction.

This was substantiated by measuring the porosity of the cristobalite by means of a mercury porosimeter. The results in terms of pore size are shown in Fig. 6.12. It is seen that about 2/3 of the volume of total porosity is present as pores with less than 2 μm equivalent diameter. Considering that our assumed reaction mechanism demands gas phase diffusion of SiO and CO_2 away

138

from the reacting surface, it may safely be concluded that
diffusion through pores or cracks of this small size will not
contribute materially to the observed reaction rate. On the other
hand, the cracking or porosity of the cristobalite affords a very
likely explanation of its increased reactivity relative to quartz.
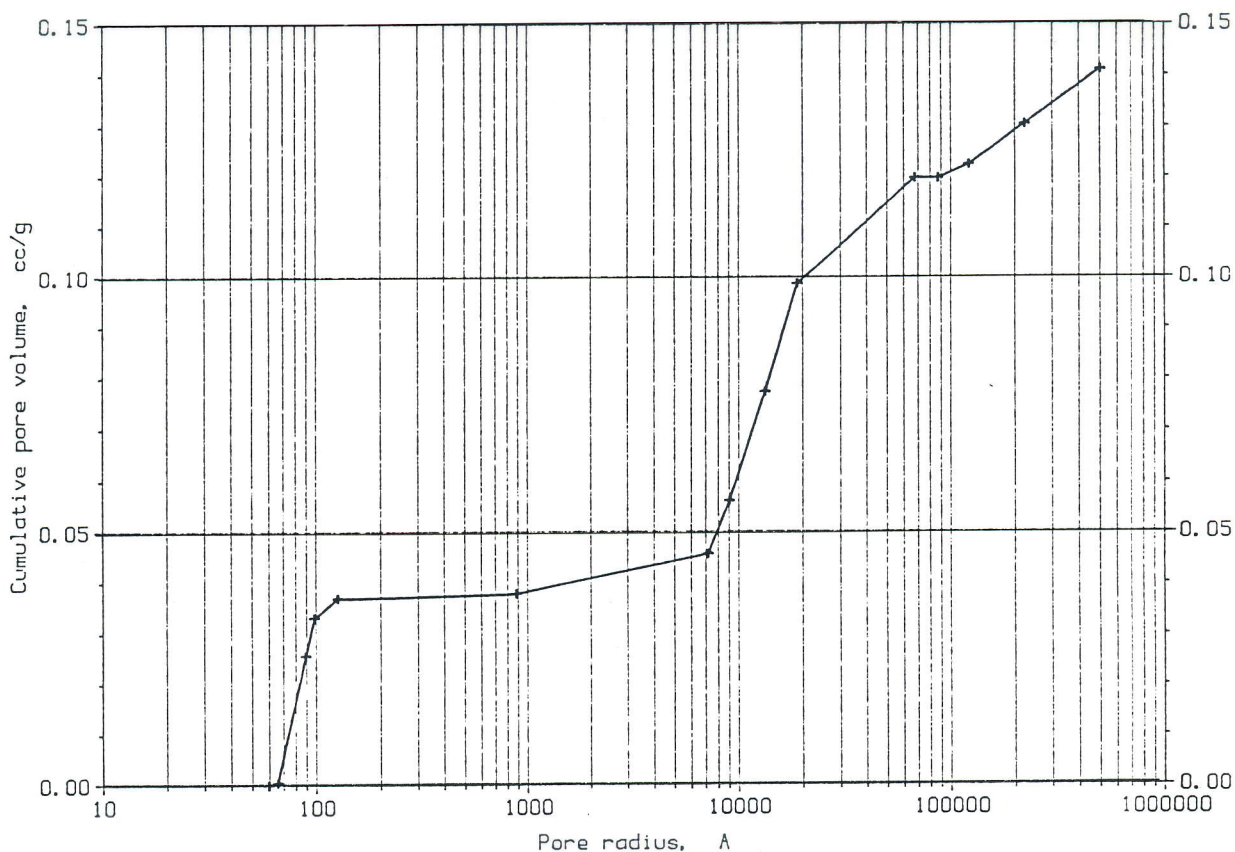
Fig. 6.12. Pore size distribution of the cristobalite particles
from run 42 (Fig. 6.10) as measured by a mercury
porosimeter. The analyses was conducted on the
particles after the run. The particle density was
found to be 1.55 g/cm^3 whereas the solid density was
1.99 g/cm^3, giving a total porosity of 22 %.

It is not equally simple to explain the enhanced rate
observed with a charge of quartz plus graphite as a result of
repeated evacuation and re-admittance of carbon monoxide. Possibly
the evacuation also aids in producing micro-cracks in the silica.
A full explanation on this point, however, would demand further
experimental work which was not undertaken.

6.5.   Final experiments

Through rather lengthy series of experimental trial and errors we have come to the conclusion that, in order to obtain representative and reproducible results, the runs shall be done

- with silica in the form of cristobalite
- with pre-mixed compositions of carbon monoxide and argon
- and in such a way that evacuation between each change in gas composition or pressures is avoided as far as possible.

The last requirement is not absolutely essential since the reaction with cristobalite appears relatively insensitive to evacuations, cf. Fig. 6.10. Nevertheless an excessive number of evacuations should be avoided, considering the time taken in the runs shown in Fig. 6.8 both for evacuations and for the preparation of new gas compositions.

6.5.1.   Constant gas composition, lowered pressure

In accordance with the above guide-lines, run 41 was conducted as follows. Cristobalite in the amount of 2.423 g was used in the charge together with 0.726 g graphite, both with grain size in the range 0.51 to 0.71 mm (molar ratio $C/SiO_2 = 3/2$, not counting the graphite crucible). The charge was held in a "type C" open crucible. After the usual procedure of degassing, temperature was raised to 1558°C and pure CO was admitted to 1.333 bar. After recording the rate of weight loss for about 20 minutes the pressure was lowered to 1.066 bar and again kept constant for about 20 minutes. The procedure was then repeated for 0.800 bar and 0.400 bar. After this, the furnace was evacuated to about 1 mbar, and a gas mixture of composition $X_{CO} = 0.80$ was admitted to a total pressure of 1.333 bar. From there onwards the procedure was repeated, that is, the pressure was stepwise lowered in the sequence 1.066, 0.800 and 0.400 bar, with about 20 minutes at each pressure, just as described for pure CO. Once again the furnace was evacuated, and the same procedure repeated for gas mixtures with $X_{CO} = 0.60$, 0.40, 0.20 and 0.10. Thus with 6 different gas

compositions at 4 different total pressures, a total of 24 observations of rate were obtained. A final measurement was made in pure CO at 1.066 bar, to see whether this gave the same result as obtained in the very beginning, which in fact it did.
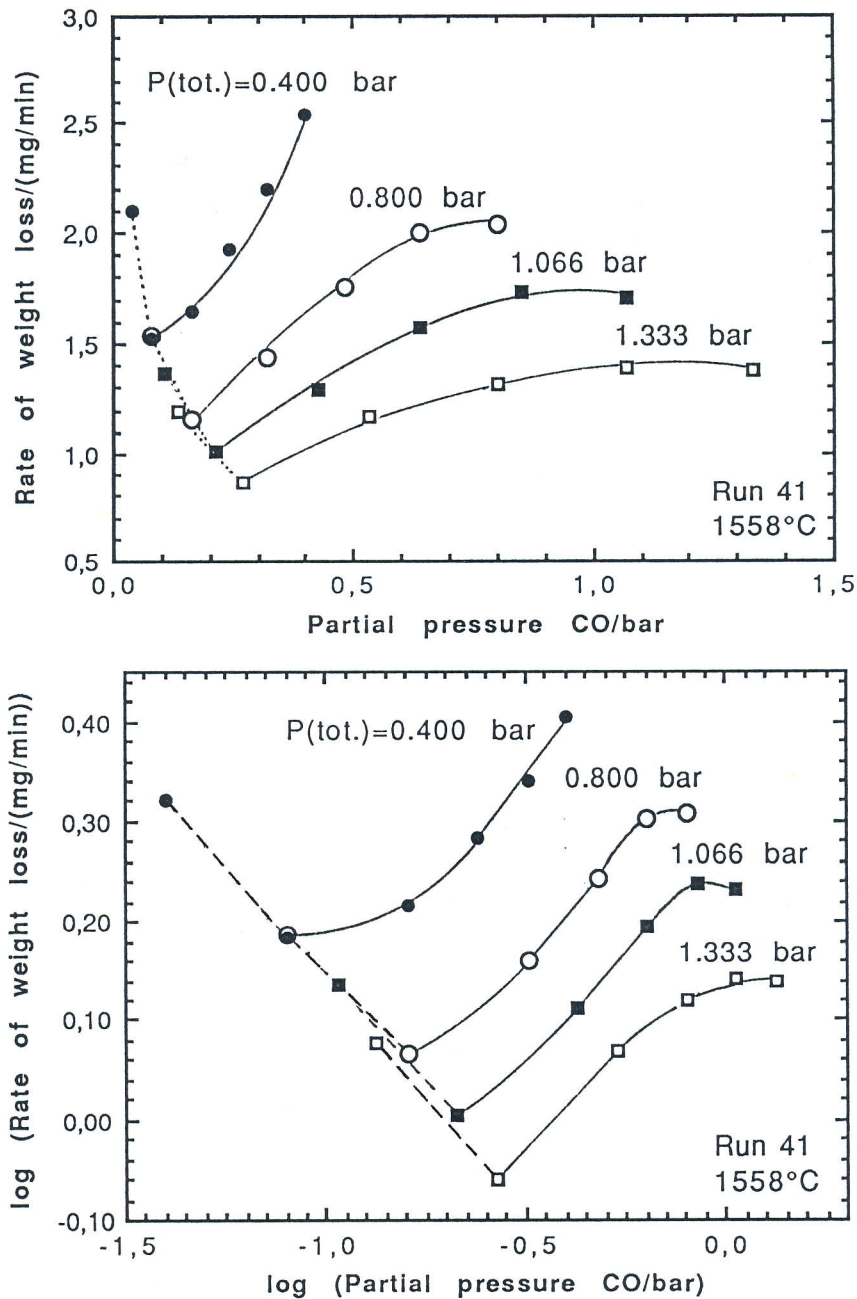
Fig. 6.13. Rate of weight loss of a cristobalite/graphite-charge (run 41) as function of partial pressure CO at temperature 1558°C and total pressures 1.333, 1.066, 0.800 and 0.400 bar (1000, 800, 600, and 300 torr) respectively. Upper and lower graph are on linear and log-log scales, respectively. (Weight data in Table A2.10 and rate data in Table A2.21.)

The results are shown graphically in Fig. 6.13. Note that each series of measurements with fixed gas composition yields one point on each of the four curves. Thus a curve through the

outermost point to the right on each curve, describes the rate of weight loss as it varies with the pressure of pure carbon monoxide. Here we recognize the steep increase in rate with decreasing pressure which was also shown in the curves of Fig. 6.4. This is clearly an effect of the concurrent decrease in total pressure. With decreasing CO pressure at constant total pressure, on the other hand, the rate decreases, as one would expect from our proposed reaction mechanism. An attempt at a quantitative treatment of these results will be given in Chapter 7.

6.5.2. Enhanced rates and the formation of silicon carbide

Apart from the rounded maxima shown by three of the four curves, they all show decreasing rate with decreasing partial pressure of carbon monoxide down to a certain point, and then a sharp increase in the rate at still lower partial pressures. It is suggested that this rise in pressure at low partial pressures is associated with the formation of silicon carbide. After the end of the run, silicon carbide was detected by XRD both on the residual graphite particles in the charge and on the inner walls of the crucible.

The conditions for formation of silicon carbide were discussed in Paragraph 6.2.3. Silicon carbide is formed by the reaction

$$SiO(g) + 2C = SiC + CO \qquad (1.8)$$

At our experimental condition, however, this reaction will proceed to the right only at low pressures of CO, because of the low pressures of SiO generated by the primary reaction

$$SiO_2 + CO = SiO + CO_2 \qquad (3.9)$$

This is most clearly seen from Fig. 3.2, where the line for reaction (3.9) crosses that for reaction (1.8) at a CO pressure of about 0.03 bar. Below this pressure the formation of SiC by reactions (3.9) and (1.8) is possible. The quoted value of the CO pressure at the crossing point, 0.03 bar, depends on the temperature and the assumptions stated for Fig. 3.2 which may not quite correspond to the reality of our experiments. But generally speaking, the observations of Fig. 6.13 are explained by the

formation of SiC when the CO pressure is decreased below a certain value at each total pressure. When silicon carbide is formed by reaction (1.8), the carbon surface acts as a "sink" for the SiO gas which thus gets a much shorter diffusion path relative to the diffusion out of the crucible, and the result is an enhanced rate of weight loss.
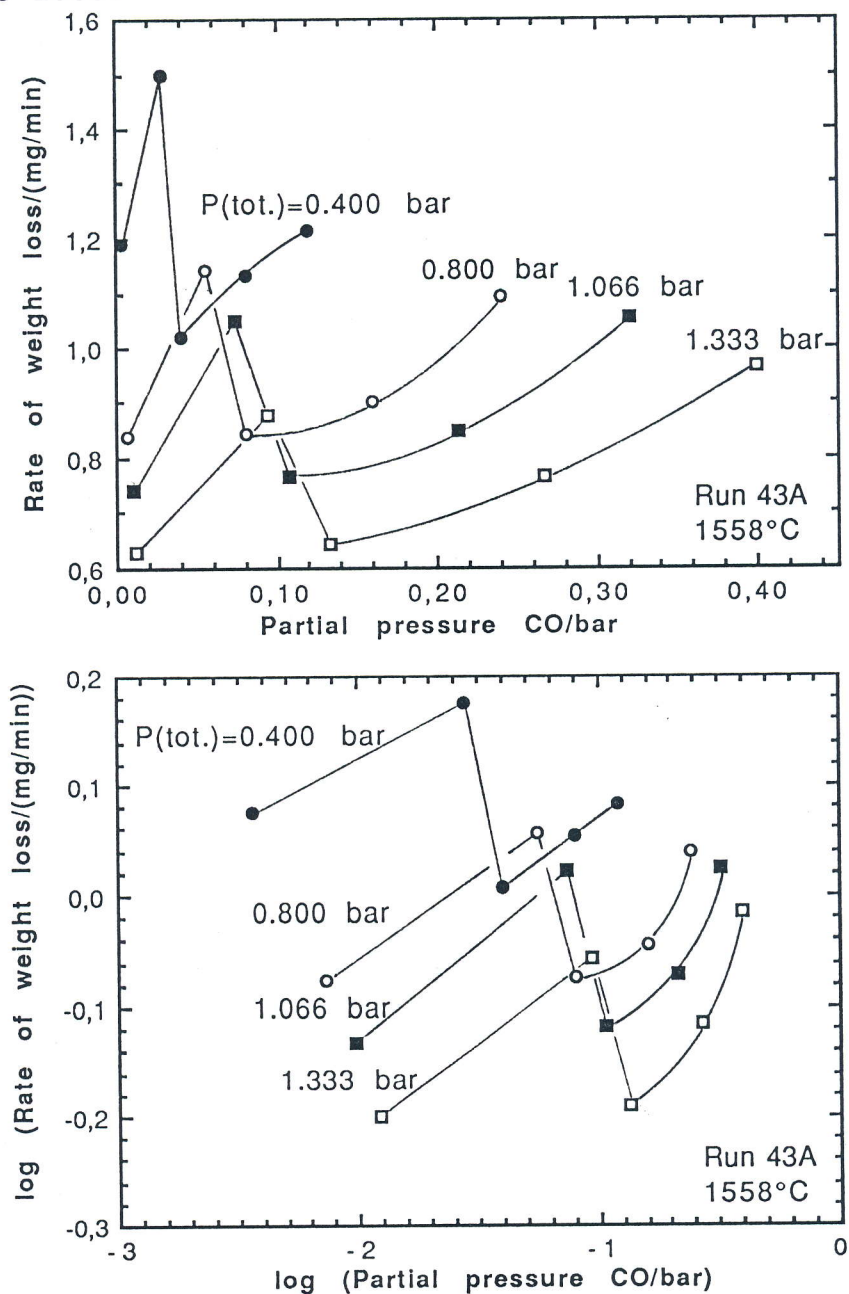
Fig. 6.14. Rates of weight loss of a cristobalite/graphite-charge (run 43A) as functions of partial pressure CO at temperature 1558°C and total pressures 1.333, 1.066, 0.800 and 0.400 bar (1000, 800, 600, and 300 torr), respectively. Upper and lower curve are on linear and logarithmic scales, respectively. (Weight data in Table A2.11 and rate data in Table A2.22.)

In order to obtain more detailed information on the behaviour of the cristobalite/graphite-charge at low partial pressures of

CO, another experiment (run 43A) was conducted in exactly the same manner as described above, but with gas compositions of X_{CO} = 0.30, 0.20, 0.10, 0.07 and 0.009. The results are given in Fig. 6.14. The sharp increase in rate at low partial pressures of CO is recognized from Fig. 6.13, but then, at still lower partial pressures, the rates drop again. Qualitatively this is explained by the fact that the rate of the primary reaction subsides when the CO pressure goes towards zero.

A closer inspection of Figs. 6.13 and 6.14 reveals that the minimum rate before the increase occurs at somewhat lower partial pressures of CO in Fig. 6.14. This may in part be due to the larger number of experimental points at low partial pressures in Fig. 6.14, partly it may also be ascribed to the fact that the nucleation and growth of silicon carbide depend on kinetic circumstances that are not easily controlled. The conditions for formation of SiC will be further discussed in Chapter 7.

6.5.3 Some further experiments

After yielding the results shown in Fig. 6.14, this run was directly continued in pure carbon monoxide (run 46B), with stepwise variation of the CO pressure from 1.33 bar down to 2 mbar. The results are shown in Fig. 6.15.

The rate of weight loss in dependence of the CO pressure is seen to exhibit a rather linear behaviour in the range 1.33-0.20 bar. As the CO pressure is decreased below 0.2 bar a substantial increase in rate is seen to take place. The formation of SiC was confirmed by XRD both on the inner walls of the graphite crucible and on the residual graphite particles. By comparing the results with run 26 (Fig. 6.2), in which silicon carbide was not formed, it is seen that the linear behaviour at the higher CO pressures is exhibited in both cases, but the rate at low pressure is very much affected by the presence of SiC.

In a number of the foregoing experiments it was found that the behaviour as a result of evacuation was difficult to predict. Most frequently the rate of weight loss was found to decrease considerably when the pressure was lowered below a few millibar. In some cases, however, a substantial increase in rate was found

to take place. In order to investigate this phenomenon, the following experiment was carried out (run 46A):
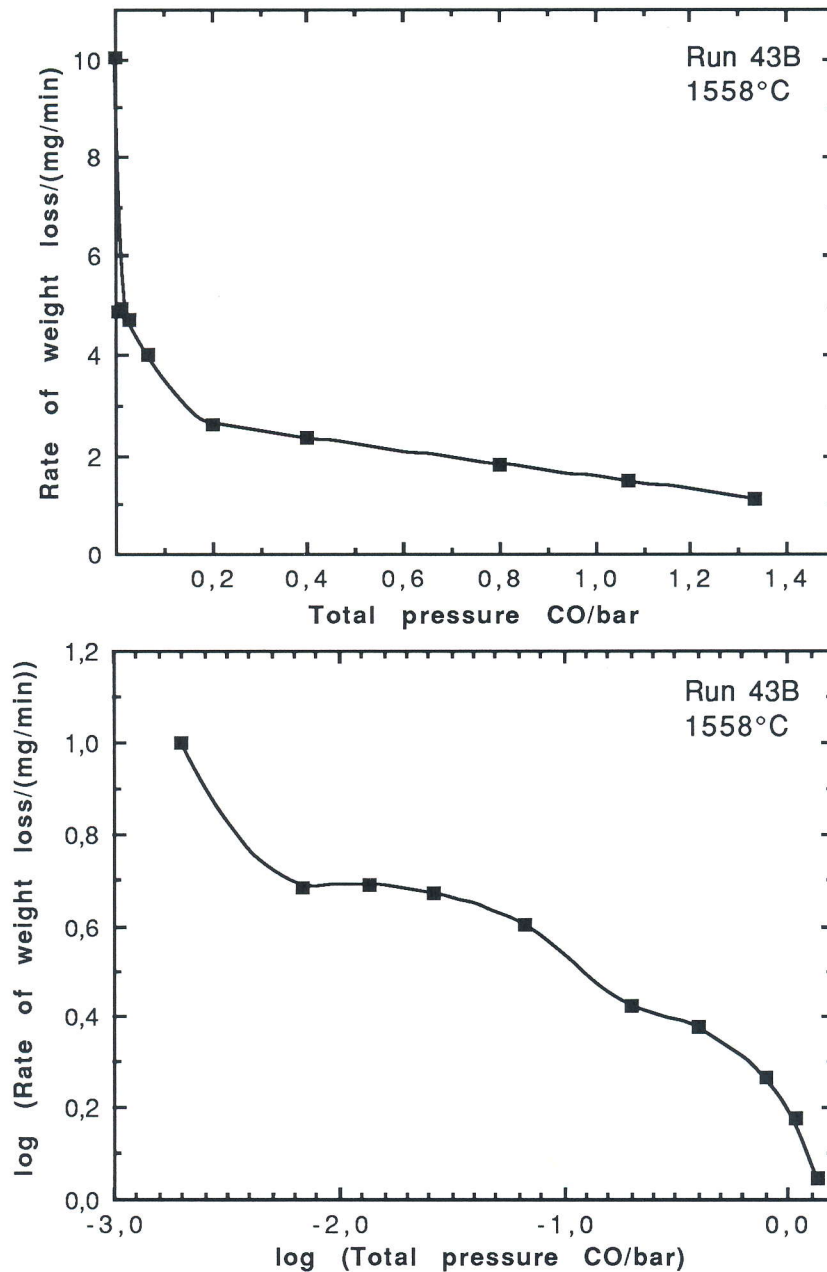
Fig. 6.15. Rate of weight loss of a cristobalite/graphite-charge (run 43B) in dependence of total pressure CO (X_{CO} = const. = 1.0) at 1558°C. Open ("type C") graphite crucible applied. Upper and lower graph are on linear and logarithmic scales respectively (Weight data in Table A2.11 and rate data in Table A2.23).

A cristobalite/graphite-charge of the same composition as the previous was held at 1558°C in pure CO of 0.040 bar for about one-half hour. The observed rate of weight loss was about 2 mg/min as illustrated by the first column of Fig. 6.16. The furnace was subsequently evacuated to about 1 mbar, and the corresponding rate

of weight loss was found to be 0.5 mg/min as given by the second column. Next a gas mixture of argon and carbon monoxide with X_{CO} = 0.1 was admitted to the furnace, and the pressure was kept constant for about 0.5 h at each of the total pressures 1.066, 0.800 and 0.400 bar. The recorded rate at 0.400 bar is illustrated by column 3. The furnace was then again evacuated to about 1 mbar, this time with the result that the rate of weight loss increased very markedly to 14.3 mg/min as illustrated by column 4 in Fig. 6.16.
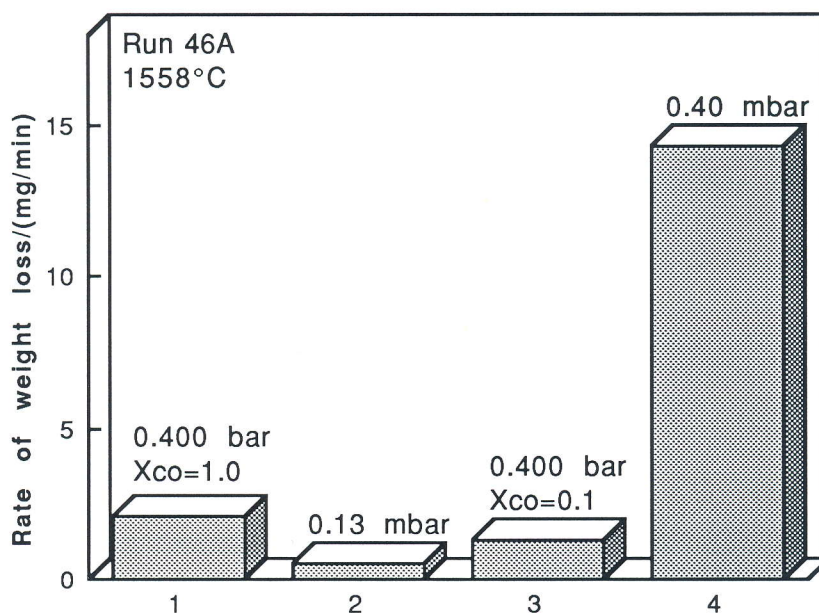
Fig. 6.16. The rate of weight loss of a cristobalite/graphite-charge at 1558°C (run 46A) in dependence of total pressure and gas composition. A low rate is observed (column 2) when the furnace is evacuated from total pressure 0.400 bar and X_{CO} = 1.0 (column 1). The rate is substantially enhanced (column 4) by evacuation from total pressure 0.400 bar and X_{CO} = 0.1 (column 3).

The explanation must be that silicon carbide was not formed during the heating in 0.40 bar of pure CO (nor would one expect SiC formation under these conditions). On the other hand, SiC was formed during heating in 0.40 bar of a gas mixture with X_{CO} = 0.1, that is, P_{CO} = 0.040. Once silicon carbide crystals are nucleated and have started to grow on the graphite surfaces, the further formation is greatly facilitated. As a consequence the system responds to a reduced total pressure with increased reaction rate, and in the vacuum region it appears that the system now produces its own carbon monoxide at a rate which is sufficient to sustain the primary reaction (3.9).

The last experiment (run 46B) was a direct continuation of the above run 46A. After recording the rate of weight loss shown as column 4 of Fig. 6.16, the furnace was maintained at 1558°C under vacuum. The rotary pump was kept running throughout the whole run, and carbon monoxide was produced at such a rate that the furnace pressure remained at about 0.4 mbar during most of the run. The results are given as weight loss in dependence of time in Fig. 6.17.
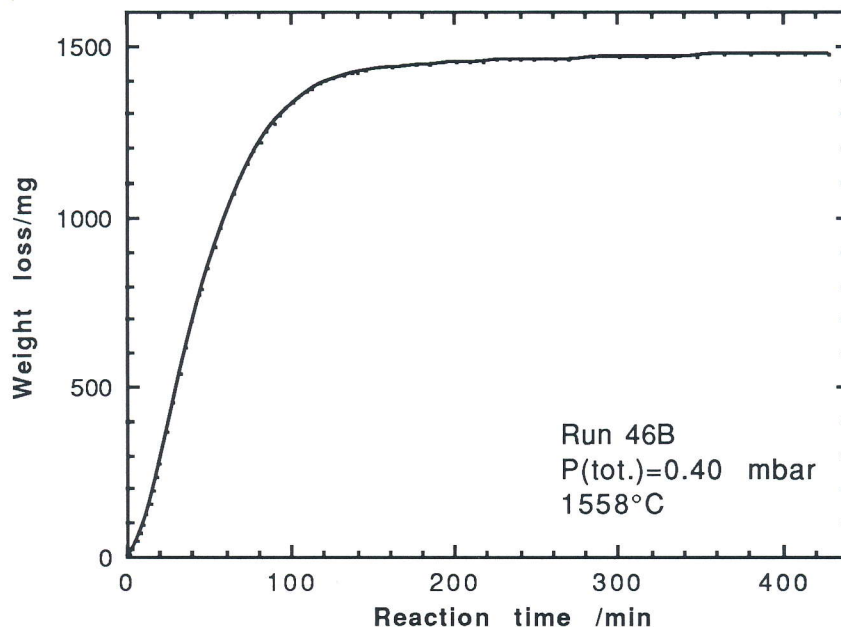
Fig. 6.17. Progress of weight loss of a cristobalite/graphite-charge (run 46B) in dependence of time when SiC is formed continuously at 1558°C and total pressure 0.4 mbar (0.3 torr) (weight data in Table A2.12).

The rate of weight loss in this case is seen to increase up to about 28 min, corresponding to nearly 50 % reaction, with a maximum rate of 21 mg/min at the turning point. After that the rate gradually decreases. Visual inspection of the charge after the run confirmed that all the silica was consumed, and XRD examination confirmed the presence of silicon carbide. Comparing with the previous experiment with reaction to completion, Fig. 6.3 (upper curve), it is seen that the time to completion in the present case is about 1/40 of that observed with quartz plus graphite in 1.5 bar of carbon monoxide.

7. DISCUSSION

7.1. The silicon monoxide pressure; an equilibrium approach

The reaction we have been studying throughout the last part of the present work is assumed to consist of two main steps. At the surface of the silica, the following reaction takes place:

$$SiO_2 + CO = SiO + CO_2 \qquad (3.9)$$
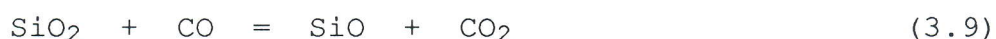
The carbon dioxide will react at the nearest carbon surface:

$$CO_2 + C = 2CO \qquad (1.4)$$

The sum of the two gives the over-all reaction

$$SiO_2 + C = SiO + CO \qquad (1.7)$$

For the time being we will ignore the possibility of silicon carbide formation and the SiO gas is assumed to diffuse away, out of the reacting system. Thus the reactions (3.9) and (1.4) are the two steps we are considering. The equilibrium constants of these two reactions are designated K_4 and K_2, respectively.

We will assume that equilibrium is established at the silica surface, this gives

$$P_{SiO} = K_4 \frac{P_{CO}}{P_{CO_2}} \qquad (7.1)$$

Likewise we assume equilibrium on the carbon surface, which gives

$$P_{CO_2} = \frac{(P_{CO})^2}{K_2} \qquad (7.2)$$

Now, in order to advance, we have to decide on the magnitude of the CO_2 pressure to be inserted in Eq. (7.1)

From Eq. (3.9) it follows that SiO and CO_2 are produced in equimolar amounts. This has led us, in some preceding sections of this work, to assume $P_{SiO} = P_{CO_2}$. This relation, however, cannot be strictly correct. We assume that the carbon monoxide gas is in equilibrium with carbon in the reaction zone, and the carbon dioxide pressure given by Eq. (7.2) represents a minimum partial pressure of CO_2 which must always be present in a carbon monoxide atmosphere in equilibrium with carbon. This minimum partial pressure comes in addition to that produced by reaction (3.9), so that the correct expression for the carbon dioxide pressure in this case will be

$$P_{CO_2} = \frac{(P_{CO})^2}{K_2} + P_{SiO} \qquad (7.3)$$

This gives the carbon dioxide partial pressure when considering only the local equilibrium very close to the silica surface.

On the other hand, we might assume that the carbon dioxide produced at the silica surface very quickly diffuses to the nearest carbon surface where it is reduced according to Eq. (1.4), so that the CO_2 pressure close to the silica surface is in fact maintained at a lower value than that given by Eq. (7.3). In the extreme case we might assume that it is in fact lowered to the minimum value.

$$P_{CO_2} = \frac{(P_{CO})^2}{K_2} \qquad (7.2)$$

These are the two cases. Quoting Motzfeldt's (1988): "--it appears that what really takes place is somewhere in-between the two extremes." It was the aim of the present author to formulate this statement in more quantitative terms. Let χ be a quantity such that $0<\chi\leq1$. We may then write

$$P_{CO_2} = \frac{(P_{CO})^2}{K_2} + \chi P_{SiO} \qquad (7.4)$$

The parameter χ may somewhat loosely be referred to as "the reaction parameter". It is a dimensionless factor which, for a given temperature and experimental arrangement, is postulated to have a constant value, independent of the CO pressure. Within the limits 0 and 1 it is expected to have a high value when there is a

scarcity of carbon in the charge, or when there is a long distance between the silica and the carbon, or a very unreactive carbon. On the other hand it is expected to have a low value when there is ample surface area of reactive carbon very close to the silica.

Introduction of P_{CO_2} from Eq. (7.4) into Eq. (7.1) yields a second-order equation which is solved for P_{SiO}:

$$P_{SiO} = - \frac{P_{CO}^2}{2 \chi K_2} + \left(\left(\frac{P_{CO}^2}{2 \chi K_2} \right)^2 + \frac{K_4 \, P_{CO}}{\chi} \right)^{1/2} \qquad (7.5)$$

Values of K_2 and K_4 are known from thermodynamic data (JANAF, 1985), and thus P_{SiO} may be calculated from Eq. (7.5) for various values of χ. Fig. 7.1 shows the results for a temperature of 1558°C and the χ-values 0.005, 0.1 and 1.0, respectively, plotted as functions of the CO pressure.
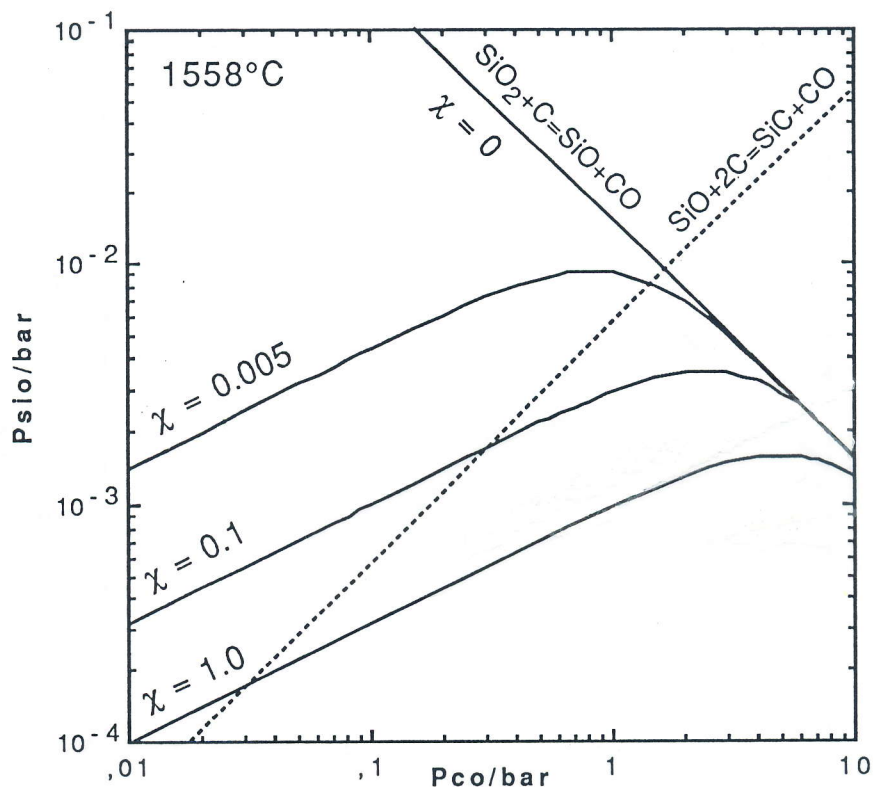
Fig. 7.1. Equilibrium SiO pressure in dependence of CO pressure calculated according to Eq. 7.5 for the reaction parameter, χ, being 0.005, 0.1 and 1.0, respectively at 1558°C. The SiC producing reaction (1.8) is included. (Data from JANAF, 1985).

Setting $\chi = 1$ in Eq. (7.5) gives the equation previously developed by Motzfeldt (1988). From Fig. 7.1 it is seen that the maximum of the curve for P_{SiO} in this case occurs at CO pressures well above those attainable in the present work. With diminishing

value of χ the maximum moves to the left and into the region of pressures we have been studying experimentally. In the extreme case of $\chi = 0$, Eq. (7.5) breaks down. We may readily see, however, that this case corresponds to the straight line in Fig. 7.1 with slope -1, continuing upwards indefinitely[1].

The curve for the SiC producing reaction (1.8) is also included as the dashed line in Fig. 7.1. The formation of SiC is thermodynamically possible at CO pressures lower than those corresponding to the crossing between the dashed line and the full-drawn curves for the various values of χ. It is seen that SiC formation is possible at higher CO pressures as χ decreases.

In fact the parts of the solid curves to the left of the crossing points are thermodynamically inconsistent. From an equilibrium point of view, the system should be invariant with the gas composition given by the crossing point in the presence of the three solid phases SiO_2, C and SiC. Experimentally it has been found that SiC quite often has not been formed, presumably for kinetic reasons, and the full-drawn curves then maintain a physical meaning also to the left of the dotted line.

7.2. A model for the rate of reaction

The reaction referred to is that of Eq. (1.7), with the net production of SiO(g) and CO(g). The rate in question is that observed experimentally as the rate of weight loss in our experimental arrangement.

We have assumed that the reaction mechanism consists of the two steps represented by Eq.s (3.9) and (1.4), and we have assumed that each of these reactions come to local equilibrium, although spatially separated. We have developed an equation for the SiO pressure, Eq. (7.5), based on these concepts. The equation contains a reaction parameter, χ, which may be said to occur as a result of the spatial separation; it is a measure of to what

---

[1]This case is impossible in a dynamic system since it would correspond to maintaining a high partial pressure of SiO by means of reaction (3.9) without any trace of the concurrently produced CO_2 remaining in the gas. It may be realized in a static system, however, where the said straight line corresponds to equilibrium of the reaction $SiO_2 + C = SiO + CO$ (1.7).

extent the local equilibrium on the carbon surface influences that on the silica surface.

We now assume that, apart from possible local gradients, Eq. (7.5) expresses an SiO pressure which is essentially the same throughout the charge. Furthermore we assume that the observed rate of weight loss is mainly determined by the rate of diffusion of the SiO gas from the charge to the surrounding furnace atmosphere, where the partial pressure of SiO is assumed to be zero. This diffusion takes place through an "interface" between charge and surroundings which need not be further specified; it is assumed to have an area A and a thickness Δs which remain unknown. With these assumptions, the gradient in partial pressure of SiO becomes

$$\frac{dP_{SiO}}{ds} = \frac{P_{SiO}}{\Delta s} \qquad (7.6)$$

From Fick´s first law for steady-state diffusion we have

$$J_{SiO} = \frac{dn_{SiO}}{A\ dt} = -D_{SiO-CO}\frac{dc_{SiO}}{ds} = -\frac{D_{SiO-CO}}{R\ T}\frac{dP_{SiO}}{ds}$$

$$= -\frac{D_{SiO-CO}}{R\ T}\frac{P_{SiO}}{\Delta s} \qquad (7.7)$$

Conversion of molar flux into weight loss of SiO per unit time, dw_{SiO}/dt, gives:

$$\frac{dw_{SiO}}{dt} = M_{SiO}\frac{dn_{SiO}}{dt} = \frac{A\ M_{SiO}\ D_{SiO-CO}}{R\ T}\frac{P_{SiO}}{\Delta s} \qquad (7.8)$$

In our assumed reaction (1.7) a charge of silica plus carbon loses equimolar amounts of SiO and CO, thus the total weight loss rate will be

$$\frac{dw_{tot}}{dt} = \frac{M_{SiO} + M_{CO}}{M_{SiO}}\frac{dw_{SiO}}{dt} = 1,635\frac{dw_{SiO}}{dt} \qquad (7.9)$$

For simplicity we will collect all parameters that are constant in our experiments, known and unknown, into a single new constant

$$k = \frac{1.635\ A\ M_{SiO}}{R\ T\ \Delta s} \qquad (7.10)$$

152

Combination of Eq.s (7.8), (7.9) and (7.10) gives

$$\frac{dw_{tot}}{dt} = k \, D_{SiO-CO} \, P_{SiO} \qquad\qquad (7.11)$$

where P_{SiO} is given by Eq.7.5. Eq.7.11 is thus expected to predict the rate of weight loss of a silica/carbon-charge in terms of the CO pressure.

The experiment given in Fig.6.11 shows the rate of weight loss of a cristobalite/graphite-charge as a function of the partial pressure of CO at various constant total pressures. The diffusivity, D_{SiO-CO}, is expected to be constant and thus independent of CO pressure at a given total pressure. The experimental data at total pressure 1.333 bar is chosen as a basis for optimalizing χ and kD_{SiO-CO} in order to obtain a close fit between the experimental data and Eq.7.11. However, the rate at 0.133 bar CO is not included in the curve fitting; because, as pointed out in Paragraph 6.5.2., SiC is formed in this region.

The fitting between the empirical data and Eq.7.11 is performed by means of a least squares-method; which calculates the parameters (in this case χ and kD_{SiO-CO}) which minimize the least squares function F:

$$F(x,y) = (f(x_1) - y_1)^2 + (f(x_2) - y_2)^2 + \cdots + (f(x_n) - y_n)^2 \qquad (7.12)$$

Eq.7.12 represents the F-function for n data points. The variable, x, in the present case is the partial pressure of CO, the function f is given by Eq.7.11 while y is the empirical rate of weight loss at the CO pressure in question. The calculations were carried out on an Apple MacIntosh computer by means of the program "Eureka:The solver".

The numerical values for kD_{SiO-CO} and χ, resulting from the computer fit, are given in Table 7.1 along with the values for the equilibrium constants applied in Eq.7.5.

Table 7.1.   Numerical values for χ (reaction parameter) and kD_{SiO-CO} in Eq.7.5 and Eq.7.11 resulting from the computer fit between empirical data at 1.333 bar and Eq.7.11.   Included are the numerical values for the equilibrium constants at 1558°C applied in Eq.7.5, calculated with data from JANAF, 1985.

$k\ D_{SiO-CO}$ [mg/bar min]	χ	K_4	K_2
217.38	1.4727×10^{-2}	9.7067×10^{-7}	15992

A study of Fig.7.2 shows a rather close fit between the experimental data and Eq. 7.11. Table A2.26 shows a maximum deviation between calculated and measured rate of weight loss of 1.3 %.

As previously pointed out, the diffusivity is inversely proportional to the total pressure, P_{tot}, hence:

$$D_{SiO-CO} = \frac{D'}{P_{tot}} \qquad (7.13)$$

where D´ is the diffusivity at a given temperature and 1 bar total pressure. D´ is assumed to be independent of gas composition (this is justified in Appendix A4). Combining Eq.7.11 and Eq.7.13 and introducing a new constant K = k D´ gives:

$$\frac{dw}{dt} = \frac{K}{P_{tot}} P_{SiO} \qquad (7.14)$$

According to Table 7.1 kD_{SiO-CO} = 217.38 mg/bar min at total pressure 1.333 bar, hence the K-factor in Eq.7.14 equals 217.38x1.333 = 289.77 mg/min and Eq.7.14 turns into:

$$\frac{dw}{dt} = \frac{289.77}{P_{tot}} P_{SiO} \qquad (7.15)$$
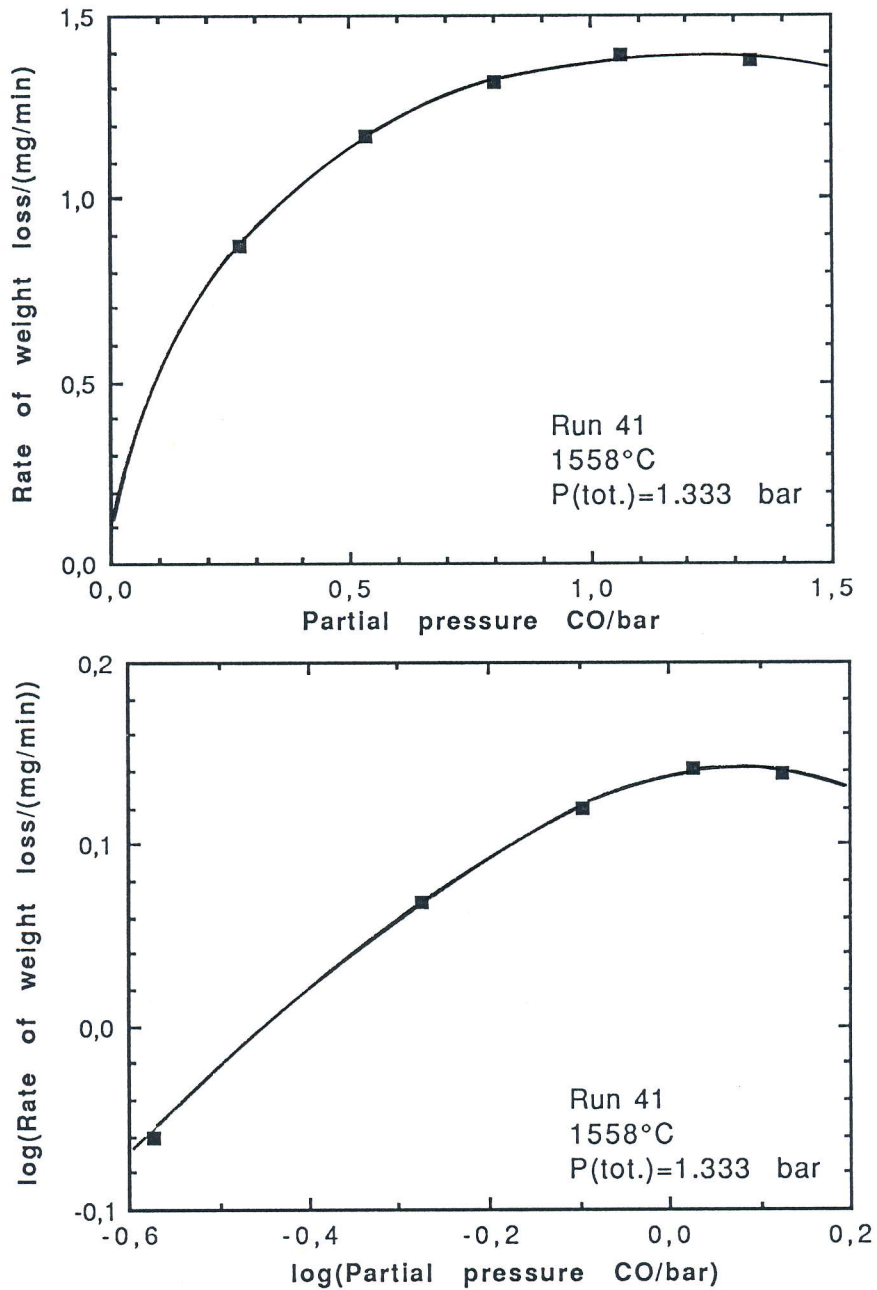
Fig. 7.2. Result of the fitting between empirical data (run 41) at total pressure 1.333 bar (Fig. 6.13/Table A2.26) and Eq. 7.11. The best fit was obtained with the parameters given in Table 7.1. Upper and lower graph are on linear and logarithmic scales, respectively.

Introduction of P_{SiO} from Eq.7.5 gives the following general expression for the rate of weight loss in units of mg/min:

$$\frac{dw_{tot}}{dt} = \frac{289.77}{P_{tot}} \left(- \frac{P_{CO}^2}{2\chi K_2} + \left(\left(\frac{P_{CO}^2}{2\chi K_2} \right)^2 + \frac{K_4 P_{CO}}{\chi} \right)^{1/2} \right) \quad (7.16)$$
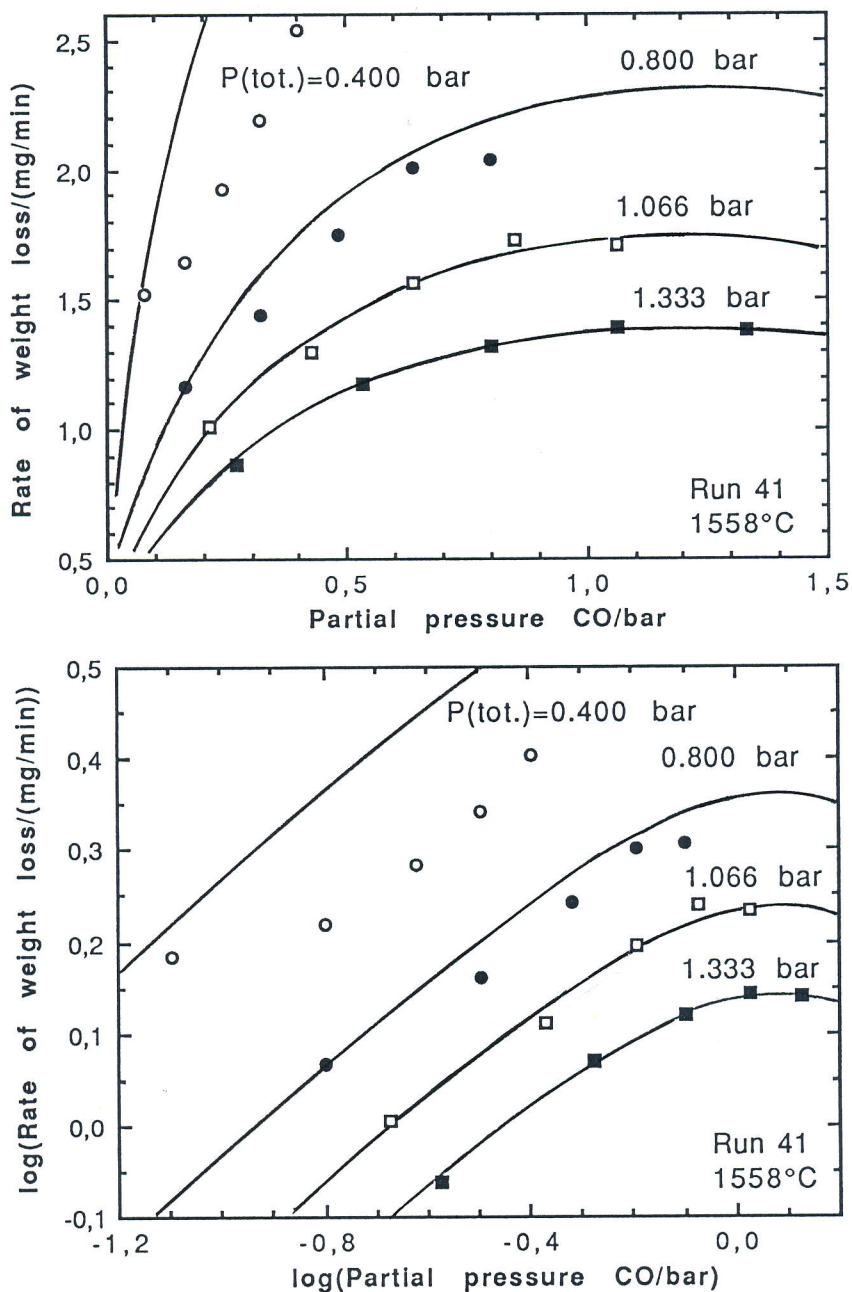
Fig. 7.3. Calculated rate of weight loss (solid lines), from Eq. 7.16, compared to observed rates (Fig. 6.13/Table A2.26-27) at total pressures 1.333, 1.066, 0.800 and 0.400 bar. Upper and lower graph are on linear and logarithmic scales, respectively.

Eq.7.16 offers the opportunity to check how the model fits with the remainder of the experimental data shown in Fig.6.13, that is, at total pressure 1.066, 0.800 and 0.400 bar respectively. The results, including the data at 1.333 bar, are given in Fig.7.3 while numerical values are given in Table A2.27.

7.3. Discussion of the model

It is seen from Fig. 7.3 that the model, represented by Eq. (7.16), describes the experimental data quite well for the total pressures 1.33 and 1.07 bar. At 0.80 bar total pressure the rates predicted by the model are somewhat higher than those observed, and at 0.40 bar they are much higher (except the lowest point at 0.4 bar). It is felt that although the model represents a step in the right direction, some explanation has to be offered for the deviation.

Generally speaking, no rate may increase indefinitely. Thus if the constraints due to one step in the reaction is lifted, another rate limiting step takes over. This is exactly what is observed in Fig. 7.3. Still we may proceed to consider the various steps or parameters that may be responsible for the lower rates compared to those predicted at low total pressures.

7.3.1. Possible variation of χ with gas pressure.

In Sect 7.1 the reaction parameter χ was postulated to be independent of the partial pressure of CO as well as of the total pressure. We may consider whether or not these are reasonable assumptions.

The excellent fit at the higher total pressures over a wide range of total partial pressures of CO indicate that χ in fact is independent of the CO pressure. With respect to the total pressure, one line of thought is as follows: A lowered total pressure would mean more rapid diffusion of CO_2, which might in turn lower the value of χ, which would result in higher SiO pressures. This result works in the wrong direction compared to the experimental results. On the other hand, the enhanced rate of diffusion might be assumed primarily to affect the SiO which now would leave the reaction zone before it has reached the full partial pressure prescribed by the model. This would correspond to a higher χ and and would work in the direction observed. Thus the

discrepancy for P_{tot}=0.800 and 0.400 bar in Fig. 7.3 may possibly be explained by a change in the value of χ.

7.3.2. Chemical reaction control at the silica surface

Lowered total pressure means an increase in calculated rate because of the P_{tot} in the denominator of Eq. 7.16. For this to be realized, the reaction (3.9) would have to take place with ever increased speed so that the equilibrium value of P_{SiO} is maintained. This is obviously not a very likely supposition, hence the disagreement between calculated and observed rates at the lower total pressures may well indicate that chemical reaction control on the silica surface is taking over.

This supposition seems reasonable, considering that Ozturk and Fruehan (1985) concluded from their studies of the reaction between SiO_2 and CO that reaction (3.9) is chemically controlled. In principle, rate data from their work could be used for a correlation with the rates shown in Fig. 7.3. In practice, however, their experimental conditions, with silica in a streaming gas at 1650°C, are so different from the present ones that any attempt at quantitative application of their data would appear questionable, and it has not been attempted in the present work.

Next we will return to the question of the expected pressure dependence. In Fig. 7.3 it is seen that the results for the higher total pressures are proportional to the square root of the CO pressure over a considerable range. This is inherent in the model that led to Eq. 7.16, based on the concepts of equilibria plus gas diffusion. Now it is interesting to note that this square-root dependence is also expected from the model for chemical control presented in Paragraph 5.2.4; it was found experimentally for the free-hanging silica tube as seen in Fig. 5.11. In Fig. 7.3 it is seen that, although the points at 0.4 bar total pressure fall short of the calculated curve, the square-root relationship is still quite well obeyed, as one would expect if chemical control takes over.

This is even better seen in Fig. 7.4, in which the rates from Fig. 7.3 for the lowest total pressure are re-plotted on log-log scales. It is seen that the "best" straight line through the four

points to the right gives a slope of 0.46, very close to the predicted 0.5.

The deviation of the two points at the lowest partial CO pressures shows the effect of silicon carbide formation, described in Paragraph 6.5.2 and to be further discussed in Sect. 7.4.
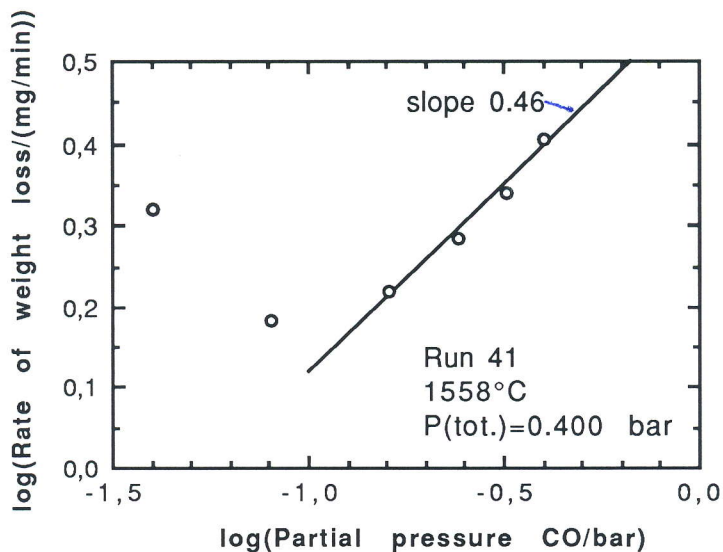
Fig. 7.4. Rate of weight loss of a cristobalite/graphite charge (run 41) in dependence of partial pressure CO at 1558°C and total pressure 0.400 bar (data from Table A2.21).

7.3.3. Chemical control at the carbon surface

The reaction in question is the Boudouard reaction, Eq. (1.4). It was concluded already in Sect. 3.4 that the application of available kinetic data for this reaction to our experimental conditions would appear difficult. The only conclusion we may tentatively draw is that the reaction probably is quite fast at temperatures around 1560°C. The solid reactant in this case is highly porous and offers a large surface area for the reaction, this holds even for well-crystallized commercial graphite. Another observation which supports the idea of a rapid reaction may be anticipated from the discussion in the next section. It was observed in the experiments described in Sect. 6.5 that at certain low partial pressures of CO, a marked increase in the weight-loss rate occurred. This increase was always associated with the formation of silicon carbide. Now, maintaining our ideas of the reaction mechanism with reactions (3.9), (1.4) and (1.8) in

sequence, it is realized that a high weight-loss rate means that the Boudouard reaction (1.4) also goes fast. And this it does, even when SiO reacts to form silicon carbide on the carbon surfaces which are thus in part made inaccessible to the reaction with CO_2. With this in mind it appears very likely that the rate of the Boudouard reaction has not in any way been impeded by chemical reaction control under the conditions of the experiments shown in Fig. 7.3.

7.4. On the formation of SiC

The model, which describes the rate of reaction between silica and carbon in terms of the CO pressure (Eq. 7.16), is based on the assumption that the SiO pressure throughout the silica/graphite-charge is adequately given by Eq. 7.5. The optimum value of the reaction parameter, based on the experimental results at 1558°C, was found to be $\chi=0.0147$ (Table 7.1), and the resulting SiO pressure in terms of the CO pressure is given in Fig. 7.5.
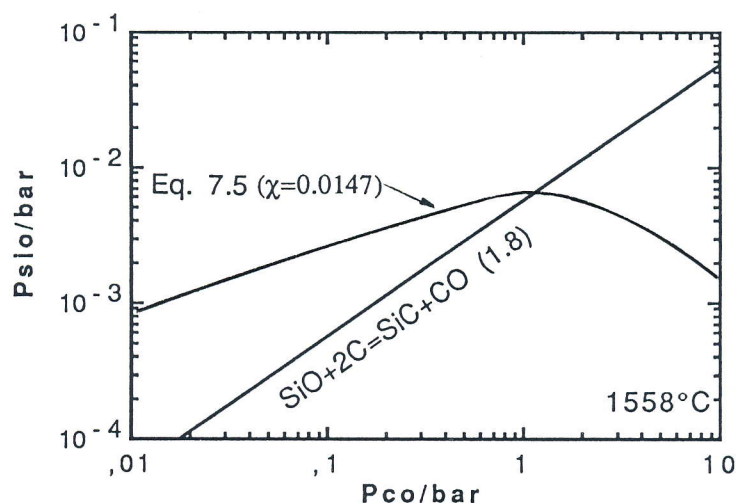
Fig. 7.5. SiO pressure in dependence of CO pressure at 1558°C as calculated from Eq. 7.5 with numerical values from Table 7.1. Included is the SiC producing reaction (1.8) (data from JANAF, 1985).

The SiC generating reaction (1.8) is included as well, and from a thermodynamic point of view the formation of SiC is seen to be possible at CO pressures below ≈1 bar. It is noted that this limiting value depends only on the temperature (which is held

160

constant) and on the value of the reaction parameter χ, which is assumed to be independent of the gas pressure. Thus this limiting value of ≈1 bar should be independent of the total gas pressure. Experimentally, however, it was found that the marked increase in rate, which we associate with the formation of SiC, occurred at considerably lower pressures, generally below 0.3 bar[2]. We may thus conclude that the formation of SiC needs a certain "overpressure" of SiO in order to proceed.

This is further corroborated by the observations shown in Fig. 7.6, which shows the behaviour of a cristobalite/graphite charge (run 43B) where initial nucleation of SiC has taken place on the graphite grains (upper curve) and a quartz/graphite charge (run 26) where SiC is not present (lower curve). The molar ratio between C and SiO_2 is 1.5 in both runs.
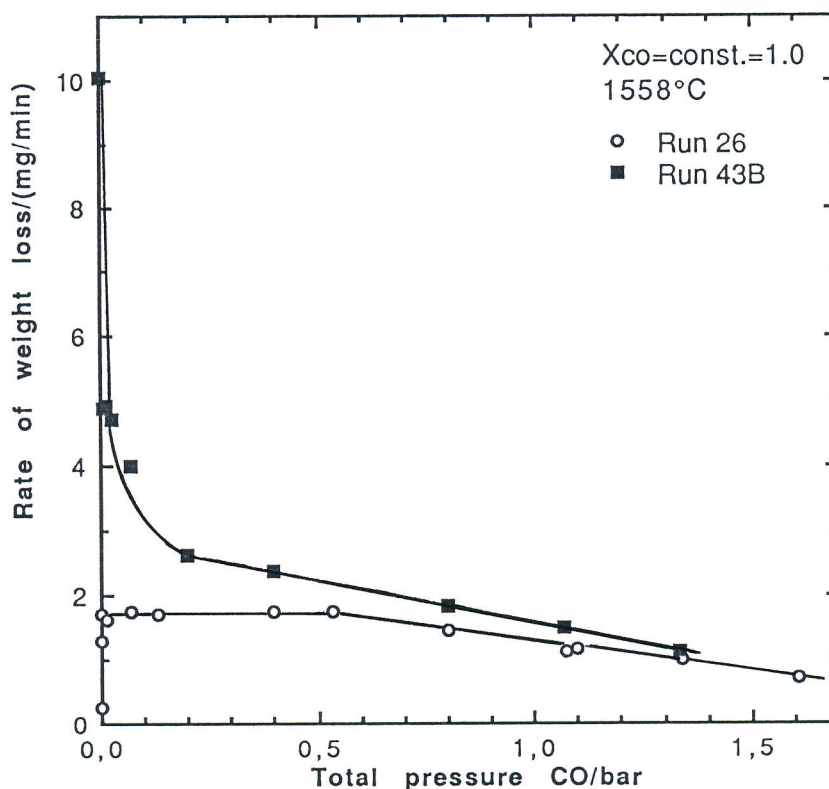
Fig. 7.6. Rate of weight loss of a cristobalite/graphite-charge where initial nucleation of SiC has taken place (Run 43B) and a quartz/graphite-charge without SiC (Run 26), in dependence of total pressure CO (X_{CO}=const.=1.0).

[2] From Fig. 6.13 it may also appear that the limiting CO pressure for formation of SiC is lower for lower total pressure. This cannot, however, be inferred from these results. Remember that the runs have not been made in sequence along the curves; on the contrary the sequence of observations go "crosswise" to the curves, and all the observations with enhanced rates were done in the same, final part of run 41.

Apart from the fact that silica is present in the forms of cristobalite and quartz, respectively, it should also be noticed that the mass of the charge with silica was three times larger than that with cristobalite. Thus the results simultaneously demonstrate the lower reactivity of silica relative to cristobalite which was discussed in Sect. 6.4.

It is seen that both curves show rates of weight loss that increase linearly with decreasing CO pressure down to pressures of about 0.5 bar. But whereas the rate of weight loss of the charge with only silica plus carbon at lower pressures levels off and becomes practically independent of the pressure, the weight loss rate of the charge with silicon carbide present shows a continued linear variation down to about 0.2 bar, and thereafter a very substantial increase.

We will first briefly give the reason why the formation of silicon carbide may lead to enhanced rates. The model described in Sections 7.1-7.2 was based on the assumption that the rate of weight loss ultimately is determined by the rate of diffusion of SiO(g) away from the reacting system. Now we assume that carbide is formed by the reaction

$$SiO + 2C = SiC + CO \tag{1.8}$$

This means that the diffusion path for SiO is very much shortened, that is, from its origin on the silica surface to the nearest carbon surface, so that SiO diffusion probably is no more rate determining. The CO which is formed instead, may be formed at a slight overpressure so that it leaves the reacting system by gas flow, which is generally much faster than diffusion.

From an equilibrium point of view the presence of SiC defines a monovariant equilibrium (coexistence of three condensed phases) which becomes invariant at a given temperature, viz.:

$$SiO_2 + 3C = SiC + 2CO \tag{1.12}$$

The corresponding equilibrium CO pressure at 1558°C is 1.6 bar (corresponding SiO pressure is 0.010 bar). That is, if equilibrium is established at the given temperature, the charge mixture would define a CO pressure substantially higher than the ambient pressure. It is of course unlikely that the two solid reactants in the form of coarse grains should come to anything

near equilibrium through the reaction given by Eq. (1.12). We may see from Fig. 7.5, however, that the concept of increased CO pressure may still be maintained. Assuming that the SiO pressure calculated from Eq. (7.5) is reasonably correct, it is seen that at. e.g., a CO-pressure of 0.2 bar, the SiO pressure is about 3×10^{-3} bar. Assuming now that this SiO reacts to form SiC, we may follow the horizontal line representing this pressure to the right until it crosses the line for reaction (1.8). From the crossing point we realize that the said SiO pressure may give rise to an equilibrium pressure of CO equal to 0.6 bar, i.e.. three times the CO pressure we assumed to begin with. Thus it is verified that the reaction, once SiC forms, may produce its own CO at substantially higher pressure than that applied.

This is also verified by the results of Fig. 6.17, which showed the progress of weight loss of a cristobalite/graphite-charge (run 46B) prepared in such a way that initial nucleation of SiC had taken place on the graphite grains. The ambient CO pressure was maintained at 0.4 mbar throughout the run by means of a rotary pump. The gas evolved from the charge at such a rate that the rotary pump in fact was unable to lower the pressure below 0.4 mbar.

Klinger, Strauss and Komarek (1966) performed similar experiments at vacuum conditions, although the silica source applied in their investigation was α-quartz. They determined the progress of reaction by measuring the amount of CO evolved. SiC was found in the solid residues. Furthermore, they found the progress of reaction to be proportional to the 1.5 power of time, and it is interesting to notice that the observations of Fig. 6.17 also obey the $t^{1.5}$ proportionality reasonably well in the accelerating region, cf. Fig. 7.7.

Klinger et al. assumed that the reaction between silica and carbon proceeded by the thermal decomposition of silica, Eq. 3.8. The transformation of quartz into cristobalite is known to proceed via a transitional noncrystalline phase, and Klinger et al. postulated that the intermediate phase was much more reactive than quartz with respect to decomposition. The formation of the intermediate transitional phase is a nucleation and growth type of process. The number of nuclei formed will increase with time and hence accelerate the rate of decomposition of silica. This would, accordingly, explain the accelerating region observed by Klinger et al. Khalafalla and Haas (1972) also concluded in their work

that the rate of carbothermal reduction of quartz is controlled by its rate of transformation into the transitional phase, which is consistent with the assumptions of Klinger et al. This assumption, however, is in contradiction with the present observations described in Paragraph 6.4.2, where it was found that the continuous transformation of quartz into cristobalite at constant temperature and gas pressure did not affect the rate of reaction.
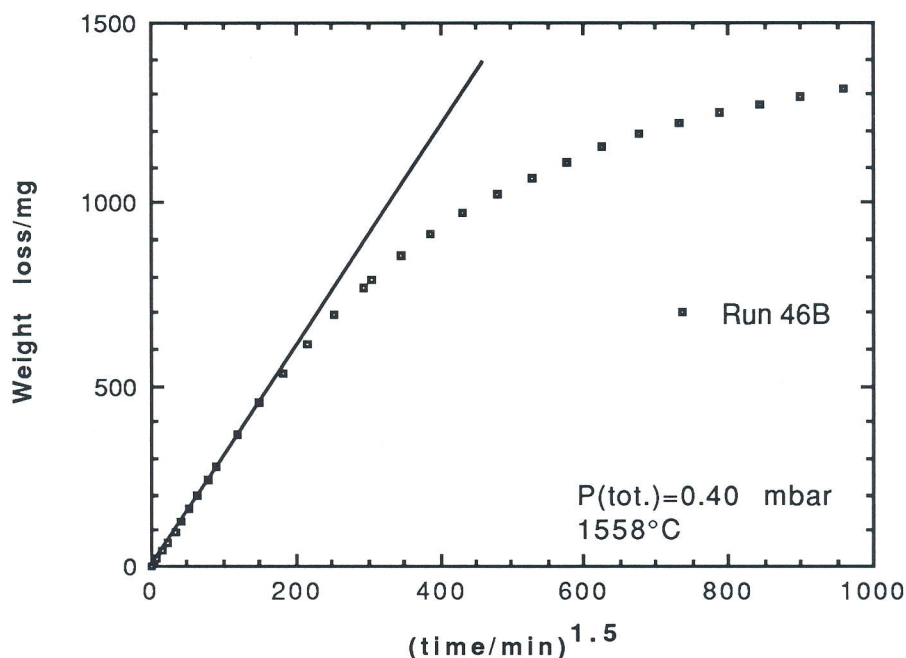
Fig. 7.7. Weight loss of a cristobalite /graphite charge (run 46B) in against the 1.5 power of time when SiC is formed continuously at 1558°C and total pressure 0.40 mbar (rate in dependence of time is given in Fig. 6.17).

Furthermore, the present final experiments were conducted with cristobalite as the silica source, thus the silica is not supposed to undergo any phase transformation during the experiment (except for the low-temperature α-β transition during heating up). In spite of this, the present results do resemble the observations of Klinger et al. and Khalafalla and Haas. The accelerating region in run 46B is probably due to the continuous nucleation of SiC on the C-surface: Once a stable SiC nucleus is formed on the C-surface, this site becomes an active consumer of SiO and subsequent growth of SiC takes place. As the number of stable nuclei increases during the run, the number of active sites consuming SiO will correspondingly increase, and so does the observed reaction rate. This is quite possibly the explanation for the accelerating region in the experiments of the above-mentioned authors as well.

At a certain point in the course of the reaction, the increase in the number of active sites levels off. At the same time the area of carbon surface available for the Boudouard reaction has decreased, the amount of silica has decreased, and the observed rate of reaction will then also decrease, as seen in Fig. 7.7. A more quantitative interpretation of this curve is beyond the scope of the present contribution.

Run 46B, illustrated in Fig. 6.17, was also mentioned above as an example to show that the reaction is quite able to supply its own carbon monoxide for the reaction when silicon carbide is formed. Given that this statement presupposes the correctness of the reaction mechanism which has been advocated throughout this thesis, it also poses a problem. The highest rates shown in Fig. 7.3 are of the order of 2.5 mg/min, and in the discussion (Paragraph 7.3.2) the fact that these rates fall short of the calculated ones was tentatively explained by the assumption that the chemical reaction on the silica surface takes over as rate controlling. Furthermore it was forwarded that the rate in this case should be proportional to the square root of the CO pressure. In the presence of SiC, however, the observed rates are of the order of 10 to 20 mg/min, that is, almost an order of magnitude larger, as shown for two different runs in Fig. 7.6 and 7.7. Furthermore these high rates occur at very low CO pressures. In e.g., run 46B (Fig. 7.7) the prevailing CO pressure inside the charge must have been higher than the 0.4 mbar recorded on the pressure gauge, but still it must have been quite low. These high rates combined with low CO pressures are difficult to reconcile with the idea of chemical control on the silica surface, but we do not as yet have a solution to this part of the puzzle.

8. CONCLUDING REMARKS

In the introductory remarks on the background of the work, it was stated that the primary aim of the present investigation has been to elucidate the mechanism or mechanisms by which solid silica may react with solid carbon at elevated temperatures. This turned out not to be an easy task. For one thing, the reactions of silicon dioxide are more difficult to study than those of many other oxides, because of the many modifications and phase transformations of silica. These, in the introductory part of the experimental work, showed up in the form of a severe lack of reproducibility. Transforming the quartz to cristobalite by heat treatment prior to the runs resulted in a much improved reproducibility. At the same time, however, it resulted in a markedly increased reaction rate, not because the crystal form of cristobalite in itself is more reactive than quartz, but because the low-temperature $\alpha-\beta$ transition in cristobalite (at about 270°C) is accompanied by a substantial volume change that introduces micro-cracks in the oxide. The effect of these may be interpreted either as an increase in surface area or as an enhanced reactivity of the given surface area; either way it gives increased reaction rate for a given grain size.

The reaction between materials in the form of grains cannot be studied without a container, and it was found experimentally that the design of the container had a pronounced influence on the observations. This question of the design of container introduces a variable which is irrelevant to the problem at hand, but it cannot be avoided. It is hoped that the design chosen for the final series of experiments, with a perforated body and a lid with a number of large holes, has yielded results that may be of some general significance.

A further consequence of the difficulties with reproducibility has been that most of the experiments have been performed at one and the same temperature. A limited number of reproducible results at one temperature was thought to be of more value than a large number of scattered results at many temperatures.

Furthermore, most of the experiments have been done with one and the same grain size of the reactants for the same reason.

These remarks are given to indicate that, strictly speaking, the results presented in this thesis are valid only for the experimental arrangement and the temperature used in these studies. Within this limitation, and based on studies of the variation in reaction rate with the systematic and independent variations of total gas pressure and of carbon monoxide partial pressure, it may be concluded that the equations

$$SiO_2(s) + CO(g) = SiO(g) + CO_2(g) \qquad (3.9)$$

$$\text{and} \quad CO_2(g) + C(s) = 2CO(g) \qquad (1.4)$$
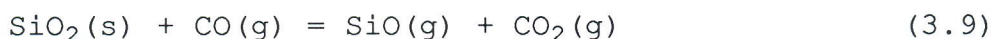
do indeed represent the initial mechanism in the reaction between silica and carbon. This is further corroborated by the model presented in Chapter 7, based on the concepts of local equilibrium of reaction (3.9) on the silica surface and of reaction (1.4) on the carbon surface, coupled with gaseous diffusion of CO_2 between the surfaces, and of SiO out of the reacting system. The rates calculated from the model show satisfactory agreement with the observed weight loss rates over a wide range of total pressures and partial pressures.

In order to see whether the model, or the whole concept of local equilibria of reactions (3.9) and (1.4), is valid for other conditions, experiments should be conducted with variation in

-grain size   -container design
-carbon to silica ratio   -temperature
-quality of carbon material   -and gas pressures as above
-total mass of charge

This in itself may amount to a formidable task unless restrictions are placed on the number of variables to be studied.

In the majority of experiments carried out during the present work, silicon carbide was not formed. This was in accordance with the intentions, since the primary aim was the study of the above reactions, or rather their sum, which gives

$$SiO_2(s) + C(s) = SiO(g) + CO(g) \qquad (1.7)$$

The SiO gas may subsequently react on the carbon surfaces to form silicon carbide:

$$SiO(g) + 2C(s) = SiC(s) + CO(g) \qquad (1.8)$$

From the thermodynamics of this reaction it is found that silicon carbide should be stable and should have been formed under conditions of several of the present experiments where it was not detected. This indicates that the nucleation and growth of silicon carbide on a graphite surface meets with some kinetic hindrance, as one would expect.

On the other hand, when silicon carbide is formed, or when experiments are performed with graphite on which prior formation of silicon carbide has taken place, a strong increase in the rate of reaction at low gas pressures is observed. Qualitatively this is explained by the fact that the SiO(g) formed by reactions (3.9) + (1.4) = (1.7) may now only diffuse to the nearest carbon surface where it is consumed by the reaction (1.8), instead of diffusing the much longer path out of the reacting system. But this explanation also poses a problem: It would appear that reaction (3.9) requires a certain pressure of carbon monoxide to proceed, and that the rate would increase with the carbon monoxide pressure (as is actually observed). But in the presence of silicon carbide the observable reaction (which is then the sum of reactions (1.7) and (1.8)) proceeds with a high rate even at very low CO pressures.

The behaviour of the reactions in the presence of silicon carbide is another area that definitely deserves further study. In the opinion of the present author it seems that the same concept of the primary reaction (3.9) may be maintained also in this case, since it appears difficult to propose any other viable mechanism for the reaction.

REFERENCES

Abrahamson, J. and Wiles, P. G. (1978), Carbon **16**, 341-349.

Ainslie, N. G., Morelock, C. R. and Turnbull, D. (1962), in "Symposium on Nucleation and Crystallization in Glasses and Melts". Eds. M. K. Reser, G. Smith and H. Insley. The Am. Ceram. Soc., Columbus, Ohio, 97-107.

Barin, I., and Knacke, O. (1973), "Thermochemical Properties of Inorganic Substances", Springer-Verlag Berlin, Verlag Stahleisen, Düsseldorf, 921 pp.

Bell, T., Hetherington, G. and Jack, K. H. (1962), Phys. Chem. Glasses, **3**, 141-146.

Bentsen, S., Jørgensen, S., Wiik, K. and Motzfeldt, K., (1985), in "Reactivity of Solids" (10th ISRS), ed. by P. Barret and L.-C. Dufour, Elsevier, Amsterdam, 621-626.

Biernacki, J. J. and Wotzak, G. P. (1989), J. Am. Ceram. Soc., **72**, 122-129.

Bihuniak, P. P. (1983), J. Am. Ceram. Soc., **66**, C188 - C189.

Blaha, H and Komarek, K. L. (1989), High. Temp. Science, **28** (in print).

Blegen, K. (1976), "Equilibria and Kinetics in the System Si-N, Si-O-N and Si-C-O-N", dr. ing. thesis, Inst. uorganisk kjemi, NTH, Trondheim, Norway, 260 pp.

Bonner, F. and Turkevich, J. (1951), J. Am. Chem. Soc., **73**, 561-564.

Borisov, K. G. (1967), Tr. Vses. Inst. Nauch.-Issled. Proekt. Rab. Ogneupor. Prom., **39**, 128-45.

Bousheri, A., Bzowski, J., Kestin, J., Mason, E. A. (1987), J.
        Phys. Chem. Ref. Data, **16,** p. 452, Table 4.

Bundy, F. P. (1980), J. Geophysical Research, **85,** 6930-6936.

Chaklader, A. C. D. (1963), J. Am. Ceram. Soc., **46,** 66-71.

Chaklader, A. C. D. and Roberts, A. L. (1961), J. Am. Ceram. Soc.,
        44, 35-41.

Coes, L. (1953), Science, **118,** 131-133.

Dolloff, R. T. (1960), WADD Tecnical Report 60-143, Wright Air
        Development Division; U.S. Dept. Comm., Office Tech.
        Service, PB Rept. 171,365, 28 pp.

Drowart, J., De Maria, G. and Inghram, M. G. (1958), J. Chem.
        Phys. **29,** 1015-1021.

Ergun, S. (1956), J. Phys. Chem., **60,** 480-485.

Ergun, S. and Mentser, M. (1965), "Reactions of Carbon with Carbon
        Dioxide and Steam" in "Chemistry and Physics of Carbon",
        Vol. 1, ed. by P. L. Walker(jr.), 203-263.

Ergun, S. and Mentser, M. (1967), Carbon **5,** 331-337.

Essenhigh, R .H. (1981), "Fundamentals of Coal Combustion" in
        "Chemistry of Coal Utilization", Second supplementary
        volume, ed. by M. A. Elliott, Wiley, New York, 1153-1312.

Flørke, O. W. (1956), Naturwiss, **43,** 419-420.

Fredersdorff, C. G. von and Elliott, M. A. (1963), "Coal
        Gasification" in "Chemistry of Coal Utilization",
        Supplementary Volume, ed. by H. H. Lowry, Wiley, New
        York, 892-1022.

Fromhold(jr.), A. T. and Fromhold, R. G. (1984), "An Overview of
        Metal Oxidation Theory" in "Comprehensive Chemical
        Kinetics", Vol. 21, ed. by C. H. Bamford, C. F. H. Tipper
        and R. G. Compton, Elsevier, Amsterdam, 1-117.

Gadsby, J., Hinshelwood, C. N. and Sykes, K. W. (1946),
        Proc.Roy.Soc.(London), **A187**, 129.

Gjerstad, S. (1968), "Kjemisk-metallurgiske undersøkelser
        vedrørende karbotermisk reduksjon av aluminiumoksyd og
        silisiumoksyd", dr.ing. thesis, Inst. uorganisk kjemi,
        NTH, Trondheim, 127 pp.(in Norwegian).

Hirata, H. and Hoshikawa, K. (1980), Jpn. J. Appl. Phys. **19**, 1573-
        1574.

Hong, J. D. and Davis, R .F. (1980), J. Am. Ceram. Soc., **63**, 546-
        552.

Hong, J. D., Davis, R. F. and Newbury, D. E. (1981), J. Mater.
        Sci., **16**, 2485-2494.

JANAF Thermochemical Tables, 3rd. ed., Ed. by M. W. Chase et al.,
        J. Phys. Chem. Ref. Data, Vol. 14, 1985.

Johannessen, J. S., Spicer, W. E. and Strausser, Y. E. (1976),
        "Use of Auger Electron Spectroscopy to Determine the
        Structure of Silicon Oxide Films", in "Surface Analysis
        for Silicon Devices", ARPA/NBS Workshop IV, 1975, A. G.
        Lieberman, ed., NBS Spec. Publ. 400-423. See also J. Appl.
        Phys. **47** (1976) 3028-3037.

Johnson, R. E. and Muan, A. (1968). J. Am. Ceram. Soc. **51**, 430-
        433.

Keat, P. P. (1954), Science, **120**, 328-330.

Khalafalla, S. E. and Haas, L. A. (1972), J. Am. Ceram. Soc. **55**,
        414-417.

Klinger, N., Strauss, E. L. and Komarek, K. L. (1966), J. Am. Ceram. Soc. **49**, 369-375.

Koga, Y. and Harrison, L. G. (1984), "Reactions of Solids with Gases Other than Oxygen" in "Comprehensive Chemical Kinetics", Vol. 21, ed. by C. H. Bamford, C. F. H. Tipper and R. G. Compton, Elsevier, Amsterdam, 119-149.

Konijnenburg, J. T. van (1977), Sci. Ceram. **9**, 339-347.

Kozhevnikov, G. N., Vodop´yanov, A. G. and Chufarov, G. I. (1972), Russ. Met. **1972** (4) (Engl. trans) 51-54.

Kozhevnikov, G. N., Vodop´yanov, A. G. and Nefedov, P. Ya. (1973), Russ. Met. **1973** (5) (Engl. trans.) 24-27.

Kvande, H., Linga, H., Motzfeldt, K. and Wahlbeck, P. G. (1979), Acta Chem. Scan., **A33**, 281-288.

Lamoreaux, R. H., Hildenbrand, D. L. and Brewer, L. (1987), J. Phys. Chem. Ref. Data, **16**, 419-443.

Lee, L.G., Miller, P. D. and Cutler, I. B. (1977), in "Reactivity of Solids" (8th ISRS), ed. by J. Wood, O. Lindqvist, C. Helgesson and N.-G. Vannerberg, Plenum Press, 701-711.

Leko, V. K. and Komarova, L. A. (1975), Russ. Inorg. Materials **11** (Engl. trans.) 950-953.

Levenspiel, O. (1972), "Chemical Reaction Engineering", 2. ed., John Wiley & Sons, 578 pp., p. 374.

Long, F. J. and Sykes, K. W. (1948), Proc. Roy. Soc. (London), **A193**, 377.

Marrero, T. R. and Mason, E. A. (1972), J. Phys. Chem. Ref. Data, **1**, 3-118.

Massalski, T. H., Ed., (1986), "Binary Alloy Phase Diagrams", Am. Soc. for Metals, Columbus, Ohio, Vol. 1 + 2, 2224 pp.

172

Miller, P. D., Lee, J. G. and Cutler, I. B. (1979), J. Am. Ceram. Soc., **62**, 147-149.

Minnear, W. P. (1979), Ext. Abstr. Program, Bienn. Conf. Carbon **14**, 181-182.

Minnear, W. P. (1982), J. Am. Ceram. Soc., **65**, C10-C11.

Mitra, S. (1977), Trans. J. Brit. Ceram. Soc., **76**, 71-74.

Motzfeldt, K. (1961), "En vurdering av ferrosilisiumprosessens kjemi", Inst. silikatforskning/Inst. uorg. kjemi, NTH, Trondheim, 74 pp. (in Norwegian).

Motzfeldt, K. (1988), "Oxides Plus Carbon", in "Terkel Rosenqvist Symposium", Proceedings, ed. by S. E. Olsen and J. K. Tuset, Division of Metallurgy, NTH, Trondheim, 127-150.

Motzfeldt, K. and Steinmo, M. (1989), "Vaporization of Silicon Carbide Studied by Mass-Loss Effusion", SINTEF Report STF34 A89061.

Muan, A. and Osborn, E. F. (1965), "Phase Equilibria among Oxides in Steelmaking", Addison-Wesley, Reading, Mass., 236 pp.

Nagamori, M., Malinsky, I. and Claveau, A. (1986), Met. Trans. **17B**, 503-514.

Nagamori, M., Malinsky, I. and Claveau, A. (1987), Met. Trans. **18B**, 472-477.

Olesinski, R. W. and Abbaschian, G. J. (1984), Bull. Alloy Phase Diagr. **5**, 486-489.

Ozturk, B. and Fruehan, R. J. (1985), Met. Trans., **16B**, 801-806.

Paule, R. C. and Margrave, J. L. (1967), "Free-Evaporation and Effusion Techniques" in "The Characterization of High Temperature vapors", ed. by J. L. Margrave, Wiley, New York, 130-151.

Philipp, R. H. (1972), J. Non-Cryst. Solids, **8-10**, 627-632.

Poch, W. and Dietzel, A. (1962), Ber. Dtsch. Keram. Ges. **39**, 413-426.

Present, R. (1958), "Kinetic Theory of Gases", McGraw-Hill, New York, 280 pp.

Pulz, W. W. and Hertl, W. (1966), "Part 1. Kinetics and Mechanism" Trans. Faraday Soc., **62**, 2499-2504. "Part 2. Effect of Added Gases" ibid. 3440-3445.

Raaness, O. and Tuset, J .K. (1972) "Reaktivitet av reduksjonsmaterialer" Rapp. for NTNF og Norske Ferrosilisiumprodusenters Sentralkontor, SINTEF, Trondheim (in Norwegian).

Ranz, W. E. and Marshall(jr.), W. R. (1952), Chem. Eng. Progr., **48**, 141-146.

Rao, C. N. R. and Gopalakrishnan, J. (1986), "New Directions in Solid State Chemistry", Cambridge Univ. Press, 503 pp.

Rao, Y. K. (1971), Met. Trans. **2**, 1439-1447.

Rao, Y. K. (1974), Chem .Eng. Sci., **29**, 1435-1445.

Rao, Y. K. and Jalan, B. P. (1972), Met. Trans., **3**, 2465-2477.

Reif, A. E. (1952), J. Phys. Chem. **56**, 785-788.

Richet, P., Bottinga, Y., Denielou, L., Petitet, J .P. and Tequi, C., Geochim. et Cosmochim. Acta, **46**, 2639-2658.

Robertson, D. G. and Sohn, H. Y., eds., (1986), "Gas-Solids Reactions in Pyrometallurgy", Center for Pyrometallurgy, Univ. of Missouri-Rolla, Rolla, Missouri. 408 pp.

Rosenqvist, T. and Tuset, J. Kr. (1987), Met. Trans. **18B**, 471-472.

174

Ruff, O. (1935), Trans. Electrochem. Soc. **68**, 87-109.

Ryabchikov, I. V., Gorokh, A. V., Krushchev, M. S., Rusakova, A.
        G., and Maksimov, Yu. S. (1966b), Metally **1960** (4) 38-43,
        Russ. Met. **1966** (4) (abridged transl.) 15-16.

Ryabchikov, I. V., Krushchev, M. S. and Shchedrovitskii, Ya. S.
        (1966a), Izv. Akad. Nauk. SSSR **167**, 155-157.

Sandberg, B. (1981), "Karbotermisk reduksjon av aluminiumoksyd",
        dr. ing. thesis, Inst. uorganisk kjemi, NTH, Trondheim,
        Norway, 140 pp (in Norwegian).

Scace, R. I. and Slack, G. A. (1959), J. Chem. Phys. **30**, 1551-
        1555.

Schei, A. (1977), "Ferrosilisiumprosessens metallurgi", Elkem R&D
        Center, Kristiansand, 256 pp.(in Norwegian).

Schei, A. and Sandberg, O. (1966), "Back Reactions During
        Production of Silicon Metal in a Submerged Arc Electric
        Furnace" in "Selected Topics in High Temperature
        Chemistry", ed. by T. Førland, K. Grjotheim, K. Motzfeldt,
        and S. Urnes, Universitetsforlaget, Oslo, 141-150.

Schwerdtfeger, K. (1966), Trans. Met. Soc. AIME **236**, 1152-1156.

Seltveit, A., (1980), "Ildfaste materialer", Tapir Forlag,
        Trondheim, 274 pp. (in Norwegian).

Shaffer, P. T. B. (1969), Acta Cryst. **B25**, 477-488.

Sigurjonsson, K. (1986), final student project ("diplomarbeid"),
        Inst. uorganisk kjemi, NTH, 75 pp. (in Norwegian).

Sohn, H. Y. and Wadsworth, M. E., eds., (1979), "Rate Processes of
        Extractive Metallurgy", Plenum Press, New York, 472 pp.,
        Sect. 4.2, 285-320.

Sosman, R. B. (1955), Trans. Brit. Ceram. Soc., **54**, 655-670.

Sosman, R. B. (1964), Bull. Am. Ceram. Soc., **43**, 213.

Stishov, S .M. and Popova, S. V. (1961), Geokhimiya, **10**, 837-839.

Szekely, J. and Themelis, N. J. (1971), "Rate Phenomena in Process
        Metallurgy", Wiley-Interscience, New York, 784 pp.

Szekely, J., Evans, J. W. and Sohn, H. Y. (1976), "Gas-Solid
        Reactions", Academic Press, New York, 400 pp., Chap. 5,
        176-204.

Temkin, R. J. (1975), J. Non-Cryst. Solids, **17**, 215-230.

Turkdogan, E. T. and Vinters, J. V. (1970), Carbon **8**, 39-53.

Tuset, J. K. (1972), Foreløpig fremdriftsrapport for SINTEF-
        prosjektene 340534 og 340536, NTH, Trondheim (in
        Norwegian).

Vodop´yanov, A. G., Baranov, S. V. and Moiseev, G. K. (1983b),
        Russ. Met. **1983** (5) (Engl. trans.) 18-23.

Vodop´yanov, A. G., Baranov, S. V., Moiseev, G. K. and
        Kozhevnikov, G. N. (1983a), Russ. Met. **1983** (3) (Engl.
        trans.) 28-32.

Vodop´yanov, A. G., Zlokazov, B. G., Kozhevnikov, G. N. and
        Ovchinnikova, L. A. (1978), Russ. Met. **1978** (2) (Engl.
        trans.) 30-35.

Wagstaff, F. E., Brown, S. D. and Cutler, I. B. (1964), Phys.
        Chem. Glasses, **5**, 76-81.

Walker(jr.), P. L., Rusinko(jr.), F. and Austin, L. G. (1959),
        Advances in Catalysis, **11**, Academic Press; New York, 133-
        221.

Wecht, E. H. P. (1977), "Feuerfest-Siliciumcarbid", Springer-
        Verlag, 276 pp., p. 17.

Weiss, A. and Weiss, A. (1954), Z. Anorg. Chem., **276**, 95-112.

Wells, A. F. (1984), Structural Inorganic Chemistry, 5th. Ed.,
        Oxford University Press, 1382 pp., p. 1006.

White, F. M. (1974), "Viscous fluid flow" McGraw-Hill, New York,
        725 pp.
Wilke, C. R. (1950), Chem. Eng. Prog., **46,** 95-104.

Yudin, B. F., Makarova, N. L. and Borisov, V. G. (1968), J. Appl.
        Chem. USSR, **41** (Engl. trans.) 29-33.

APPENDICES

A1. The electronic weighing system

This is included as a service to the future operators of the thermobalance Versatilie and, for that matter, partly written in norwegian. The computer program, which enables the BBC micro-computer to comunicate with the multimeter (cf. Fig. 4.6), is written in BASIC and listed in Appendix A1.2.

A1.1. Procedure for running the weight program "W.RATE" on a BBC-microcomputer.

Programmet er skrevet i BASIC og "leser" veiesignalet [V] fra en "5405 Sartorius veiecelle" via et "7151 Solartron computing multimeter" samt styrer utskriftformatet på skriver.

1.   Slå på strømforsyningsenhet (Sartorius A7048) til veiecelle (bryter i front av instrumentet).

2.   Slå på "7151 Solartron computing multimeter" (bryter bak på instrumentet).

Trykk så **MENU** tasten på tastaturet til multimeteret. Tasten **SKIP** trykkes fortløpende til display viser "PROGS?", deretter trykkes **ENTER** og **SKIP** trykkes til display viser "RECALL?". **ENTER** trykkes og dersom display viser "ANALOG?" trykkes **EXIT** og **TRACK**. Multimeteret er nå operativt, gå til pkt. 3.
Dersom display ikke viser "ANALOG?" (f.eks. "EMPTY" eller noe annet) trykkes **EXIT** og deretter **MENU** (samme tast som **EXIT**). **SKIP** trykkes til display viser "PROGS?", deretter trykkes **ENTER** og **SKIP** trykkes til display viser "ANALOG?". **ENTER** velges og **SKIP** trykkes til display viser "CHART?", deretter trykkes **ENTER**. **SKIP** trykkes til display viser "RUN?" deretter **ENTER**. Display viser nå "YMAX=" for deretter å vise "1.0000". **ENTER** trykkes og display viser "YMIN=" for deretter å vise "-1.0000", trykk så **ENTER** (tallverdiene til YMAX og YMIN er likegyldige siden dataprogrammet "W.RATE" beregner de korrekte verdier, YMAX og YMIN må forøvrig ha et innhold for at mikrodatamaskinen og multimeteret kan

kommunisere). Display viser "OK" deretter trykkes **EXIT** og **TRACK**.
Multimeteret er nå operativt, gå til pkt. 3.

3.   Slå på BBC-mikrodatamaskin (bryter bak på maskinen) og dens
      monitor (bryter i front).

4.   Diskett merket "W.RATE" legges i diskettdrevet.

5.   Kommandoen: CHAIN "W.RATE" skrives med etterfølgende **RETURN**
      (dvs. return tasten på tastaturet)

      Nedenfor er listet spørsmålene som deretter i tur dukker fram
på monitor etterhvert som de blir besvart:

6.   HOW MANY MEASUREMENTS TO CALCULATE RATE (max. 100)?
      Svar f.eks. 100   **RETURN** (En rutine som beregner
      vekttapshastighet ved hjelp av lineær regresion gjør nå
      dette på basis av hundre enkelt målinger).

7.   WEIGHT OF SAMPLE (mg):
      Svar f.eks. 10000 **RETURN** (dette betyr at innveid prøve
      veier 10 g og en prosedyre som beregner % vektendring bruker
      dette som utgangsvekt.)

8.   CHOOSE MEASUREMENT MODE (TIME):

      1. NINES 3 (6.6 ms)
      2. NINES 4 (40 ms)
      3. NINES 4 (50 ms)
      4. NINES 5 FILTER OFF (400 ms)
      5. NINES 5 FILTER ON (1.6 s)
      6. NINES 6 (6X9/800 ms)

      Svar f.eks. 6 (Solartron multimeteret måler nå
      spenningssignalet [V] fra veiecellen med en nøyaktighet på
      seks desimaler. Målemoden anbefales siden den også gir en
      god skjerming mot eventuelt støy. Se forøvrig:"7151
      COMPUTING MULTIMETER, OPERATING MANUAL, Solartron
      Instruments." for en nærmere beskrivelse av de enkelte
      målemoder.

9. FULL RANGE CHART (mg):

Svar f.eks. 100 **RETURN**. Med 10 V full skala på skriver vil dette nå tilsvare 100 mg. Følsomheten kan man selvfølgelig velge fritt, men bedre enn 50 mg full skala er ikke å anbefale. Selv 50 mg full skala kan gi ubehagelig langtidsdrift. (Generelt bør "FULL RANGE CHART" velges i forhold til forventet totalt vekttap. Det har liten hensikt å la skriveren gå en mengde ganger tversover skalaen i ett forsøk.)

10. START%=

Svar f.eks. 50 **RETURN** (Skriverpapiret er tenkt inndelt i 100%, i dette tifelle vil skriverpennen begynne å skrive midt på skriverpapiret. Forøvrig må verdiene velges i området: 11<START%<89, andre verdier vil ligge i "dødbåndsområdet" til Solartron multimeteret og er således ulovlige).

Etter at siste spørsmål er besvart vil monitorskjermen se omtrent slik ut:

<div align="center">

FULL RANGE CHART(mg):100

WEIGHT OF SAMPLE(mg):10000

</div>

A. CHANGE RANGE CHART

B. CHANGE MEASUREMENT TIME (6X9/800 ms)

C. TERMINATE

D. PRINT RESULT

E. # MEAS. TO CALC. RATE (100)

m(mg)	%weight loss	rate(mg/min)	cor.coeff.
Absolute weight change from initial weight	Calculates % weight change from initial weight	Calculates weight change per unit time	The rate calculation rutine is based on linear regression. Corr.coeff. should be close to 1.

182

11. Program-parametrene kan endres ved å velge fra ovenstående
meny. Ved å velge "A" på tastaturet kan fullt utslag på
skriver endres til en annen ønsket verdi. Ved å velge "D"
for man skrevet ut en resultatlinje på printer (dvs. m(mg),
%weight loss, rate(mg/min) og corr.coeff.).

12. Programmet avsluttes ved å velge "D". Ny programkjøring
startes ved å gi kommandoen: RUN **RETURN**.

A1.2. Listing of the BASIC-program "W.RATE".

```
10 CLS
11 INPUT"  HOW MANY MEASUREMENT TO CALCULATE THE    RATE(max.100)";ANT
12 TIME=0:HAST=0:CORR=0
13 DIM SUM(100,2)
15 PRINT
20 INPUT"WEIGHT OF SAMPLE (mg):"WSAMPLE
30 REM   KALIBRERING 14/10-87
40 CALFACT=43897.4
50 REM----VELG OENSKET MAALETID--------------------------------------------------
60 GOSUB 80
70 GOTO450
80 A=&5000
90 CLS
100 *FX21,0
110 PRINT"CHOOSE MEASUREMENT MODE(TIME):"'
120 PRINT"1. NINES 3 (6.6ms)"'
130 PRINT"2. NINES 4 (40ms)"'
140 PRINT"3. NINES 4 (50ms)"'
150 PRINT"4. NINES 5 FILTER OFF (400ms)"'
160 PRINT"5. NINES 5 FILTER ON (1.6s)"'
170 PRINT"6. NINES 6 (6X9/800ms)"
180 B=GET
190  IF B=49 THEN $A="IO":TM$="(6.6ms)":GOSUB330
200 IF B=50 THEN $A="I1":TM$="(40ms)":GOSUB330
210 IF B=51 THEN $A="I2":TM$="(50ms)":GOSUB330
220 IF B=52 THEN $A="I3":TM$="(400ms)":GOSUB330
230 IF B=53 THEN $A="I5":TM$="(1.6s FILT ON)":GOSUB330
240 IF B=54 THEN $A="I4":TM$="(6X9/800ms)":GOSUB330
250 IF B<49 OR B>54 THEN GOTO90 ,
260 CLS
270 *FX3,4
280 VDU28,26,5,41,4
290 CLS
300 PRINT TM$
310 *FX21,1
320 RETURN
```

```
330 *FX2,2
340 *FX2,2
350 *FX7,7
360 *FX8,7
370  *FX21,1
380 OSBYTE=&FFF4
390 FOR I=0 TO LEN($A)
400 A%=138:X%=2
410 Y%=A?I
420 CALL OSBYTE
430 NEXT I
440 RETURN
450 MODE3
460 VDU 28,0,8,79,0
470 *FX21,0
480 CLS
490 INPUT"FULL RANGE CHART(mg):"W
500 DELU=0.78*(W/CALFACT)
510 PRINT
520 INPUT"START%="START
530 CLS
540 PRINT TAB(26);"***FULL RANGE CHART(mg):";W;"***"
550 PRINT TAB(26);"WEIGHT OF SAMPLE(mg):";WSAMPLE
560 PRINT
570 PRINT"A. CHANGE RANGE CHART"
580 PRINT"B. CHANGE MEASUREMENT TIME";TM$
590 PRINT"C. TERMINATE"
595 PRINT"D. PRINT RESULT"
597 @%=&20009:PRINT"E. # MEAS. TO CALC. RATE (";ANT;")"
600  VDU28,0,10,79,9:PRINT;TAB(4);"m(mg)";TAB(20);"%weight loss";
605  TAB(37);"rate(mg/min)";TAB(54);"cor.coeff."
610 REM----LES VOLTMETER(MIDDEL AV 10 MAALINGER)------------------
620 GOSUB1130
630 REM----BEREGN YMIN,YMAX----------------
640 N=UMAALT-DELU*((START-11)/78)
650 M=UMAALT+DELU*((89-START)/78)
660 GOSUB680
670 GOTO910
```

```
 680 REM----SKRIV KOM. TIL VOLTM. F.O.M. LAGERCELLE &5000----------------------
 690 A=&5000
 700 REM---LAGE KOMMANDO STRENG--------
 710 A$="MODIFY ANALOG "
 720 B$="YMAX="
 730 C$=" YMIN="
 740 D$=STR$(M)
 750 E$=STR$(N)
 760 COM$=A$+B$+D$+C$+E$
 770 $A=COM$
 780 OSBYTE=&FFF4
 790 REM----SEND KOMMANDO STRENG---------
 800 *FX2,2
 810 *FX7,7
 820 *FX8,7
 830 *FX21,1
 840 FOR I=0 TO LEN($A)
 850 A%=138:X%=2
 860 Y%=A?I
 870 CALL OSBYTE
 880 NEXT I
 890 *FX21,1
 900 RETURN
 910 REM---FORETA 5 MAALINGER-----------
 920 GOSUB1330
 930 *FX3,4
 935 VDU28,32,7,40,6:CLS
 940 REPEAT
 945 FOR NUMB=1 TO ANT
 950 *FX2,2
 960 IF INKEY(-66) THEN GOTO460
 970 IF INKEY(-101) THEN GOSUB80
 980 IF INKEY(-83) THEN PRINT:PRINT"LOG.PROGRAM TERMINATED":GOTO 1110
 985 IF INKEY(-51) THEN PROCprint
 987 IF INKEY(-35) THEN PROCmeas
 990 *FX2,1
1000 *FX3,6
1010 INPUT VDC$
1020 VDC=VAL(LEFT$(VDC$,9))
1022 SUM(NUMB,1)=VDC*CALFACT:SUM(NUMB,2)=TIME/6000
```

```
1030  IF VDC<N OR VDC>M THEN GOSUB1280
1040  @%=&20409
1050  *FX3,4
1060  VDU 28,0,24,79,11
1070  DELM=CALFACT*(VDC-UMAALT)
1080  PRINT DELM;TAB(22);100*DELM/WSAMPLE;TAB(39);HAST;TAB(57);CORR
1090  *FX2,2
1095   NEXT NUMB
1097  PROCRATE
1100  UNTIL FALSE
1110  *FX21,0
1120  END
1130  REM----BEREGN MIDDEL AV 10 MAALINGER(SUBRUTINE)-------------------
1140  C=0
1150  GOSUB1330
1160  FORK=1 TO 10
1170  *FX2,1
1180  *FX3,6
1190  INPUT F$
1200   G$=LEFT$(F$,9)
1210   C=C+VAL(G$)
1220  *FX2,2
1230  *FX3,4
1240   NEXT K
1250   UMAALT=C/(K-1)
1260  RETURN
1270  REM----SLUTT SUBRUTINE--------------------------------------------
1280  REM----KORREKSJONSRUTINE----------------
1290  IF VDC<N THEN M=VDC:N=VDC-DELU ELSE N=VDC:M=VDC+DELU
1300  GOSUB680
1310  GOSUB1330
1320  RETURN
1330  REM----LES KOM. STRENG I OUTP.BUFFER-----------------------------
1340  *FX2,1
1350  *FX3,6
1360  INPUT BEG$
1370  RETURN
```

```
1390 REM-----RUTINE FOR BEREGNING AV VEKT TAPSHASTIGHET-----------------
1400 DEF PROCRATE
1410 STIDVKT=0:SUMTID=0:SUMVEKT=0:KVADTID=0:KVADVKT=0
1420 FOR NUMB=1 TO ANT
1430 STIDVKT=STIDVKT+((SUM(NUMB,1)-SUM(1,1))*SUM(NUMB,2))
1440 SUMTID=SUMTID+SUM(NUMB,2)
1450 SUMVEKT=SUMVEKT+(SUM(NUMB,1)-SUM(1,1))
1460 KVADTID=KVADTID+((SUM(NUMB,2))^2)
1465 KVADVKT=KVADVKT+((SUM(NUMB,1)-SUM(1,1))^2)
1470 NEXT NUMB
1480   HAST=(STIDVKT-((SUMTID*SUMVEKT)/(NUMB-1)))/
        (KVADTID-(((SUMTID)^2)/(NUMB-1)))
1483   CORR=((STIDVKT-((SUMTID*SUMVEKT)/(NUMB-1)))^2)/((KVADTID
      -(((SUMTID)^2)/(NUMB-1)))*(KVADVKT-(((SUMVEKT)^2)/(NUMB-1))))
1490 TIME=0
1593 ENDPROC
1595 REM----RUTINE FOR UTPRINTING AV RESULTAT--------------------------
1600 DEF PROCprint
1610 *FX3,0
1620 VDU2
1625 VDU1,27,69
1630   PRINT;TAB(4);"m(mg)";TAB(20);"%weight loss";
        TAB(37);"rate(mg/min)";TAB(54);"cor.coeff."
1640 PRINT
1650   PRINT DELM;TAB(22);100*DELM/WSAMPLE;
        TAB(39);HAST;TAB(57);CORR
1660 PRINT
1661 PRINT
1665 VDU1,27,70
1670 VDU3
1680 ENDPROC
1690   REM----RUTINE FOR ENDRING AV ANT. MAALINGER
        FOR BEREGN. AV VDUTANHAST.--------
1700 DEFPROCmeas
1705 *FX21,0
1710   INPUT"HOW MANY MEASUREMENTS TO CALCULATE THE RATE
1711 (max. 100)";ANT
1720 @%=&20009:VDU28,25,8,30,7:CLS:PRINT"(";ANT;")"
1725 NUMB=1
1730 ENDPROC
```

A2.   Experimental data

A2.1. Comprehensive review on all of the experiments with respect to experimental parameters being relevant

All pressures are reported as they were measured, that is, in units of torr. To convert into units of bar multiply by 1.333×10^{-3}.

Table A2.1. A listing of parameters relevant to the experiments performed with vitreous and devitrified quartz glass tubings. P_{CO} and P_{Ar} means that the furnace atmosphere is composed of pure CO and pure Ar, respectively, while a furnace atmosphere of 4×10^{-5} torr is virtually vacuum conditions.

Run no.	Silica sample	Furnace atmosphere [torr]	Temperature [°C]	Max. rate [mg/min]	Purpose
1	Quartz glass tubing(vitreous)	4×10^{-5}	1506	0.10	Rate of decomp.(Fig. 5.1)
2	"	"	1606	1.92	"
3	"	"	1618	9.04	"
4A	"	"	1568	5.70	Rate of decomp.(Fig. 5.2)
4B-I	"	"	1582	6.34	"
4B-II	"	"	1632	14.23	"
4B-III	"	"	1682	20.77	"
5	"	$P_{Ar}=745$	1550	0.04	Synthesizing cristobalite
6	Devitrified quartz glass (cristobalite)	4×10^{-5}	1563	1.04	Rate of decomp.(Fig. 5.3)
7	"	4×10^{-5}	1563	0.38	Rate of decomp.
8	"	$4 \times 10^{-5} < P_{CO} < 427$	1566	0.78	React. with CO
9	"	$4 \times 10^{-5} < P_{CO} < 778$	1575	1.25	React. with CO (Fig.5.5)

Table A2.1. Continued.......

Run no.	Silica sample	Furnace atmosphere [torr]	Temperature [°C]	Max. rate [mg/min]	Purpose
10	Devitrified quartz glass (cristobalite)	$4\times10^{-5}<P_{CO}<821$	1570	1.15	React. with CO (Fig.5.6)
11	"	$4\times10^{-5}<P_{CO}<269$	1572	1.11	React.with CO in the presence of C
12	"	$P_{CO}=75$	1430–1574	1.74	Activation energy at 75 torr CO (Fig.5.7)
13	"	$P_{CO}=200$	1412–1573	1.31	Activation energy at 200 torr CO (Fig.5.8)
14	"	$31<P_{CO}<156$	1575	2.08	Effect of bulk gas flow on react. rate (Fig.5.10)
15	Quartz glass tubing(vitreous)	4×10^{-5} $P_{CO}=200$	1609	0.05	Decomp.and react. with CO

Table A2.2. A listing of parameters relevant to the experiments performed with silica and silica/carbon mixtures. P_{CO}, P_{Ar} and P_{TOT} means that the furnace atmosphere is composed of pure CO, pure Ar and a mixture of Ar and CO respectively, while X_{CO} means the molar fraction of CO in the furnace atmosphere. The crucible types A, B and C refers to Fig. 6.1.

Run no	Purpose	Quality and particle size [mm] of reactants silica	Quality and particle size [mm] of reactants carbon	Molar ratio n_C/n_{SiO_2}	Crucible type	Furnace atmosphere [torr]	Temp. [°C]	Results
16	Rate at const. CO pressure	Quartz 1.003-1.19	-	-	B	$P_{CO}=1140$	1537	Low rate (short duration)
17	Complete conversion at const CO pressure	"	-	-	"	$P_{CO}=1140$	1570	Cfr. Fig. 6.3
18A	Rate when amount silica is 3 times run no. 17	"	-	-	"	$P_{CO}=1140$	"	Rate is 1.3 the rate of run no. 17
18B	Rate in dependence of CO pressure	"	-	-	"	$4\times10^{-5}<P_{CO}<1142$	"	Cfr. Fig. 6.4
18C	Rate at const. Ar pressure	"	-	-	"	$P_{Ar}=760$	"	Succesively increasing rate
19	Complete conversion at const. CO pressure	"	Graphite CS-49 0.105-0.177	8.7	"	$P_{CO}=1140$	"	Cfr. Fig. 6.3

Table A2.2. continued........

Run no	Purpose	Quality and particle size [mm] of reactants		Molar ratio n_C/n_{SiO_2}	Crucible type	Furnace atmosphere [torr]	Temp. [°C]	Results
		silica	carbon					
20	Rate in depend. of CO pressure	Quartz 1.003-1.19	Graphite CS-49 0.105-0.177	8.7	B	$2 \times 10^{-4} < P_{CO} < 1140$	1570	Cf. Fig. 6.2 and 6.4
21	Reproduce run no. 20	"	"	"	"	$2994 < P_{CO} < 1000$	"	Short duration (obstruction of optical path due to condensation)
22	Rate in depend. of CO pressure	Quartz 0.513-0.710	–	–	A	$1 < P_{CO} < 1405$	1558	Decreasing rate with CO pressure
23	Same as 22, type B crucible	"	–	–	B	$1 < P_{CO} < 1319$	"	Same behaviour as run no. 22, but generally higher rates.
24	Same as 22, effect of addition of graphite	"	Graphite CS-49 0.513-0.710	1.5	A	$3 < P_{CO} < 1350$	"	Same behaviour as run no. 23, but generally higher rates (Fig. 6.2).
25	Same as 22, effect of addition of charcoal	"	Charcoal o.513-0.710	~0.3	"	$2 < P_{CO} < 1199$	"	Same behaviour as run no. 24, but generally higher rates. SiC is formed.
26	Same as 24, effect of open crucible	"	Graphite CS-49 0.513-0.710	1.5	C	$8 \times 10^{-5} < P_{CO} < 1206$	"	Cf. Fig. 6.2.

Table A2.2. continued.......

Run no	Purpose	Quality and particle size [mm] of reactants		Molar ratio n_C/n_{SiO_2}	Crucible type	Furnace atmosphere [torr]	Temp. [°C]	Results
		silica	carbon					
27-30	Rate in depend. of CO partial pressure	Quartz 0.513-0.710	Graphite CS-49 0.513-0.710	1.5	C	$600 \leq P_{TOT} \leq 1000$ $0.001 \leq x_{CO} \leq 1$ (gases mixed in furnace chamber)	1558	There is a considerable scatter in the observed rates.
31	Testing mixing procedure	"	"	"	"	$P_{TOT} = 800$ $0.125 \leq x_{CO} \leq 1$	"	Rate is seriously affected whether CO or Ar is allowed first into the furnace chamber (Fig. 6.7).
32-35	Rate in depend. of CO partial pressure	"	"	"	"	$P_{TOT} = 800$ $0.025 \leq x_{CO} \leq 1$ (gas mixing equipm. applied)	"	There is a considerable scatter in the observed rates (Fig. 6.8).
36	Rate in vacuum	"	"	"	"	4×10^{-5}	"	Const. low rate in terms of time
37	Rate in depend. of CO partial pressure	"	"	"	"	$P_{TOT} = 800$ $0.125 \leq x_{CO} \leq 1$	"	Considerable scatter in the observed rates (Fig. 6.8).
38	Effect of evacuation on rate	"	"	"	"	$P_{CO} = 800$ and $P_{CO} = 0.4$	"	Increasing rate with number of evacuation (Fig. 6.9).

Table A2.2. continued.......

| Run no | Purpose | Quality and particle size [mm] of reactants | | Molar ratio n_C/n_{SiO_2} | Crucible type | Furnace atmosphere [torr] | Temp. [°C] | Results |
		silica	carbon					
39-40	Effect of evacuation on rate	Cristobalite 0.513-0.710	Graphite CS-49 0.513-0.710	1.5	C	$P_{CO}=800$ and $P_{CO}=0.4$	1558	Short duration (obstruction of optical path due to condensation).
41	Rate in depend. of CO partial pressure	"	"	"	"	$300 \leq P_{TOT} \leq 1000$ $0.1 \leq X_{CO} \leq 1$ (Gas mixing equipm. applied)	"	SiC is formed (Fig. 6.13).
42	Effect of evacuation on rate	"	"	"	"	$P_{CO}=800$ and $P_{CO}=0.4$	"	Rate independent of number of evacuation (Fig. 6.10).
43A	Rate in depend. of CO partial pressure	"	"	"	"	$300 \leq P_{TOT} \leq 1000$ $0.009 \leq X_{CO} \leq 1$ (Gas mixing equipm. applied)	"	SiC is formed (Fig. 6.14).
43B	Rate in depend. of CO pressure	"	"	"	"	$1.5 \leq P_{CO} \leq 1000$	"	Fast rate at low CO pressures (Fig. 6.15).
44A	Effect of evacuation on rate	Quartz 0.513.0.710	"	"	"	$P_{CO}=800$ and $P_{CO}=0.4$	"	Increasing rate with number of evacuation (Fig. 6.10).

Table A2.2. continued........

Run no	Purpose	Quality and particle size [mm] of reactants		Molar ratio n_C/n_{SiO_2}	Crucible type	Furnace atmosphere [torr]	Temp. [°C]	Results
		silica	carbon					
44B	Stability of rate in depend. of time	Quartz 0.513-0.710	Graphite CS-49 0.513-0.710	1.5	C	$P_{TOT}=800$ $X_{CO}=0.4$	1558	Rate essentially constant during 2 h.
45	Effect of quenching on rate	"	"	"	"	$P_{CO}=800$ and $P_{CO}=0.4$	"	Substantial increase in rate after quenching (Fig. 6.11).
46A	Generate SiC on the graphite particles	"	"	"	"	$P_{CO}=300$ and $300 \leq P_{TOT} \leq 800$ $X_{CO}=0.1$	"	A large rate is observed when furnace is evacuated below 1 torr (Fig. 6.16).
46B	Development of rate when SiC is formed	Cristobalite 0.513.0.710	"	"	"	$P_{CO}=0.3$	"	Wheight loss curve exhibit "sigmoidal" behaviour (Fig. 6.17).

Table A2.3.   A listing of parameters relevant to the thermogravimetric investigation on the kinetics of the transformation of quartz into cristobalite (KR.1-6) and the possible influence of these transformations on the rate of interaction between silica and carbon. The composition of the residual silica was analyzed by means of XRD. Run Al-1A, Al-1B and Al-2 investigated the quality of alumina (alsint) as a possible inert crucible material for future experiments with silica/carbon mixtures.

Run no.	Purpose	Quality and particle size [mm] of silica	Crucible (Cfr.Fig. 6.1)	Temp. [°C]	Furnace CO pressure at given temp. [torr]	Reaction time at given temp. and atmosph. [h]	Results
KR.1	Kinetics of the quartz/ cristobalite transformation	Quartz 0.513-0.710	type C (graphite)	1200	774	18	Cristobalite was not found
KR.2	"	"	"	1211 1558	773 800	18 4	A considerable transformation into cristobalite, but some quartz left
KR.3	"	"	"	1210 1558	775 800	18 7	Most of the quartz was transformed into cristobalite
KR.4	"	"	"	1210 1558	774 4×10^{-5}	13 5	"
KR.5	Synthesizing cristobalite from quartz	"	Al_2O_3 (alsint)	1430	1 atm air	120	"
KR.6	"	"	"	"	"		"

Table A2.3. Continued.......

Run no.	Purpose	Quality and particle particle size [mm] of silica	Crucible (Cfr. Fig. 6.1)	Temp. [°C]	Furnace CO pressure at given temp. [torr]	Reaction time at given temp. and atmosph. [h]	Results
Al-1A	The stability of Al_2O_3 (alsint) in the presence of C(graphite)	Silica not present	type C (graphite)	1558	790	20	The alumina was not found to loose weight
Al-1B	"	"	"		4×10^{-5}	2.5	The alumina was found to loose weight
Al-2	The stability of Al_2O_3 (alsint) in the presence of C(graphite) and silica	Quartz 0.513-0.710	"	1520	782	5.6	The alumina pieces and silica particles were considerably sintered at the points of contact

A2.2. Weight data

Table A2.4 contains weight data relevant to the experiments with vitreous and devitrified silica tubings, while Table A2.5-12 contains weight data relevant to the experiments with mixtures of silica and graphite particles.

Table A2.4. Run 1-14.

Run no.	Initial weight [g]	Final weight [g]	Weight loss [mg]	Remarks
1	7,8143	7.6685	145.8	Silica tubing only
2	7.5455	6.5897	955.8	"
3	7.4890	5.7766	1712.4	"
4A/4B	7.7505	5.0552	2695.3	"
9	8.6697	8.3361	333.6	Silica tubing plus "black body" (Mo-cup)
10	8.3012	7.8143	486.9	"
12	7.5490	7.3863	162.7	"
13	7.3797	7.2305	149.2	"
14	7.2233	6.9846	238.7	"

Table A2.5. Run no 17

Item	Initial weight w_i [g]	Final weight w_f [g]	Weight change $\Delta w = w_i - w_f$ [mg]	Remark
Silica (quartz)	1.0220	0	1022.0	All silica consumed
Crucible (cup+lid)	23.1137	22.9122	201.5	

Table A2.6. Run no. 18

Item	Initial weight w_i [g]	Final weight w_f [g]	Weight change $\Delta w = w_i - w_f$ [mg]	Remark
Silica (quartz)	3.0662	2.5622	504.0	-
Crucible (cup+lid)	22.9110	22.8309	80.1	-

Table A2.7. Run no. 19

Item	Initial weight w_i [g]	Final weight w_f [g]	Weight change $\Delta w = w_i - w_f$ [mg]	Remark
Silica (quartz)	0.7208	0	720.8	All silica consumed
Carbon (graphite)	1.2552	1.1417	113.5	-
crucible lid	5.0001	4.9989	1.2	-
crucible cup	17.7787	17.7323	46.4	-

Table A2.8. Run no. 20

Item	Initial weight w_i [g]	Final weight w_f [g]	Weight change $\Delta w = w_i - w_f$ [mg]	Remark
Silica (quartz)	3.0664			Δw is initial weight of the charge (silica +carbon) minus charge residue
Carbon (graphite)	5.3347	7.8380	563.1	
Crucible lid	4.9989	4.9987	0.2	-
crucible cup	17.7159	17.7017	14.2	-

Table A2.9. Run no. 24.

Item	Initial weight w_i [g]	Final weight w_f [g]	Weight change $\Delta w = w_i - w_f$ [mg]	Remark
Silica (quartz)	7.2704			Δw is initial weight of the charge (silica +carbon) minus charge residue
		8.8686	579.0	
Carbon (graphite)	2.1772			
Crucible lid	5.7141	5.7200	-10.3	-
crucible cup	17.5306	17.5409	-19.4	-

Table A2.10. Run no. 41.

Item	Initial weight w_i [g]	Final weight w_f [g]	Weight change $\Delta w = w_i - w_f$ [mg]	Remark
Silica (cristob.)	2.4233			Δw is initial weight of the charge (silica +carbon) minus charge residue. SiC is formed
		1.9999	1149.7	
Carbon (graphite)	0.7263			
Crucible lid	5.0160	5.0156	0.4	SiC formed
crucible cup	17.9440	17.8888	55.2	"

Table A2.11. Run no. 43A + 43B.

Item	Initial weight w_i [g]	Final weight w_f [g]	Weight change $\Delta w = w_i - w_f$ [mg]	Remark
Silica (cristob.)	2.4233			Δw is initial weight of the charge (silica +carbon) minus charge residue. SiC is formed.
		1.6910	1458.6	
Carbon (graphite)	0.7263			
Crucible lid	5.0136	5.0151	-1.5	SiC formed
crucible cup	17.8201	17.8152	4.9	"

Table A2.12. Run no.46A+46B

Item	Initial weight w_i [g]	Final weight w_f [g]	Weight change $\Delta w = w_i - w_f$ [mg]	Remark
Silica (cristob.)	2.4235	0	2423.5	All silica consumed
Carbon (graphite)	0.7261	0.4075	318.6	Considerabel amounts of SiC formed
Crucible lid	5.0049	5.0273	-22.4	SiC formed
crucible cup	17.5952	17.5064	88.8	"

A2.3. Rate data

Table A2.13. Run no. 9.

CO pressure [torr]	Rate of weight loss [mg/min]
1.5	0.299
5	0.338
11	0.480
20	0.677
32	0.787
50	0.911
82	1.109
125	1.202
204	1.250
409	0.954
778	0.975
4×10^{-5}	0.246

Table A2.14. Run no. 10

CO pressure [torr]	Rate of weight loss [mg/min]
4×10^{-5}	0.299
205	1.026
50	0.909
154	1.152
101	1.115
421	1.028
348	1.012
258	1.041
307	1.046
719	1.019
515	0.997
614	1.063
821	1.129

Table A2.15. Run no. 12

Temperature [°C]	Rate of weight loss [mg/min]
1430	0.142
1452	0.243
1484	0.439
1511	0.658
1553	1.180
1574	1.519

Table A2.16. Run no. 13

Temperature [°C]	Rate of weight loss [mg/min]
1412	0.186
1451	0.300
1483	0.457
1510	0.630
1552	0.984
1573	1.233
1412	0.198

Table A2.17. Run no. 18.

CO pressure [torr]	Rate of weight loss [mg/min]
1141	0.267
760	0.350
529	0.449
304	0.506
155	0.554
76	0.582
17	0.604
5	0.442
10	0.395
50	0.457
200	0.503
800	0.336
1520	0.198
4	0.578
6×10^{-5}	0.191

Table A2.18. Run no. 20.

CO pressure [torr]	Rate of weight loss [mg/min]	Average rate [mg/min]
1140	0.462	
758	0.731	
1140	0.497	
761	0.878	
2×10^{-4}	2.391	2.060
5	2.414	2.442
11	2.097	2.306
20	2.097	2.097
50	2.184	2.434
76	2.488	2.586
152	2.762	2.898
304	2.333	2.424
543	1.257	1.225
760	0.821	0.801
912	0.637	0.619
1140	0.442	0.442
911	0.601	
760	0.781	
543	1.192	
304	2.514	
152	3.033	
76	2.683	
50	2.683	
10	2.514	
5	2.470	
2×10^{-4}	1.730	

Table A2.19. Run no. 24.

CO pressure [torr]	Rate of weight loss [mg/min]
751	0.450
1352	0.118
1109	0.228
808	0.419
604	0.640
401	1.025
198	2.621
97	3.470
10	3.813
3	2.856

Table A2.20. Run no. 26.

CO pressure [torr]	Rate of weight loss [mg/min]
822	1.183
803	1.134
1206	0.705
1005	0.983
601	1.477
402	1.750
300	1.768
99	1.698
50	1.732
10	1.632
1.3	1.280
1.3	1.711
801	0.857
8×10^{-5}	0.236

Table A2.21. Run no 41.

Total pressure $P_{CO} + P_{Ar}$ [torr]	Partial pressure CO [torr]	Rate of weight loss [mg/min]
1000	1000	1.376
	800	1.387
	600	1.315
	400	1.171
	200	0.869
	100	1.192
800	800	1.711
	640	1.732
	480	1.570
	320	1.294
	160	1.011
	80	1.366
600	600	2.032
	480	2.006
	360	1.753
	240	1.444
	120	1.163
	60	1.540
300	300	2.539
	240	2.194
	180	1.921
	120	1.651
	60	1.528
	30	2.097

Table A2.22. Run no 43A.

Total pressure $P_{CO}+P_{Ar}$ [torr]	Partial pressure CO [torr]	Rate of weight loss [mg/min]
	300	0.966
	200	0.767
1000	100	0.645
	70	0.879
	9	0.630
	240	1.056
	160	0.848
800	80	0.765
	56	1.050
	7	0.740
	180	1.095
	120	0.904
600	60	0.845
	42	1.140
	5	0.839
	90	1.213
	60	1.130
300	30	1.018
	21	1.499
	3	1.192

Table A2.23. Run no. 43B.

CO pressure [torr]	Rate of weight loss [mg/min]
1000	1.118
800	1.494
600	1.823
300	2.356
150	2.632
50	4.011
20	4.705
10	4.915
5	4.872
2	10.054

Table A2.24. Thermogravimetric data for run no. 17. w_{tot} is total weight loss recorded at time t, w_i is initial weight of silica (1.0220 g) and τ is time for complete reaction (185 h). M_{SiO_2} and M_C are formula weights of silica and carbon respectively (Cfr. Fig. 6.3 and 6.6).

Reaction time t	Total weight loss w_{tot}	Fraction silica reacted $R = \dfrac{w_{tot}}{\left(1+\dfrac{M_C}{M_{SiO_2}}\right)w_i}$	Fractional time t/τ	Ratio between radius of silica particle at time t, r, and initial radius, r_i. $\dfrac{r}{r_i} = (1-R)^{1/3}$
[h]	[mg]			
0	0	0.00	0.00	1.00
10	85	0.07	0.05	0.98
20	163	0.13	0.11	0.95
30	240	0.20	0.16	0.93
40	318	0.26	0.22	0.91
50	398	0.32	0.27	0.88
60	478	0.39	0.32	0.85
70	556	0.45	0.38	0.82
80	639	0.52	0.43	0.78
90	712	0.58	0.49	0.75
100	786	0.64	0.54	0.71
110	858	0.70	0.60	0.67
130	994	0.81	0.70	0.57
150	1106	0.90	0.81	0.46
170	1188	0.97	0.92	0.32
180	1209	0.99	0.97	0.24
185	1226	1.00	1.00	≈ 0

Table A2.25. Thermogravimetric data for run no. 19. w_{tot} is total weight loss recorded at time t, w_i is initial weight of silica (0.7208 g) and τ is time for complete reaction (90 h). M_{SiO_2} and M_C are formula weights of silica and carbon respectively (Cfr. Fig. 6.3 and 6.6).

Reaction time t [h]	Total weight loss w_{tot} [mg]	Fraction silica reacted $R = \dfrac{w_{tot}}{\left(1+\dfrac{M_C}{M_{SiO_2}}\right)w_i}$	Fractional time t/τ	Ratio between radius of silica particle at time t, r, and initial radius, r_i. $\dfrac{r}{r_i} = (1-R)^{1/3}$
0	0	0.00	0.00	1.00
10	180	0.21	0.11	0.93
20	350	0.41	0.22	0.84
30	485	0.56	0.33	0.76
40	593	0.69	0.44	0.68
50	682	0.79	0.56	0.60
60	757	0.88	0.67	0.50
70	815	0.94	0.78	0.39
80	852	0.99	0.89	0.25
90	868	$\approx$1.00	1.00	$\approx$0.00

A2.4. Fitting between empirical data and model

Table A2.26. Result from the fitting between empirical data (measured) and calculated according to Eq.7.11. The best fit was found with the parametres given in Table 7.1. The empirical data refer to a cristobalite/graphite-charge (run 41) at 1558°C and total pressure 1.333 bar (1000 torr). Empirical data from Table A.21.

Total pressure [torr]	Mole fraction x_{CO}	Rate of weight loss [mg/min]		% deviation $\dfrac{calc.-meas.}{meas.} \times 100$
		Measured	Calculated	
	1.00	1.376	1.376	0.0
	0.80	1.387	1.372	−1.1
1000	0.60	1.315	1.311	−0.3
	0.40	1.171	1.164	−0.6
	0.20	0.869	0.880	1.3
	(0.10)	(1.192)	Formation of SiC	

Table A2.27 Result from the fitting between empirical data (measured) and calculated according to Eq.7.16. The empirical data refer to a cristobalite/graphite-charge (run 41) at 1558°C and total pressure 1.066, 0.800 and 0.400 bar (800, 600 and 300 torr) respectively. Empirical data from Table A2.21.

Total pressure [torr]	Mole fraction X_{CO}	Rate of weight loss [mg/min]		% deviation $\dfrac{calc.-meas.}{meas.}$ x100
		Measured	Calculated	
	1.00	1.711	1.715	0.2
	0.80	1.732	1.661	−4.1
800	0.60	1.570	1.545	−1.6
	0.40	1.294	1.341	3.6
	0.20	1.011	0.993	−1.8
	(0.10)	(1.366)	Formation of SiC	
	1.00	2.032	2.184	7.5
	0.80	2.006	2.059	2.6
600	0.60	1.753	1.868	6.6
	0.40	1.444	1.587	9.9
	0.20	1.163	1.157	−0.5
	(0.10)	(1.540)	Formation of SiC	
	1.00	2.539	3,482	37.1
	0.80	2.194	3.173	44.6
300	0.60	1.921	2.794	45.4
	0.40	1.651	2.314	40.2
	0.20	1.528	1.654	8.2
	(0.10)	(2.097)	−	−

A3. Gas velocity distribution inside the graphite heating element as calculated by "FLUENT".

We want to calculate the distribution of gas velocity inside the experimental arrangement which is shown schematically in Fig A3.1. Inside the silica tube is a cup of molybdenum (for temperature measurements) which prevents gas flow through the tube. The temperature distribution observed experimentally, and the distribution assumed for the calculations, are shown in the figure. (We will return below to the reasons why the assumed temperature gradient is steeper than the observed one.)

The uneven temperature inside the heating element will cause convection in the gas, so that a flow pattern will be established. The computation of this pattern is based on the equations of fluid dynamics as given below. The symbols have the following meaning:

t = time (s) c_p = heat capacity (J kg^{-1} K^{-1})

T = temperature (K)   k = thermal conductivity (W m^{-1} K^{-1})

P = pressure (Pa) r_{ij} = position[1]

v = gas velocity (m s^{-1}) τ_{ij} = shear stress tensor

ρ = density (kg m^{-3})   g = gravitational acceleration (m s^{-2})

e_i = unit vector β = coeff. of volume expansion (K^{-1})

Mass balance or the equation of continuity:

$$\frac{D\rho}{Dt} = -\rho \ \text{div} \ v \tag{A3.1}$$

Energy balance or the equation of energy:

$$\rho \ c_P \ \frac{DT}{Dt} = \beta \ T \ \frac{DP}{Dt} + \tau_{ij} \ \frac{\partial v_i}{\partial r_j} + \text{div} \ (k \ \text{grad} \ T) \tag{A3.2}$$

Impulse balance or the equation of motion (Navier-Stokes):

$$\rho \ \frac{Dv}{Dt} = - \ \text{grad} \ P + \rho \ g + e_i \ \frac{\partial \tau_{ij}}{\partial r_j} \tag{A3.3}$$

---

[1] Tensor notation e.g. $\frac{\partial \tau_{xx}}{\partial x} + \frac{\partial \tau_{xy}}{\partial y} + \frac{\partial \tau_{xz}}{\partial z} = \frac{\partial \tau_{xj}}{\partial r_j}$, where x,y and z are cartesian coordinates
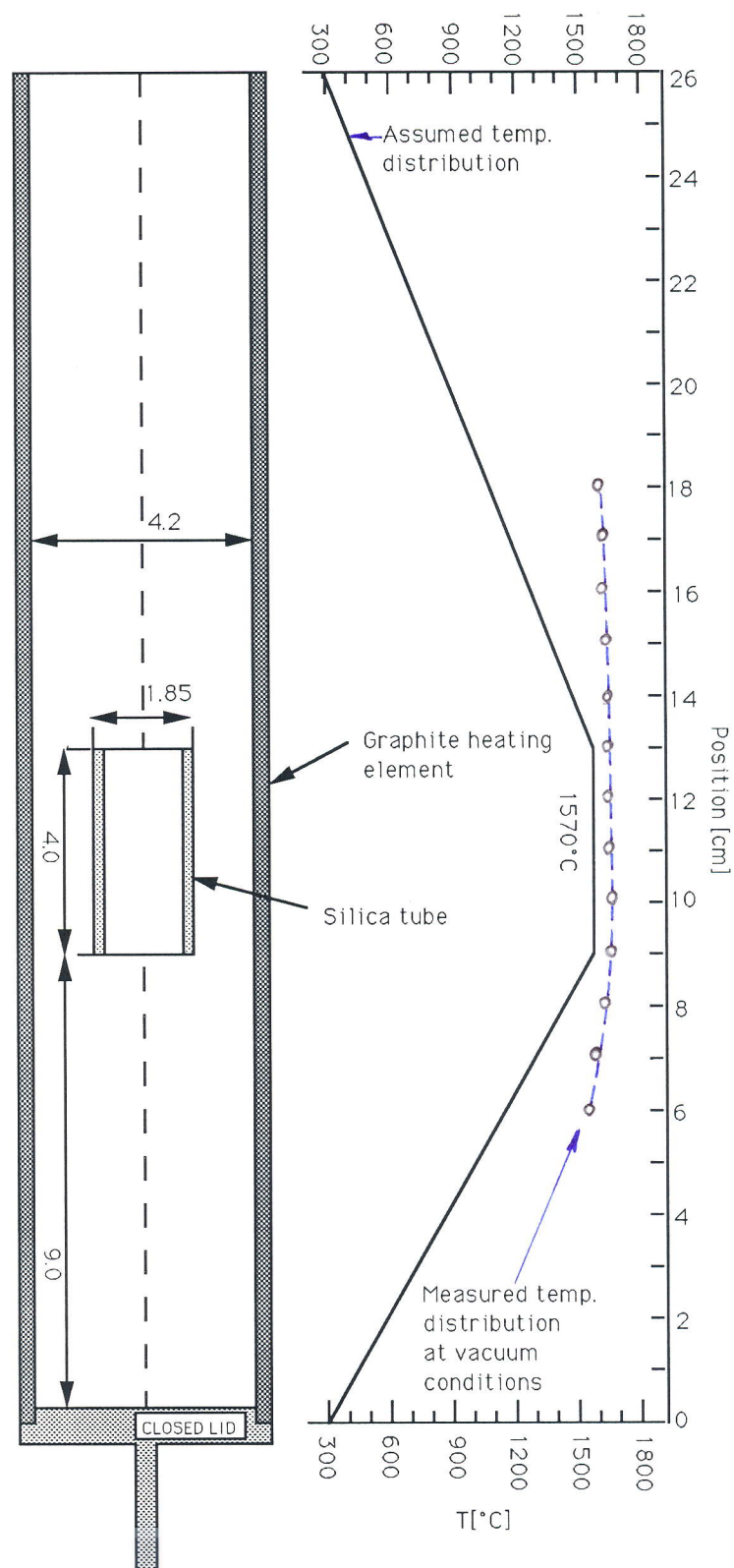
Fig. A3.1.   Geometry and dimensions [cm] of the graphite heating
element   and   silica   tubing.   The   experimental
temperature distribution is shown by the dashed curve
and open points (data from Fig. 3.2, measured in an
empty heating element in a vacuum).   The steeper
temperature gradients assumed for the calculation are
shown by full-drawn lines.

The viscosity η of the gas does not enter explicitly in these equations, but it enters in the expression for the shear stress tensor.

The gas in question is carbon monoxide, and data for the density and the coefficient of volume expansion are simply derived by assuming ideal gas behaviour.

The heat capacity as a function of temperature is taken from Barin and Knacke (1973). Transformed into units of J kg^{-1} K^{-1} it becomes:

$$C_{P,CO} = 1015 + 0.1464\ T - 1.644\times10^6\ T^{-2} \qquad \text{(A3.4)}$$
$$298K \leq T \leq 2500K$$

The heat capacity is assumed to be independent of pressure in the range of interest, i.e. 0.1 to 1 bar.

The viscosity is taken from Bousheri et al. (1987). A third-power regression gives the following polynomial for the viscocity in units of 10^{-6} Pa s:

$$\eta_{CO} = 5.88 + 0.0444\ T - 9.76\times10^{-6}\ T^2 + 1.38\times10^{-9}\ T^3 \qquad \text{(A3.5)}$$
$$273K \leq T \leq 3273K$$

The viscosity at a given temperature departs from a constant value at very low and very high pressures, but it is taken to be independent of pressure at the pressures in question. (This is correct as long as the mean free path is small compared to the dimensions of the apparatus, but not so small as to be comparable with molecular dimensions, cf. Present (1958) p. 41.)

The following relation exists between the thermal conductivity, heat capacity and viscosity of a polyatomic gas (cf., e.g., Sohn and Wadsworth (1979), p. 342):

$$k = (C_P + \frac{9\ R}{4\ M})\eta \qquad \text{(A3.6)}$$

where R is the gas constant and M formula weight of the gas species in question.

Using values from the above Eqs. A3.4 and A3.5, the following polynomial is obtained for the thermal conductivity in units of W m^{-1} K^{-1}:

$$k_{CO} = 5.3 \times 10^{-3} + 9.44 \times 10^{-5} \, T - 3.34 \times 10^{-8} \, T^2 + 1.15 \times 10^{-11} \, T^3$$
$$-1.36 \times 10^{-15} \, T^4 \tag{A3.7}$$

$$298K \leq T \leq 2500K$$

Now we will return to Fig. A3.1. It is seen that, compared to the experimentally determined temperature distribution, the distribution assumed for the calculations shows more pronounced gradients in the vicinity of the silica tube. This was a deliberate choice in order to enhance somewhat the effects of temperature gradients. Radial temperature gradients, on the other hand, are assumed to be negligible, and the temperature profile is assumed to be independent of the gas pressure.

The calculations were carried out on an "APOLLO 1000" computer by means of the data program "FLUENT" (Fluid flow simulation program. Version 2.9. Creare Incorporated. Hanover, New Hampshire 03755), which was available at the Department of metallurgy, NTH.

The velocity distribution is obtained by solving Eqs. A3.1 to A3.3 by an iterative procedure. The solution is acceptable when low values is obtained for the residuals of P (pressure), v (velocity) and H (enthalpy), that is, indicating that the iterative calculation converges to a specific solution. In order to compute the velocity distribution, the system is divided into a finite number of volume elements. A cross section of the volume elements in the surroundings of the silica tubing is shown in Fig. A3.2 for illustration. Velocity vectors are computed for each and all of the volume elements throughout the system, that is, from bottom to top of the heating element.

The results for the case of closed heating element and 0.1 bar CO are shown graphically in Fig. 5.12 to 5.14 in the main text, where these results are also discussed. Likewise, the results for the open tube and 0.1 bar CO are shown in Fig. 5.15.

The results for 1.0 bar CO are not displayed graphically, but selected numerical values for the surroundings of the silica tube are given in Tables A3.1 to A3.4 for both pressure values and for the cases of closed as well as open heating element.
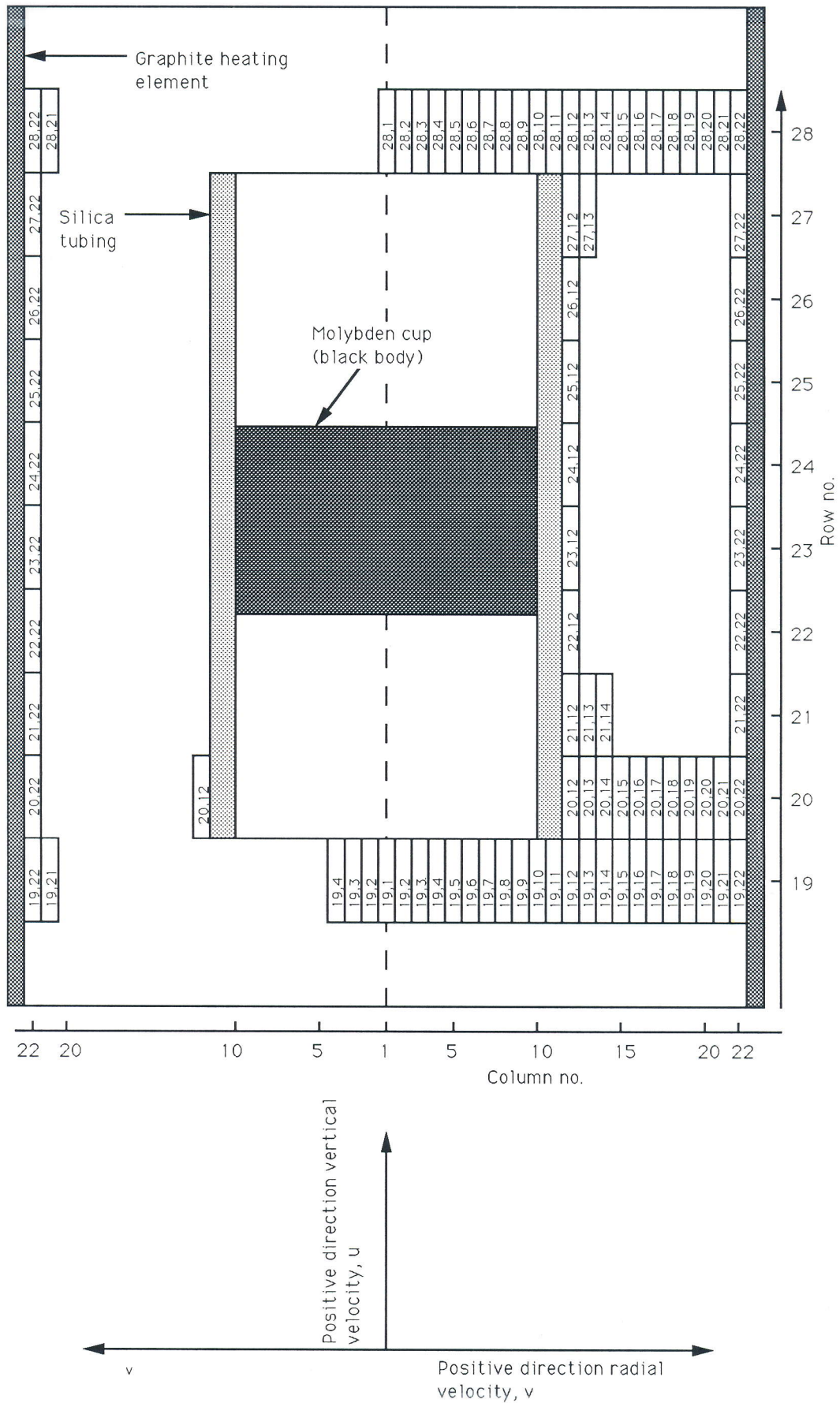
Fig. A3.2. Details in the surroundings of the silica tubing. Position and magnitude of some of the volume elements, which the system is devided into in order to compute the velocity distribution, is indicated. Notation volume element: (Row no, Column no.)

Table A3.1. The gas velocity distribution in the surroundings of the
            silica tubing at 1 bar CO pressure and closed heating
            element. The vertical velocity component (denoted u) is
            taken to be positive in the direction opposite the
            gravitational acceleration while the radial component
            (denoted v) is positive in the direction from centerline
            heating element to the perepheriy. The residuals given are
            dimensionless. "Row no." and "Column no." refer to Fig.
            A3.2.

Gas velocity $u \times 10^7$ / $v \times 10^7$ [m/s]

Row no. Column no.	19	21	23	25	27
22	5190/-519	504/-46.1	199/0.529	500/40.1	4060/404
20	15900/-5660	949/-402	333/6.67	930/337	12000/4460
18	16100/-15200	331/-757	290/16.8	319/599	9500/11300
16	9030/-26500	340/-744	323/22.8	-317/528	-724/16900
14	-1510/-37600	-293/-373	432/18.9	-224/197	-12700/17400
12	-11700/-46500	443/-36.5	459/5.01	472/-5.65	-18200/6660
10	-18200/-50400	-	-	-	-

RESIDUALS: P(pressure):2.6×10^{-9}, u(velocity):1.2×10^{-5}, v(velocity):2.1×10^{-4},
           H(enthalpy):5.4×10^{-8}

Table A3.2. The gas velocity distribution in the
            surroundings of the silica tubing at 1 bar
            CO pressure and open heating element.

Gas velocity u [m/s]

Row no. Column no.	19	21	23	25	27
22	0.318	0.428	0.403	0.385	0.350
20	0.998	1.36	1.43	1.44	1.39
18	1.14	1.51	1.71	1.84	1.89
16	1.08	1.37	1.57	1.76	1.93
14	0.962	1.16	1.29	1.47	1.71
12	0.684	0.354	0.393	0.449	0.556
10	0.288	-	-	-	-

RESIDUALS: Not reported.

Table A3.3. The gas velocity distribution in the surroundings of the silica tubing at 0.1 bar CO pressure and closed heating element.

	Gas velocity $ux10^7$ / $vx10^7$ [m/s]				
Row no.	19	21	23	25	27
Column no.					
22	281/-22.7	31.3/-3.40	4.76/-0.0554	24.2/2.50	141/6.99
20	704/-232	51.6/-26.2	7.22/-0.313	39.9/18.7	273/66.2
18	577/-599	-6.36/-43.3	-2.25/-0.201	-2.99/30.0	100/151
16	183/-1100	-64.3/-32.9	-9.98/0.441	-45.9/22.6	-176/214
14	-247/-1660	-30.2/-2.15	-2.64/0.717	-25.8/2.78	-324/163
12	-439/-1980	23.4/2.05	3.40/0.120	10.4/-0.852	-113/24.9
10	-699/-2010	-	-	-	-

RESIDUALS: P(pressure):$2.4x10^{-4}$, u(velocity):$2.0x10^{-5}$, v(velocity):$1.8x10^{-4}$, H(enthalpy):$5.3x10^{-8}$

Table A3.4. The gas velocity distribution in the surroundings of the silica tubing at 0.1 bar CO pressure and open heating element.

	Gas velocity u [m/s]				
Row no.	19	21	23	25	27
Column no.					
22	0.0601	0.0782	0.0779	0.0780	0.0763
20	0.254	0.325	0.326	0.326	0.317
18	0.385	0.480	0.483	0.483	0.473
16	0.453	0.536	0.540	0.541	0.539
14	0.407	0.415	0.420	0.420	0.434
12	0.217	0.105	0.108	0.108	0.105
10	0.134	-	-	-	-

RESIDUALS: P(pressure):$7.7x10^{-4}$, u(velocity):$2.1x10^{-4}$, v(velocity):$2.0x10^{-4}$, H(enthalpy):$1.5x10^{-7}$

A4.   The effect of composition on the diffusivity

Throughout the present work it has been assumed that the diffusivities of the diffusing species in the gaseous mixture are independent of gas composition and a function of temperature and total pressure only.

First, for a binary gas mixture of e.g. the species A and B it is commonly assumed that D_{A-B} is independent of composition. The rigorous Chapman-Enskog theory of hard spheres molecules gives, however, small corrections which makes D_{A-B} vary by a few percent as X_A goes from 0 to 1. The order of magnitude of the correction depends on the mass ratios between A and B. Marrero and Mason (1972) have visualized how the correction term vary with composition for two given mass ratios, and reports about 4% increase in D_{A-B} at mass ratio $M_A/M_B=0.1$ as X_A goes from 0 to 1. At mass ratio $M_A/M_B=0.5$ the correction is less than 2 %. However, for the molar masses of the gaseous species in question (SiO, CO, CO_2 and Ar) the lowest possible mass ratio is $M_{CO}/M_{CO_2}=0.64$ which gives a maximum variation in the diffusivity of less than 1 %. Hence, the binary diffusivities may be assumed to be independent of composition.

Second, the final experiments investigated the rate of interaction between the reactants at constant total pressures as the CO-pressure was varied as a partial pressure. The gas mixture was obtained by mixing CO and Ar and the compositional variation was rather large as X_{CO} varied from 0.009 to 1. The diffusivity of the diffusing species was assumed to be independent of composition. However, while taking the diffusivity of CO_2 as an example, the maximum attainable variation in $D_{CO_2-Ar/CO}$ is expected to be the difference between the diffusivity of CO_2 in pure Ar, D_{CO_2-Ar}, and pure CO, D_{CO_2-CO}, respectively. Computing the diffusivities from the relations recommended by Marrero and Mason (1972) at 1558 ^oC and $P_{tot.}=$ 1 atm gives $D_{CO_2-Ar}=$ 3.889 cm^2/s and $D_{CO_2-CO}=$ 3.925 cm^2/s. That is a maximum increase in the diffusivity of 0.9 % as X_{CO} goes from 0 to 1. Thus the assumption of constant diffusivity is relatively well fullfilled.

On the other hand, if the molar masses of the gaseous species, which the mixture is composed by, are substantially different the composition dependence have to be accounted for.

Wilke (1950) recommended the following relationship for computing the effective diffusion coefficient of a gas with respect to a multicomponent mixture of stagnant gases:

$$D_A = \frac{1 - X_A}{\frac{X_B}{D_{AB}} + \frac{X_C}{D_{AC}} + \frac{X_D}{D_{AD}} + \cdots} \qquad (A4.1)$$

Thus if the binary diffusion coefficients and the composition of the gas phase respectively, are known, Eq. A4.1 enables the calculation of the diffusivity. The diffusivity of a specie A in a stagnant binary mixture of B and C, may, according to Wilke (1950) be calculated by the following relationship:

$$D_A = \frac{1}{\frac{X'_B}{D_{AB}} + \frac{X'_C}{D_{AC}}} \qquad (A4.2)$$

Where X'_B and X'_C are the mole fractions of B and C in the inert gas portion considered separately from diffusing gas A. Eq. A4.2 may thus be applied for computing the diffusivity of CO_2 (A) in a binary mixture of CO (B) and Ar (C). However, as the numeric value of D_{CO_2-CO} is very close to D_{CO_2-Ar}, Eq. (A4.2) describes a relationship between D_{CO_2-mix} and X_{CO} which is essentially linear.

A5.   NBS, report of calibration

U.S. DEPARTMENT OF COMMERCE

NATIONAL BUREAU OF STANDARDS

WASHINGTON, D.C.   20234

REPORT OF CALIBRATION

RIBBON FILAMENT LAMP

Submitted by

Universitetet I Trondheim
Norges Tekniske Høgskole
Institutt for Silikat-Og Høytemperaturkjemi
N-7034 Trondheim-NTH, Norway

Brightness Temperature (at 655 nanometers) versus Lamp Current

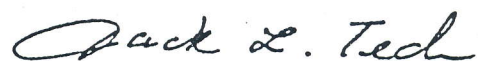| Degrees C (IPTS-68)	Direct Current (amperes)	Degrees C (IPTS-68)	Direct Current (amperes)
1000	13.31	1700	25.80
1100	14.56	1800	28.12
1200	16.01	1900	30.54
1300	17.66	2000	33.05
1400	19.49	2100	35.65
1500	21.47	2200	38.34
1600	23.58	2300	41.12

The maximum uncertainties of the temperature values reported are estimated to vary from ±2.5 degrees at 800°C, to ±1.5 degrees at 1100°C, and to ±3 degrees at 2300°C. The values in the above table and the uncertainties apply at the conclusion of the calibration. The typical change when the lamp is operated at the higher temperatures is a decrease of about one degree per ten hours at all temperatures.

These values apply when the lamp is operated base down and the portion of the filament at the notch made vertical. The center contact should be at a positive potential and the room temperature at 25°C. The sighting should be made on the center of the filament across from the notch, with the arrow, etched on the back of the envelope, appearing at the notch. Sightings were made such that the angle subtended at the lamp filament by the entrance pupil of the pyrometer was 0.14 radian.

P.O. No. Letter dated April 9, 1980
Test No. 534/223113
December 1, 1980

The calibration was performed using the NBS photoelectric pyrometer described in the paper, "The NBS Photoelectric Pyrometer and Its Use in Realizing the International Practical Temperature Scale Above 1063°C", R. D. Lee, Metrologia 2, 150 (1966). The magnitudes of the effects when altering these conditions are discussed in NBS Monograph 41, Theory and Methods of Optical Pyrometry (1962). The text of the International Practical Temperature Scale of 1968 Amended Edition of 1975 may be found in Metrologia 12, 7 (1976).

For the Director

Jack L. Tech

Jack L. Tech, Chief
Radiometric Physics Division
Center for Radiation Research

P.O. No. Letter dated April 9, 1980
Test No. 534/223113
December 1, 1980